DOT-TST-77-59

STAND-UP TIME OF TUNNELS IN SQUEEZING GROUND

Part I: A Physical Model Study

JUNE 1977

FINAL REPORT
UNDER CONTRACT
DOT-OS-50108

Document is availble to the U.S. Public through
The National Technical Information Service,
Springfield, Virginia 22161

Prepared for

U.S. DEPARTMENT OF TRANSPORTATION
Office of the Secretary
Office of University Research
Washington, D.C. 20590

Technical Report Documentation Page

1. Report No.	2. Government Accession No.	3. Recipient's Catalog No.
DOT-TST-77-59		

4. Title and Subtitle	5. Report Date
STAND-UP TIME OF TUNNELS IN SQUEEZING GROUND Part I: A Physical Model Study Part II: General Constitutive	June 30, 1977 6. Performing Organization Code
7. Author(s) L. R. Myer, T. L. Brekke, G. E. Korbin E. Kavazanjian and J. K. Mitchell	8. Performing Organization Report No.
9. Performing Organization Name and Address University of California 434B Davis Hall Berkeley, California 94720	10. Work Unit No. (TRAIS) 11. Contract or Grant No. DOT-OS-50108
12. Sponsoring Agency Name and Address	13. Type of Report and Period Covered Annual Report July 1, 1976-June 30, 1977 14. Sponsoring Agency Code

15. Supplementary Notes

OST Technical Monitor: Russell K. McFarland, TST-45

16. Abstract

The effect of tunnel size, advance rate, and depth of cover on the stand-up time of tunnels in squeezing ground was investigated through a series of 12 physical model tests. The stand-up time, defined as the time elapsed before instability develops, was found to be characterized by increasing deformations and deformation rates rather than a catastrophic collapse of the tunnel.

Test results showed a 25% increase in stand-up time was realized by halving the size of the opening (from 5.0 m dia. to 2.4 m dia. when scaled to prototype dimensions) or by decreasing the advance rate by a factor of four (from 1.3 m/hr to 0.3 m/hr for the 5.0 m dia. tunnel). Depth of cover was described in terms of the ratio of confining pressure to material strength. Decreasing the depth (or increasing material strength) by 10% also increased stand-up time by 25%.

In order to establish a predictive capability, a constitutive theory describing the time dependent behavior of soft clays has been developed. By generalizing existing empirical rules developed for fixed boundary conditions and then unifying these empirical rules with a tensor framework, a multi-axial constitutive equation describing the stress-strain-time behavior of normally loaded soft clays was formulated.

17. Key Words	18. Distribution Statement
Tunnels, Stability Problems	Document is available to the U. S. Public through the National Technical Information Service, Springfield, Virginia 22161

19. Security Classif. (of this report)	20. Security Classif. (of this page)	21. No. of Pages	22. Price
UNCLASSIFIED	UNCLASSIFIED		

EXECUTIVE SUMMARY

Introduction

One objective of this research is to develop a fundamental understanding of the relationship between the size and rate of advance of a tunnel face and the stand-up time in squeezing ground. With this understanding, a second objective is to develop a predictive capability.

Problem Studied:

Project research developed into three separate tasks which together should fulfill the program objective. The first task, now complete, involved a set of physical model studies to develop an understanding of the interrelationship among tunnel size, advance rate, and the deformation behavior around the tunnel opening.

The second and third tasks are both concerned with developing a predictive capability. In the second task, an empirical theory describing the time dependent behavior of soft clays has been developed. Laboratory work pointed towards verification of the theory and accompanying numerical model is now underway. In the third task, a mathematical model employing a visco-plastic constitutive equation with an internal "degree of damage" variable is under investigation.

Results Achieved:

Physical model tests were performed in a cylindrical steel test chamber 0.67 m dia. x 1.22 m long. The geometrical scaling laws for model to prototype extrapolations were developed. A sand-wax model material which, subject to the appropriate scaling laws, showed behavioral characteristics considered representative of squeezing ground (and soft clays) was developed. A circumfrential pressure was applied to the sand-wax filled model chamber and a small scale tunnel excavator was advanced along the axis of the steel cylinder. Deformations resulting from tunnel excavation were measured along two radial lines and one axial line within the model using inductance coil strain gages.

A total of 12 physical model tests were performed encompassing prototype conditions corresponding to two different advance rates, three tunnel diameters, and six different depths of cover. Test results showed that it was necessary to describe stand-up time, defined as the time elapsed before instability developed, in terms of accumulated strains rather than a state of total collapse. Total, catastrophic collapse only occurred when the deformation around the tunnel intersected the model boundary. This is consistent with observed field behavior in which deformations and deformation rates become large enough to inhibit tunneling operations even though catastrophic collapse does not necessarily occur. Thus, on the basis of the studies, it can be inferred that if catastrophic collapse does occur when tunneling in squeezing ground, it is caused by factors other than those encompassed by the physical models, e.g. discontinuities or intersection of tunnel deformations with the ground surface.

Stand-up, T_{ST}, was defined as the time to reach a specified "critical" deformation expressed as a percent of the unsupported period. The unsupported period is the time in a continually advancing excavation that an element of ground remains unsupported. The effect on stand-up time of size of opening, rate of advance, and depth of cover (expressed as a ratio of material strength to confining pressure) was investigated.

Test results showed that if the rate of advance and ratio of tunnel diameter to distance from the face to the first support remain constant, increasing the tunnel size decreases T_{ST}. Increasing the prototype dimensions from 2.4 m dia. to 5.0 m dia. decreases stand-up time by 20%. A similar 20% decrease in T_{ST} was achieved when advance rate was reduced from 1.3 m/hr to 0.3 m/hr for a 5.0 m dia. tunnel.

Changes in stand-up time behavior due to changes in depth of cover, expressed as a ratio of confining pressure to material strength, were related to changes in tunnel size or advance rate. A confining pressure (or depth of cover) decrease of 10% was found equivalent to a 50% decrease in tunnel size or an increase in advance rate by a factor of four (T_{ST} reduced by 20%). The same correlations exist for a 10% increase in material strength (depth of cover held constant).

In order to develop a predictive capability, constitutive equations for the time dependent behavior of squeezing ground are required. By generalizing existing empirical laws for the time-dependent behavior of soft clays, a multi-axial constitutive relationship has been developed. In this relationship the stress and strain states are represented as Cartesian tensors and separated into volumetric and deviatoric components. Each strain tensor component is assumed to have immediate (time independent) and delayed (time dependent) contributions. Relationships describing the four terms of the constitutive equation were generalized from Bjerrum's one dimensional consolidation model, Ladd and Foott's concept of normalized soil properties, and the Singh-Mitchell creep equation. The validity of the theory and an accompanying numerical model is currently under investigation through a laboratory test program.

Work is also progressing on development of a mathematical model of the mechanical behavior of the sand-wax material used to simulate "squeezing ground." A visco-plastic constitutive equation with an internal "degree of damage" variable has been employed to represent the rate and pressure dependence of strength and modulus observed in laboratory triaxial compression tests. Volumetric response is assumed rate independent but non-linear. Deviatoric response is taken to be rate and confining pressure dependent. The softening phenomenon is introduced through the internal variable measuring "degree of damage." Study of the necessary generalization of the mathematical model to reproduce stress and deformation states found in practical tunneling operations has been undertaken. This includes defining the mathematical structure, material parameters, and laboratory experiments required to simulate three dimensional, non-triaxial stress and deformation states.

Utilization of Results:

Tunneling through squeezing ground is one of the most troublesome and least understood areas in underground construction. This research project advances the state-of-the-art of tunneling in squeezing ground. The understanding gained from the physical model tests of the interrelationship between size of the tunnel opening, advance rate, and the stability of the opening should allow for more effective design and construction procedures and thus provide for significant economies.

The work on constitutive equations is of benefit not only in the field of underground construction but also in any geotechnical problem involving time dependent strengths or deformations. Most geotechnical material models currently in use do not address this problem of time dependence of strength and deformation.

Conclusion:

Fundamental knowledge of the interrelationship among stand-up time, size of tunnel opening, rate of advance, and depth of cover (or material strength) has been gained through a series of 12 physical model tests. The effect of increasing the opening size, of decreasing the advance rate, and of increasing the depth of cover on stand-up time of tunnels in squeezing ground has been quantified. Progress has been made towards developing the constitutive equations required to establish a numerical technique for predicting these effects. Knowledge gained from the physical model tests alone should provide for significant improvement in design and construction procedures for the construction of tunnels in squeezing ground.

PREFACE

The objective of the research described herein is to develop a fundamental understanding of the relationship between the size of an advancing tunnel face, the rate of excavation, and the stand-up time in squeezing ground. Stand-up time is defined as the time elapsed after excavation that an unsupported tunnel face will remain stable. Squeezing ground is argillaceous rock or soil that exhibits pronounced time dependence of deformation and strength properties in-situ.

This annual report for the second year of a three-year research effort has two parts. Part I presents the findings from a study of case histories and from a series of physical model tests. Part II describes the present status of an experimental effort to establish the constitutive equations for the time dependent behavior of squeezing ground. The concurrent effort to develop a mathematical model will be reported in the final report.

The project personnel has been the following:

Principal Investigator:

T. L. Brekke, Professor of Geological Engineering

Co-principal Investigators:

I. Finnie, Professor of Mechanical Engineering

J. K. Mitchell, Professor of Civil Engineering

R. L. Taylor, Professor of Civil Engineering

Research Engineer:

G. E. Korbin, Ph.D.

Research Assistants:

L. R. Myer

E. Kavazanjian

M. Panaahande

ACKNOWLEDGMENTS

The technical representative for this contract is Mr. R. K. McFarland, Office of Systems Engineering. His continued support of and detailed interest in this work is greatly appreciated.

The physical model tests as well as the material characterization work was carried out at the Richmond Field Station. Mr. C. Chan, Research Engineer, Mr. B. Debeling, Machinist, and Mr. T. Pickrell, Electronics Technician, all of the Institute of Transportation Studies, were most helpful in their aid in designing and constructing the testing equipment.

Professors I. Finnie, K. S. Pister, and R. L. Taylor have made valuable contributions to the reported work.

PART I

A MODEL STUDY OF STAND-UP TIME IN SQUEEZING GROUND

L. R. Myer

T. L. Brekke

G. E. Korbin

TABLE OF CONTENTS

LIST OF FIGURES

LIST OF TABLES

SYMBOLS

P	Pressure
P_z	Confining pressure (model), overburden pressure (prototype)
P_a	Air pressure
S_u	Undrained shear strength
UC	Unconfined compression strength
σ	Stress
ε	Strain
ε_r	Radial strain
ε_θ	Circumferential strain
$\dot{\varepsilon}$	Strain rate
Q_m	Value of quantity Q in model
Q_p	Value of Quantity Q in prototype
Q^*	Scale of quantity Q
ρ	Density
g	Gravity
t	Time
ℓ^*	Length scale
ξ	Displacement scale
U	Displacement
E	Youngs Modulous
ν	Poisson's Ratio
r	Radius
C	Compressibility coefficient
F	Flexibility coefficient

A	Strain rate at t_1 and $\bar{D} = 0$ (in creep equation) Radius of tunnel (in model results)
$\bar{\alpha}$	Slope of linear portion of plot of log $\dot{\epsilon}$ vs $\bar{D}$
$\bar{D}$	Normalized stress
m	Slope of plot of log $\dot{\epsilon}$ vs. log t
A_r	Ratio of advance rate to tunnel radius (model)
F_{sr}	Strain rate factor
T_{st}	Stand-up time factor

Chapter 1

INTRODUCTION

The objective of the research described herein was to develop a fundamental understanding of the relationship between the size of an advancing tunnel face, the rate of excavation, and the stand-up time in squeezing ground. Stand-up time is defined as the time elapsed after excavation that an unsupported tunnel face will remain stable. Squeezing ground is argillaceous rock or soil that exhibits pronounced time dependence of deformation and strength properties.

Stand-up time problems are expressions of unstable behavior of ground in underground excavation. Displacements and time are the only practically measurable quantities that can be used to describe this behavior. Thus, displacement and time become the dependent variables of this investigation. The stability of the ground depends on the interaction of certain physical properties of the ground with physical characteristics of the excavation. These properties and characteristics become the independent variables.

A definition of instability in terms of the deformation-time history of an opening after excavation, may take more than one form. Such a history might be represented as in Figures I-1 and I-2 (Lang, 1972). In Figure I-1 instability is imminent when the slope of the curve, $\frac{dD}{dt}$, begins to increase. The stand-up time in this case would be the cumulative time up to the beginning of accelerating deformations. Practically speaking, large and fast deformations may inhibit tunnelling progress before the unstable portion of Figure I-1 is reached; for example, large, fast deformations may trap a shield before it can

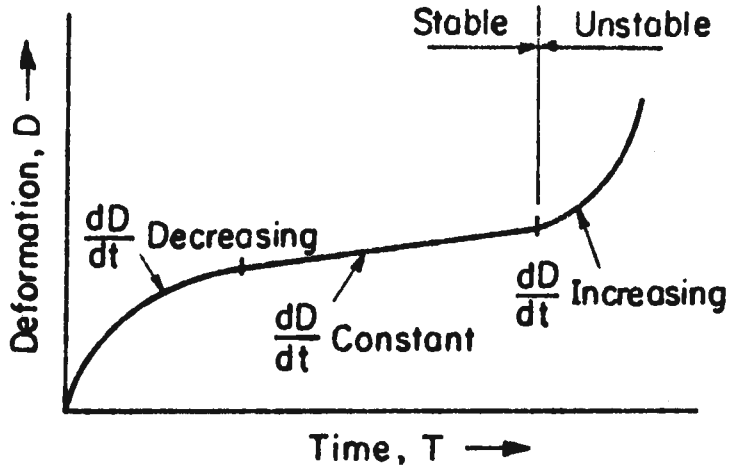

FIGURE I-1 POSSIBLE DEFORMATION-TIME HISTORY OF A TUNNEL AFTER EXCAVATION. (after Lang, 1972)

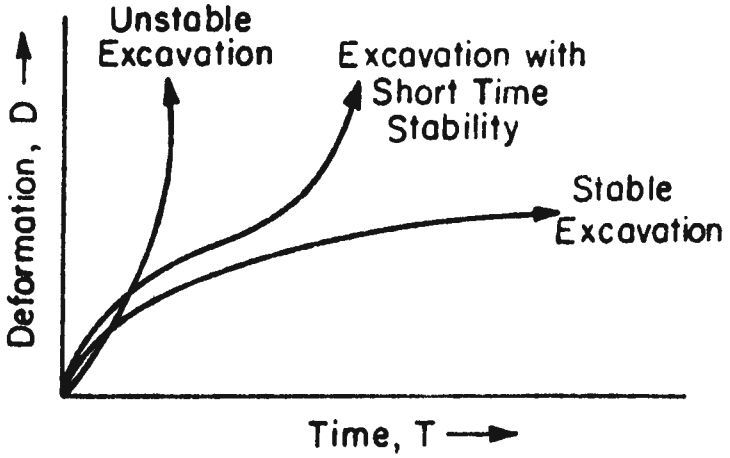

FIGURE I-2 COMPARISON OF DEFORMATION-TIME HISTORIES OF STABLE, TEMPORARILY STABLE, AND UNSTABLE TUNNELS. (after Lang, 1972)

progress. In this case, the stand-up time would be the time elapsed before a certain amount of deformation has occurred. Field studies in unsupported openings (Merrill, 1954, 1957, and Waddell, 1971) have yielded results which substantiate the shape of the stable portion of Figure I-1.

The stability of a tunnel will also be affected by the deformations of the material ahead of an advancing tunnel face. Of numerous studies measuring such deformations (Wood, 1969, Moretto, 1969, Hansmire, 1972, Attewell and Farmer, 1974), one example is the work of Ward (1969) in the Victoria Line tunnel in London clay. Instrumentation placed as shown in the inserts of Figures I-3, I-4 measured the axial and radial deformations of the clay as the shield approached the instrumentation. These figures will be referred to later for comparison with model test results.

As mentioned, one of the objectives of this research is to define more clearly the independent variables pertinent to the stand-up time problem. Terzaghi (1946) observed that the stand-up time of a tunnel depended to a large extent on the distance from the face to the first support. From a number of observations in Europe, Lauffer (1958) found that stand-up time for a given tunnel decreased as the ground conditions worsened. More importantly, he observed that for any given ground condition the stand-up time decreased dramatically with increasing length of the active span as shown in Figures I-5, I-6. Since there must be a reasonable relation between the active span and the height of the tunnel face, what Lauffer found is, in reality, a very pronounced reduction of the stand-up time with increasing tunnel size. Lauffer's results have remained essentially the only semi-quantitative

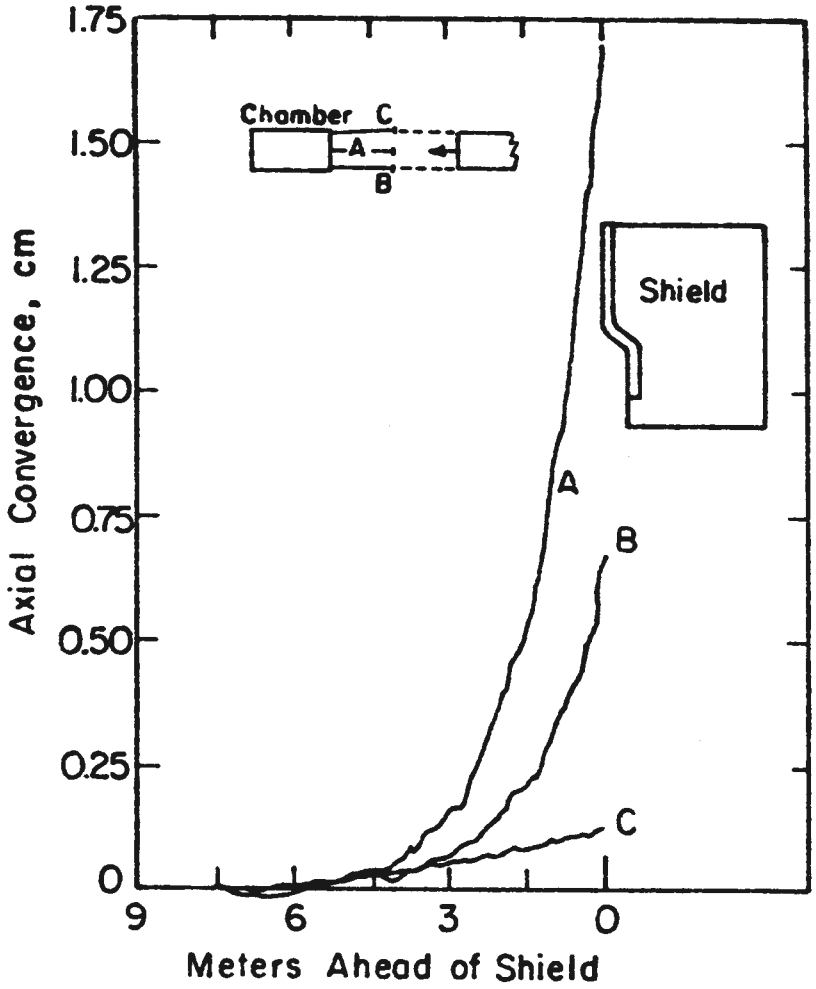

FIGURE I-3 AXIAL DEFORMATIONS AHEAD OF AN ADVANCING SHIELD IN LONDON CLAY. (after Ward, 1969)

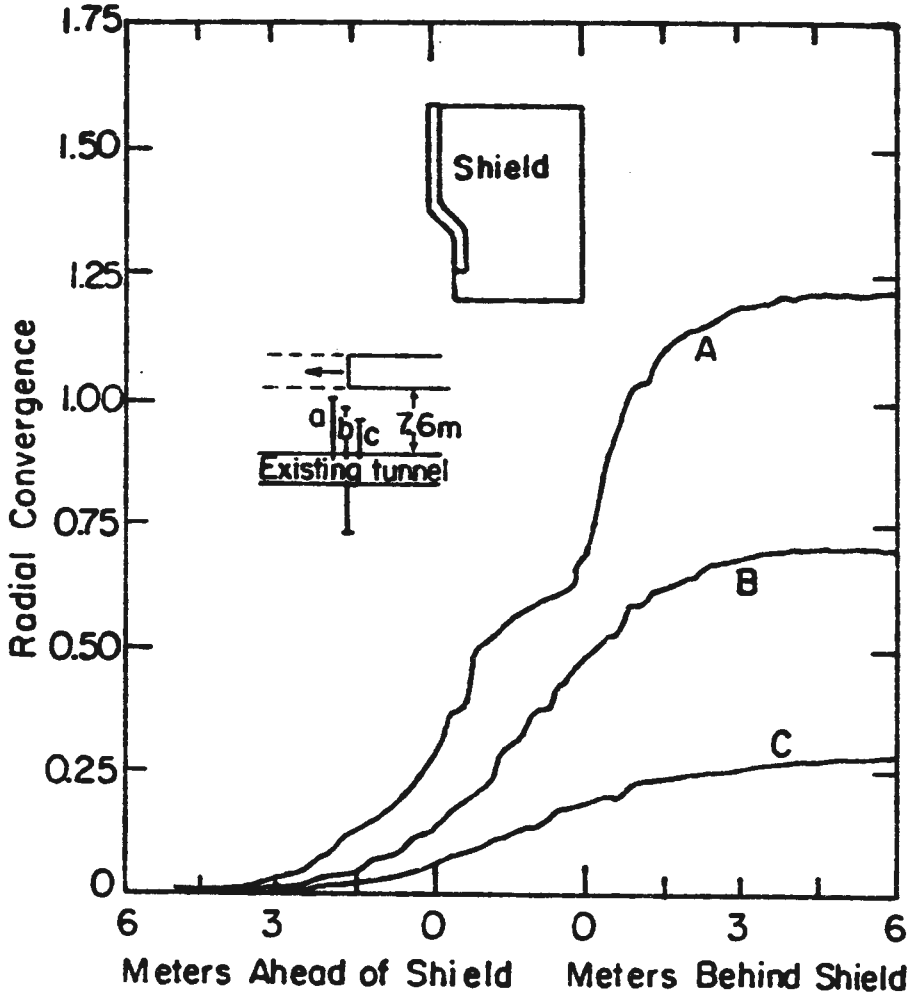

FIGURE I-4 RADIAL DEFORMATIONS AHEAD OF, AND BEHIND, AN ADVANCING SHIELD IN LONDON CLAY. (after Ward, 1969)

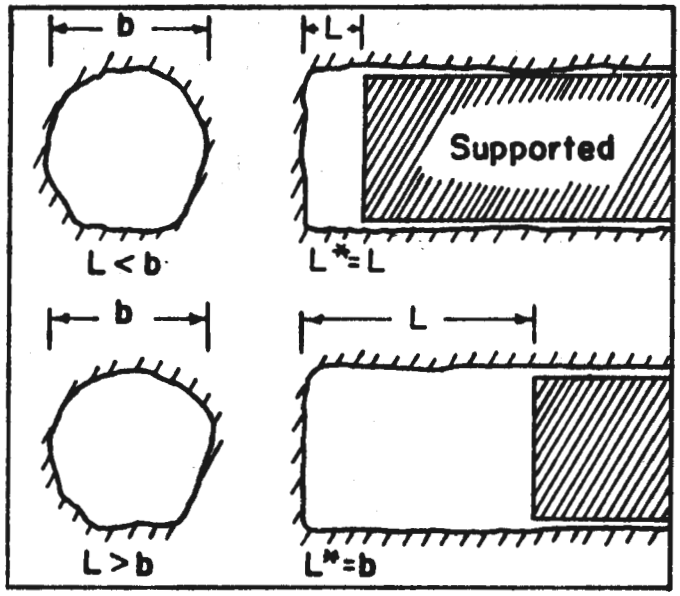

FIGURE I-5 DEFINITION OF "ACTIVE SPAN", L*. (after Lauffer, 1958)

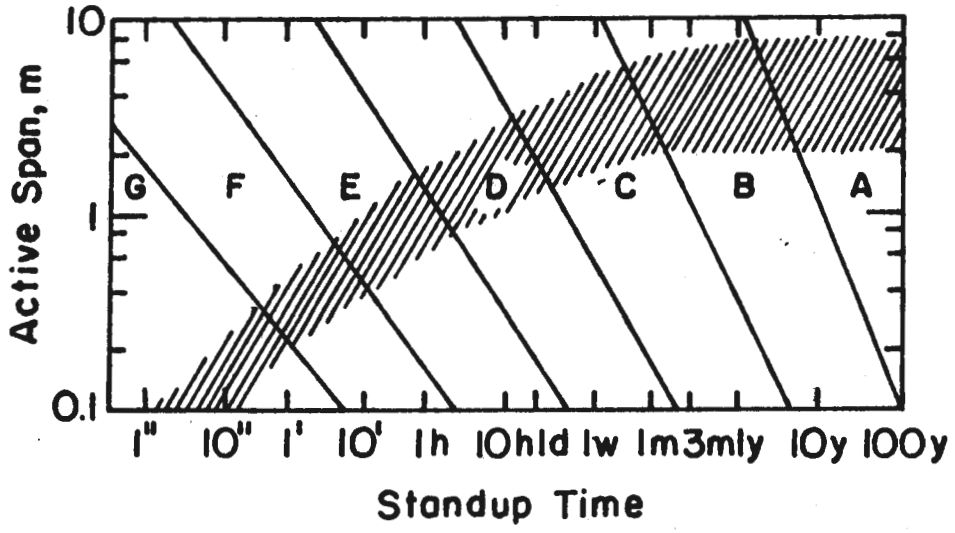

FIGURE I-6 ACTIVE SPAN VERSUS STAND-UP TIME. A - BEST ROCK MASS, G - WORST ROCK MASS. SHADED AREA INDICATES THE PRACTICAL RANGE. (after Lauffer, 1958)

assessment of stand-up time problems, although his work has been somewhat updated and modified by Underwood (1968) and Bieniawski (1974).

Previous work thus defined one independent variable to be some measure of the size of a tunnel. The study of case histories (Chapter 2) further substantiated this choice.

It is appreciated that changes in geometry of the unsupported space, the presence of weak zones, discontinuities, and other inhomogeneities could all affect the relative stand-up time of a large and small tunnel in the same ground. However, the simplest and most fundamental approach was taken, and a hypothesis was proposed to explain the size effect in a homogeneous continuum. Figure I-7 illustrates the hypothesis. Tunnels I and II are advancing at the same rate and at the same depth. The ratio of face diameter to unsupported length is equal for each. A and B are elements ahead of the advancing faces at which stress field changes induced by the openings are first felt. The elements accumulate damage while in the changed stress field. A has time t_1 to accumulate damage, whereas B has time $t_2 < t_1$. Thus, A will be nearer to failure when it reaches the face, and the stand-up time for tunnel I will consequently be less than for tunnel II.

Justification for a hypothesis of accumulating damage should be supported by knowledge of the time dependent deformation and strength characteristics of squeezing ground. Semple (1973) has shown that some fault gauge (a typical example of squeezing ground) can be treated analytically as a clayey soil. Thus, it seems reasonable to apply the literature on material properties of clayey soils to squeezing ground.

There have been numerous investigations on creep rupture of clayey soils (e.g. Murayama and Shibata, 1964, Singh and Mitchell, 1968,

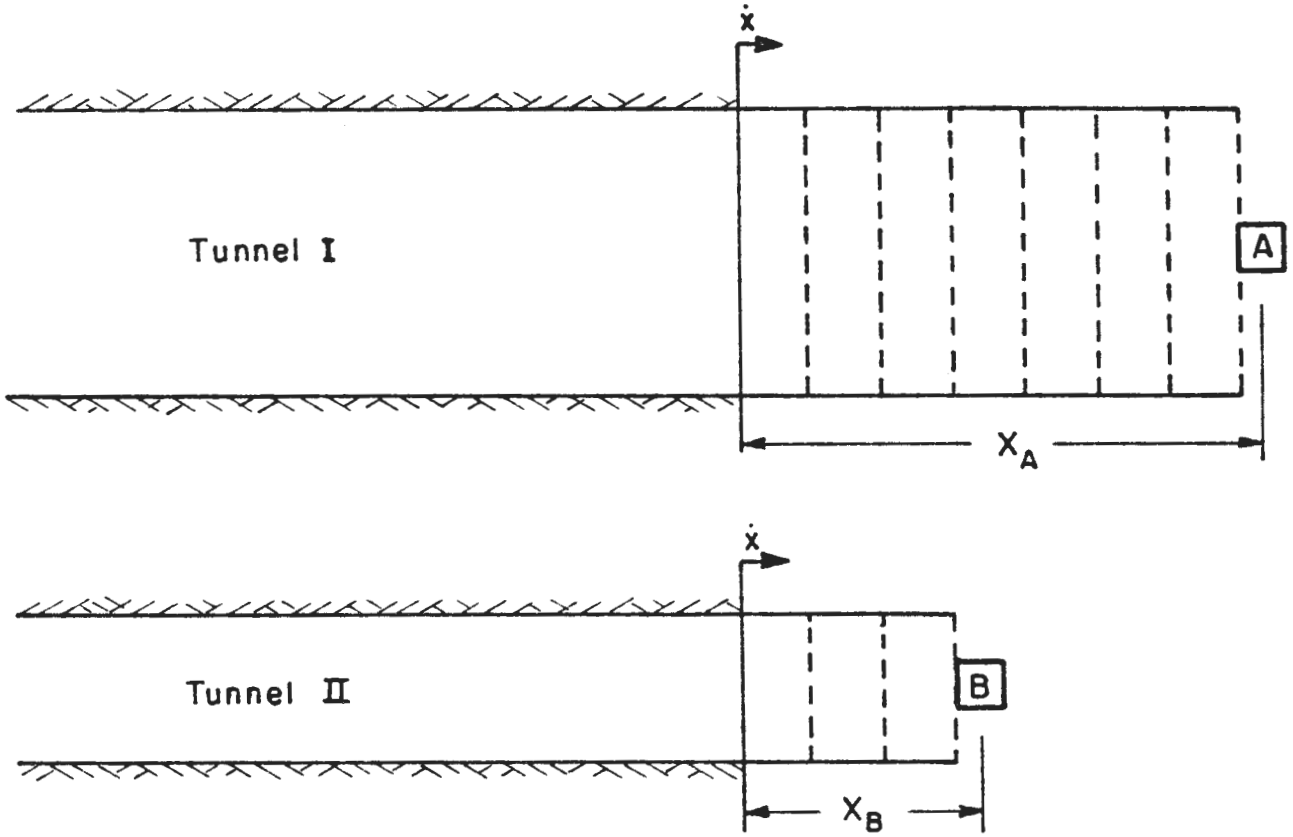

FIGURE I-7 ILLUSTRATION OF HYPOTHESIS. $\dot{x}$ = ADVANCE RATE. X_A, X_B = DISTANCE FROM TUNNEL FACE TO POINT OF FIRST EFFECT OF INDUCED STRESS FIELD. $t_1 = \frac{X_A}{\dot{x}}$, $t_2 = \frac{X_B}{\dot{x}}$ STIPLED LINES INDICATE ROUNDS EXCAVATED.

Shibata and Karube, 1969, Sekiguchi, 1973, Campanella and Vaid, 1974). However, most testing has been done under conditions of invarient loads so the effect of variable loading path is still largely unknown. Elements A and B might also be described as undergoing slow, triaxial unloading following complex paths. Casagrande and Wilson (1951) and Bishop and Henkel (1962) demonstrated that a slower rate of loading led to a lower strength value for some clayey soils tested. These results are suggestive that the strength of element B would be reduced less than A by the time the face had reached the elements.

The case history study (Chapter 2) also indicated that a decrease in excavation rate leads to a decrease in stand-up time. Thus, excavation rate becomes the second independent variable. From the preceding discussion of rate of loading effects on strength, a hypothesis naturally arises that material at a quickly advanced tunnel face exhibits a higher strength than the material at a slowly advanced tunnel face. Higher strength results in a more stable tunnel, and a longer stand-up time.

A material of a given strength which is unstable at one depth may be stable at a more shallow depth. A ratio of a material strength to depth of cover would be a reasonable indication of material strength relative to stand-up-time. Such a ratio was first suggested by Broms and Bennermark (1967) for vertical openings, e.g. a hole in a sheet pile retaining wall. These authors also assumed a tunnel face was analogous to an opening in a vertical wall. In a laboratory model, they determined that stable conditions would be maintained for $\frac{P_z - P_a}{Su} < 6.3\text{-}7.5$ where P_z = total overburden pressure, P_a = air pressure greater than atmospheric pressure used to help maintain stability, and

Su = undrained shear strength. A similar study by Attewell and Boden (1971) found the minimum ratio for stability to be 4.5. From a compilation of case histories Peck (1969) suggested that a stability ratio of 5 be used. There is scatter in stability ratio values determined from case histories reflecting, in part, the influence of other factors on the stability of tunnels.

Other material properties are needed to describe the apparent time dependence of the strength of material around an opening. For laboratory tests on clayey soils, Singh and Michell, (1968) described a parameter m (minus slope of log strain rate v.s. log time curve); if $m < 1$, a material appears to have the potential for creep rupture. Mitchell (1976) also described a parameter $C=(1-m)\varepsilon_f$, (where ε_f = failure strain in constant rate of strain or creep rupture test) which could be used to predict the time to failure of laboratory creep tests. It is interesting to note that failure tests (t_f) of laboratory creep tests of clayey soils often range from 10 to 1000 minutes, values which are similar to stand-up times in bad ground. Laboratory values such as m, c, and t_f may or may not have direct application to stand-up time problems but they are suggestive.

The work carried out to study the size and rate effects as hypothesized above involved a study of case histories (Chapter 2), a discussion of model theory and application (Chapter 3), identification and characterization of a suitable model material (Chapter 4), and a series of physical model tests with different size openings and excavation rates (Chapter 5 and 6). The results obtained and discussion are presented in Chapter 6, followed by conclusions in Chaper 7.

Chapter 2

CASE HISTORY SURVEY OF STAND-UP TIME PROBLEMS

Introduction

Numerous factors influence stand-up time behavior in-situ. Some of the most important are listed in Table II-1. The case history study demonstrated that actual stand-up time problems are caused by combinations of these factors. However, the study showed the strength-deformation-time characgeristics to be important in all cases. Furthermore, two recurring solutions to the stand-up time problem became evident: (1) Adjustment of excavation procedure, often by increasing excavation rate, whereby the support could be placed before the stand-up time of the ground elapsed; or (2) Reduction of the size of the excavation.

TABLE II-1 Factors Influencing Stand-Up Time

1. Strength deformation characteristics of the ground including time dependence
2. In-situ stress conditions
3. Water regime
4. Size and shape of the opening
5. Method of excavation
6. Rate of advance
7. Method of support and/or reinforcement and lining

Cases of Changed Excavation Procedures to Increase Stand-up Time

A. Tyholt Tunnel, Norway

An 8 m (26 ft) diameter tunnel in Tyholt Norway was excavated at a depth of 20 m (65 ft) in clay which contained zones of quick clay of

low strength (Hartmark, 1964; Broms and Bennermark, 1967). The strength of the clay, as measured by the Scandinavian full cone test, varied from 19.3 KN/m^2 (2.8 psi) to 98 KN/m^2 (14.2 psi). A full diameter, open faced shield was used with provision for use of a bulkhead in front. Compressed air was also used where the clay strength was low. Pre-cast reinforced concrete segments, 75 cm (30 in) long, were used for support. Progress in free air through the stronger clay was 4.5 m (15 ft) per week using air spades. In sections of the tunnel where the clay was of the higher strength and $\frac{P_z - P_a}{S_u}$ values were less than 6, no stand-up time problems were experienced. However, at one point in a zone of low strength material the air pressure dropped from 90 KN/m^2 to 32 KN/m^2 (13.1 psi to 4.7 psi) and the face moved 0.30 m (1 ft) into the tunnel. A slide into the tunnel occurred when a zone of clay of the weakest strength was entered and an increased air pressure of 158 KN/m^2 (26.8 psi) was necessary to maintain stability.

B. Alpine Highway Tunnel

Rabcewicz (1975) reported on a 6.4 km (4 mile) long, 10 m (33 ft) diameter highway tunnel in the Alps. Overburden was up to 960 m (3150 ft) and the rock was mainly of weak phyllites. Excavation proceeded by a method of top heading followed by two benches. The average advance rate was 2.1 m (7 ft) per day. Stability problems were persistent and severe including, at one point, a large face collapse which injured two men. The major problem was one of large deformations occurring quickly which if not checked led to collapse; the stand-up time was short. At first, shotcrete reinforced with rock bolts and wire mesh was placed immediately after excavation to avert instability.

However, continued deformation cracked the shotcrete. Stabilization was finally achieved using reinforced shotcrete with gaps running along the length of the tunnel axis plus steel ribs with joints, both measures allowing for compressive displacement.

C. Bart Fairmont Hill Tunnel

During construction of the Bay Area Rapid Transit system the Fairmont Hill Tunnel was built through a faulted zone of the Franciscan formation (Moler, pers. comm.). The tunnel was 6.1 m (20 ft) in diameter and under a maximum of 52.6 m (140 ft) of overburden. Excavation proceeded using a mole and support consisting of steel "I" rings spaced .6 m to 1.2 m (2 ft to 4 ft) apart. The material in the fault zone was a decomposed serpentine described as a "swirly, sheared fibrous mass of green to black earthy material," that was water saturated. It had a stand-up time of one to six hours. The cutter head of the mole persistently clogged in this material, slowing excavation progress. As the stand-up time was exceeded more and more material washed and collapsed into the tunnel forming a 3 m by 3.6 m (10 ft by 12 ft) cavity in the roof and a 2 m (6 ft) cavity in the tunnel wall. Cribbing alone was used to support the roof cavity but cribbing plus shotcrete were required to stabilize the wall cavity.

D. BART Berkeley Hills Tunnel

Twin tunnels were driven through the Berkeley hills between Oakland and Orinda for the BART project. The tunnels were 6.4 m (21 ft) diameter horseshoe shaped and were driven full face using a jumbo (Ayres, 1969). A pilot bore had been driven in the crown along one tunnel line. The geology consisted of complex sections of

conglomerates, siltstones, sandstones, shale, and volcanics. Numerous seams and faults containing gouge crossed the tunnel line. Support consisted of steel sets on .6 m to 1.2 m (2 ft to 4 ft) centers. Four foot rounds were driven. Squeezing ground caused stability problems in both supported and unsupported sections of the heading but only instability in the unsupported section will be discussed here. Squeezing ground became a problem near a portal of one tunnel under 12 m (40 ft) of cover. Steel sets were being augmented by crown bars and a breastboard. At one point the breastboard fell out and the face caved in. Excavation continued using two breastboards and crown bars or spiling. Only a small portion of the face could be open at any one time. The face advanced 11 m (36 ft) in one week as compared to 9 m (30 ft) per day in sections of the tunnel in better ground. The ground movement continued to accelerate, and the tunnel was declared unsafe when cracks from the caving ground reached the surface. Extra support was added to stabilize the ground behind the face before excavation continued. The author noted that more prompt installation of crownbars, breastboards and steel support would have averted the problem.

E. Oake Dam Tunnels

The Oake Dam Tunnels were excavated in Pierre shale, a clay soil with an unconfined compressive strength of about 483 KN/m^2 to 1430 KN/m^2 (70 psi to 208 psi) (Underwood, 1965). The shale could be easily cut with air spades. The ground tended more toward blocky and seamy than pure squeezing. The cover over the 9 m (29 ft) diameter tunnels was up to 24 m (73 ft). A mole was used in the full face excavation. Support consisted of ring beams on 1.2 m (4 ft) centers. In one tunnel, the advance was 21 m (68 ft) per day until a fault was

intersected and fallout stopped the machine. Progress decreased drastically to 28 m (91 ft) in 30 days and an average overbreak of 6 m (20 ft) was experienced over this distance. In another fault zone 4.6 m (15 ft) of unsupported ground was left over the weekend. By Monday the face had collapsed. In another tunnel on the project shale fallouts in one area were so frequent and of such magnitude that only 4 m (13 ft) were mined in 31 days. Overbreak averaged 6 m to 9 m (20 ft to 30 ft). Finally a very large fallout buried the machine and the remainder of the tunnel was handmined using side drifts and top heading and bench methods. The author pointed out that the major excavation problem was the lack of appreciation of the short stand-up time of the material. At first when a fault was encountered and fallout blocked the cutter head of the mole, the practice was to withdraw the machine and "take another run at it." This took too much time and large cave-ins ahead of the machine resulted. When this practice was reversed and the machine was not backed off in bad ground, progress improved.

Increased Stand-up Time Through Size Reduction

A. Kensico and Tygart Tunnels

Terzaghi (1946) cited two examples to illustrate that the top heading and bench method should be used when the stand-up time is too short to allow for full face operations. The Kensico tunnel was built as part of the Delaware aquaduct. The 7.3 m (24 ft) diameter, hand dug tunnel encountered jointed and partly decayed to crushed and decayed gneiss in faults which necessitated the top heading and bench method.

On the Tygart River dam project a 6.7 m by 9.4 m (22 ft by 31 ft) tunnel was driven in ground consisting of thin strata of sandstone separated by immature shale. The shale provided little resistance to slippage between layers and thus top heading and bench methods were used. On the same project a few hundred yards away, a tunnel was driven full face without difficulty because the crown was in a layer of sandstone, eliminating the stand-up time problem.

B. Carly V. Porter tunnel

The Carly V. Porter tunnel was built in the Tehachapi mountains as part of the California aquaduct (Arnold et. al., 1972). It is 7.2 km (4.8 miles) long with a finished diameter of 6 m (20 ft). The rock was of various types, including igneous, metamorphic, and Pliocene lakebed deposits. The lakebed deposits consisted of faulted and sheared claystones and siltstones with plastic clay and marl mixed in. The overburden in the lakebed area, the eventual collapse zone, averaged 41 m (135 ft). The tunnel was excavated full face using a shield followed by the installation of 1.2 m (4 ft) wide, six piece liner plates for support. The advance rate was 1.8 m to 5.5 m (6 ft to 18 ft) per day. Voids between the liner plates and the ground were not filled. Breastboarding was often necessary, and the lake deposits tended to squeeze. During mining of the lake deposits grade was lost, and remining was required. During remining, excessive squeeze began and led to collapse of the tunnel. The remining of the collapse zone met with stand-up time problems. At first, the full face method was attempted with steel sets placed .6 m (2 ft) on center. 11.5 m (38 ft) were remined in this manner; the ground squeezed into the tunnel at rates which varied from a couple of inches per day to a couple of

feet per day. Then the squeeze accelerated, and in one 48 hour period the ground advanced 4.5 m or 6 m (15 or 20 ft) into the tunnel, sweeping away the breastboards at the face. The excavation method was changed to top heading and wallplate drift, but ground pressure collapsed the drifts. Finally, a multiple drift system was successful in mining through the zone.

C. Tehachapi Tunnel No. 3

The Tehachapi tunnel No. 3 is also in the Tehachapi mountains as part of the California Aquaduct (Peters, 1972). The tunnel is 1706 m (5400 ft) long with a finished diameter of 7.3 m (24 ft). The rock mass consisted of granite, gneiss and quartz diorite with numerous shears and faults containing gouge material. The tunnel was advanced by the full face method until heavy ground was encountered in fault zones and a top heading and bench system was initiated. When the top heading entered the hanging wall, in one fault zone, water inflow and very unstable blocky material with gouge zones was encountered. A 1.2 m by 1.5 m (4 by 5 ft) pilot bore was begun but the ground was still unstable. Finally, the top heading was advanced with the aid of crown bars and spiling.

D. Wilson tunnel

The Wilson tunnel in Hawaii is 10 m (33 ft) in diameter and was built under 15 m to 30 m (50 ft to 100 ft) of cover (Peck, 1969), It was hand mined full-face with air spades. The ground was a residual silty clay derived from lava flows and had brittle stress-strain characteristics. At points of excessive overbreak and poor support ravelling became excessive, eventually filling the tunnel and causing

a set of three sinkholes at the surface. After this, the face was attacked by the multiple drift method and the stand-up time was increased so that overbreak and ravelling were eliminated.

E. Antwerp Gas Storage Chambers

At Antwerp, Belgium, liquified gas storage chambers were constructed at a depth of 80 m (262 ft) in Boom clay (Peck, 1969; debeer and Buttiens, 1966). This clay is fissured and plastic with undrained shear strength of about 607 KN/m^2 (88 psi). The P_z/S_u ratio in this case was 4.1. Some of the 5.5 m (18 ft) diameter galleries were hand mined and supported with wooden timbers. The full face method of excavation was tried but the ground was too unstable to continue in this manner; a 45° talus slope formed at the face at one point leaving 5.5 m (18 ft) of unsupported crown in danger of collapse. The excavation method was then changed to one of preceding the main face by a pilot bore of 1.5 m to 3 m (5 ft to 10 ft) in length. Only enough material was excavated at one time in the pilot bore to allow erection of a set of steel ribs, leaving a core of material in the middle of the bore. The pilot bore was then enlarged set by set to full diameter. Another cycle was then begun by advancing the pilot bore 1.5 m to 3 m (5 ft to 10 ft). It was noted that the clay not only deformed into the tunnel at the face but in the crown it also deformed toward the face and into the tunnel, tending to pull in the top of the support.

F. Schewaikheim Railway Tunnel

Rabcewicz (1969) discussed a railway tunnel at Schewaikheim, Germany, built by the multiple drift method because the stand-up time

of the ground was very short. It was a 9 m (30 ft) diameter tunnel 300 m (984 ft) long under 20 m (65 ft) overburden. The tunnel was mixed face; the lower part was in limestone with thin layers of clay; the upper part was in a weak clay. Instrumentation placed ahead of the face noted movement of the clay three diameters ahead of the face.

G. Henderson Haulage Tunnel

The Henderson Haulage tunnel is a 16 km (10 mile) long mine haulage tunnel running beneath the Continental Divide in Colorado. The 4.6 m by 5.2 m (15 ft by 17 ft)tunnel is beneath as much as 400 m (1200 ft) of cover. The rock consists of gneiss and granite. The tunnel was driven full face and little support was needed except in fault zones. In one 19 m (62 ft) long zone the tunnel encountered gouge consisting of a mixture of dark clay and coarse to fine sand. The gouge began to squeeze into the tunnel so a bulkhead was erected at the face. However, the squeeze pushed the bulkhead into the tunnel at about 2.5 cm (1 in) per hour, and finally accelerated to a run over the bulkhead, filling the tunnel. The heading was advanced through the zone using a top heading and bench with crown bars. Some index tests on the gouge material indicated significant swell potential for the gouge, yet in-situ behavior was predominantly that of squeezing ground. The high in-situ stresses produced large time dependent deformations which overshadowed the swelling behavior of the gouge (Brekke and Howard, 1969).

H. Dwight D. Eisenhower Tunnel (Straight Creek Tunnel)

One of the most thoroughly investigated and best documented tunnel projects involving stand-up time problems the Eisenhower tunnel,

North Bore, a highway tunnel which crosses the Continental Divide west of Denver, Colorado. A comprehensive review of the case was given by Hopper, et. al. (1972). The main rock type was granite and the major structural feature was the Loveland fault zone. The 2700 m (8900 ft) long, 14.6 m by 15 m (48 ft by 50 ft) tunnel had up to 442 m (1450 ft) of overburden. A pilot bore had been excavated close to the tunnel, and laboratory index testing was performed. The tunnel line was divided into zones for reference (FigureII-1),based on assessed ground conditions. Excavation proceeded simultaneously from the east and west portals. An attempt was made to drive Zone II full face using a shield. The shield was erected at the end of Zone I about 38 m (125 ft) from the Loveland fault. It had advanced 21 m (70 ft) when it developed mechanical problems in its support rollers. By the time the roller support was changed to a sled system, ground pressures had frozen the shield into place. Concurrently with these problems, stability problems had developed in the top heading of Zone III. The ground in Zone III was very blocky and seamy to highly decomposed. Stand-up time problems at the face, and high loads and distortion of sets were experienced. These problems led to the adoption of the multiple drift method for excavation of Zone II. The crown drift was driven first. The worst material encountered was gouge consisting of stiff clay with blocks of decomposed weak rock. Squeezing rock was a problem even in this 2.4 m x 2.7 m (8 ft x 9 ft) drift. It was advanced at a rate of 1.8 m to 2.1 m (6 ft to 7 ft) per day. Displacements of 1.3 cm (0.5 in) were noted within one to 1 1/2 hours after excavation. Behind the face squeeze continued and ground movements up to 15 cm (6 in) were noted. The lower sidewall drifts experienced some stand-up time and

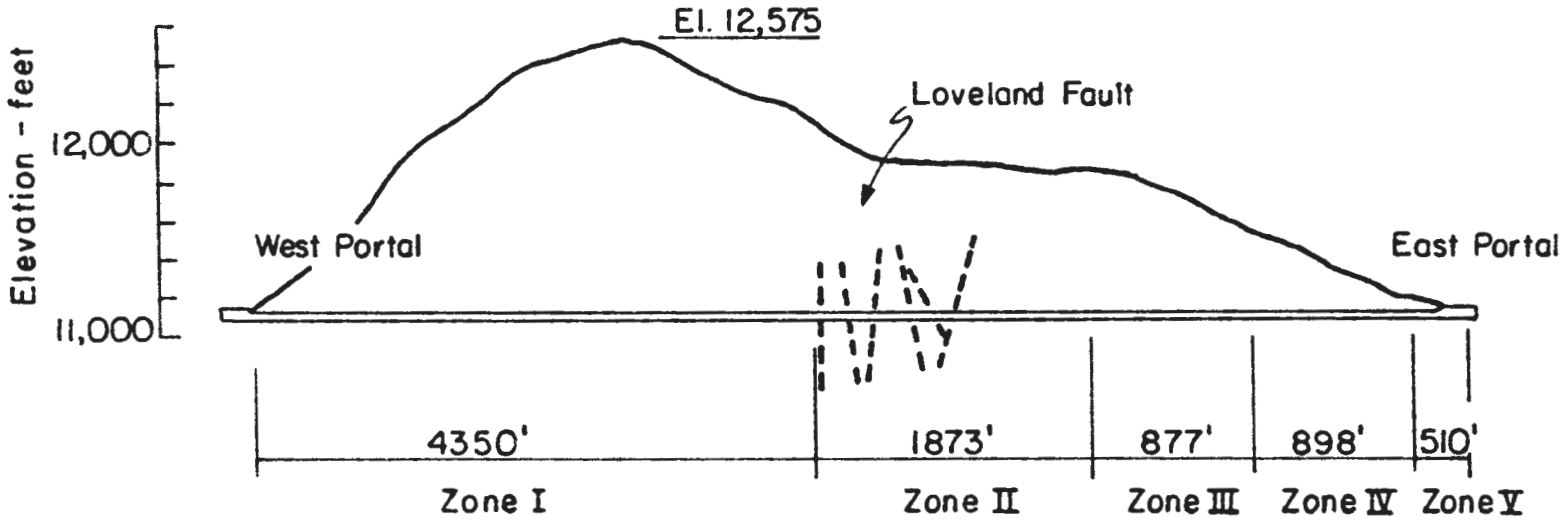

FIGURE II-1 SECTION OF EISENHOWER TUNNEL. (after Hopper et. al., 1972)

squeeze problems, but successive drifts in general had fewer stability problems.

Conclusions

It was clear from the case history study that the factors listed in Table II-I all interact in affecting the standup time of a given tunnel. It was also clearly impossible to single out any one factor as the most important. Nevertheless, several factors persistently reappeared in the case histories and these warranted further study:

(1) Strength of the ground. Inadequate stand-up time was a problem when the ratio of depth of cover to strength of the ground was too large.

(2) Time dependence of deformation and strength characteristics of the ground. Deformations continued even when an excavation boundary was stationary and the accumulation of deformation over time apparently led to failure.

(3) Excavation size. When stand-up time was too short and instability threatened or occurred, stable conditions were often attained through a reduction in tunnel size.

(4) Advance rate. A decrease in advance rate often led to a reduction in stand-up time.

Chapter 3

PHYSICAL MODEL THEORY AND APPLICATION

Introduction

A physical model is a device so related to a physical system (prototype) that the behavior of all or part of the prototype can be predicted by observing the behavior of the model. This definition is similar to one given by Murphy (1950). The first, most important, and in some ways most difficult step in proceeding with a physical model study is to determine those characteristics and quantities (primary quantities) needed to ensure that the model behavior is an accurate representation of the prototype behavior. Selection of too few primary quantities leads to an inaccurate model but inclusion of too many may result in too complex a model to study practically. Secondly, the appropriate rules or scales (similitude relations) for quantitatively relating the primary and predicted quantities of the model to those of the prototype must be determined. Lastly, an equation (predictive equation) relating the primary and predictive quantities to each other may be developed. These three steps will first be discussed in general terms and then specifically with regard to the stand-up time problem.

Physical Model Theory

Selection of Primary Quantities Primary quantities for most geo-mechanical models can be grouped into three general classes (Murphy, 1950): forces, geometry, and properties of materials. Forces of interest can often be limited to boundary loads, gravity, or body loads, inertial forces and fluid pressures. Geometric primary

quantities include the spacial and time distribution of forces and all pertinent dimensions. Pertinent material properties include instantaneous and time dependent deformation and strength characteristics. A correct selection of material properties depends on a knowledge of the mechanical behavior of the prototype material. Unfortunately this knowledge is often incomplete for complex geological materials.

Development of Similitude Relations Conditions of similitude can be determined from the field equations governing the problem (Mandel 1963). The field equations for most geo-mechanical problems are equilibrium, compatibility, and constitutive equations. In the following development, the ratio between a model quantity (Q_m) and a prototype quantity (Q_p) will be defined by: $Q^* = \frac{Q_m}{Q_p}$. Q^* is called the scale of quantity Q.

The equilibrium equations for a static problem are:

$$\sigma_{ij,j} + \rho g_i = 0$$

where σ represents a stress tensor and ρg is the body force Writing out one equation

$$\frac{\partial \sigma_{yx}}{\partial x} + \frac{\partial \sigma_{yy}}{\partial y} + \frac{\partial \sigma_{yz}}{\partial z} + \rho_g = 0 \qquad (3.1)$$

Suppose, for a moment that the scales of each of the quantities in Eq. 3.1 is changed, i.e. let $\sigma^* = \frac{\sigma_m}{\sigma_p}$, $\rho^* = \frac{\rho_m}{\rho_p}$, $\ell^* = \frac{\ell_m}{\ell_p}$ etc.

Thus, Eq. 3.1 would be written:

$$\frac{\sigma^*}{\ell^*}\left(\frac{\partial \sigma_{yx}}{\partial x} + \frac{\partial \sigma_{yy}}{\partial y} + \frac{\partial \sigma_{yz}}{\partial z}\right) + \rho^* g^* \rho g = 0 \tag{3.2}$$

Eq. 3.2 is the same as Eq. 3.1 only if

$$\sigma^* \ell^{*-1} = \rho^* g^*$$

or $$\sigma^* = \rho^* g^* \ell^*$$

Since under natural conditions $\rho^* = g^* = 1$,

$$\sigma^* = \ell^* \tag{3.3}$$

This result means that the stress and length scales must be equal. Problems soon develop in reduced scale models where the strength of the material is a factor; if the scale of material strength equals the scale of stresses, the strength of the model material must be proportionately less than the strength of the prototype material. Centrifugal models (Roscoe, 1970, Polshin et al.,1973, etc.) in which $g^* \neq 1$ can be used to circumvent this problem.

The problems presented by Eq. 3.3 can also be avoided if the body forces can be ignored. For this case Eq. 3.1 becomes

$$\frac{\partial \sigma_{yx}}{\partial x} + \frac{\partial \sigma_{yy}}{\partial y} + \frac{\partial \sigma_{yz}}{\partial z} = 0 \tag{3.4}$$

If scales are changed in Eq. 3.4

$$\frac{\sigma^*}{\ell^*}\left(\frac{\partial \sigma_{yx}}{\partial x} + \frac{\partial \sigma_{yy}}{\partial y} + \frac{\partial \sigma_{yz}}{\partial z}\right) = 0 \tag{3.5}$$

Eq. 3.5 and Eq. 3.4 are the same if σ^*/ℓ^* = constant, or

$$\sigma^* = c\ell^* \tag{3.6}$$

The constant c can be any value, so the scales of stress and length are effectively uncoupled.

The most general compatibility equation relating strains and displacement can be given as Jaunzemis, (1967)

$$2\varepsilon_{ij} = \delta_{mi}\, U_{m,j} + \delta_{mj}\, U_{m,i} + U_{m,i}\, U_{m,j} \tag{3.7}$$

Writing out one equation

$$2\varepsilon_{xx} = 2\,\frac{\partial U_y}{\partial x} + \left(\frac{\partial U_x}{\partial x}\right)^2 + \left(\frac{\partial U_y}{\partial x}\right)^2 + \left(\frac{\partial U_z}{\partial x}\right)^2 \tag{3.8}$$

If the scales of the quantities in Eq. 3.8 are changed

$$2\,\overset{*}{\varepsilon}\varepsilon_{xx} = 2\,\frac{\overset{*}{\xi}}{\overset{*}{\ell}}\,\frac{\partial U_x}{\partial x} + \frac{\overset{*2}{\xi}}{\overset{*2}{\ell}}\left[\left(\frac{\partial U_x}{\partial x}\right)^2 + \left(\frac{\partial U_y}{\partial x}\right)^2 + \left(\frac{\partial U_z}{\partial x}\right)^2\right] \tag{3.9}$$

Where $\overset{*}{\xi}$ is the displacement scale; $\overset{*}{\ell}$ is the length scale.

If Eq. 3.9 is to be the same as Eq. 3.8, then

$$\overset{*}{\varepsilon} = \overset{*}{\xi}/\overset{*}{\ell} = \overset{*2}{\xi}/\overset{*2}{\ell} = 1 \tag{3.10}$$

This result fulfills the condition of simple similitude and means that the strains in the model must equal the strains in the prototype. But if a small strain assumption is valid, Eq. 3.7 becomes

$\varepsilon_{ij} = 1/2\,(U_{i,j} + U_{j,i})$ and Eq. 3.8 becomes

$$\varepsilon_{xx} = 1/2\,(\partial U_y/\partial x + \partial U_x/\partial x = \partial U_x/\partial x \tag{3.11}$$

Changing scales, Eq. 3.11 becomes

$\overset{*}{\varepsilon} = \overset{*}{\xi}/\overset{*}{\ell} \neq 1$ necessarily. This result meets the condition of extended similitude. By allowing a different scale for displacements and lengths the strains in the prototype and model can be different.

Scales for forces, lengths, deformations and strains have been developed. For static problems the only remaining quantities to be

scaled are material properties. This requires a knowledge of the general constitutive behavior of the prototype material as well as a reasonable guess as to what part of this behavior is applicable to the problem at hand. As an illustrative example, consider the constitutive equation from isotropic linear elasticity:

$$\sigma_{ij} = \lambda\varepsilon_{kk}\delta_{ij} + 2\mu\varepsilon_{ij} \tag{3.13}$$

Is scales are changed:

$$\overset{*}{\sigma}\overset{*}{\sigma}_{ij} = \overset{*}{\lambda}\overset{*}{\varepsilon}\overset{*}{\varepsilon}_{kk}\delta_{ij} + 2\overset{*}{\mu}\overset{*}{\varepsilon}\overset{*}{\varepsilon}_{ij} \tag{3.14}$$

In order for Eq. 3.13 and Eq. 3.14 to be the same,

$$\overset{*}{\lambda} = \overset{*}{\mu} = \overset{*}{\sigma}\overset{*}{\varepsilon}^{-1} \text{ or } \overset{*}{E} = \overset{*}{\sigma}\overset{*}{\varepsilon}^{-1} \text{ and } \overset{*}{\nu} = 1 \tag{3.15}$$

If $\overset{*}{\varepsilon} = 1$, Eq. 3.15 yields the result that the elastic modulous and stress scales must be equal. Extended similitude provides greater latitude in the choice of model material moduli.

If rheologic or post-yield behavior are important the equations describing this behavior would have to be examined in a similar fashion.

Development of Prediction Equations One form of prediction equation is a direct result of the determination of similitude relations. As in the preceeding discussion:

$$\overset{*}{Q} = \frac{Q_m}{Q_p} \tag{3.16}$$

If Q_m is measured in the model, Eq. 3.16 will yield the predicted quantity Q_p in the prototype. This approach requires that a model test be performed for each set of boundary conditions that a prototype may encounter. It may be more desirable to do only enough model tests to determine a general equation describing a phenomenon.

Such a relation of the form

$$Q_{1m} = f(Q_{2m}, Q_{3m} \cdots Q_{nm}) \tag{3.17}$$

is also a prediction equation. The predicted quantity Q_{1m} of the model would then be related to the similar quantity Q_{1p} of the prototype by a relation of the same form as Eq. 3.16.

$$Q_{1p} = Q_{1m}/Q_1^*$$

The process of determining the form of Eq. 3.17 involves the standard application of the theory of dimensional analysis. Thorough discussion of the theory and application of dimensional analysis can be found elsewhere (Murphy, 1950, Langhaar, 1951).

Model Laws for the Stand-up Time Model

Stand-up time problems occur during the construction of tunnels, so it was necessary to model as accurately as possible the actual tunnel construction procedure in squeezing ground. With this in mind the primary quantities were established.

The only forces of consequence were body forces, i.e., the weight of the ground. Geometric quantities included the diameter of the tunnel, advance rate, distance from face to first support, and bead size of the tunnel shield. The most pertinent material properties were assumed to be the time dependent deformation and strength characteristics. The predicted quantities or dependent variables were the deformations of the material at and beyond the tunnel wall. The scaling laws for these quantities will now be discussed in detail.

As shown previously a modeling process can be greatly simplified if body forces can be eliminated from the equilibrium equation, thus uncoupling stress and length scales. This simplification was

accomplished by limiting the study to tunnels "at depth" and by assuming that a tunnel at depth is equivalent to a hole in a thick wall cylinder with appropriate boundary conditions. The equilibrium equation for stresses in this problem can be written as $\sigma_{ij,j} = 0$. As noted above this equation yields the result that stress ($\overset{*}{\sigma}$) and length ($\overset{*}{\ell}$) scales are uncoupled.

The length scale, $\overset{*}{\ell}$, was selected for convenience. Three sizes of model tunnels would be excavated. The largest diameter of 18 cm (7 in) was chosen so that the ratio $\frac{\text{diameter of model chamber}}{\text{diameter of tunnel}}$ would not be too large. Too large a ratio would indicate that the stress field around the tunnel might intersect the boundary of the model. By letting the 18 cm tunnel model a 7 1/2 m (25 ft) diameter prototype, the length scale of $\overset{*}{\ell}$ = 1/40 was chosen.

The value of $\overset{*}{\sigma}$ was selected so the model would represent a tunnel at sufficient depth to make a "deep tunnel" assumption valid. The depth of a prototype tunnel can be expressed as: $DP = \frac{\sigma_{zp}}{\rho_p}$

where σ_{zp} is the vertical stress in the ground at tunnel depth and ρ_p is the weight density of the prototype ground. If $\overset{*}{\sigma} = 1$ then σ_{zp} equals the confining pressure on the model. Letting the confining pressure be 576 KN/m^2 (83 psi), and ρ= 15 KN/m^3 (96 lbs/ft^3), then, since $\overset{*}{\rho} = 1$, D_p = 38 m (126 ft). This figure yielded a depth to diameter ratio of about 5 which was large enough to satisfy the "deep tunnel" assumption.

The scale of strains, ε^* , was set equal to 1 and consequently the displacement scale $\overset{*}{\xi}$ equaled ℓ^*. The scale of $\varepsilon^* = 1$ was chosen for two reasons: first, large deformations were suspected

which would invalidate the small strain assumption; second, an analysis of the ground-liner interaction,as discussed later in this chapter, suggested $\varepsilon^* = 1$.

The constitutive behavior of squeezing ground is unfortunately not well defined. As discussed in Chapters 1 and 2, the time-dependent deformation and strength behavior of the ground seemed to be of greatest importance and the theory of the rheologic behavior of clayey soils also appeared applicable to squeezing ground.

The creep (one dimensional) behavior up to failure of many clayey soils has been satisfactorily described by an equation developed by Singh and Mitchell(1969):

$$\varepsilon = Ae^{\bar{\alpha}\bar{D}} \left(t_1/t\right)^m \qquad (3.18)$$

A = Strain rate at time t_1 and $\bar{D}$ = 0 (projected value)

$\bar{\alpha}$ = Slope of linear portion of plot of log $\dot{\varepsilon}$ vs. log $\bar{D}$ at constant time

$\bar{D}$ = Normalized stress level, deviator stress divided by stress at failure

t = time

m = minus slope of plot of log $\dot{\varepsilon}$ vs. log t

This equation was assumed to describe the rheologic behavior of squeezing ground. Note that the number of dimensionless quantities in 3.18 dictated that the behavior of the model material be quite "realistic" since dimensionless quantities must have the same

magnitude in model and prototype. If the scales are changed in Eq. 3.18

$$\varepsilon^* t^{*-1} \dot{\varepsilon}^* = A^* e^{\bar{\alpha}\bar{D}} (t_1/t)^m \tag{3.19}$$

Thus $$\varepsilon^* t^{*-1} = A^*$$

The scale of time, t*, could be adjusted relative to the value of A but further investigations (Chapter 4) showed that A* = 1 and so, conveniently, t* = 1.

Scales of other quantities, expressed in terms of length, time, stress, etc. could now be determined. For example, the advance rate was expressed in terms of ℓ/t and so had a scale of $\ell^*/t^* = 1/40$. A summary of the scales for the various primary quantities is listed in Table III-1.

Selection of Model Specifications

Once the scaling laws were established particular specifications for model loads and dimensions could be established.

The initial value of the boundary loads or confining pressure of the models had to be chosen high enough so that stand-up time problems would exist, but not so high that catastrophic failures extending to the model boundary would occur. As noted, Peck (1969) had observed that stand-up time problems occur if the ratio P_z/S_u is greater than about 5. Earlier work by Korbin (1975) with an unlined model tunnel in material similar to that of this study had experienced short stand-up time if $P_z/UC = 2.7$ (here P_z = confining pressure and UC = unconfined compressive strength). Therefore, an initial confining pressure of 575KN/m^2 (83.psi), ($P_z/UC = 2.3$) was used in this study.

Table III-1

Scales For Primary Quantities

Quantity	Scale	Quantity	Scale	Quantity	Scale
Stress	$\sigma^* = 1$	Unsupported Span	$\ell^* = 1$		$A^* = 1$
Length	$\ell^* = 1$	Tunnel Diameter	$\ell^* = 1$	Material	$\bar{\alpha}^* = 1$
Time	$t^* = 1$	Bead Size	$\ell^* = 1$	Properties	$\bar{D}^* = 1$
Strain	$\varepsilon^* = 1$	Confining Pressure	$\sigma^* = 1$		$m^* = 1$
		Advance Rate	$\ell^*/t^* = \frac{1}{40}$		

Availability of materials to use as tunnel liners dictated the outside diameters of the three model tunnel liners to be 6.1 cm (2.4 in), 12. 1 cm (4.75 in) and 18.5 cm (7.3 in). Using a length scale of $\frac{1}{40}$ these modeled prototype tunnels having dimensions of: 2.4 m (8 ft) 4.8 m (15. 8 ft) and 7.5 m (24.5 ft) respectively.

The distance from the face to first support in all models was one radius as this seemed consistent with tunnelling practice.

A reasonable advance rate for a 5 m (16 ft) diameter tunnel in squeezing ground might be one radius per 8 hour shift. This rate was varied in some models for study of the effect of rate of advance on stand-up time.

The unobstructed deformation of the ground behind the bead of a tunnel shield was also modeled. Such movements of 6 cm (2.4 in) is not uncommon in prototype tunnels so the "bead" on the end of the model tunnel liner was made .33 cm (.13 in) larger in diameter than the liner.

Determination of the thickness of the model liners required an analysis of the soil-liner interaction in the model as well as in a prototype tunnel. A reasonable manner of characterizing a soil-liner interaction is through the relative deformabilities of the liner and the ground. Peck et. al. (1972) proposed two ratios, called compressibility and flexibility ratios, for this type of characterization. Qualitatively, the stresses on a tunnel lining can be thought of as composed of two parts: an equal-all-around pressure causing diametrical strain but no change in shape; and stresses causing distortion or bending of the liner (see Figure III-1). The stresses on the ground at the boundary with the liner are equal but opposite

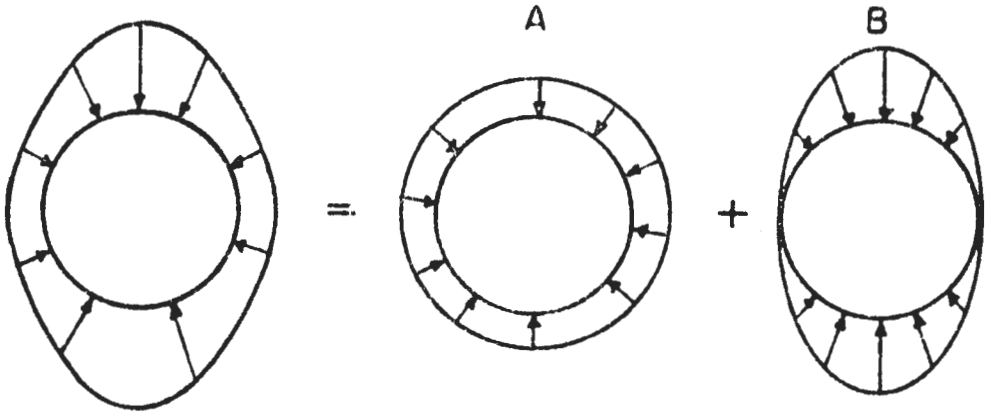

FIGURE III-1 ILLUSTRATION OF POSSIBLE STRESSES ON A TUNNEL LINER. STRESSES COMPOSED OF AN EQUAL-ALL-AROUND PRESSURE (A) PLUS STRESSES CAUSING DISTORTION OF LINER (B).

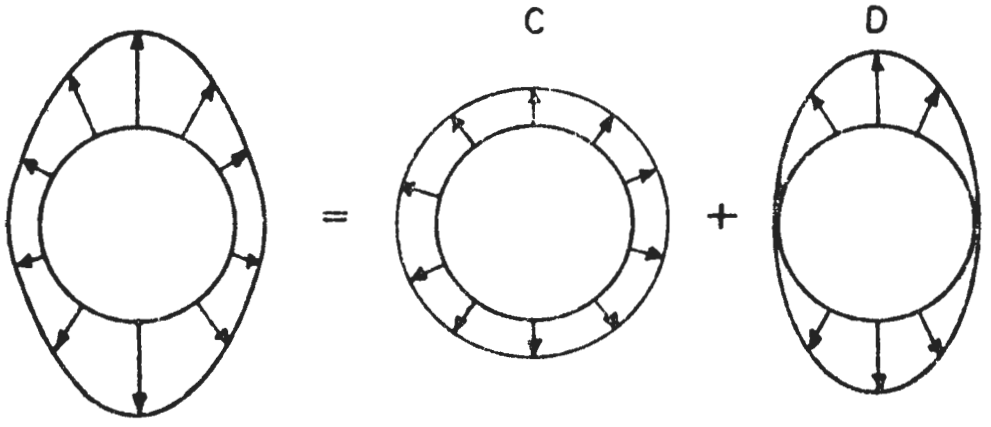

FIGURE III-2 ILLUSTRATION OF POSSIBLE STRESSES ON GROUND AT BOUNDARY WITH LINER. STRESSES EQUAL TO THOSE IN FIGURE III-1 BUT OPPOSITE IN SIGN.

in sign as shown in Figure III-2. A compressibility ratio can then be defined as a ratio of the strains under loading of Figure III-1A to the strains under loading of Figure III-2C. Similarly, a flexibility ratio is defined as a ratio of the strains under loading of Figure III- B to the strains under loading of Figure III-2D.

For purposes of comparison, a "real" stress field is not needed, so let the idealized stresses shown in Figures III-3 and III-4 represent the boundary stresses on the liner and ground respectively. The further assumption of linear elasticity reduces the significance of these results to qualitative importance.

The displacement and strain at the boundary in the ground due to pressure P_1 as shown in Figure III-4G are

$$U_{gr} = \frac{-P_1 r(1 + \nu_g)}{E_g} \quad \text{and} \quad \varepsilon_r = \frac{-P_1 (1 + \nu_g)}{E_g}$$

where ν is Poisson's ratio and E is Young's modulus. The deformations of the thin liner under pressure P_1 as shown in Figure III-3E are

$$U_{\ell r} = \frac{P_1 r^2 (1 - \nu_\ell^2)}{E_\ell t} \quad ; \varepsilon_{\ell r} = \frac{2P_1 r (1 - \nu_\ell^2)}{E_\ell t}$$

where t is thickness of the liner.

The compressibility ratio C is thus

$$C = \frac{\varepsilon_{\ell r}}{\varepsilon_{gr}} = \frac{2E_g r(1 - \nu_\ell^2)}{(1-\nu_g) t E_\ell} \approx \frac{k_1 E_g r}{t E_\ell}$$

where K_1 is a constant.

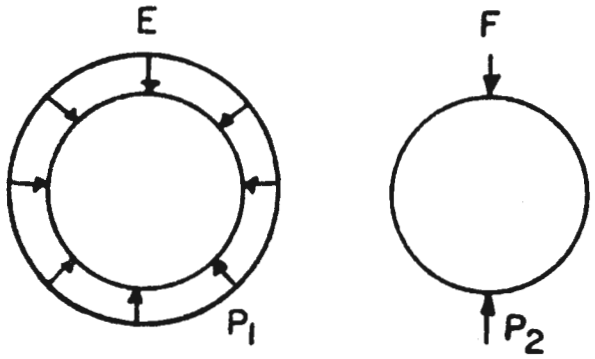

FIGURE III-3 IDEALIZATION OF STRESSES IN FIGURE III-1A AND III-1B

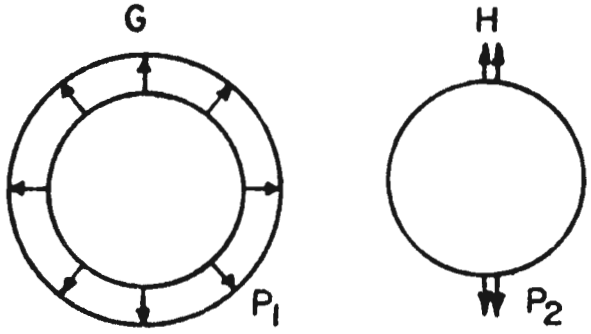

FIGURE III-4 IDEALIZATION OF STRESSES IN FIGURE III-2C AND III-2D

Similarly, the displacement and strain in the Y direction (up) of a thin walled liner loaded as in Figure III-3F is approximately

$$U_{\ell y} = .149 \frac{P_2 r^3 (1 - \nu_\ell^2)}{E_\ell I_\ell} ; \varepsilon_{\ell y} = 3(.149) \frac{P_2 r^2 (1 - \nu_\ell^2)}{E_\ell I_\ell}$$

And the deformations in the ground under stresses as in Figure III-H is

$$U_{gy} = \frac{-P_2 r (.70 - .64 \nu_g^2)}{\pi E_g}; \varepsilon_{gy} = \frac{-P_2 (.70 - .64 \nu_g^2)}{\pi E_g}$$

The flexibility ratio F is thus

$$\frac{\varepsilon_{\ell y}}{\varepsilon_{gy}} = \frac{.45\pi(1 - \nu_g^2) r^2 E_g}{(.70 - .64\nu_g^2) E_\ell I_\ell} \sim \frac{K_2' r^2 E_g}{E_\ell I_\ell} \sim \frac{K_2 r^2 E_g}{E_\ell t^3}$$

where K_2 is a constant. If the ratios F and C are large, the strain in the liner under a given load would be large in comparison to the strains of the ground under a similar load. Thus, the liner would be "flexible" in comparison to the ground.

Values of C and F were calculated and compared to distortions of several tunnel liners as described by Peck (1969), (See Appendix A, Table A-1). In those cases where moments were small, indicating a flexible liner, F was large (>1), also indicating a flexible liner. The compressibility coefficient (C in all cases was small (<1) indicating that the liners were rigid with respect to uniform diametrical deformation.

Taking, $E_g = 2.0 \times 10^4$ KN/m^2 (418 ksf), t = 0.30 cm (.01 ft), r = 6.4 cm (0.21 ft), $E_\ell = 2.1 \times 10^8$ KN/m^{2}x (4.3×10^6ksf) then

F = 4.3 and C = 0.002 for the model tunnel liners. (Note, the value of K_2 changes with units used). These numbers are consistent with the range of values in Table A-1. So the soil-liner interaction of the model was a reasonable representation of the soil-liner interaction of a prototype.Taking .318 cm (1.25 in) as the wall thickness of the liner for the 13 cm (5 in) diameter tunnel the thickness of the other two liners were determined so that the flexibility coefficient would be the same for all the liners. The final dimensions of the liners are given in Table III-2.

The lengths of the liners insured that the boundary effects of the endplates of the model chamber would not interfere with material behavior in the area of interest in the model.

A discussion of the determination of values for material property constants of the sand-wax modelling material is found in the later part of the next chapter.

Table III-2
Model Liner Dimensions

Outside Diameter		Wall Thickness		Length	
cm	(in)	cm	(in)	cm	(in)
6.1	(2.4)	.201	(.079)	81	(32)
12.1	(4.75)	.318	(.125)	91	(36)
18.5	(7.3)	.427	(.168)	102	(40)

Chapter 4

MODEL MATERIAL SELECTION AND CHARACTERIZATION

Introduction

The aim of the model material investigation was to find a material which was easy to use and yet was reasonably similar in constitutive properties to materials which lead to stand-up time problems.

Sand and wax was selected as a model material based on previous work by Korbin (1975). The sand used was a mixture of equal parts by weight of Monterey No. 0 and Monterey No. 20 sand. Various mixtures of different kinds of wax were combined with this sand mixture in order to obtain suitable material characteristics. A general description of the various components of the mixtures is found in Appendix B, Table B-1.

Sample Preparation and Testing

Samples for index testing were prepared by compacting four equal lifts by weight of hot sand-wax mixture (~80°C (27°F)) in 3.56 cm (1.40 in) diameter molds to a height of 8.9 cm (3.5 in). Tampers were 3.55 cm (1.39 in) in diameter. Specimens were allowed to cool in a constant temperature room for at least one day prior to extrusion from the molds. Density measurements were taken and all samples not within $\pm$ 10 Kg/m^3 (.6 pcf) of the target density of 1.530 T/m^3 (95.5 pcf) were discarded. Very careful preparation was necessary because it was observed that a 10% change in density would result in at least a 10% change in strength.

In the test cells all specimens were secured to top and bottom caps by a layer of epoxy cement. It was impossible to properly seat the specimens if the cement was not used.

Unconfined compression tests were performed at a constant displacement rate of about .8 cm/min. (.3in/min). Creep test loads were determined as a percentage of the ultimate load determined in the strength tests. This emphasized the need for careful preparation of samples.

Instead of applying the creep load instantaneously as is conventionally done, the specimens were loaded under the same displacement rate (.8 cm/min) as in strength tests up to the desired creep load and then allowed to creep under constant load. This was justified by noting that deformation rates do effect material strength (Casagrande & Wilson 1951, Scott, 1963 etc.). The total strain in the creep tests consisted of the sum of the strain accumulated during the constant strain-rate part of the test and the strain accumulated under constant load.

Confined tests were also performed using standard triaxial cells over a range of confining pressures up to 588 KN/m^2 (85 psi). A constant displacement rate of .8 cm/min was used for these tests also. The confining medium was air; specimens were jacketed and drained.

Material Selection Process

The process of model material selection and characterization proceeded by three stages: (1) initial selection from results of unconfined compression tests; (2) final selection and characterization from results of unconfined creep tests; (3) determination of Mohr-Coulomb Envelope using confined tests.

During stage 1 of the material selection process, numerous unconfined compression tests were performed on various sand-wax mixtures.

A summary of results of these tests is in Table IV-1. Korbin (1975) indicated that the design pressure of the model test chamber set an upper limit on unconfined strength of sand-wax mixtures usable as a model material. Mixtures with an unconfined strength exceeding 294 KN/m^2 (42 psi) were therefore rejected. Mixtures were also rejected which were too brittle or did not experience a significant amount of strain before failure. In Table IV-1 a measure of the stiffness of the material is given simply by a ratio of ultimate stress to strain at ultimate load $\sigma_{ult}/\varepsilon_{ult}$.

As a result of stage 1 investigations, six sand-wax mixtures were selected for further testing under stage 2 of the material selection process. Table IV-2 summarizes unconfined creep test results for these six mixtures. Table B-2, Appendix B lists individually the results of all creep tests. Clayey soil does not fail at unconfined creep stress levels below 40% to 60% of the unconfined soil strength (Murayama and Shibata, 1964,Singh and Mitchell, 1969). Therefore, sand-wax mixtures which failed within 10,000 minutes at a creep stress of 50% of the unconfined strength (.5 ult) of the material were rejected. It was also required that Eq. 3.18 describe the creep behavior of the sand-wax mixture and that its material property constants have model scales as indicated in Table III-1.

The following discussion supplies a few details of the selection process and characterization of the mixture finally accepted as the model material for this study.

Table IV-1

Unconfined Test Results For Possible Sand-Wax Model Material

Material	Ultimate Stress (σ_{ult}) KN/m^2 (psi)	Strain (ε_{ult}) at Ultimate Load	$\sigma_{ult}/\varepsilon_{ult}$ KN/m^2 x 10^2	Temp. °C
.6% Park .3% Paro	503. (73.0)	.412	12	20
.6% Park .2% Paro	365. (53.0)	.354	10	20
.6% Park .2% Shap	391. (56.6)	.335	12	20
*.6% Park .2% Cast	324. (47.0)	.343	9	20
.6% Park .3% Vic Am	398. (57.8)	.325	12	20
.5% Park .4% Vic Am	370. (53.7)	.361	10	20
.7% Park .5% Paro	740. (107)	.513	14	20
.8% Park	395. (57.4)	.398	10	20
.7% Cast .5% Park	640. (92.9)	.445	14	20
.8% Shap .4% Park	high	.522	—	20
.8% Paro .4% Park	528. (76.9)	.531	10	20
.5% Paro .4% Park	419. (60.8)	.441	10	20
1% CD150 .3% Vic Am	375. (54.4)	.172	22	7.2
*1.3% CD150	351. (51.0)	.171	21	7.2
*1.5% Vic Am	143. (20.7)	.368	4	20
*.7% Paro .5% Shap	361. (52.4)	.615	6	20
*.8% Vic Am 4% Shap	250. (36.4)	.335	7	20
*.6% CD150 .4% Shap	248. (35.9)	.246	10	20

*Mixtures selected for further testing under stage 2 of material selection process.

Final Selection and Characterization

The mixture containing 1.5% by weight Victory Amber (Vic Am[1]) had the lowest strength and lowest $\frac{\sigma_{ult}}{\varepsilon_{ult}}$ ratio. However, it also failed readily under a .5 ult creep load and so it was rejected. The mixture containing .6% Parakote (Park) and .2% (Casting Cast) wax had a relatively low unconfined strength. Because it included two stronger, stiffer waxes it was thought that the time to failure under creep loading of this mixture might be significantly different from that of the softer, weaker waxes. Within the scatter of results no significant difference was noted. A mixture of .8% Vic Am .4% Shaping (Shap) yielded reasonable strengths and $\sigma_{ult}/\varepsilon_{ult}$ ratios. Results of creep tests for this mix at .5 ult load were inconclusive. The mix of .7% Parowax (Paro) .5% Shap had a higher strength than the .8% Vic Am .4% Shap mixture, but the $\sigma_{ult}/\varepsilon_{ult}$ ratio was lower, strains at failure in the creep tests were higher, and results at .5 ult creep load were more acceptable. Physical properties of the wax CD 150/160 and Parowax are essentially the same (Korbin 1975). Quality control of CD 150/160 would be better than on the household Parowax yielding more faith in the constancy of the physical properties of CD 150/160. Therefore, CD 150/160 was substituted for Parowax and the percentage of wax decreased so that the finally selected sand-wax mixture was .6% CD 150/160 (CD150) .4% Shap.

---

[1]Note that as part of a mixture a wax will be referred to initally by its name followed by an abbreviation of the name in parenthesis. Thereafter reference to the wax will be made using the abbreviation.

Some tests including both unconfined strength and creep tests were run at 7.2°C (45°F) to determine if temperature could be used to significantly alter the properties of a sand-wax material. Lowering the temperature increased the strength and brittleness of the material. Under creep loading the time to failure seemed to be about the same as for materials tested at 20°C (68°F). Results of these tests are included in Tables IV-1 and IV-2.

A more complete test program was then begun to determine if the creep behavior of .6% CD150 .4% Shap sand-wax could be characterized using Eq. 3.18. First, more unconfined strength tests were performed to obtain a better average value of the ultimate unconfined load. Results of all unconfined strength tests on .6% CD150 .4% Shap are in Table B-3, Appendix B. Unconfined creep tests were then run at loads of .5, .6, .7, .8, and .9 ult. The data resulting from this test program is summarized in Table IV-2 using average values. Typical unconfined creep curves for samples tested at the various stress levels are shown in Figure IV-1. A complete listing of results of all creep tests on .6% CD150 .4% Shap is in Table B-2, Appendix B.

Figures IV-2 is a plot of log strain rate vs. log time at various stress levels*. This data can be reasonably well fit by straight lines. The slopes (m) of these plots should be equal for all stress levels ($\bar{D}$) up to about $\bar{D}$ = .9 (Mitchell, 1976). Excluding data for tests run at $\bar{D}$ = .9, the average value of m for .6% CD150 .4% shap is .6. Figure IV-3 is a plot of log strain vs. stress level for various times.

*Strain rate values were determined by curve fitting creep test strain time data using the same method as discussed in Chapter 5 for curve fitting model test results.

Table IV-2

Summary of Unconfined Creep Test Results for Possible Sand-Wax Model Materials

Material	Load (% Ultimate)	Creep Strain (Ave.)%		Total Strain (Ave.)%		Time to Failure (Ave.) min		Temp °C
1.5% Vic Am	70	.426		.509		42		20
1.5% Vic Am	50	.870		1.00		3360		20
.6% Park .2% Cast	77	.138		.399		67		20
.8% Vic Am .4% Shap	77	.4.8		.548		51		20
.8% Vic Am .4% Shap	50	.301		.606		—		20
.7% Paro .5% Shap	77-85	.781		.963		70		20
.7% Paro .5% Shap	50	. 95		1.14		Didn't fail in 10,000		20
1.3% CD150	77	.191		.250		80		7.2
		Ave	St. Dev.*	Ave	St. Dev.*	Ave	St. Dev.*	
.6% CD150 .4% Shap	90	.336	.09	.472	.14	14	8	20
.6% CD150 .4% Shap	80	.402	.08	.454	.09	89	17	20
.6% CD150 .4% Shap	70	.767	.04	.815	.05	932	116	20
.6% CD150 .4% Shap	60	.915	.18	.940	.18	3421	2591	20
.6% CD150 .4% Shap	50	. 81	.29	.927	.10	+		20

* Standard Deviation based on N weighting
+ Two samples failed in under 10,000 minutes

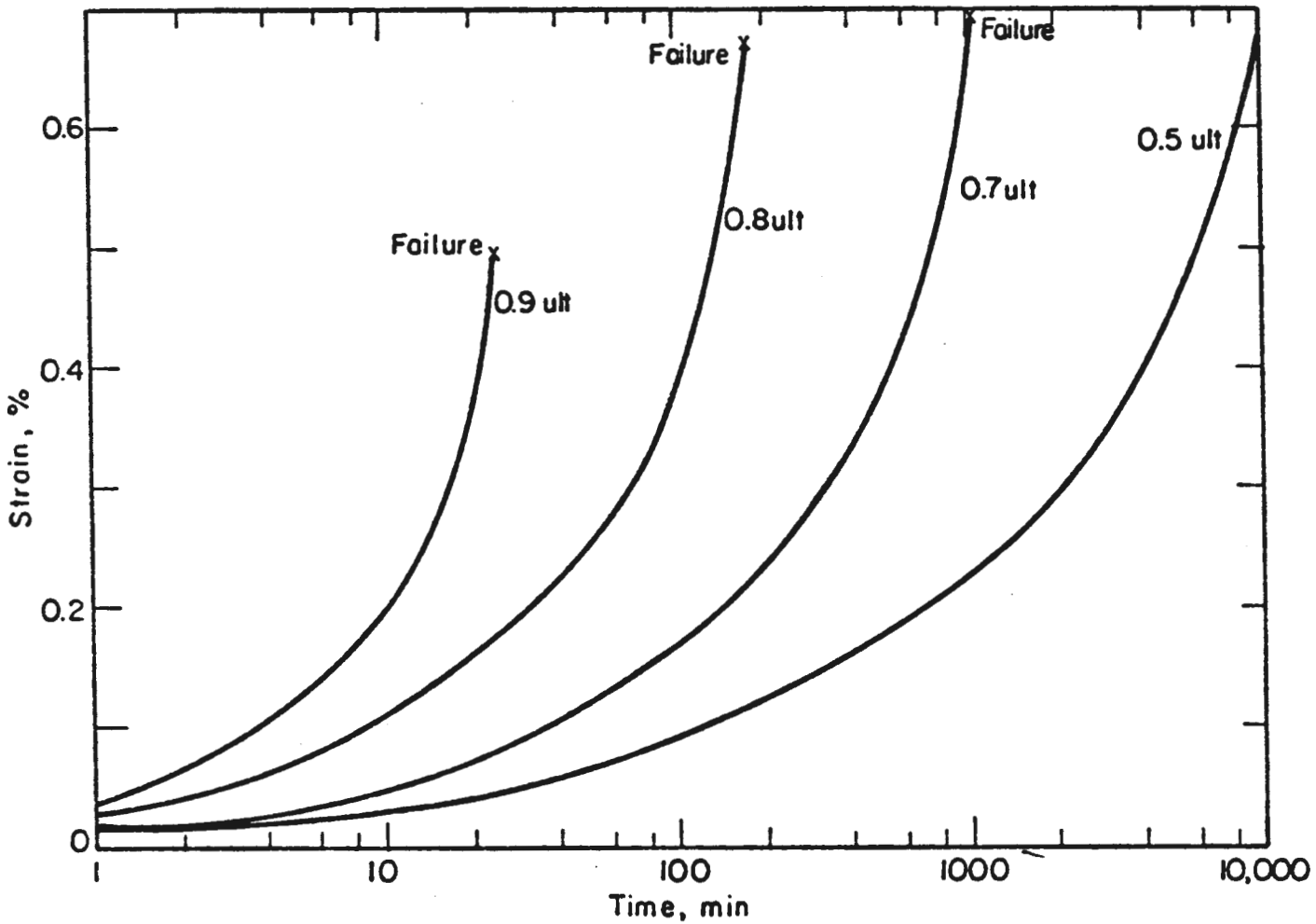

FIGURE IV-1 TYPICAL UNCONFINED CREEP CURVES OF .6% CD150 .4% SHAP SAND-WAX AT VARIOUS STRESS LEVELS.

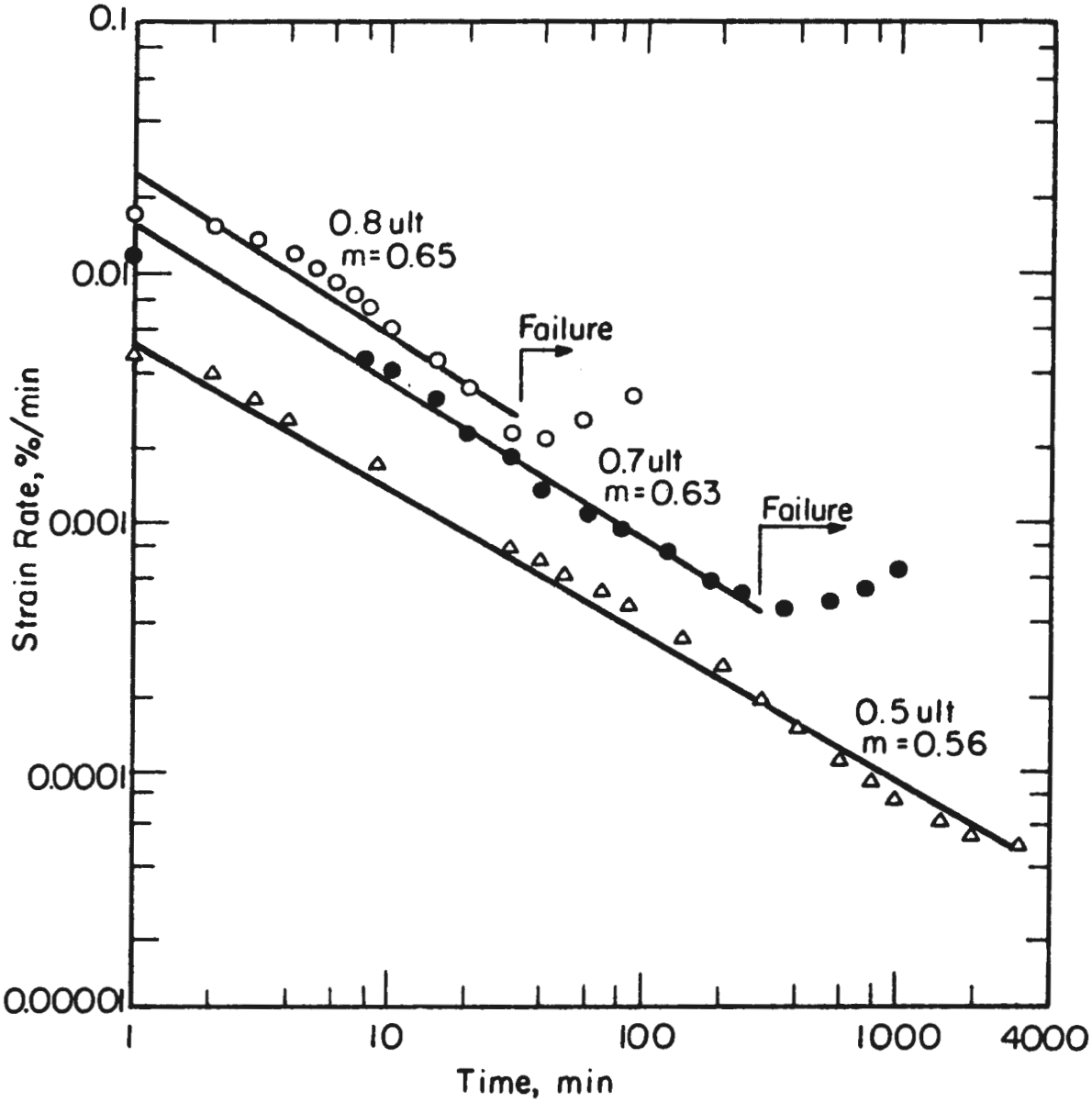

FIGURE IV-2 LOG STRAIN RATE VS. LOG TIME FOR .6% CD150 .4% SHAP SAND-WAX AT VARIOUS STRESS LEVELS.

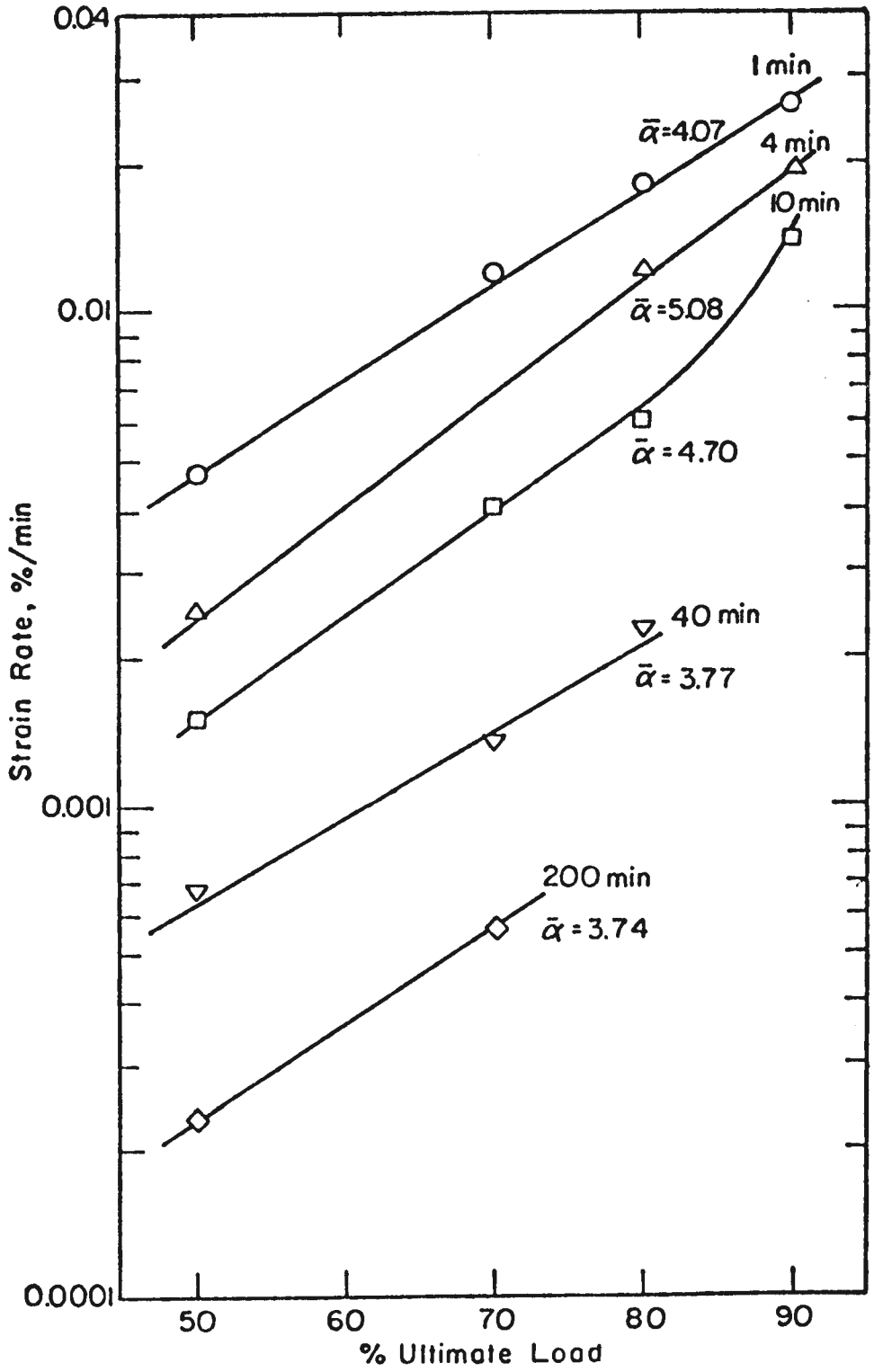

FIGURE IV-3 LOG STRAIN VS. STRESS LEVEL AT VARIOUS TIMES FOR .6% CD150 .4% SHAP SAND-Wax

Straight, parallel lines also fit this data quite well. The average value of $\bar{\alpha}$ is 4.3; and A = 6.4 x 10^{-4} %/min. Table IV-3 is a comparison of values of m, $\bar{\alpha}$, and A for .6% CD150 .4% shap with values of these constants for several real materials. The values of creep parameters for the real materials do not necessarily indicate potential stand-up time problems of a tunnel in those materials; they serve to show the similarity in the creep parameters of .6% CD150 .4% shap and some real materials and thus justify scaling material properties by the scale of Q_m/Q_p = 1. It should be noted that the time frame of the model material, particularly the time to failure under creep loads, seemed to be the same as for some real materials (see Singh & Mitchell, 1968, 1969 for examples). Thus the scale of t* = 1 was also reasonable.

To complete the characterization of .6% CD150 .4% shap a series of confined tests were performed. Figure IV-4 illustrates the effect of confining pressure on the stress strain behavior. Figure IV-5 is the Mohr-Coulomb Envelope of ultimate stresses for the material. It is curved, being steeper under low confinement than under high. This sort of behavior is typical of real materials also.

Table IV-3

Comparison of Creep Parameters for Model and Réal Materials

Material	Reference	m	$\bar{\alpha}$	A
Undisturbed Seattle Clay	Mitchell (1976)	0.5	-	-
Undisturbed London Clay	Bishop (1966)	0.97	1.4	1.4×10^{-5} %/min
Undisturbed Bay Mud	Sing and Mitchell (1968)	0.8	6.	3.4×10^{-3} %/min
Undisturbed Straight Creek Gouge	Semple (1973)	0.95	3.	1×10^{-4} %/min
.6% CD150 .4% Shap Sand and Wax		0.6	4.3	6.4×10^{-4} %/min

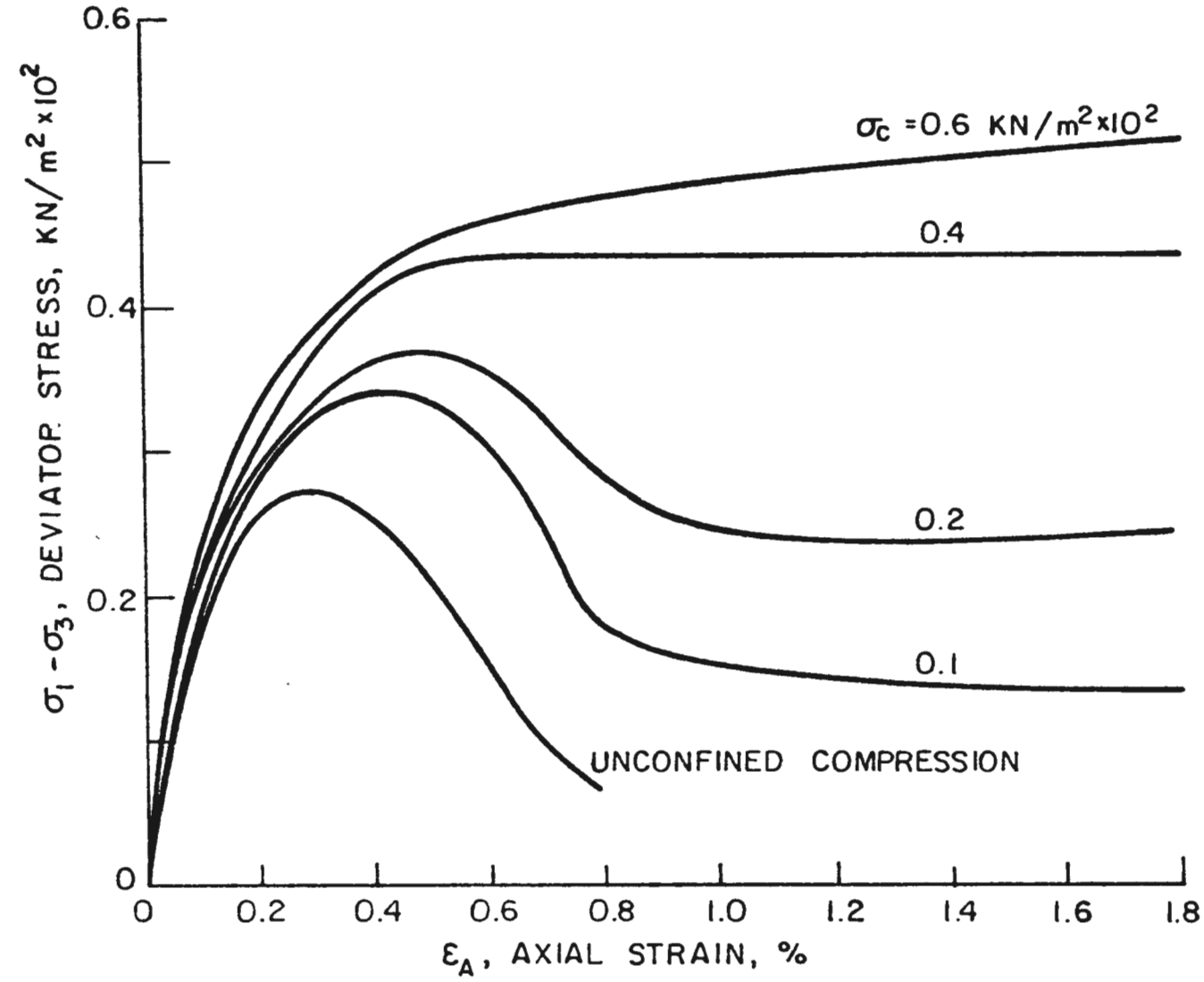

FIGURE IV-4 EFFECT OF CONFINING PRESSURE ON STRESS STRAIN BEHAVIOR OF .6% CD150 .4% SHAP SAND-WAX.

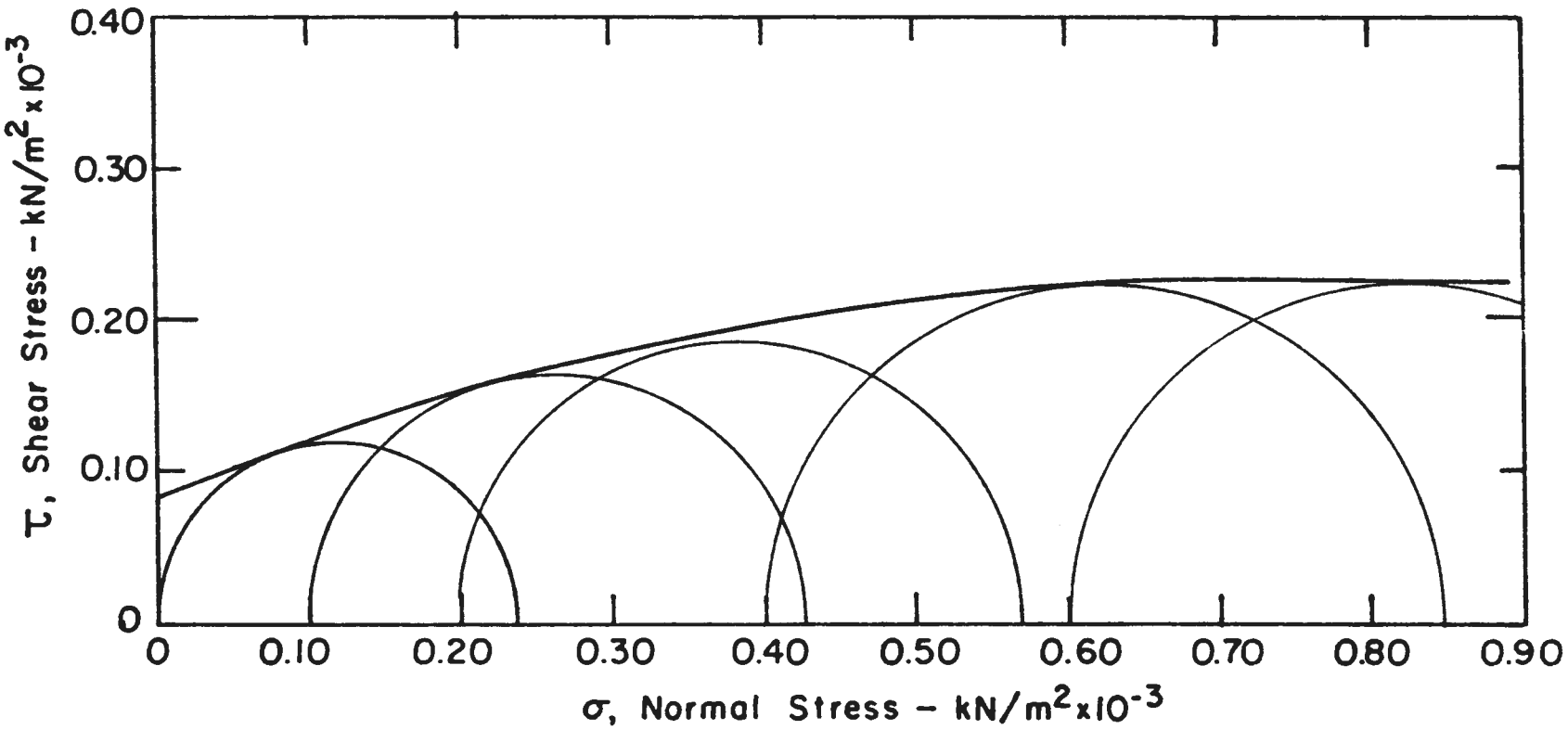

FIGURE IV-5 MOHR-COULOMB ENVELOPE OF ULTIMATE STRESSES FOR .6% CD150 .4% SHAP SAND-WAX.

Chapter 5

MODEL TEST EQUIPMENT, INSTRUMENTATION AND TEST PROCEDURES

Test Apparatus

The model testing apparatus consisted of three systems; model chamber and environmental controls, and excavating equipment.

A cross section of the model test chamber is shown in Figure V-1. This chamber was designed by Korbin (1975) for earlier model studies. The steel cylinder was designed as a standard pressure vessel for a maximum pressure of 1410 KN/m^2 (200 psi). It was constructed by rolling A-517 steel to an inside diameter of 66.6 cm (26 in). Its length was 1.22 m (4 ft). Flanges were continuously welded to the circumference of the cylinder ends and grooved for the installation of O-rings.

A rubber membrane was utilized in pressurization. The specially constructed 0.32 cm (0.81 in) thick neopreme membrane fitted tightly inside the cylinder. To form an air tight seal between the inside of the steel cylinder and outside of the membrane, the ends of the membrane were rotated flat against the flanges. Consequently, when the end plates were bolted in place, the flange, O-ring, and membrane formed a seal.

Air pressure was applied between the membrane and the steel cylinder via the system shown schematically in Figure V-2. A gas pressure booster increased "house-line" pressure in the accumulator. A regulator and calibrated pressure gage attached to the accumulator maintained constant test chamber pressure. A back-up system of bottled air was available for emergencies. The material characteristics of the

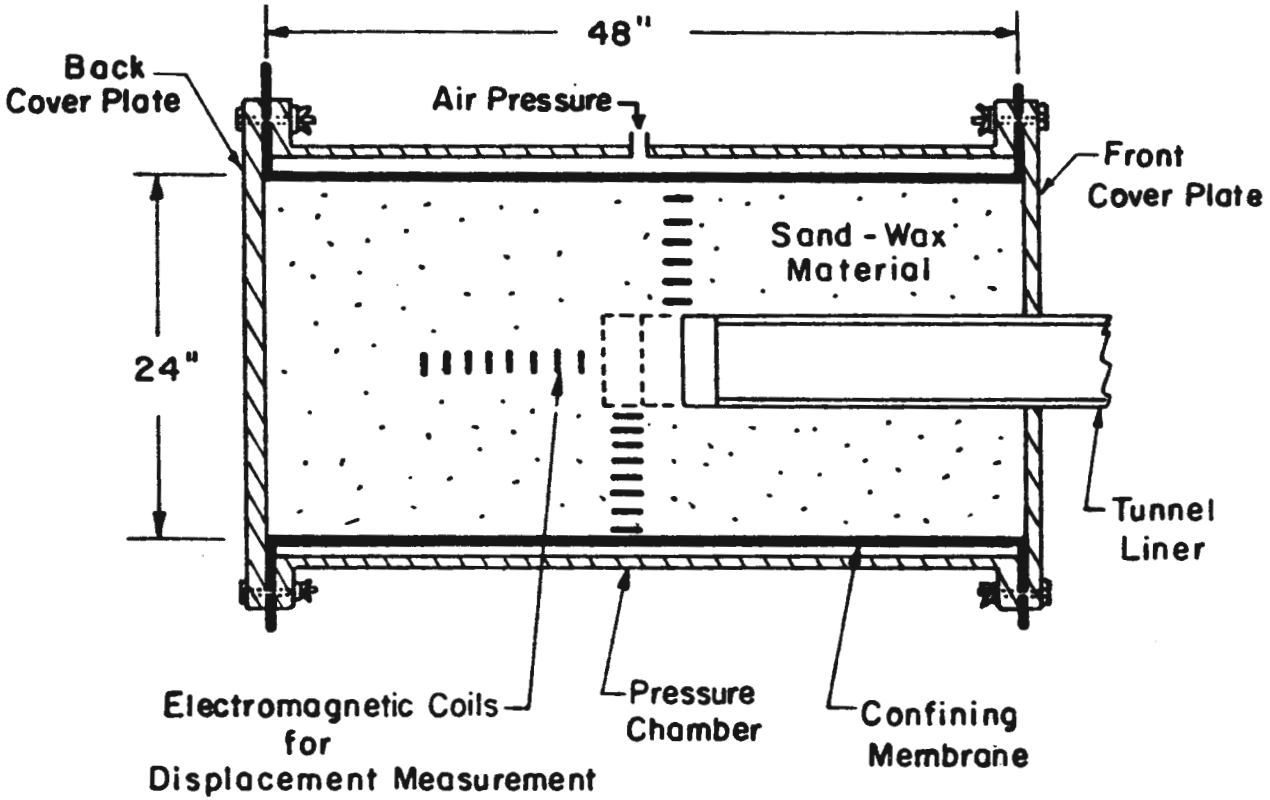

FIGURE V-1 CROSS SECTION OF MODEL TEST CHAMBER. DOTTED LINES REPRESENT ROUNDS YET TO BE EXCAVATED.

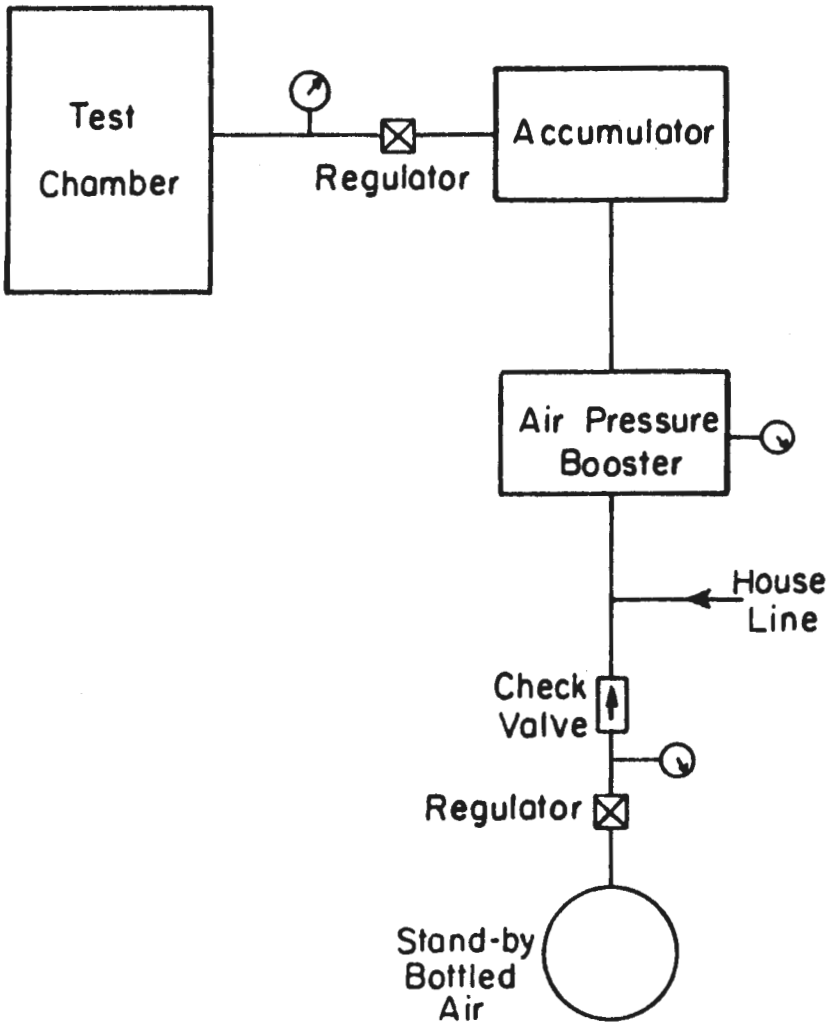

FIGURE V-2 SCHEMATIC DRAWING OF AIR PRESSURIZATION SYSTEM

sand-wax material were temperature sensitive so all tests were performed in a constant temperature room (20°C ± 1°) (68°F).

Four requirements were placed on the design of the excavating equipment: (1) Excavate and line three different diameter tunnels on precise alignments, (2) Excavate and line simultaneously at a given rate, (3) Maintain a given unsupported span, (4) Cause no material disturbance not exhibited by a real tunnelling operation.

The tunnels were excavated for a distance of about 0.5 m. (20 in.) (about half the length of the test chamber) and then excavation stopped. During the filing of the chamber with model material, instrumentation was clustered around the final position of the tunnel opening. Accurate alignment of the excavator was thus necessary in order to avoid disturbing the instrumentation. This,as well as diversified functional requirements, was achieved by designing the excavator as a nested serires of metal cylinders. A cross section of the escavating equipment is shown in Figure V-3. Figure V-4 is a photo of the completed equipment and Figure V-5 shows the excavator attached to the test chamber. Only the outer cylinder (guide tube) needed to be aligned relative to the model chamber. All inner cylinders (tunnel liner, cutting assembly) were aligned relative to the guide tube. Interchangeable bearing in the guide tube accomodated the three different liner diameters. These bearings maintained the alignment of the tunnels to within .25 cm (.1 in) in 61 cm (24 in).

The driving mechanism was the same for all tunnel sizes and was therefore attached to the liners via a flexible "spider" coupling. The drive shaft, which advances the tunnel linings, was a threaded

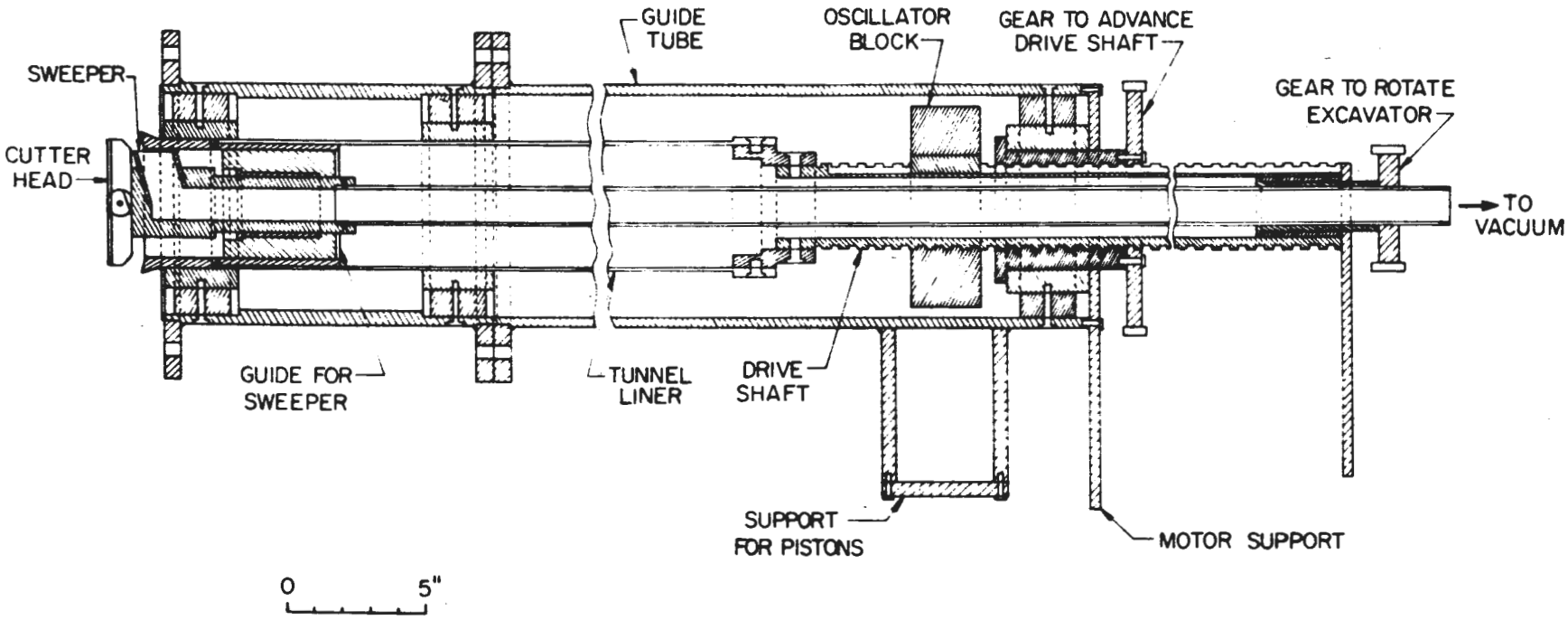

FIGURE V-3 CROSS SECTION OF MODEL TUNNEL EXCAVATOR.

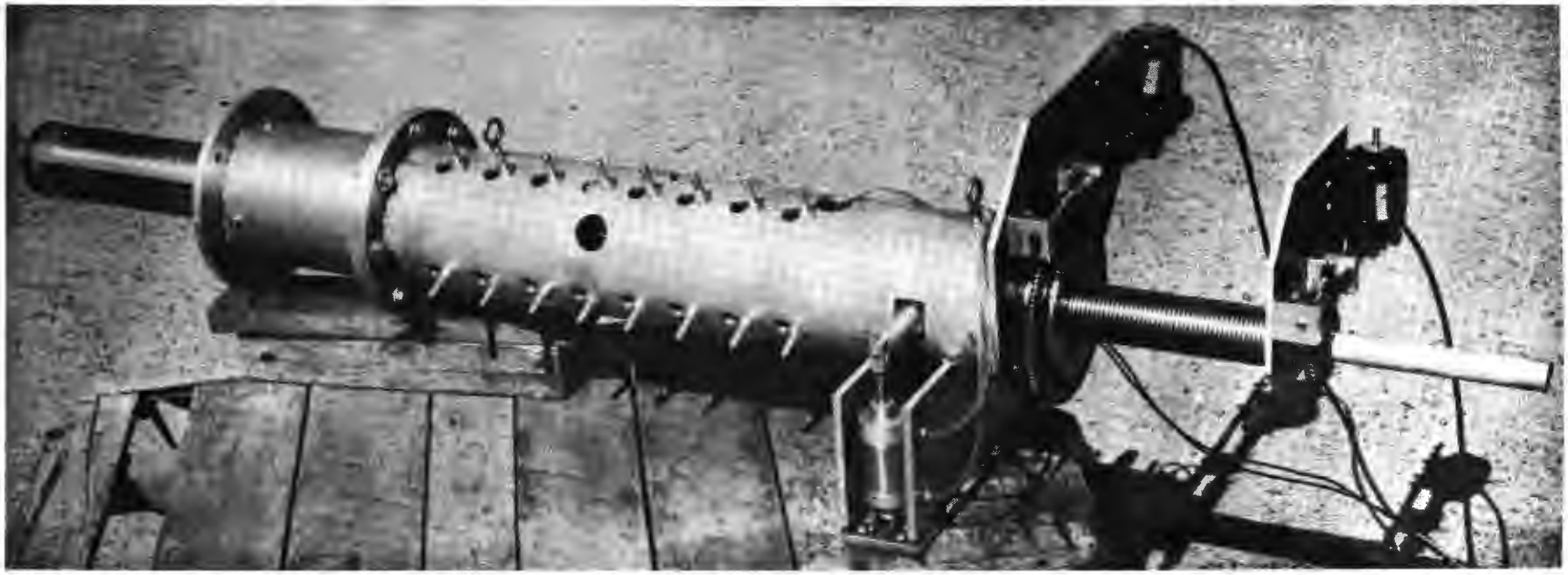

FIGURE V-4 COMPLETED EXCAVATOR

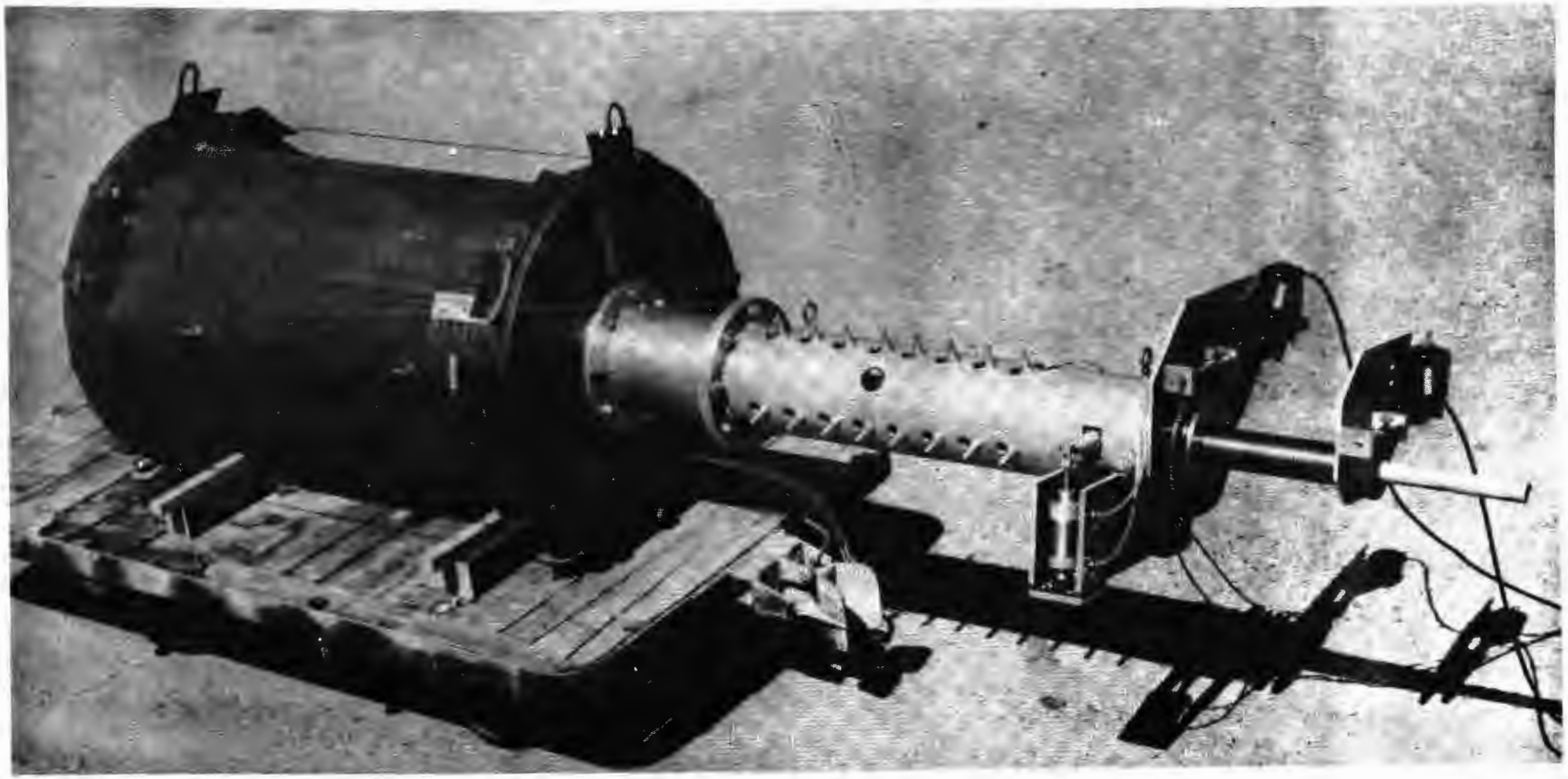

FIGURE V-5 EXCAVATOR ATTACHED TO MODEL TEST CHAMBER

hollow tube. This was connected through reduction gears to a constant speed motor. Because of the slow advance rates, a 1/50 Hp motor could be used even though the design load was 486 N-M (4300 in.-lbs.).

Both plexiglass and steel were used in fabricating the liners and cutters. All parts near the face of the excavation, such as the end of the liners and the cutter heads, were made of plexiglass in order not to disturb the magnetic fields of the embedded transducers.

Aligned within the tunnel lining mechanism was the cutting-sweeping assembly. The cutter head extended beyond the end of the liner creating the unsupported section of the tunnel. It could rotate independently of the liner but was adjusted so as to maintain a constant unsupported length. Material was excavated by scraping action of the arms of the rotating cutter head. The cutting surface of the arms was made of a carborundum chip-epoxy mix which prevented wear of the cutting arms. The arms could be collapsed together so the entire cutting-sweeping assembly could be withdrawn from the tunnel at the end of excavation. Thus, the cutter head would not interfere with deformations of the unsupported tunnel section. The cutter head excavated to within about .5 cm (.2 in) of the finished diameter of the tunnels. Tunnels were trimmed to final dimensions by rotationally oscillating motion of the liner tip. The plexiglass liner tip was beveled inward and also faced with the carborundum chip-epoxy mixture. Excavated material was swept up and removed through a long tube extending the length of the excavator and attached to a vacuum cleaner. The vacuum was small, approximately 7 KN/m^2 (1 psi) and did not affect material behavior. Figure V-6 is a view facing the excavation end of the three lines and cutter heads.

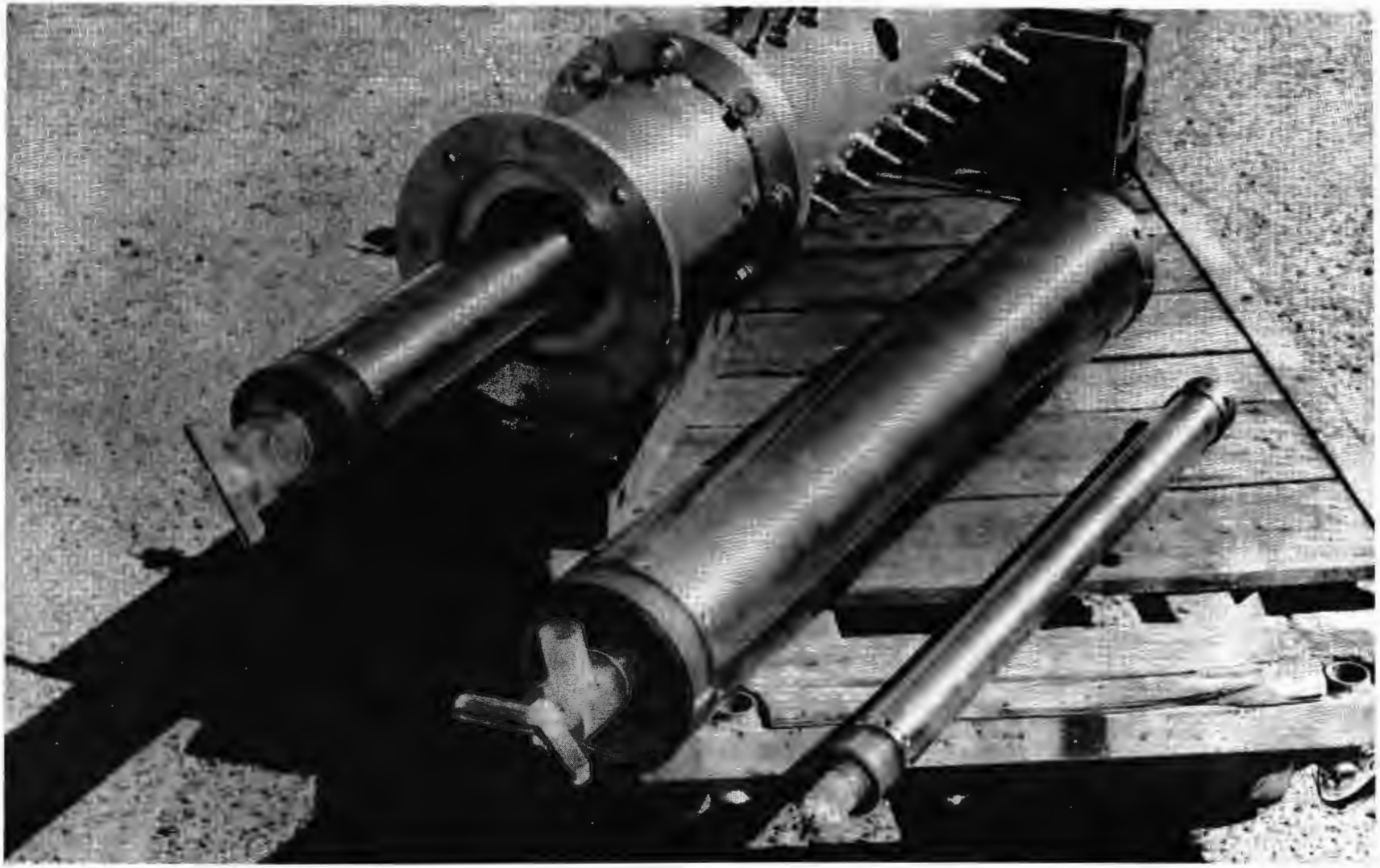

FIGURE V-6 EXCAVATION END, SHOWING CUTTING HEAD, OF THE THREE TUNNEL LINERS USED IN STUDY.

Reduction of friction due to insertion of the liner was the major concern in satisfying the fourth design requirement. Most real tunnels have the liner placed segment by segment as the tunnel advances. The driving motor of the excavator pushed the liner forward as a whole. Axially oriented (in the direction of tunnel advance) friction forces created by the motion of the liner relative to the sand-wax were undesirable in the model. Such induced shear forces would not exist in a prototype and might make the stress field around the model tunnel face different from the stress field around a prototype tunnel face.

A lining system had to be developed that would minimize friction forces and would not disturb the magnetic fields of the transducers. Preliminary tests had shown that friction forces could be especially high from some liner materials because the sand grains would tend to gouge into the liner material if it was too soft. A series of tests was performed using a direct shear testing apparatus to determine the "coefficient of friction" between sand-wax and several plausible liner materials. The results are summarized in Table V-1. Hard chromed steel was chosen because of the machinability of steel and the low coefficient of friction due to hard chroming. Heat treatment would distort a liner too much.

Friction effects were further reduced by rotationally oscillating the liners as they were pushed into the sample. Rotational oscillation had the effect of rotating the induced axial (in direction of tunnel advance) shear force to a tangential force periodically reversing in direction by 180°. In this way, almost all the friction force is directed tangentially. The oscillating motion was effected using a system shown schematically in Figure V-7.

Table V-1

Measured Coefficient of Friction μ Between Sand-Wax and Other Materials

Material	μ $\frac{\text{Normal load}}{\text{Shearing load}}$
Ceramic	.13
Hard anodized aluminum	.23
Case hardened steel	.14
Glass	.13
Hard Chromed Steel	.15

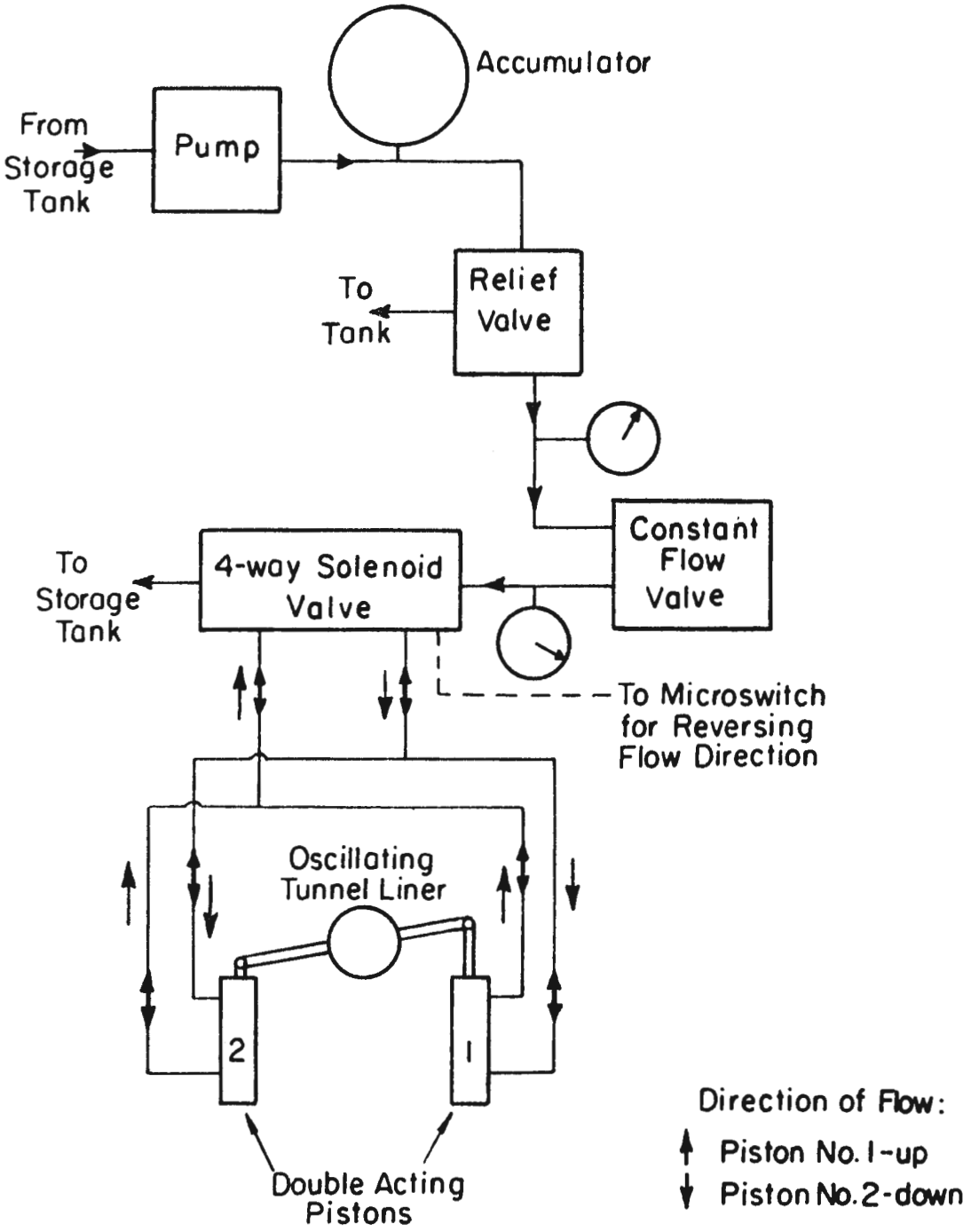

FIGURE V-7 SCHEMATIC DRAWING OF HYDRAULIC SYSTEM FOR OSCILLATING TUNNEL LINERS.

Instrumentation

For measurement of displacement, an instrumentation system with independent electromagnetic sensors was used.

The sensors were essentially flat annular coils of wire as shown in Figure V-8. Two sizes were used: .32 cm (.12 in) thick by 1.27 cm (.5 in) in diameter; and .32 cm by 2.54 cm (1.0) in diameter.

Sensors were used in pairs with their flat surfaces parallel to each other. One transmitted a constant reference signal; the other received the transmitted signal via electro-magnetic coupling of the sensors. Sensor separation was inversely proportional to the magnitude of the received signal.

These sensor pairs were incorporated into a general layout of 24 sensors as sketched in Figure V-9. Three lines of sensors were used: one radial line placed one radius back from the face; another radial line was placed one half radius back from the face; and the third line was oriented axially foreward from the center of the face. A typical pattern of sensor placement for the lines is shown in Figure V-10. This figure also shows the sensor mode, transmit or receive, and label (A1, A2, etc.). Nearest the opening 1.27 cm diameter sensors were used as the first and second sensor in each line. Elsewhere, the larger sensors were used and were spaced from 2.8 cm to 3.8 cm (1.1 in to 1.5 in) apart.

The sensors provided a complete record of displacement along three different lines in the models but their small size minimized disturbance of material movement. To minimize another source of disturbance, 1.83 mm (0.7 in) diameter Teflon coated cables were lead-in wires to the sensors. Twisted pairs of lacquer insulated

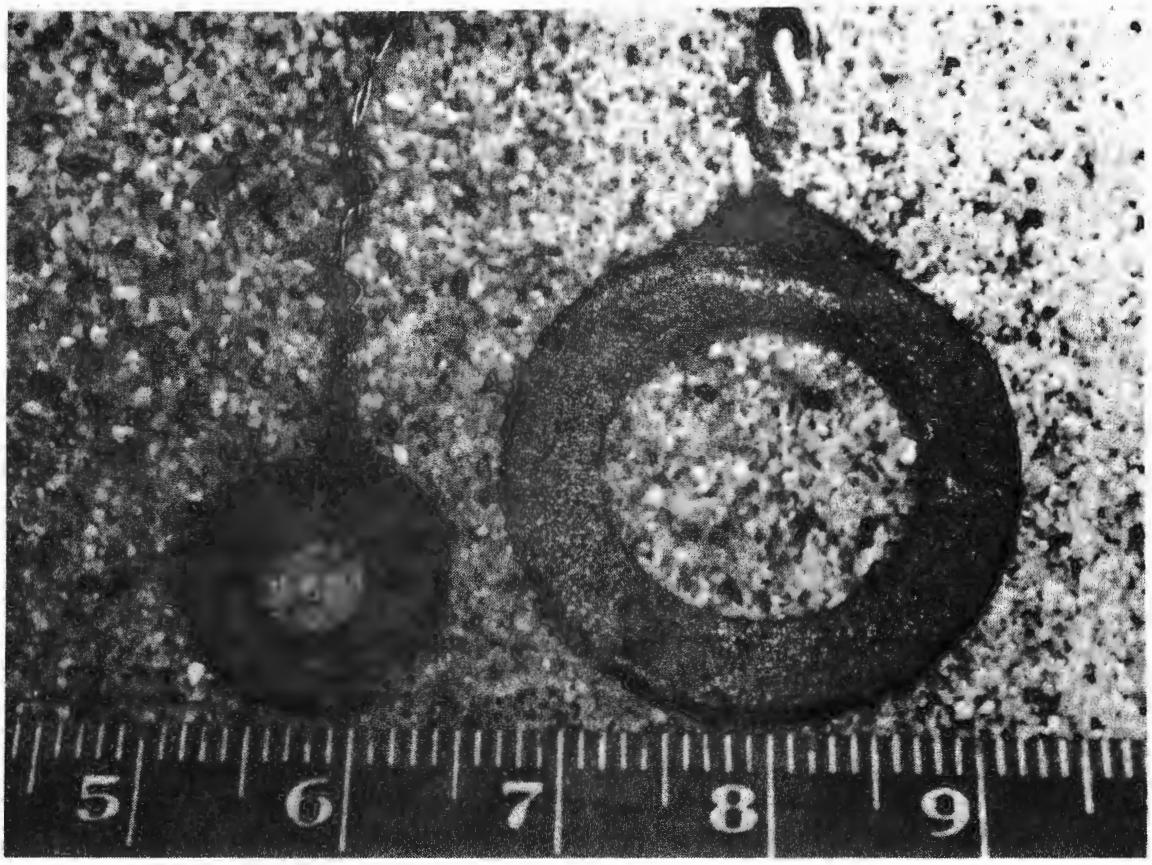

FIGURE V-8 ELECTROMAGNETIC SENSORS. (scale in cm)

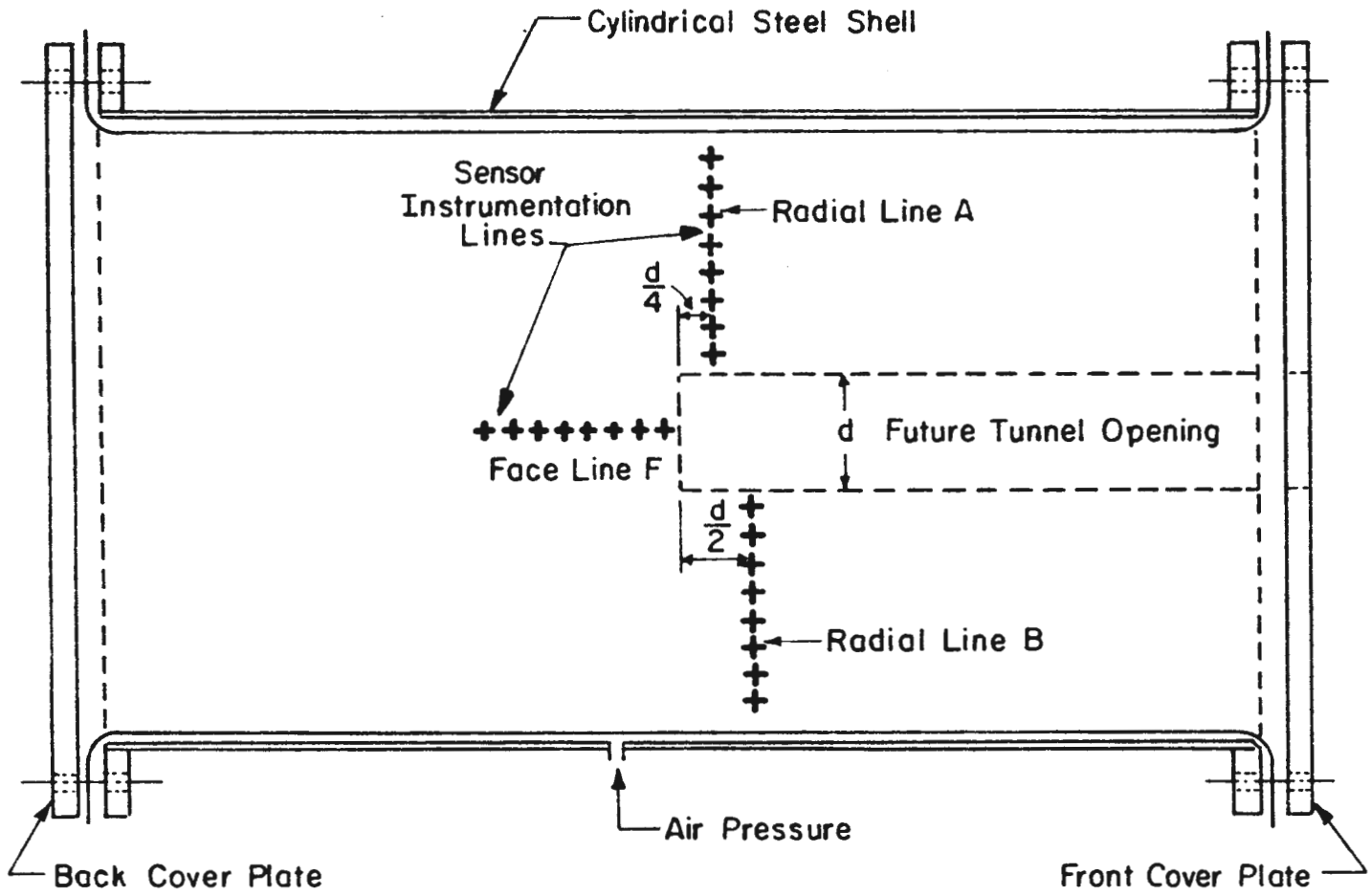

FIGURE V-9 SENSOR LINE POSITIONS. IN MODELS.

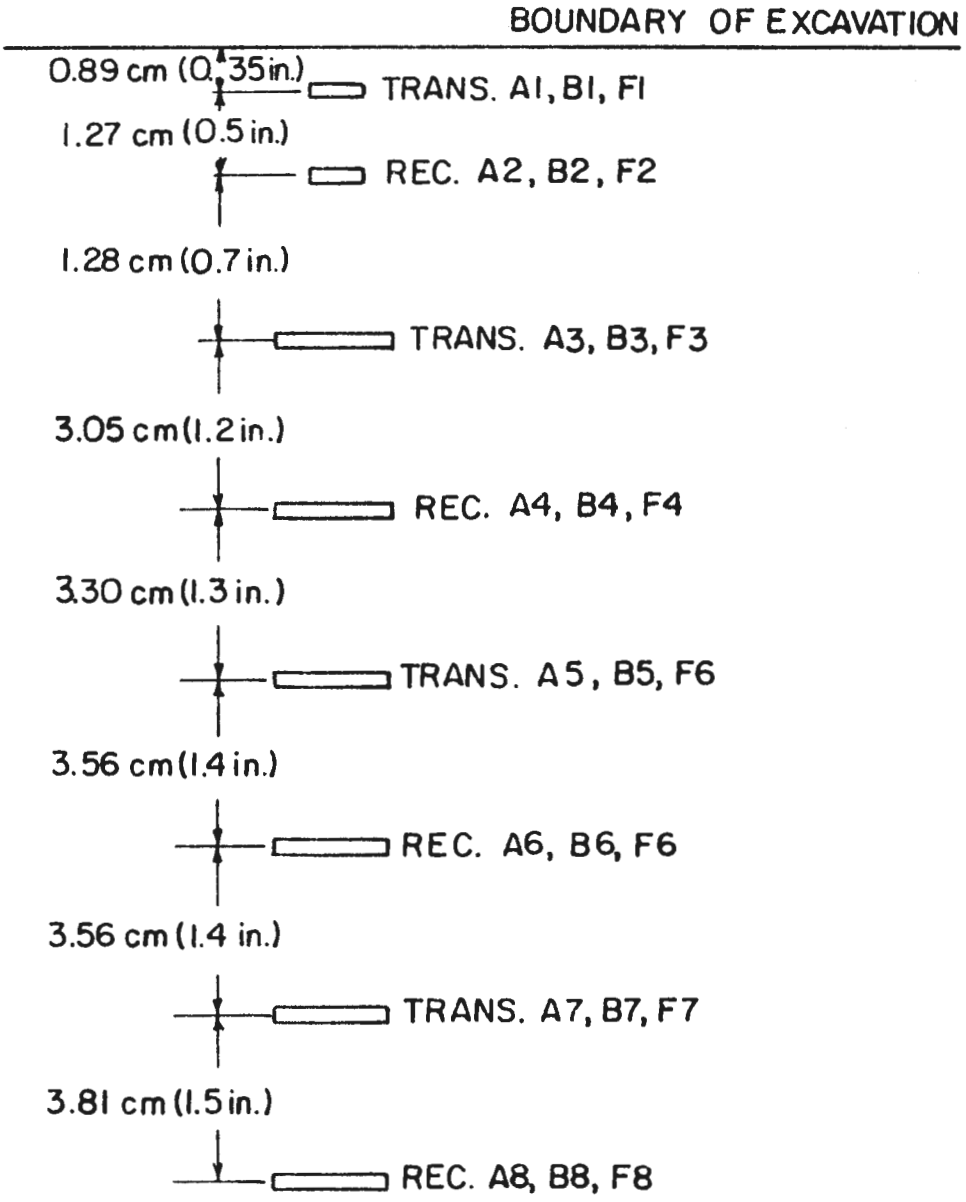

FIGURE V-10 SENSOR LABEL (e.g., A1), POSITION, MODE (Trans. or Rec.) OF SENSORS ALONG RADIAL LINES A AND B AND FACE LINE F

.25 mm. (.001 in.) diameter wires ran the last 30 cm. (12 in.) to the small sensors.

Sensors pairs were calibrated using the device shown in Figure V-11. It was constructed of plexiglass because sensor calibration was changed if they were closer than two diameters to metal. A separate calibration curve was obtained for each sensor pair. A typical curve for a pair of 2.54 cm sensors is shown in Figure V-12. The effect of differential translation and rotation of sensors on their calibration curves had been investigated by Korbin (1975). Errors from the translations up to .6 cm (.25 in) and from rotations up to 20° were small.

External instrumentation basically consisted of the transmitter and receiver circuits, Figure V-13.The transmitter hardware was designed to provide a constant amplitude 20KHZ signal.Amplitude was regulated with an automatic gain control driven with an error signal derived from a DC reference and the output. Resolution and stability was within $\pm$1 mv-RMS over the test duration. Receiver circuits provided signal conditioning prior to amplitude measurement. An integrating digital voltmeter measured the conditioned signal, which was recorded on punched tape. A scanner and program interval selector allowed for the automatic scanning and recording of a series of sensors at prescribed intervals of time. The total time required to read all sensors was 20 seconds.

Long term stability of the instrumentation was tested over a period of four days. For this test sensors were placed in approximate in-situ position. Over all accuracy of the system for this period was on the order of one-thousandths of an inch.

FIGURE V-11 DEVICE FOR CALIBRATING SENSORS

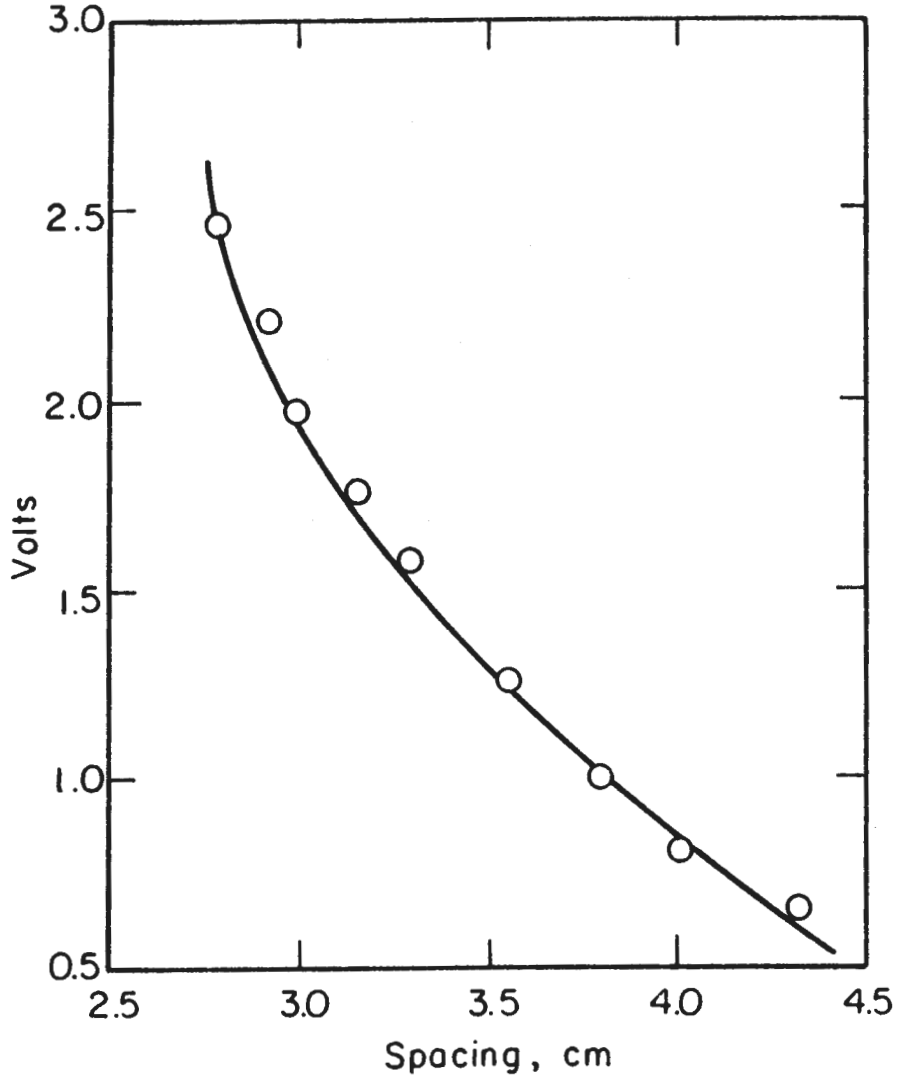

FIGURE V-12 TYPICAL EXAMPLE OF SENSOR CALIBRATION CURVE USING SENSORS A5T and A6R.

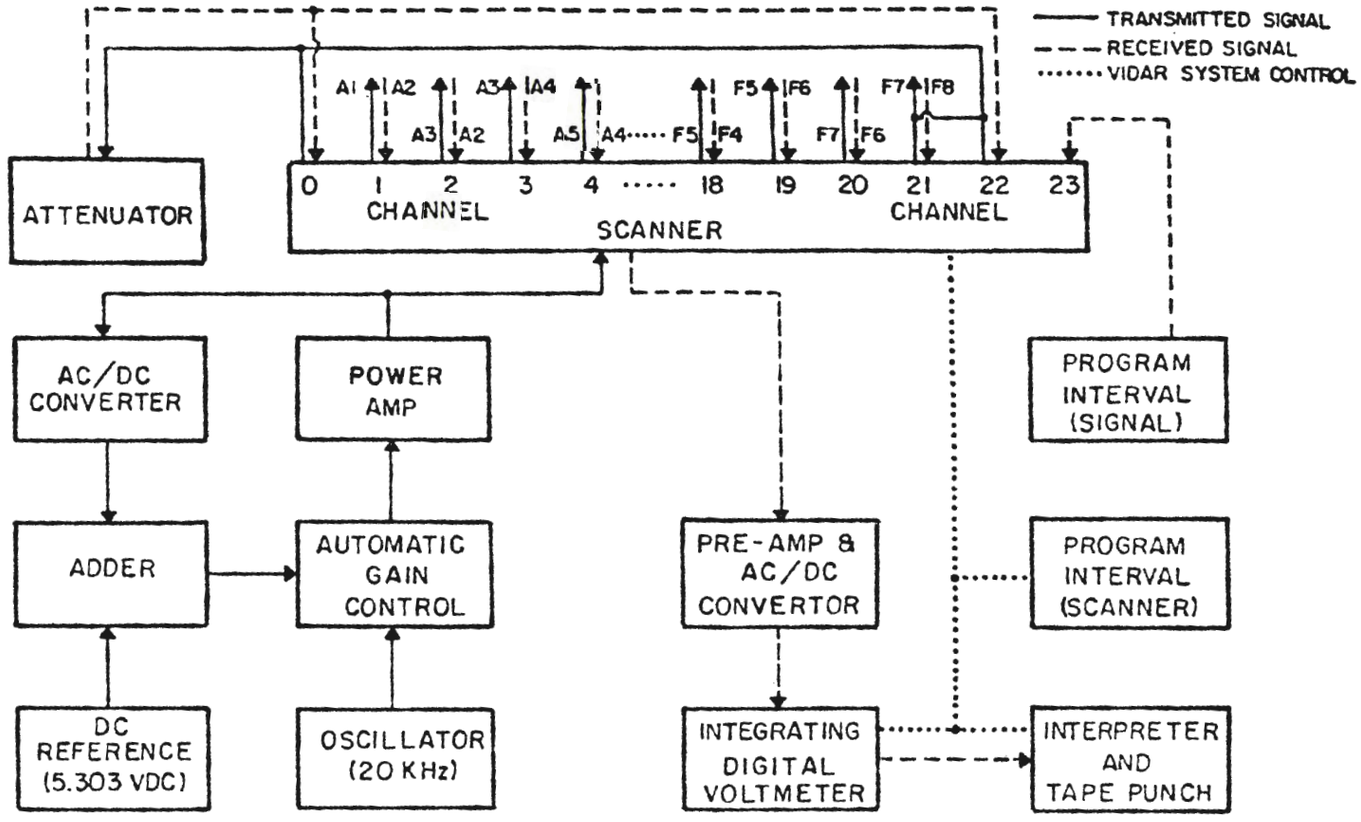

FIGURE V-13 EXTERNAL INSTRUMENTATION.

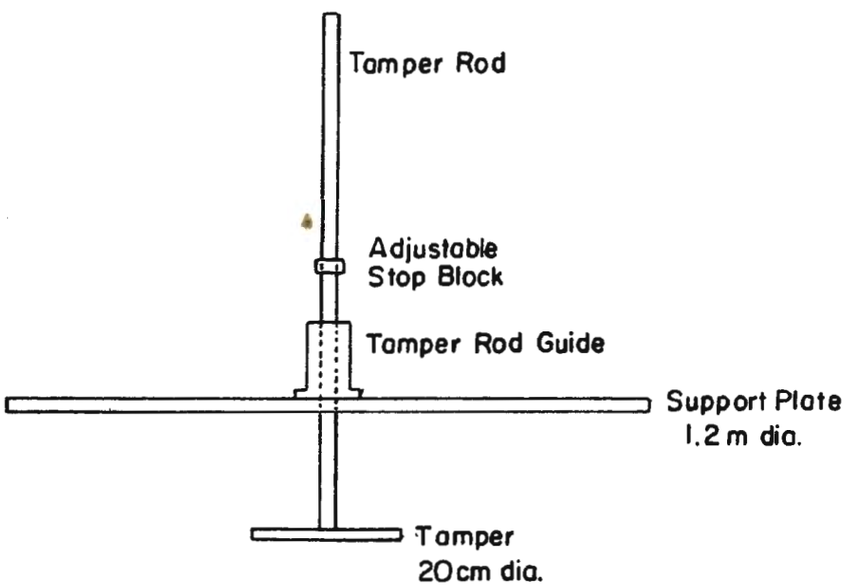

FIGURE V-15 DEVICE FOR COMPACTING HOT SAND-WAX IN MODEL CHAMBER (not drawn to scale). SUPPORT PLATE RESTED ON TOP OF MODEL CHAMBER.

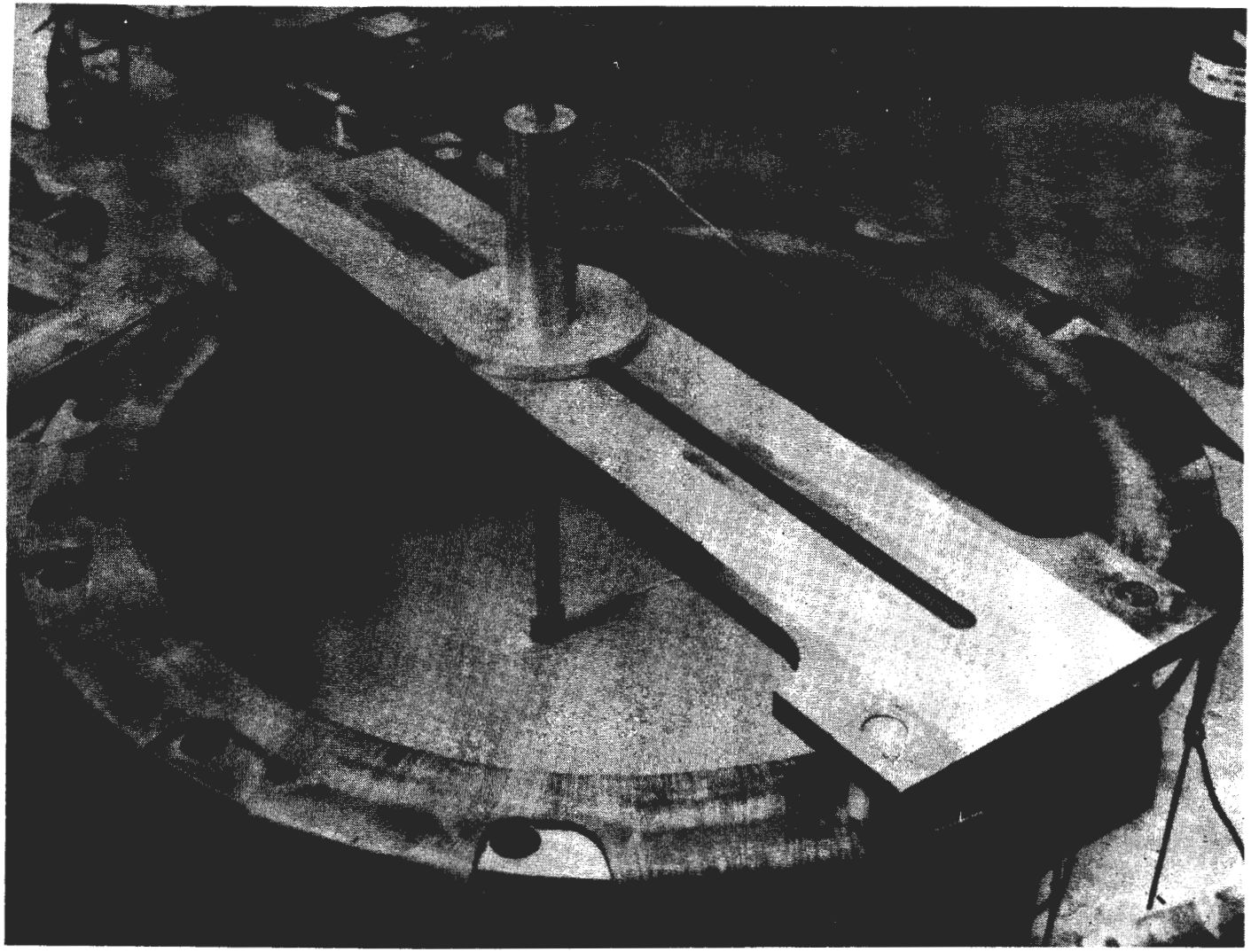

FIGURE V-16 ILLUSTRATION OF SENSOR PLACEMENT IN MODEL CHAMBER.

Data Reduction and Analysis Techniques

Non-linear curve fitting was used extensively throughout data reduction and analysis. An equation of the type

$$y = A\, x^{B}\, e^{Cx} \tag{5.1}$$

was fit to the calibration data of each sensor pair, and the constants A,B, and C were catalogued in a computer program. Figure V-17 is an example of the excellent fit obtained. During data reduction, readings from the sensors (voltages) were input into the computer, appropriate values of A,B, and C were selected, and sensor separations were computed using Eq. 5.1. By knowing initial sensor separations, cumulative displacements could easily be obtained.

As will be discussed further in Chapter 6, a knowledge of the state of strain in the models was important. A computer program was written to fit non-linear equations to the displacement vs. sensor position data. The derivative of the equations would be the strain in the direction of the sensor line. It should be noted that the result of a non-linear curve fit is the best fit for the given choice and number of variables used in the curve fitting equation. Different choices and numbers of variables yield other "best-fit" curves. How good the "best-fit" curve really is depends to some extent on how good a choice of variables is made by the user. With this in mind, the computer program was written with the option of three equations to be used as best fit curves:

$$y = \sum_{i=0}^{n} B_i X^i \tag{5.2}$$

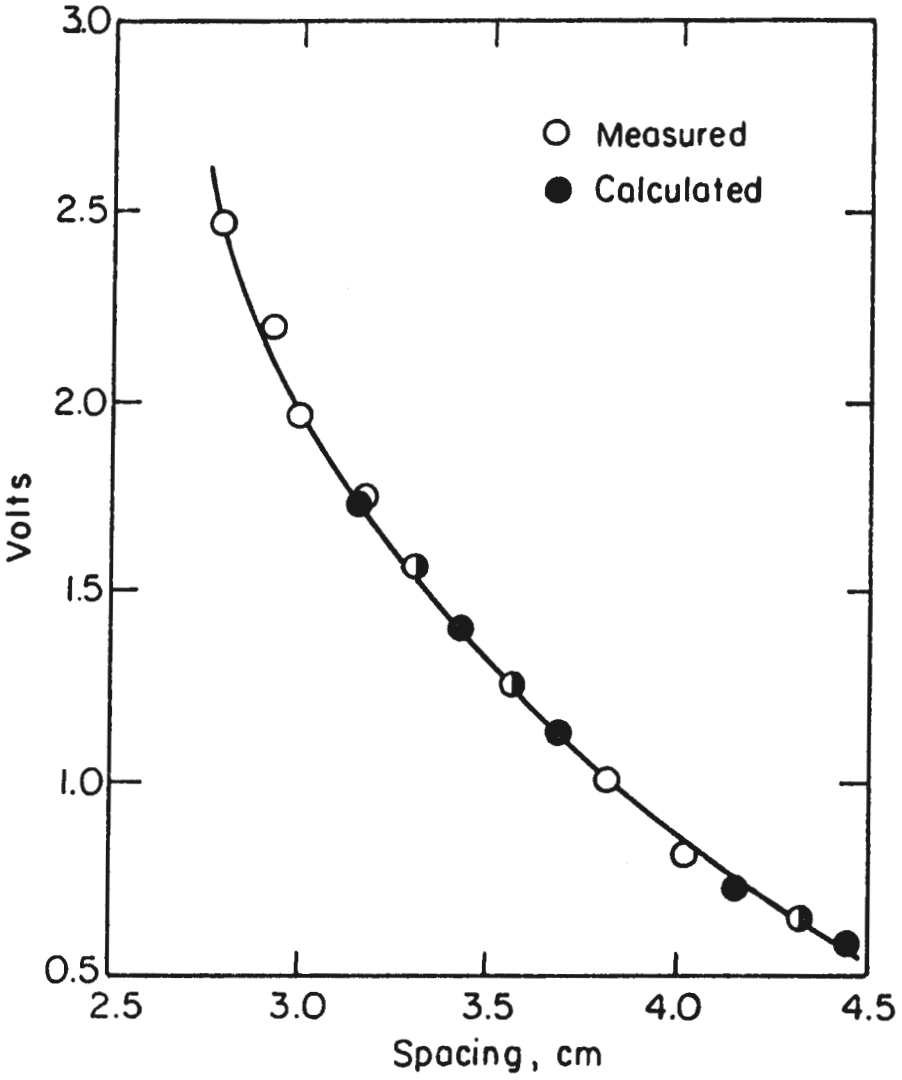

FIGURE V-17 COMPARISON OF MEASURED VALUES AND CALCULATED VALUES USING EQ. 5.1 FOR CALIBRATION CURVE OF SENSOR A5T TO SENSOR AGR. (Typical example)

$$y = \sum_{i=0}^{n} B_i X^{-i} \tag{5.3}$$

$$y = \sum_{i=0}^{n} B_i (X-1)^{-i} \tag{5.4}$$

Values of n could also be varied. These equations express the displacement y of a sensor as a function of its position x. Sensor positions were expressed as a ratio, the distance from the center of the tunnel to the sensor divided by the radius of the tunnel. Eq. 5.2 or 5.4 was used for the face line because x=0 at the face. But Eq. 5.2 and 5.3 were both used to fit data from radial lines A and B. It can be shown (Carnahan, 1969) that if the order of a polynomial equals the number of data points the polynomial will be forced to fit through each point. Therefore, in determining strains a maximum value of n=6 was used.

Appropriate best-fit curves were selected by inspection. Higher order polynomials may precisely fit the given data points of a given function, but there is no guarantee that it will fit values in-between the specified points. Calculated displacements using a best-fit equation were compared to measured displacements. Also, slopes of the equation were calculated at various points along the curve and checked to see that they were continuously decreasing. The highest order equation which had a continously decreasing slope was generally accepted as the best-fit approximation of the data. Figure V-18 is a typical example to illustrate the goodness of fit of the approximating functions. Listings of the computer programs written for use in data reduction can be found in Appendix D.

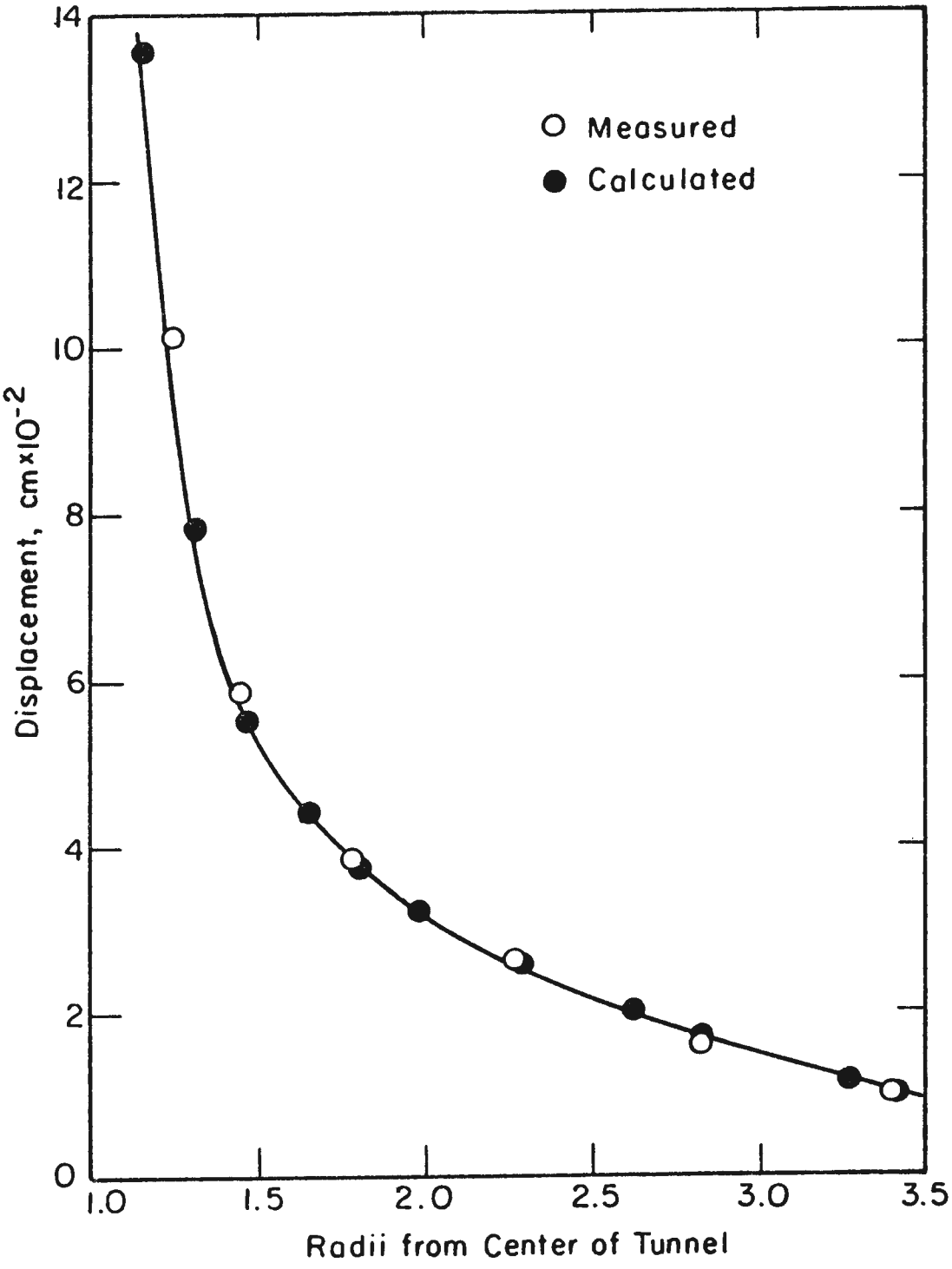

FIGURE V-18 COMPARISON OF MEASURED AND CALCULATED VALUES USING n = 5 IN EQ. 5.3 FOR RADIAL LINE A AT THE END OF EXCAVATION IN MODEL I.

As can be seen from Figure V-18 displacement gradients were high near the tunnel opening but quickly diminished farther away. This behavior produced some problems in obtaining reasonable numbers when using the approximating functions in the interval from the tunnel wall to the first sensor. In this interval slopes of the functions tended to become unreasonably high, often approaching 200%. Often there were also significant discrepancies in slopes of two different order functions in this interval even though differences between calculated and measure displacements were less than .25 mm (.001 in) (beyond the accuracy of the instrumentation). This latter behavior was a result of the steepness of the curves near the tunnel opening. The slope of a curve is the slope of a line drawn tangent to the curve. The slope of this tangent line equals the tangent of the angle the line makes with reference axes. As the angle approaches 90° a small change in the angle produces a large change in its tangent value. These difficulties were circumvented by ignoring strain values calculated for points between the tunnel wall and the first sensor in each line.

CHAPTER 6

MODEL TEST RESULTS AND DISCUSSION

Introduction And Explanation Of Notation

A total of twelve model tests was performed in which tunnel size, advance rate, and confining pressure were varied. The sand-wax mixture containing .6%CD150/160 and .4% Shaping wax was the model material used for all tests. An unsupported span between the liner and tunnel face equal to one model tunnel radius was maintained for all tests. Table VI-1 is a summary of pertinent model parameters and corresponding prototype values for all tests.

Strains, rather than displacements, were employed to facilitate comparison of deformations in tunnels of different size. In this way a better understanding might be gained of the increase in deformations with increasing tunnel size that is often observed in the field.

Because the models were axisymmetric, data from radial lines A and B could be used to obtain both radial strain, ε_r, and circumferential strain, ε_θ. Face line F yielded axial strain values, ε_z. Derivatives of non-linear curves fit to displacement data provided ε_r and ε_z values. ε_θ equaled radial displacement divided by the tunnel radius. The position of sensors relative to tunnel openings varied somewhat between models and displacement gradients were steep and non-linear. Therefore, for accuracy, strains in all models were compared at points on the sensor lines .4, .8, and 1.3 radii from the final position of the tunnel boundary. These are geometrically similar points in all models at all times during the tests.

TABLE VI-1

Model Test and Prototype Tunnel Parameters

Model				Prototype		
Model No.	Tunnel Diameter cm (in)	Advance Rate cm/hr (in/hr)	Confining Pressure KN/m^2 (psi)	Tunnel Diameter m (ft)	Advance Rate m/hr (ft/hr)	$\frac{\text{Depth of Cover}}{\text{Material Strength}} \left(\frac{P_z}{UC}^*\right)$
I	12.4 4.9	0.8 0.3	576 83.	5. 16.	0.3 1.	2.3
II	12.4 4.9	0.8 0.3	640 93.	5. 16.	0.3 1.	2.6
III	12.4 4.9	0.8 0.3	748 108.	5. 16.	0.3 1.	3.0
IV	12.4 4.9	0.8 0.3	690.100.	5. 16.	0.3 1.	2.8
V	12.4 4.9	0.8 0.3	662 96.	5. 16.	0.3 1.	2.7
VI	12.4 4.9	3.2 1.2	662 96.	5. 16.	1.3 4.	2.7
VII	12.4 4.9	3.2 1.2	576 83.	5. 16.	1.3 4.	2.3
VIII	12.4 4.9	0.8 0.3	518 75.	5. 16.	0.3 1.	2.1
IX	12.4 4.9	0.8 0.3	576 83.	5. 16.	0.3 1.	2.3
X	6.4 2.5	0.8 0.3	576 83.	2.6 8.4	0.3 1.	2.3
XI	19. 7.5	0.8 0.3	576. 83.	7.6 25.	0.3 1.	2.3
XII	19. 7.5	0.8 0.3	518. 75.	7.6 25.	0.3 1.	2.1

*UC (unconfined compressive strength) was used instead of undrained shear strength as reported in the literature because the sand-wax material had a friction angle greater than zero.

Results will be given in terms of ε_r and ε_z values more often than ε_θ values because, for some tests, the scatter in the ε_θ data was often greater than the effect of changed test conditions. The scatter resulted from drift in the reference signal sent to the transmitting sensors. The reference signal would remain constant for the time needed to read a line of sensors, so the effect of the drift was to shift the curve of displacement vs. sensor position up or down by a constant value. Such a shift would not alter the slope of these curves.

In many figures notation designating the point at which a strain was calculated has this form: x-position $\frac{x}{A}$ = . For graphs of results for radial line A and B, this notation means: the number of tunnel radii from the center of the model at which strain is calculated; x is radial distance; A is tunnel radius. For face line F the same notation means: the number of tunnel radii from the final face position at which strain was calculated; x is axial distance; A is tunnel radius.

In the figures in which strain was plotted as a function of time, positive time is the time elapsed after excavation of the model tunnel had been completed. Negative time is the time remaining until completion of excavation.

Strains before excavation was completed from models with different test conditions were compared in plots of strain as a function of tunnel face position. The face position is the distance, expressed in terms of tunnel radii, which the face had yet to advance before excavation was completed.

MODELS I and IX

Models I and IX were duplicate tests. Model I results from radial line B are not presented because sensor B1 was hit by the tunnel liner and displaced. Model IX provided data for line B as well as a check for repeatability of results. Results of Models I and IX reveal aspects of the general deformation pattern of material ahead of an advancing tunnel face. Specifications for the length of the unsupported span, advance rate and confining pressure in these models were developed in Chapter 3 to model a "typical" tunnelling operation in squeezing ground. Thus, results of these tests also provide a standard for comparison with models in which tunnel size or advance rate were changed.

Figures V1-1 to V1-4 are example plots of strain vs. time for Models I and IX. Other plots completing the results from these models are found in Figures C-1 to C-4, Appendix C. Model I ε_r and ε_z strains were within 20% of the magnitude of Model IX ε_r and ε_z strains over a large part of the duration of the tests. By the end of excavation in both models, ε_z strains were about twice as large as ε_r strains at similar points on the sensor lines. At that time the displacement of sensor F1 in both models was about .3 cm (.1 in) while the displacement of the A2 sensors was about .1 cm (.04 in). In the prototype these displacements would scale to 12 cm (5 in) and 4 cm (1.5 in) respectively. As shown in Figure I-3, Chapter 1, in a field study in a 4.3 m (14 ft) diameter tunnel in London clay, cumulative displacements at a point near the face were 1.7 cm (.7 in). This was a stable tunnel, but in a comparison the model represented a tunnel in which considerably more deformation had occurred.

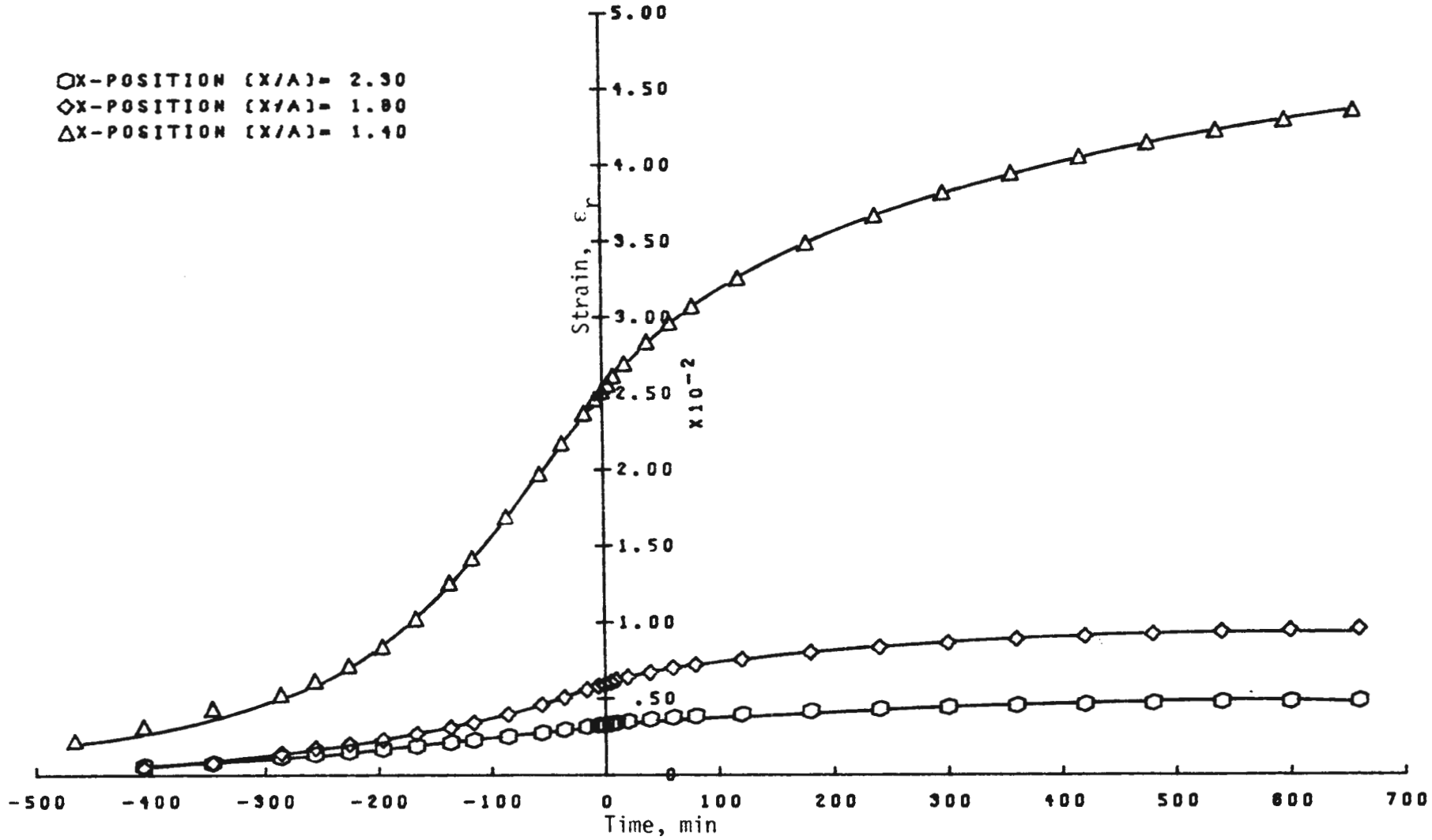

FIGURE VI-1 ε_r VS TIME AT THREE POSITIONS ON RADIAL LINE A, MODEL I

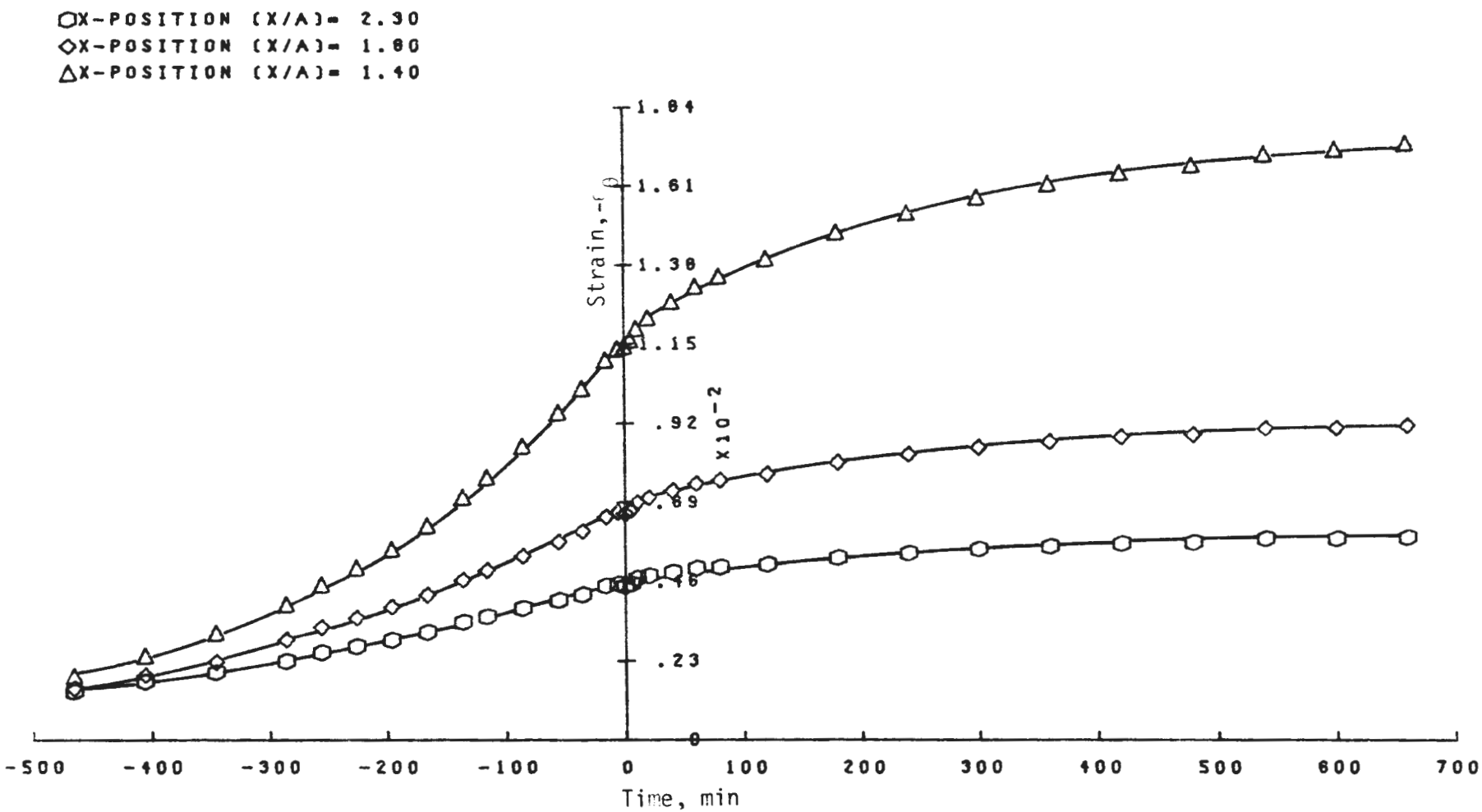

FIGURE VI-2 ϵ_θ VS. TIME AT THREE POSITIONS ON RADIAL LINE A, MODEL I

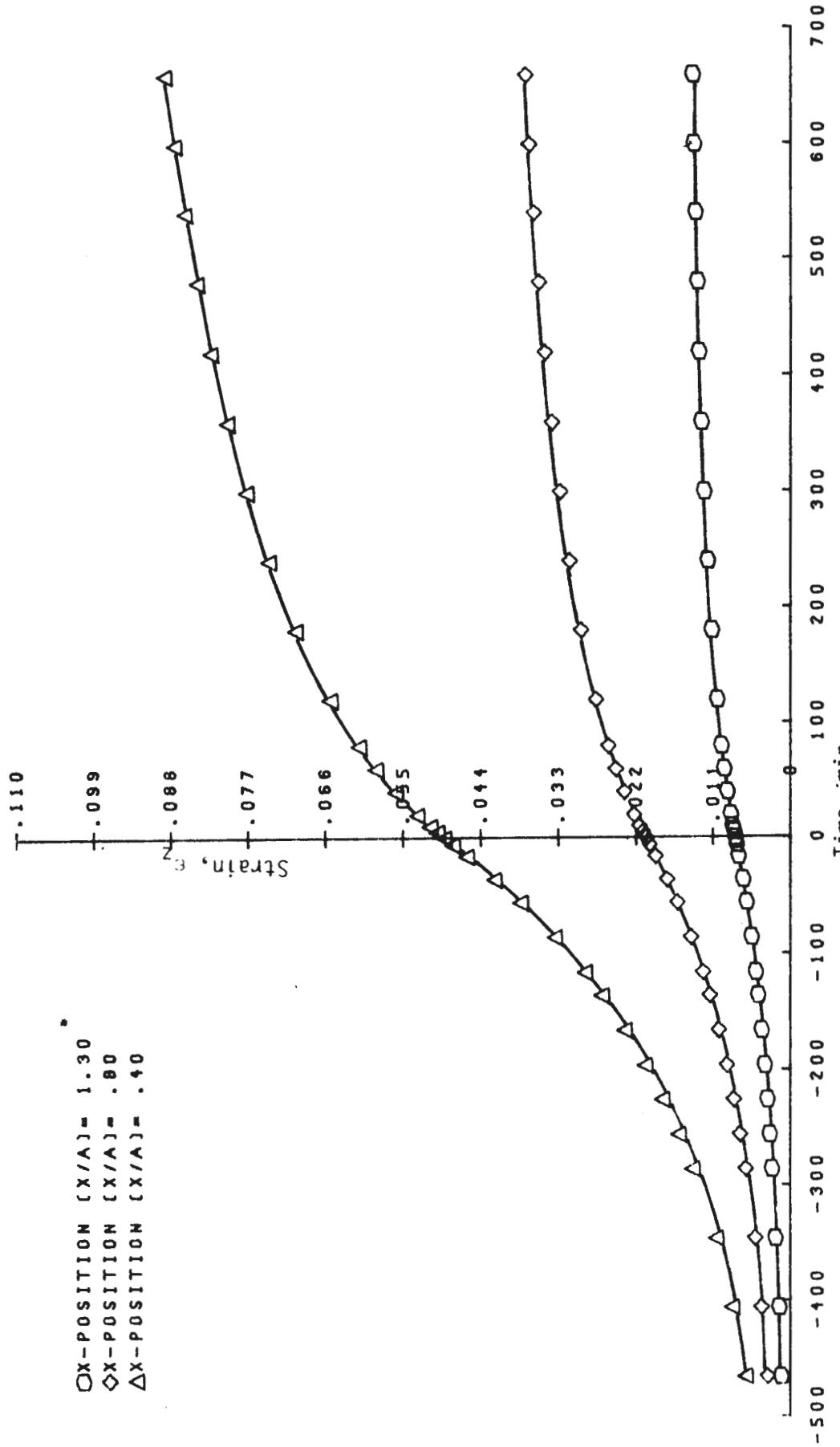

FIGURE VI-3 ε_z VS. TIME AT THREE POSITIONS ON FACE LINE F, MODEL I

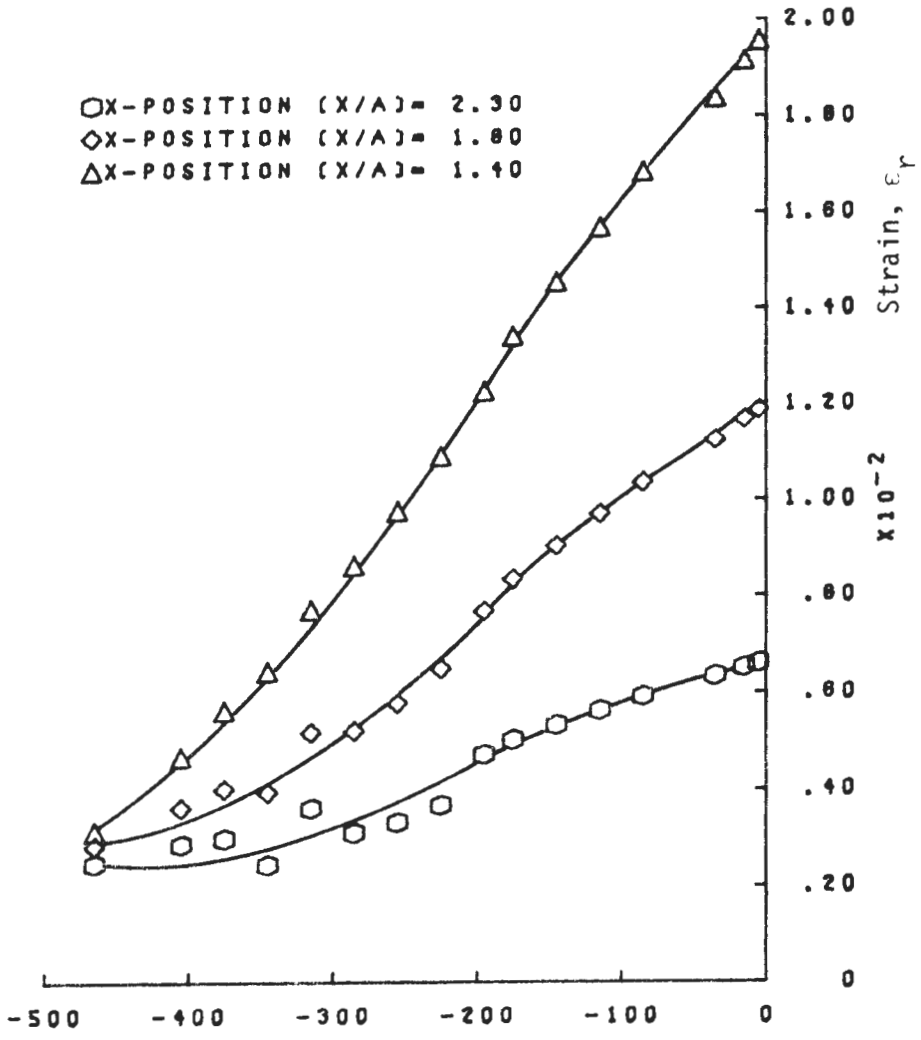

FIGURE VI-4 ε_r VS. TIME AT THREE POSITIONS ON RADIAL LINE B, MODEL IX

The value of ε_θ at sensor A1 is almost the same in both Model I and IX but the interpolated value at position $\frac{x}{A} = 1.4$, near sensor A2, is considerably larger in Model IX than in Model I. This means that proportionally more of the total displacement took place near the tunnel wall in Model I than in Model IX.

In both Models I and IX the strain rate at position $\frac{x}{A} = 1.4$ on line A became constant soon after the face had passed the sensor line. Associated with the constant strain rate, as seen in Figure VI-1, was a marked divergence in results of line A between ε_r values at position $\frac{x}{A} = 1.4$ and ε_r values only .4 radius farther away from the model center. This divergence meant that movement of sensor A2 relative to A3 was considerably greater than displacement of A3 relative to A4. Korbin (1975) found that divergence in the relative displacement of sensors indicated material failure. Also, because strains in the model near the tunnel wall were larger than strains of samples of the same material in triaxial tests with comparable confining pressure, it was concluded that by the end of excavation the material around the tunnel opening was in a failed condition.

In Figure VI-4 the effect of the approaching shield on deformations of the ground in Model IX can be seen. About 280 minutes before excavation ended, line B was positioned just beyond the middle of the unsupported span. Up to this point radial strain rates on line B had been increasing. However, as the support approached closer, strain rates became slightly decreased or became almost constant in magnitude.

At the time excavation was complete (time = 0) line A was in the middle of the unsupported span. Thus, in the time interval from -250 minutes to 0 minutes (using the notation for time as in Figure VI-1) line A was in the same position relative to the shield as line B had been in the time interval from -500 minutes to -250 minutes. If the deformation behavior of the model had been in equilibrium with the tunnel advance rate, the strains on line A in the interval from -250 to 0 minutes should have been equal to the strains on line B in the interval from -500 to -250 minutes. However, the average rate of strain accumulation at measurement positions on line A was about twice the average strain rate for similar points on line B. Perhaps the stronger, stiffer material in the front of the model had not allowed an equilibrium state to develop by the time the face had passed line B.

Immediately after excavation stopped, strain rates throughout Model I began to decrease and were reduced significantly even within the 700 minutes of deformations shown in Figures VI-1 to VI-3. As illustrated in Figure I-1, after excavation, anticipated deformation behavior was a period of almost constant rate of deformation followed by accelerated deformations leading to collapse or failure of the tunnel. However, an accelerating strain rate did not develop within 9000 minutes after excavation in Model I. At that time an attempt was made to increase the model confining pressure by 30% but collapse occurred while the pressure was being increased. Model IX was depressurized immediately after excavation was stopped and disassembled in an attempt to locate distinct failure surfaces which might have formed during excavation; but no clearly defined surfaces were found.

MODELS II, III, IV, V, VIII

The results of these models provided information on the effect of varying the ratio of depth of cover to material strength on ground behavior ahead of an advancing tunnel face. They also led to a better understanding of the mechanism of model tunnel failure and collapse. Models II, V, and VIII were used further for comparison in the analysis of size and rate effects on stand-up time behavior.

The initial confining pressure in Model II was 10% higher than the confining pressure in Model I. Figure VI-5 summarizes the strains on line F of Model II up to 700 minutes after excavation stopped. More complete results are given in Appendix C, Figures C-5 and C-6. In general, the deformation patterns of Models I, IX, and II were the same except deformations were larger in Model II. By the end of excavation at .4 radius from the tunnel boundary, Model II strains (ε_r and ε_z) were about 30% to 40% higher than in Models I and IX. Displacements at sensors A1 B1 and F1 were from 23% to 50% higher in Model II. Some difference in behavior was shown by line B which in Model II did not show a decrease in slope as the shield approached.

After 8000 minutes low deformation rates indicated Model II had attained long term stability, so the confining pressure was raised by 10% to 690 KN/m^2 (100 psi). The tunnel was still stable 15000 minutes later after another 10% increase in pressure. The pressure was then increased a third time to 806 KN/m^2 (117 psi). An equipment malfunction terminated the test after 3000 minutes though displacement rates indicated stability had not yet been attained.

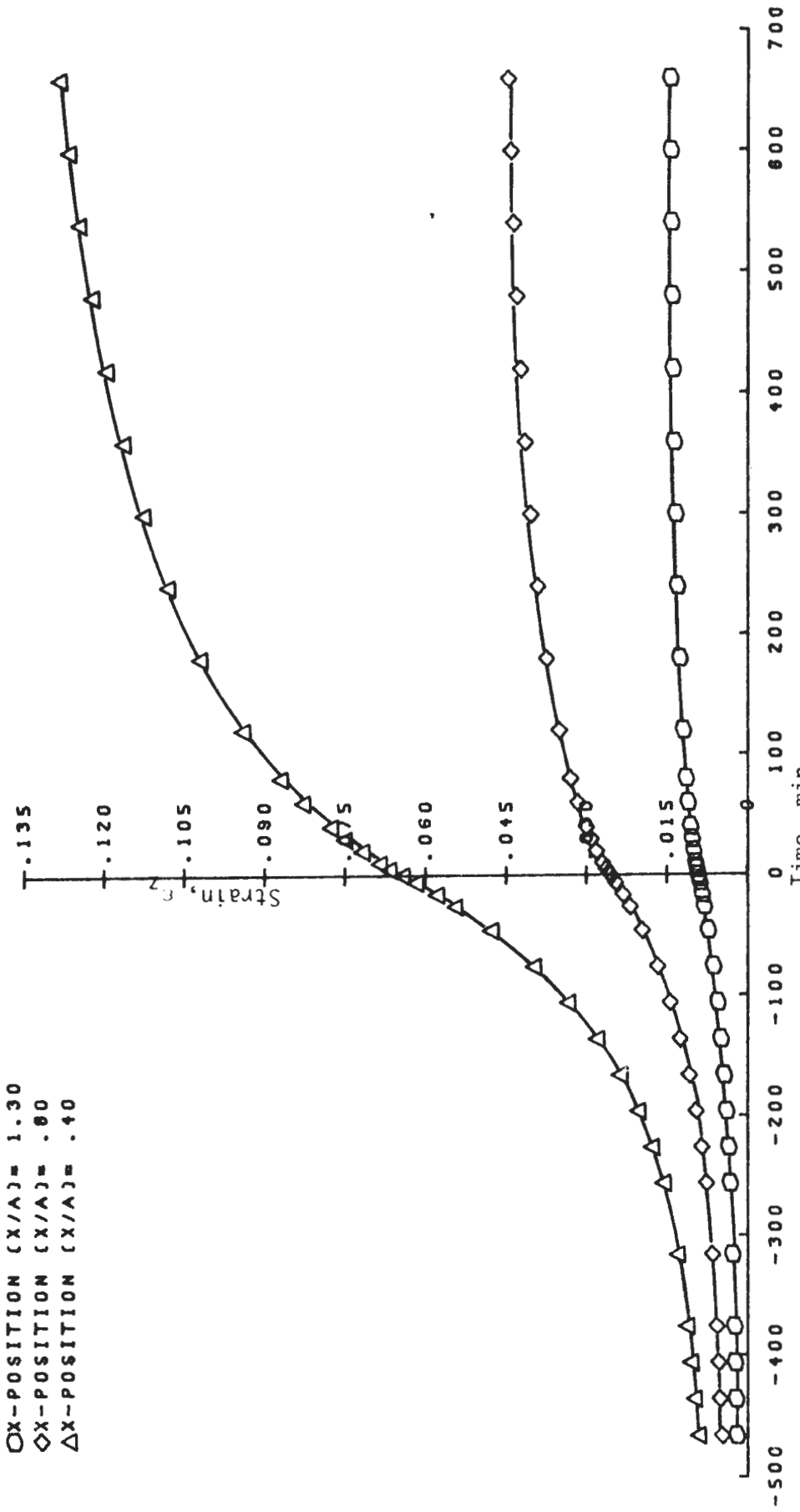

FIGURE VI-5 ε_z VS. TIME AT THREE POSITIONS ON FACE LINE F, MODEL II.

Model III was pressurized to 748 KN/m^2 (108 psi), equal to Model II confining pressure after the second pressure increase. This model tunnel collapsed during excavation when the face was still one radius from its final position. No numerical results are given because the failure occurred too far from most of the instrumentation. The collapse was catastrophic, filling the tunnel and stalling the excavator. Upon disassembly, cracks which extended to the model boundary were noted. Also, the intense deformations had the effect of crushing the sand-wax material; leaving it with only a little cohesion.

A confining pressure of 690 KN/m^2 (100 psi) was applied to Model IV. This pressure equaled the Model II confining pressure after the first increase. The Model IV tunnel face had advanced to within one half radius of its final position before catastrophic failure occurred. The mode of collapse was the same as in Model III, and since instrumentation was near the failed area, a record of pre-collapse behavior was obtained.

One hundred fifty minutes before collapse the Model IV tunnel face had advanced 1.3 cm (.5 in) beyond line B. At this time ε_r at position $\frac{x}{A}$ = 1.4 on line B was about 1.% or 40% higher than ε_r at the same point on line B in Model II when the face was at the same position. Based on previous results this was a reasonable increase in strain compared to the increase in pressure. However, ninety minutes later after the face had advanced .2 radius, ε_r at $\frac{x}{A}$ = 1.4 on line B had increased to 3.4% or 4 1/2 times the strain in Model II at the same time and place. At this time ε_r and ε_z near sensors A1 and F1 were .8% and 1.7% respectively, almost two times the strain at similar points in Model II. Thirty minutes before collapse the displacement

at sensor B1 was .5 cm (.2 in), having increased 150% in thirty minutes. This scaled to 20 cm (18 in) of movement in a 15 m (16 ft) prototype tunnel. Also at this time, the smallest measurable strain (.2 %) was within 11 cm (4.5 in) of the model boundary. In summary, the Model IV tunnel progressed from stability to collapse within 150 minutes during a face advance of .3 radius.

These results could be physically interpreted as follows: as the region of failed material around the tunnel enlarged, stress was redistributed to more competent material further away from the opening. Collapse became imminent when the region of failed material had increased to such an extent that stress was being redistributed to material at or near the model boundary.

The confining pressure on Model V was 5% higher than in Model II and 5% lower than in Model IV. A comparison of Model V results as in Figure VI-6 (see also Appendix C, Figure C-7) with results of Model I, IX and II shows the behavior of Model V to be of the same general form but of greater magnitude. At the end of excavation Model V radial and axial strains were from 70% to 85% greater than Model II strains. Radial strain rates continued to increase up to the end of excavation, when the shield bead had just passed line B. Passage of the bead left a void between the liner and the tunnel wall. Figure Vl-7 clearly shows how the ground moved into the void and came to rest against the liner. Though strain rates were higher for a longer period of time in Model V than in models at lower pressures, it did not collapse during the duration of the test.

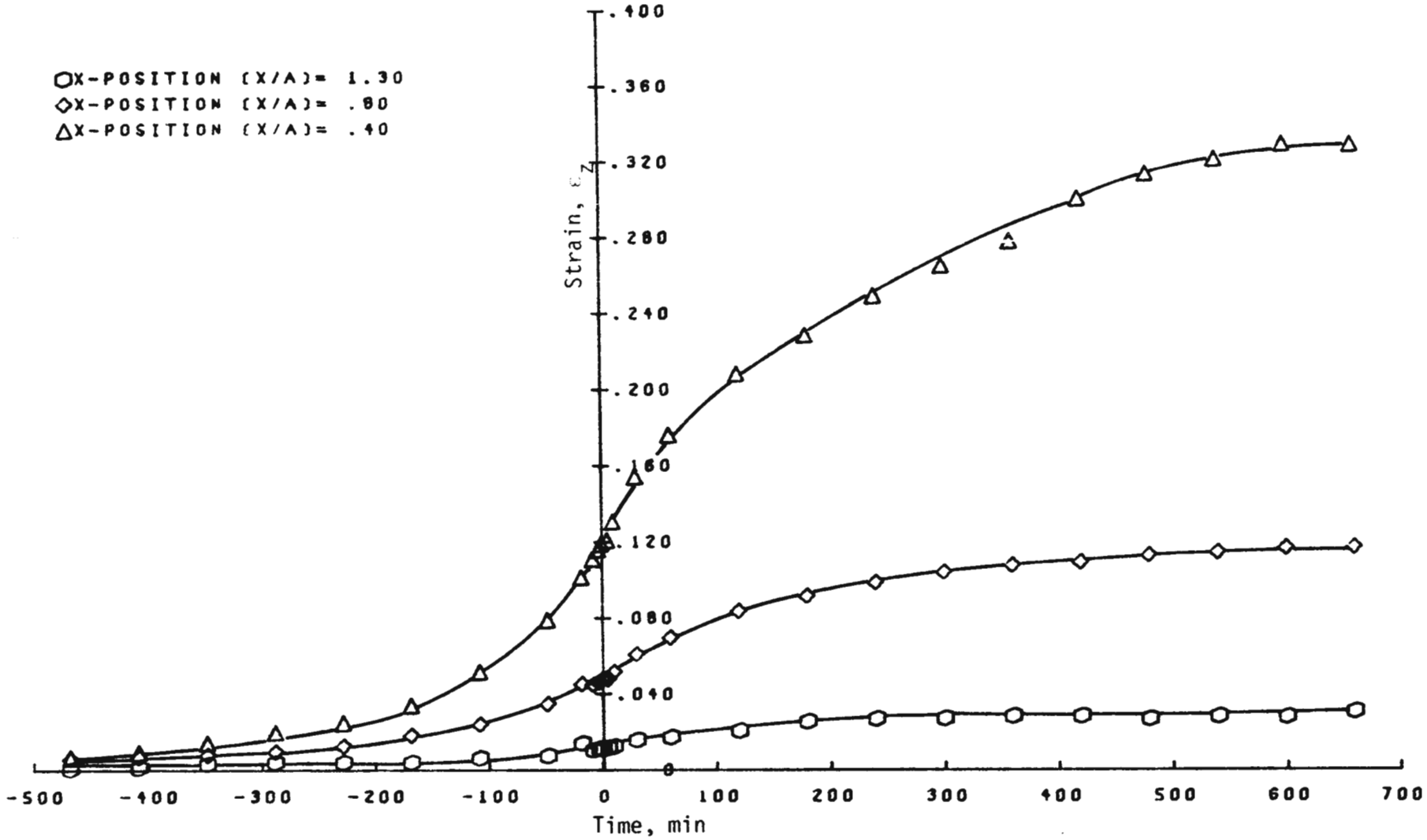

FIGURE VI-6 ε_z VS. TIME AT THREE POSITIONS ON FACE LINE F, MODEL V

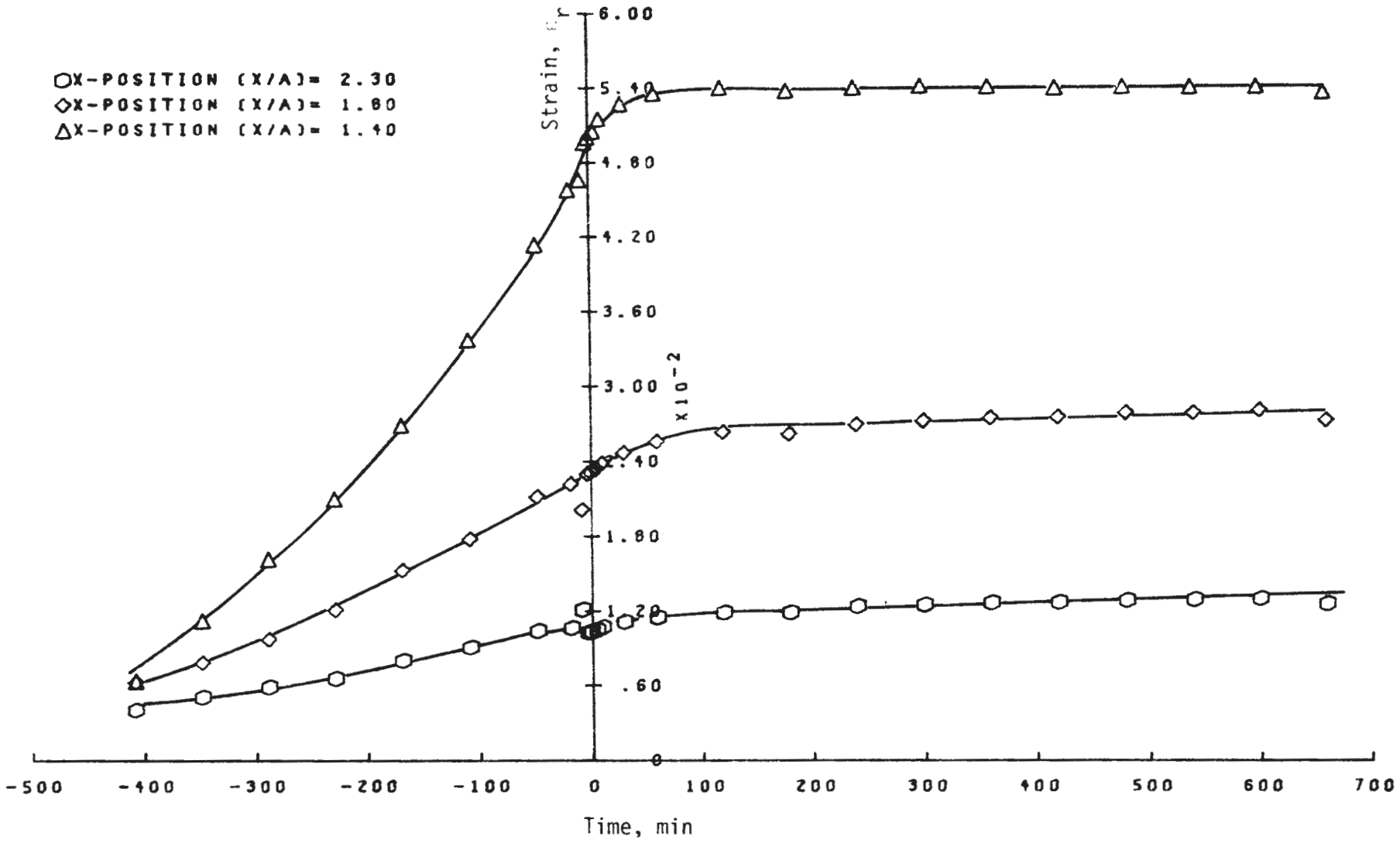

FIGURE V1-7 ε_r VS. TIME AT THREE POSITIONS ON RADIAL LINE B, MODEL V

In Model VIII the confining pressure of 518 KN/m^2 (74 psi) was 10% less than the pressure in Models I and IX. This lower pressure is reflected, as seen in Figure VI-8 (see also Appendix C, Figures C-8 to C-11), by lower strains at the end of excavation and lower strains after excavation stopped. Line A strain rates continued to increase up to the end of excavation instead of becoming constant as in models at higher pressures. Line B strain rates changed from increasing to decreasing or almost constant when the shield was about .6 radius away. In Models I and IX this change occurred when the shield was closer to line B. Model VIII also exhibited less divergence in plots of ε_r vs. time for line A. A ratio between the strain at position $\frac{x}{A} = 1.4$ and the strain at $\frac{x}{A} = 1.8$ on line A can be used to compare the amount of divergence in Models VIII and II. In Model II this ratio equaled 3.4; for Model VIII it equaled 2.5.

Figure VI-9 is a plot of the radial and axial strains at the end of excavation .4 radius from the tunnel wall in Models I, II, V, VIII, and IX as a function of the ratio $\frac{P_z}{UC}$ for the models. P_z is the confining pressure; UC is the model material unconfined compressive strength which was constant in all tests. Tunnel sizes and advance rates were the same in all these models. Within data scatter the increase in strain varied linearly with the increase in confining pressure up to $\frac{P_z}{UC} = 2.55$. Beyond this point, as shown by Model V, a small increase in pressure produced a much larger increase in strain than an extrapolation of results at lower pressures would predict. Radial strains on line B of Model V were greater at the end of excavation than the line B radial strains in Model IV sixty minutes before collapse. Yet, after excavation stopped deformation rates continuously decreased,

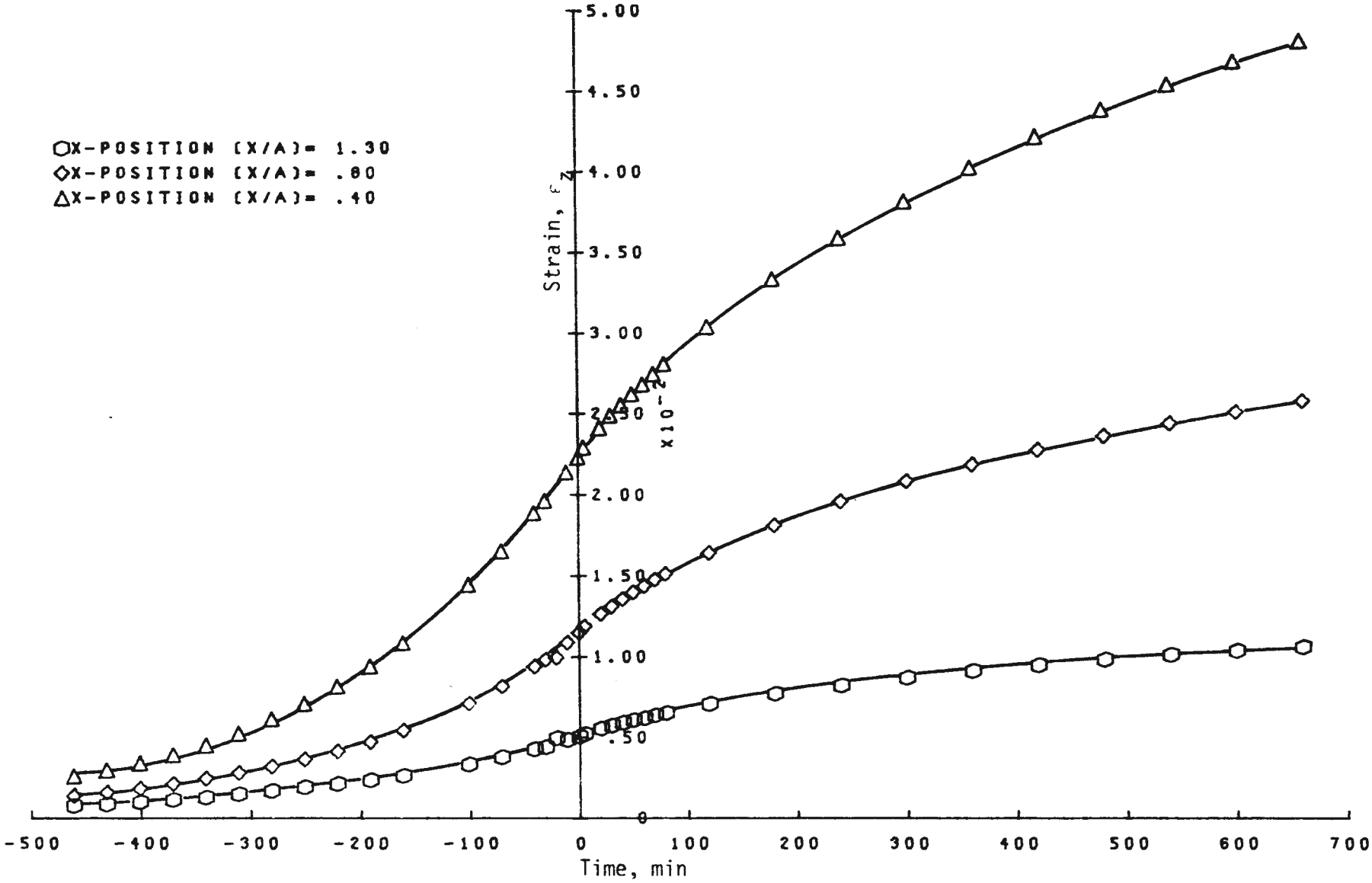

FIGURE VI-8 ε_z VS. TIME AT THREE POSITIONS ON FACE LINE F, MODEL VIII

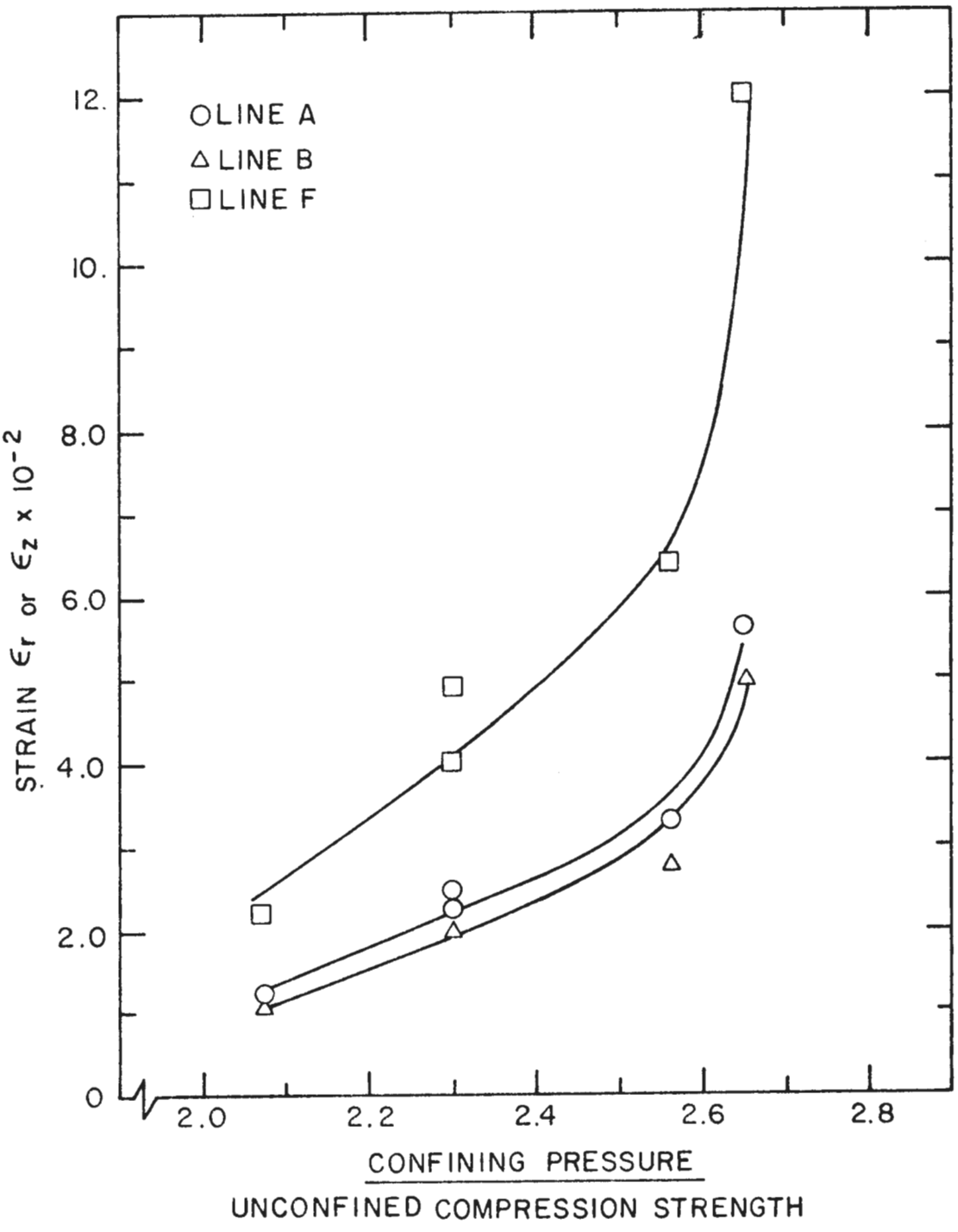

FIGURE VI-9 EFFECT OF CONFINING PRESSURE ON MAGNITUDE OF STRAINS. STRAINS CALCULATED AT END OF EXCAVATION .4 RADII FROM TUNNEL BOUNDARY.

leading to apparent long term stability. This behavior was common to all tests, including those yet to be discussed, which did not fail during excavation of the tunnel.

These results showed that the development of deformation patterns leading to instability in the models was affected most by the process of material removal. Deformations accumulated after excavation did not have a significant effect on the stability of the models.

When collapse did occur in the models it resulted from interaction of the model boundary and the region of deformed and failed material around the tunnel. Part of the deformations seen in Model V were also due to this interaction. Since a model boundary does not represent any prototype characteristic, the model collapses were not true stand-up time failures. If the model boundary had not been present, collapse would have been averted at model confining pressures by the continued redistribution of stresses farther away from the tunnel boundaries. The ground would react to stress redistribution by continuously reducing the diameter of the tunnel but collapse would not occur as long as the failed material around the tunnel maintained enough strength to overcome gravity and restrain it from falling out of the roof.

MODELS VI, VII, X, XI, XII

In these models the effects of variations of tunnel size and advance rate on tunnel deformations and stand-up time were studied. Based on results of the previous models, differences in behavior during model tunnel excavation were considered most important. To aid in

describing the size and advance rate effect on deformations during excavation, a strain rate factor, F_{sr}, was defined as in the following expression

$$\frac{\bar{\dot{\varepsilon}}_{mq}}{\bar{\dot{\varepsilon}}_{ms}} = F_{sr} \frac{A_{rmq}}{A_{rms}}$$

where m is the model number and q and s refer to quicker or slower advance rates. The ratio, A_r, of advance rate to tunnel radius expressed the advance rate in terms of equivalent number of tunnel radii advanced per unit time. $\bar{\dot{\varepsilon}}$ is the average strain rate in models mq and ms before excavation stopped and was defined as

$$\bar{\dot{\varepsilon}} = \frac{\varepsilon_f - \varepsilon_i}{t_f - t_i}$$

where i and f refer to initial and final values. To establish initial values (see Figure VI-11), the distance in tunnel radii (nr) to the final face position from the point at which either strain first began to accumulate or the final unsupported period began was determined for each of the two models being compared. As shown in Figure VI-10 the unsupported period is the time, in a continually advanced tunnel, that an element remains unsupported. In the models, the unsupported period corresponded to the time needed to advance the face a distance equal to one tunnel radius. In Figure VI-11, if n = 1, $A_r$nr = unsupported period. The minimum value of the quantity nr was determined for the two models being compared and this value was used in each to find the face position at which to calculate initial values of strain

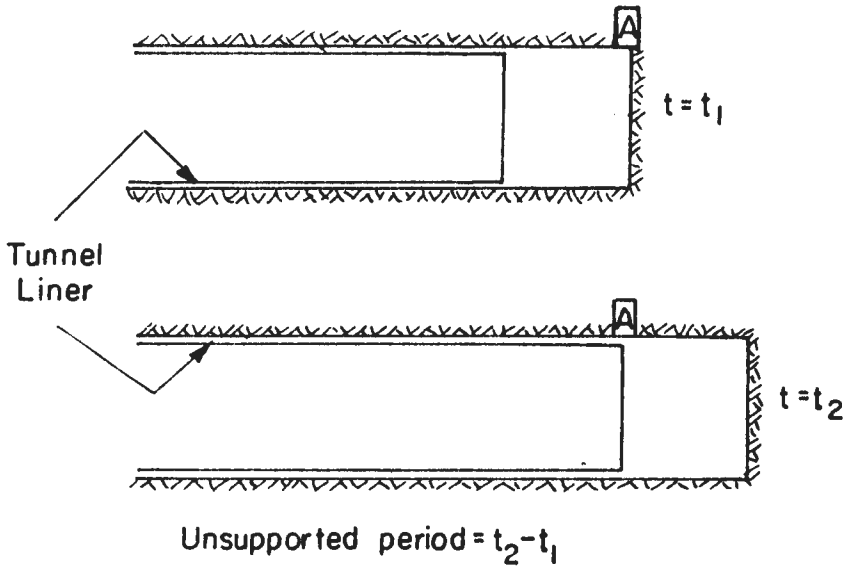

FIGURE V1-10 DEFINITION OF UNSUPPORTED PERIOD. ELEMENT A FIRST EXPOSED AT TIME t_1 AND FINALLY SUPPORTED AT TIME t_2.

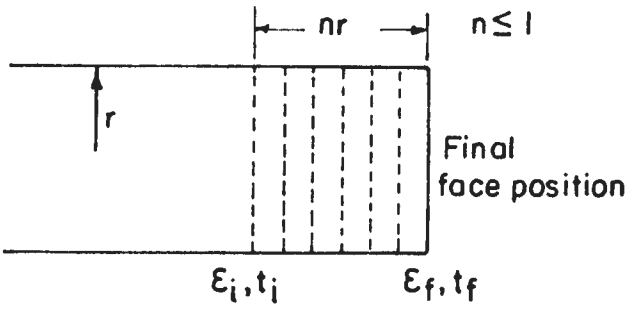

FIGURE V1-11 DETERMINATION OF FACE POSITION AT WHICH INITIAL VALUES OF STRAIN TAKEN FOR CALCULATION OF F_{sr}. DOTTED LINES REPRESENT FACE POSITIONS PRIOR TO COMPLETION OF EXCAVATION.

and time. Thus, the quantity F_{sr} relates the change in average strain rates between two models to the change in advance rates as expressed by A_r. A value of $F_{sr} = 1$ means a proportional change in A_r produced an equal proportional change in average strain rate.

Effects of tunnel size and advance rate changes on stand-up time in the models during excavation were expressed by a stand-up time factor, T_{st}, which is the time to reach a prescribed strain divided by the length of the unsupported period. If T_{st}, < 1, the stand-up time, or time to reach a given strain in the tunnel, was less than the unsupported period.

The advance rate of the tunnel in Model V was about .3 cm/hr (1.2 in/hr), or about four times the advance rate in Model VI. Otherwise test conditions in the two models were equal. (Comparitive test conditions are summarized in Table VI-2). As shown in Figure VI-12 (see also Appendix C, Figures C-12 and C-13), strain rates in Model VI were higher before excavation was complete than in Model V (Figure VI-6). However, as shown in the following analysis, higher strain rates did not lead to a greater accumulation of strain during the time interval of one unsupported period. For line A of Models V and VI, average strain rates were

$$\dot{\bar{\varepsilon}}_{vs} = 2. \times 10^{-4} \%/\text{min} \ , \ \dot{\bar{\varepsilon}}_{vlf} = 4.2 \times 10^{-4} \%/\text{min}$$

and advance rates were

$$A_{vs} = .14/\text{hr} \text{ and } A_{vlf} = .5/\text{hr}$$

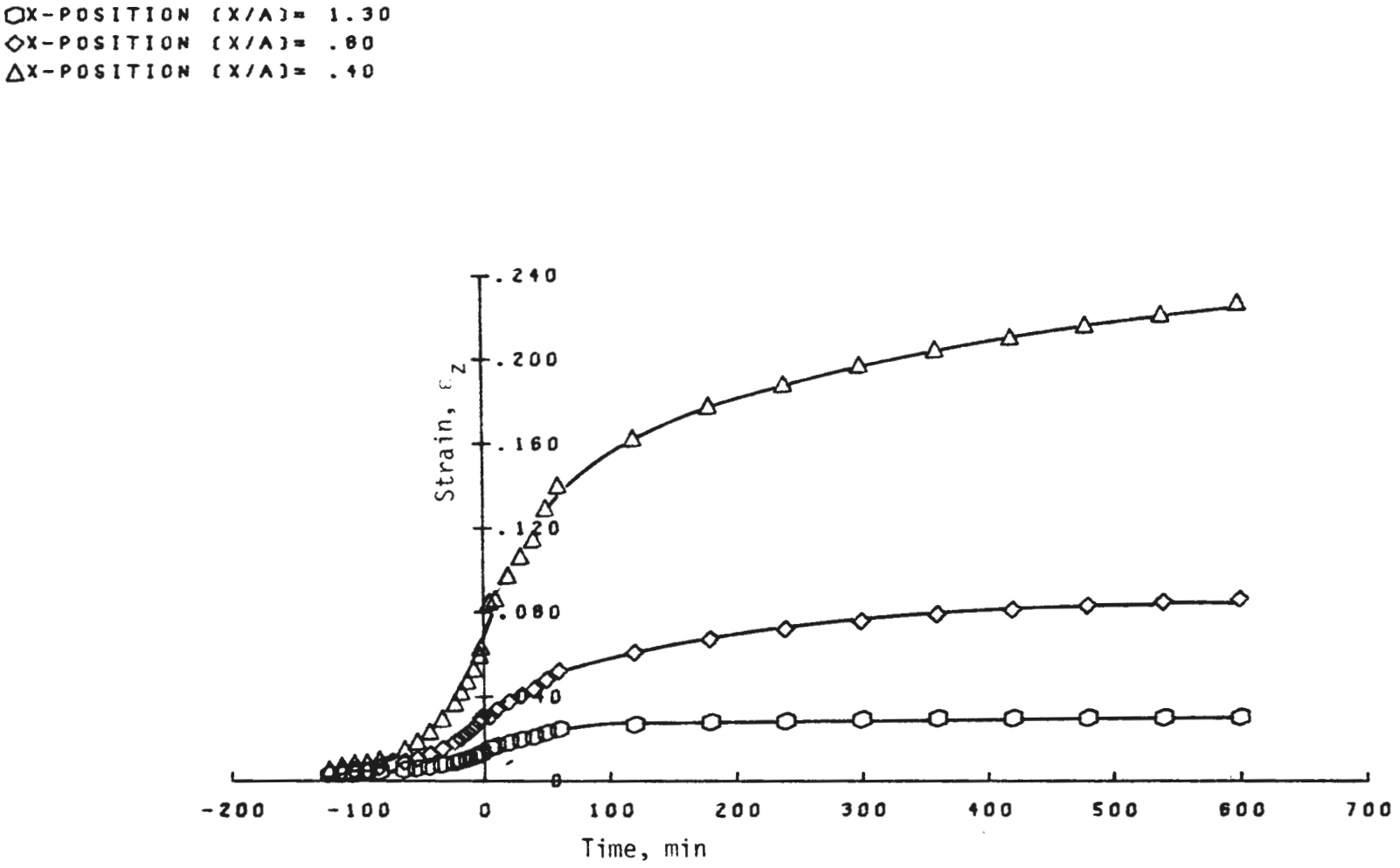

FIGURE V1-12 ε_z VS. TIME AT THREE POSITIONS ON FACE LINE F, MODEL V1.

Thus F_{sr} = .6 for a comparison of strain rate values at position $\frac{x}{A}$ = 1.4 on line A in both models. In comparison at similar points on all three sensor lines, F_{sr} varied from .5 to .6 (see Table VI-2). This means that a factor of 4 increase in advance rate produced only a factor of 2 to 2.4 increase in average strain rates. Since, by definition in this comparison, $t_f - t_i$ in Model VI equaled 1/4 $(t_f - t_i)$ in Model V, and $\varepsilon = \dot{\varepsilon}\Delta t$, the strain at the end of excavation in Model VI was less than in Model V. As exemplified by Figure VI-13 for line F (see all Appendix C, Figures C-14 and C-15), the increase in advance rate by a factor of four yielded a decrease in strain of 45% to 55% at the measurement positions.

Figure VI-13 also shows that the axial strain at $\frac{x}{A}$ = .4 on line F in Model V 72 minutes before excavation ended was equal to ε_z at the same position in Model VI at the end of excavation. The stand-up time factor, T_{st}, of line F for Model V as compared to Model VI was therefore

$$T_{st} = \frac{441 - 72}{441} = .8$$

where 441 minutes was the unsupported period in Model V. For all three sensor lines T_{st} varied from .6 to .8 (see Table VI-2). Thus, for similar positions on the sensor lines, at a time 20% to 40% before the end of excavation of Model V the strains were already equal to the strains at the end of excavation in Model VI.

Results of Model VII, line F at $\frac{x}{A}$ = .4 are compared with results of Models I and IX at a similar point in Figure VI-14. Results of line A and B comparisons are in Appendix C, Figure C-16 and C-17.

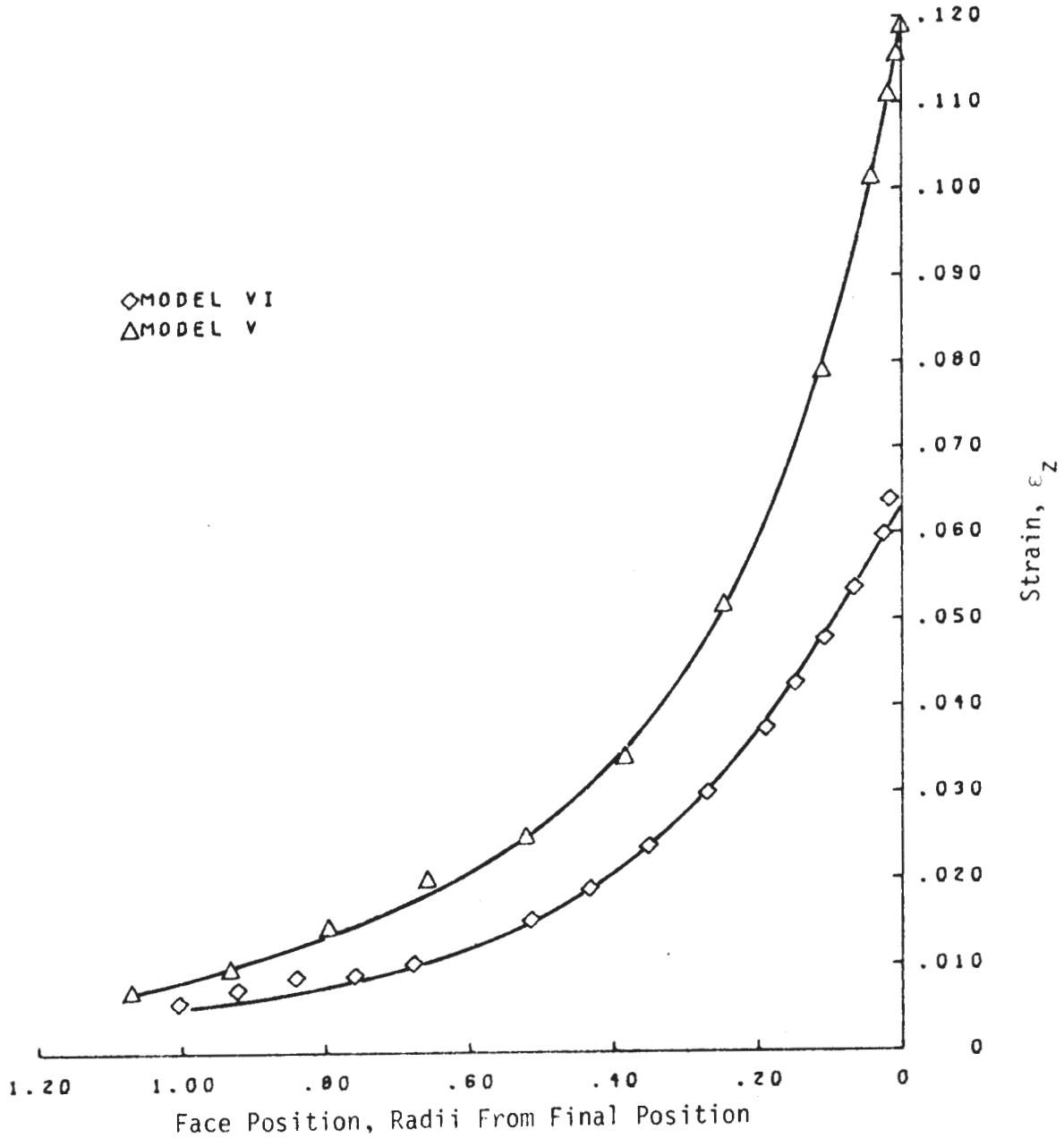

FIGURE VI-13 COMPARISON OF ε_z IN MODELS V AND VI ON LINE F AT POSITION $\frac{x}{A} = .4$

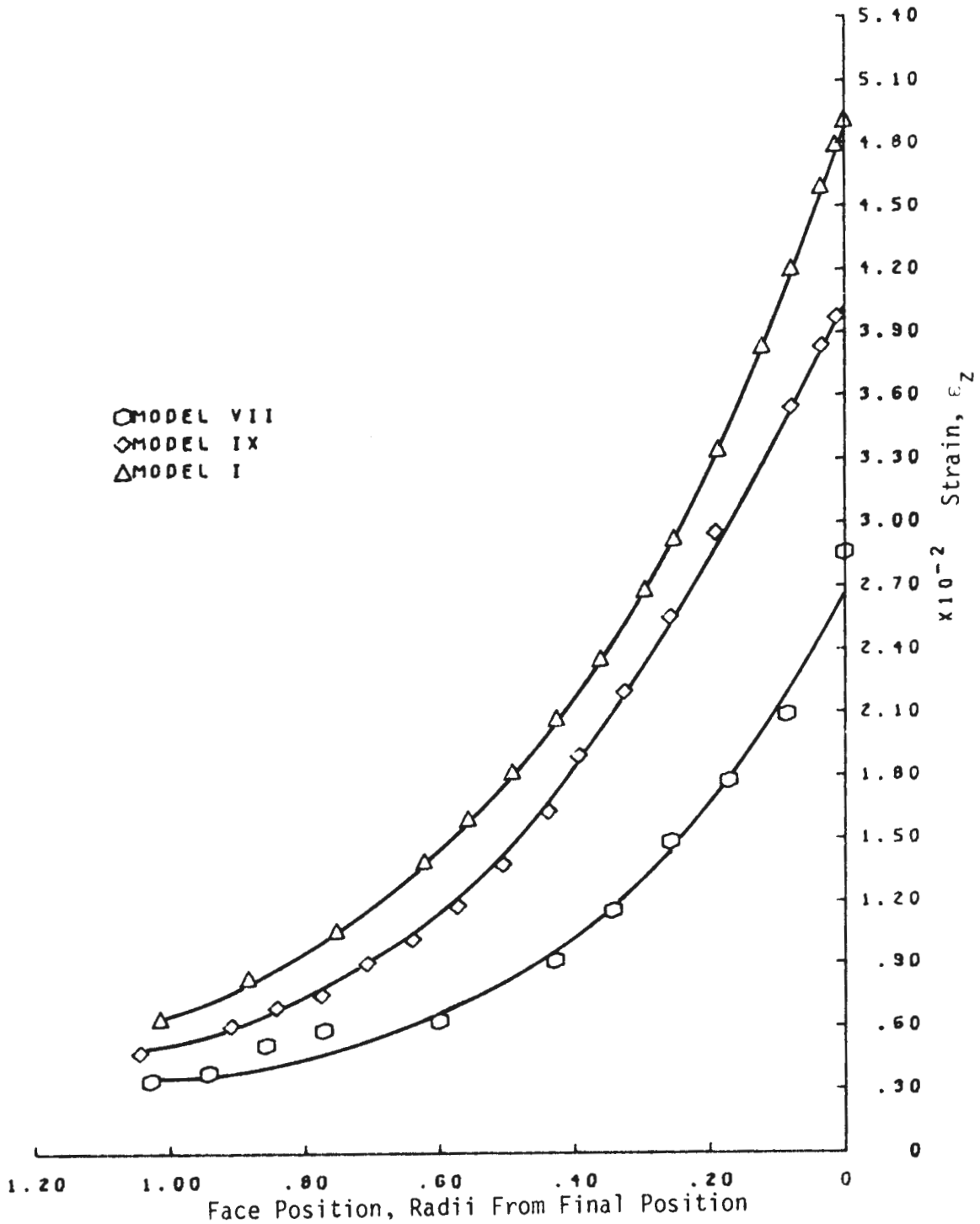

FIGURE VI-14 COMPARISON OF ε_z IN MODELS VII, I AND IX ON LINE F AT POSITION $\frac{X}{A} = .4$

As shown in Table VI-2, values of F_{sr} varied from .7 to .9 for the three sensor lines and values of T_{st} varied from .8 to .9. Correspondingly, the strains at the end of excavation at similar points on the sensor lines were reduced by 20% to 48%. The higher post excavation strain rate as shown in Figure VI-15 (see also Appendix C Figures C-18 and C-19) caused the total strain at some points in Model VII to exceed the total in Models I and IX. However, the greater magnitude of strain after excavation did not affect stability of the model. A comparison of the results of Models V vs. Model VI and of Models I and IX vs. Model VII shows that an increase in excavation rate had more of an influence on deformation patterns at the higher confining pressure. Model V was closer to collapse than Model I and IX, consequently the increase in excavation rate had a stabilizing influence on the unstable conditions.

The tunnel of Model X was about one half the diameter of the Model I and IX tunnels but the confining pressure and advance rates were equal. A decrease in displacement at sensors A1, B1, and F1 of about 75%, 85%, and 80% respectively resulted from the size decrease. In the prototype 2.4 m (8 ft) diameter tunnel, displacements at similar points would be only 1. cm (.4 in), .8 cm (.3 in), and 2. cm (.9 in). A true size effect exists only if the strains are different at geometrically similar positions in two different sized tunnels. Figure VI-16 is a plot of axial strain vs. time for Model X, line F, and Figure VI-17 compares axial strain on line F at $\frac{x}{A} = .4$ in Models X, I and IX up to the end of excavation (Complete Model X results are in Appendix C, Figures C-20 to C-23). A reduction in

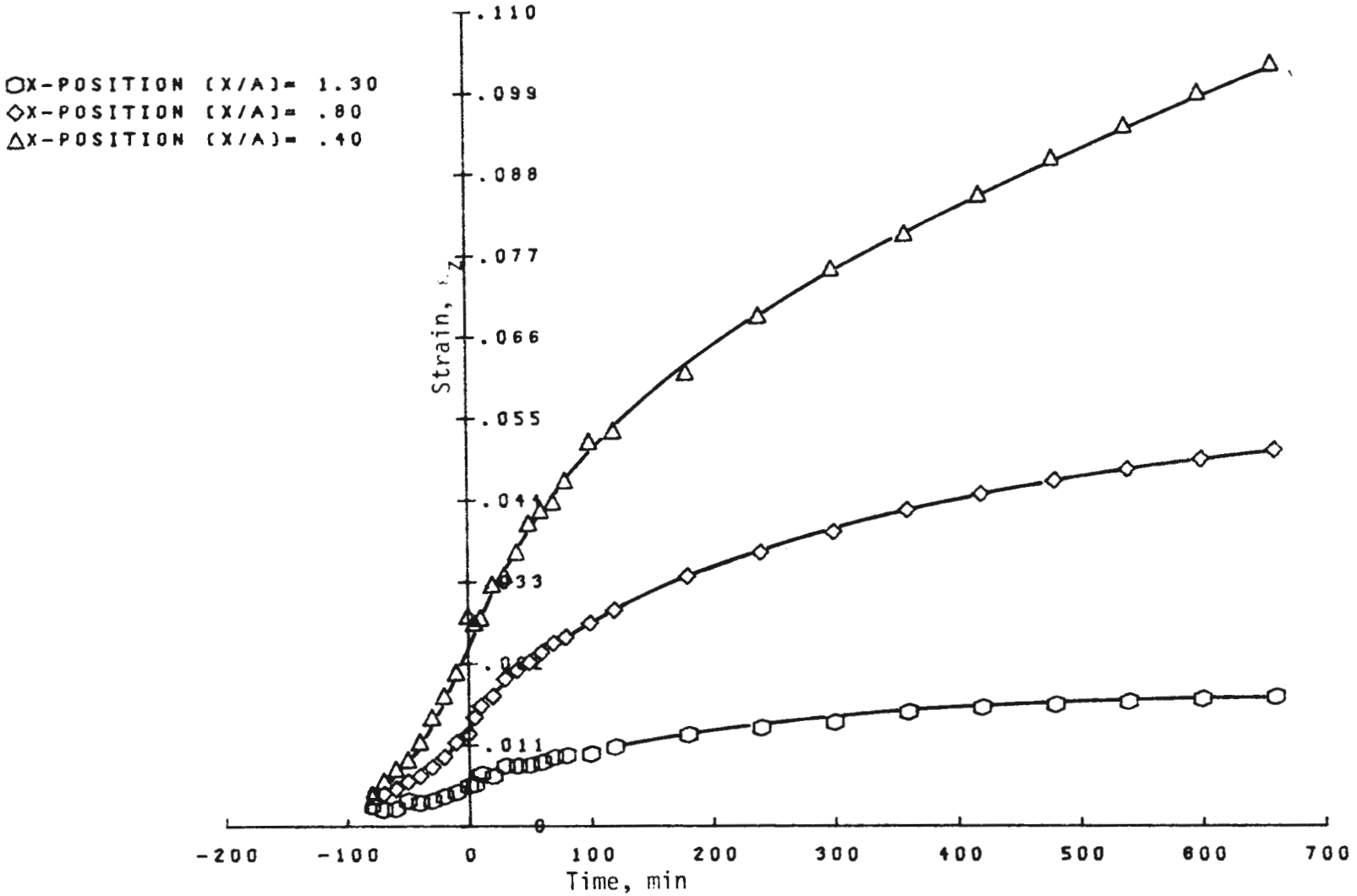

FIGURE V1-15 ε_z VS. TIME AT THREE POSITIONS ON FACE LINE F, MODEL V11

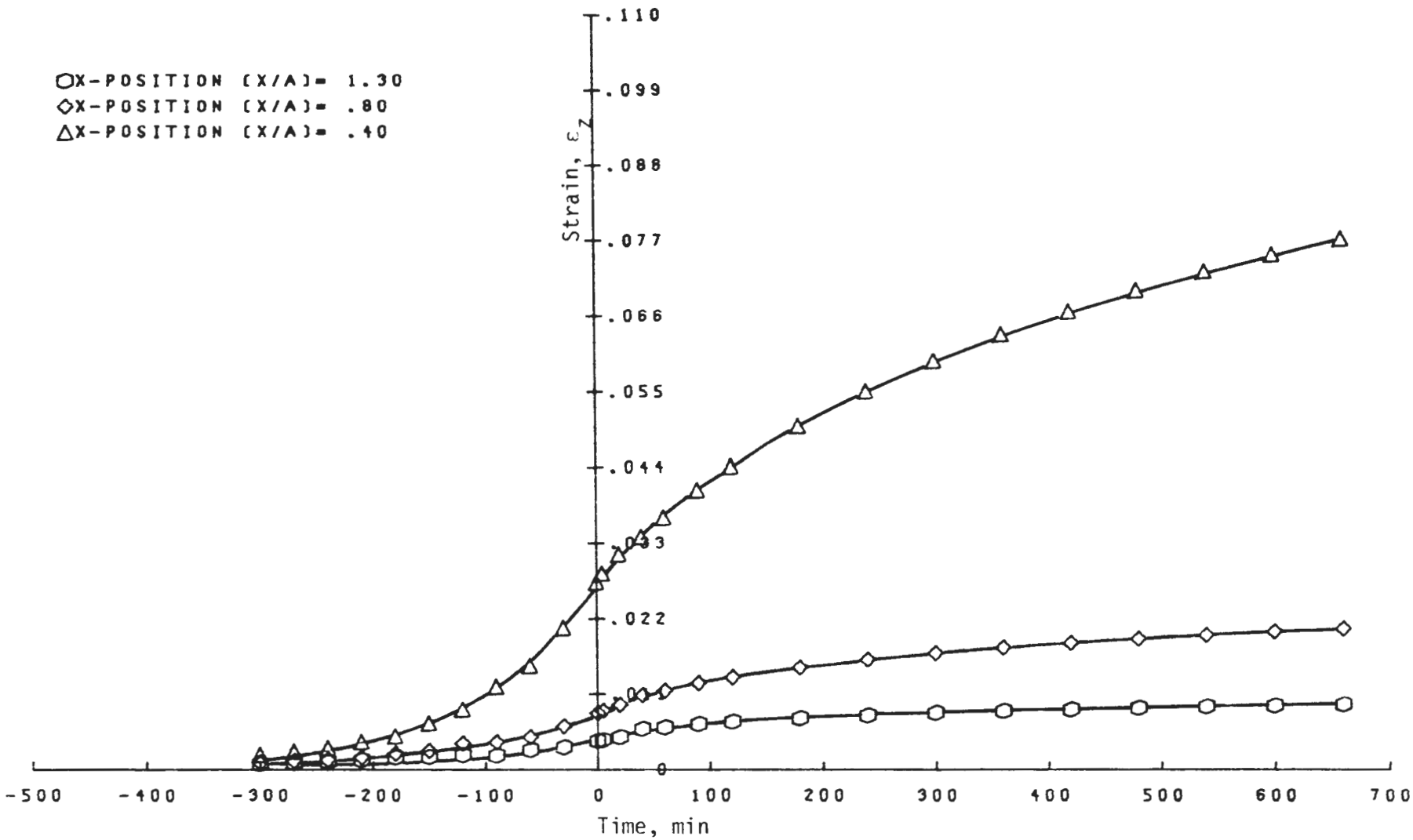

FIGURE VI-16 ε_z VS. TIME AT THREE POSITIONS ON FACE LINE F, MODEL X

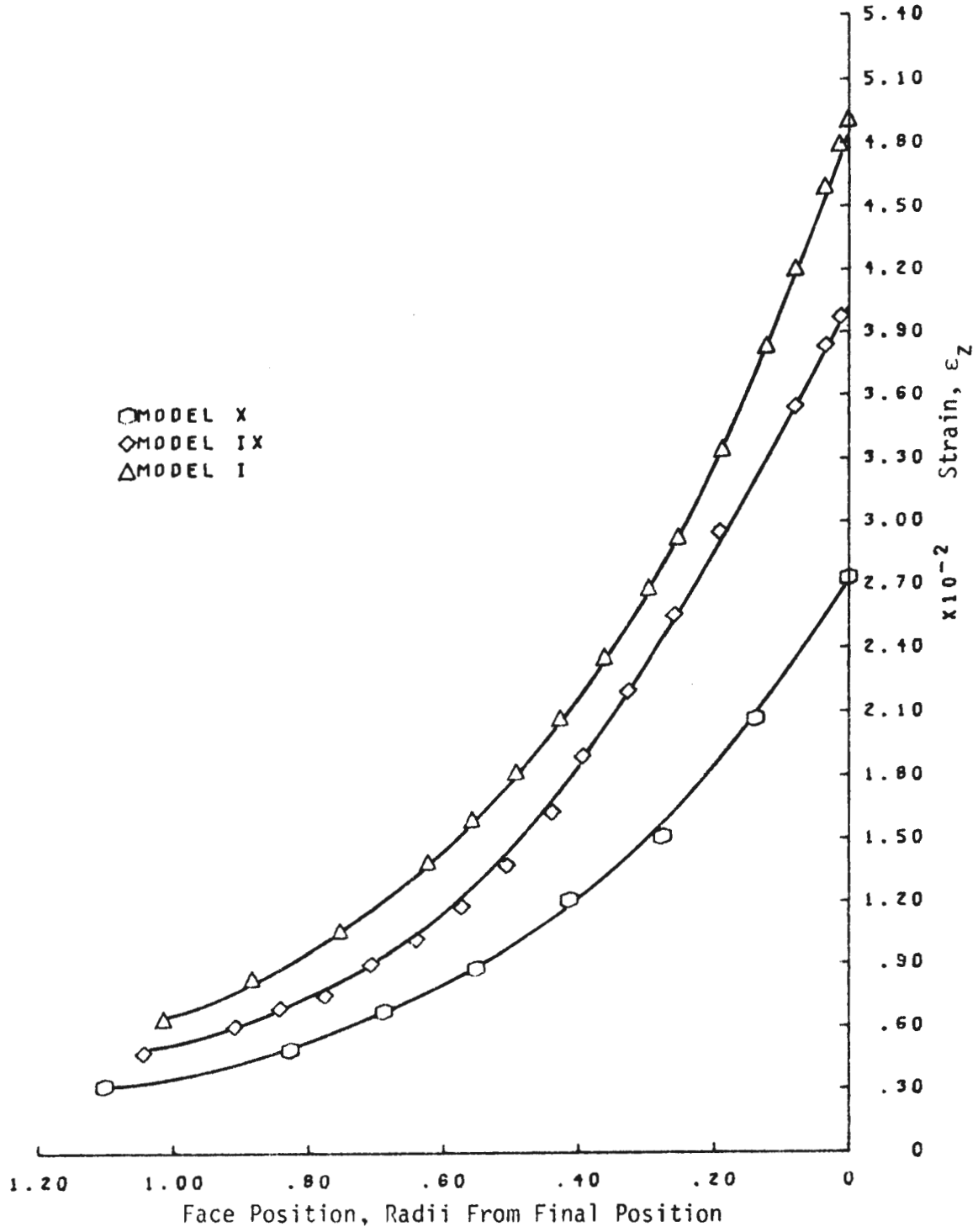

FIGURE VI-17 COMPARISON OF ε_z IN MODEL X, I AND IX ON LINE F AT POSITION $\frac{x}{A} = .4$

size by one half led to a 35% to 60% decrease in strain at similar points on the three sensor lines by the end of excavation. Values of T_{st} varied from .35 to .8 in comparing Models X and IX (see Table VI-2). Therefore, strains equivalent to strains at the end of excavation in Model X had occurred at similar points on the sensor lines in Models I and IX 108 to 290 minutes before excavation had been completed.

By expressing advance rates in terms of the ratio A_r, it had been hoped that an equivalence could be established between the changes in strain rates due to altered advance rates and the changes in strain rates due to altered tunnel size. For example, doubling the advance rate or halving the diameter of a tunnel yields the same value of $A_r = 2$. Thus, F_{sr} should also be the same in each case. In the model tests, A_r of Model X was twice A_r of Models I and IX. At an equal confining pressure, the advance rate of Model VII was four times the advance rate of Models I and IX and in comparing Models VII and IX (see Table VI-2) $F_{sr} = .8$ on the average. Assuming a linear relationship between A_r and F_{sr}, a comparison of Models IX and X for a two fold increase in A_r should have yielded $F_{sr} = .9$. However, the true values of F_{sr} varied from .4 to .7 for the three sensor lines. The discrepancy between the predicted and true value of F_{sr} for Model I as compared to Model X indicates independence of the effects of size and advance rate changes.

The diameter of the Model XI tunnel was three times the diameter of the Model X tunnel. The advance rates and the confining pressures were equal in the two models. Collapse of the larger tunnel

(Model XI) occurred when the face was 1.1 radii from its final position. The mode of failure was similar to that in Models III and IV with failure planes extending to the boundary of the model.

The tunnel of Model XII was the same diameter as the Model XI tunnel but the confining pressure was reduced to 518 KN/m^2 (75 psi), or equal to the Model VIII confining pressure. After advancing to within .25 radius of its final position the tunnel collapsed. Figure VI-18 shows the axial strain vs. time behavior of Model XII and Figure VI-19 compares the very unstable bevavior at $\frac{x}{A}$ = .4 on line F of Model XII with the stable behavior at the similar position in Model VIII. Other results are shown in Figures C-24 and C-25, Appendix C. Shortly before failure, displacements at A2, B2, and F2 were .4 cm, .61 cm, and .51 cm (.16 in, .24 in, .2 in) respectively. These scaled to 16 cm, 24 cm, and 20 cm (6. in, 9.4 in, 8 in) at similar positions in a prototype tunnel. In comparing Models VIII and XII, (see Table VI-2) T_{st} was found to vary from almost 0 for line B to .5 for line A. It is not clear at what point the boundary of the model began to affect deformations around the tunnel. Boundary effects would cause deformations to increase in magnitude and rate and thus the value of T_{st} would be low.

Changes in model behavior ahead of an advancing face due to changes in advance rate, tunnel size and confining pressure are interrelated as shown, for example, in Figures VI-20 and VI-21. (See Appendix C, Figures C-26 to C-29 for complete results). Figure VI-20 is a plot of ε_z at $\frac{x}{A}$ = .4 relative to the face position in Models II and VI, and it shows that, relative to the face position during

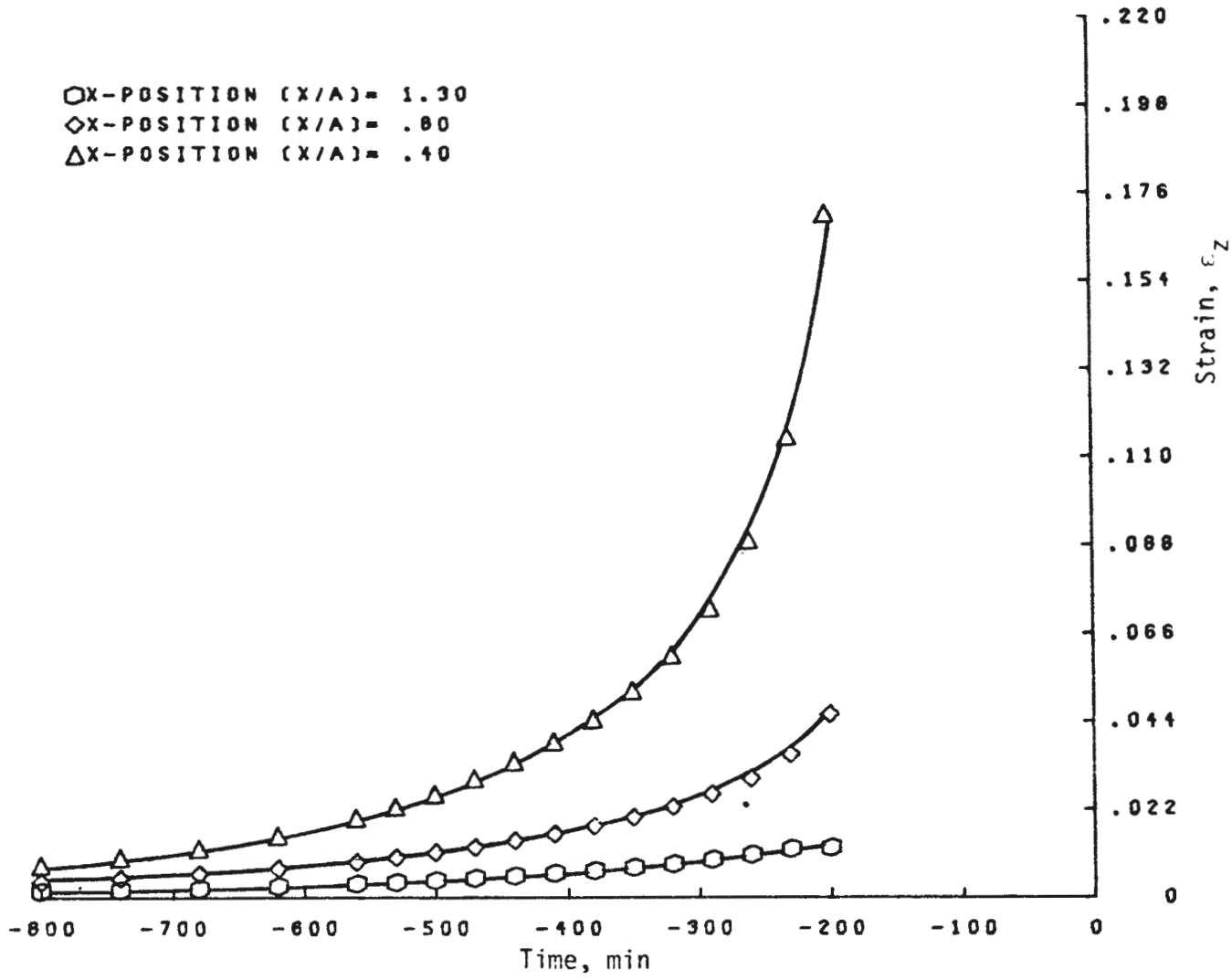

FIGURE VI-18 ε_z VS. TIME AT THREE POSTIONS ON FACE LINE F, MODEL X11

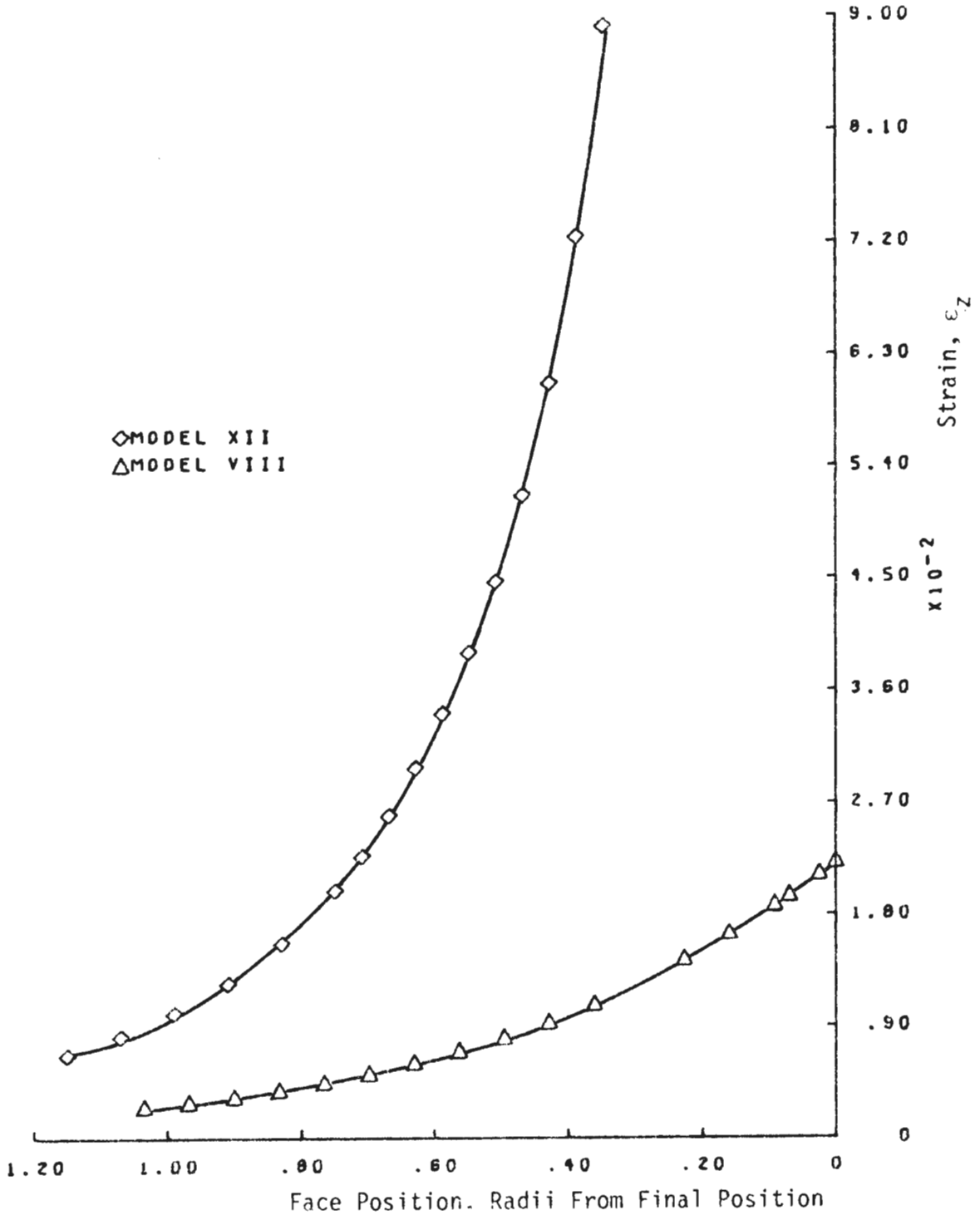

FIGURE V1-19 COMPARISON OF ε_z IN MODELS X11 AND V111 ON LINE F AT POSITION $\frac{x}{A}$ = .4

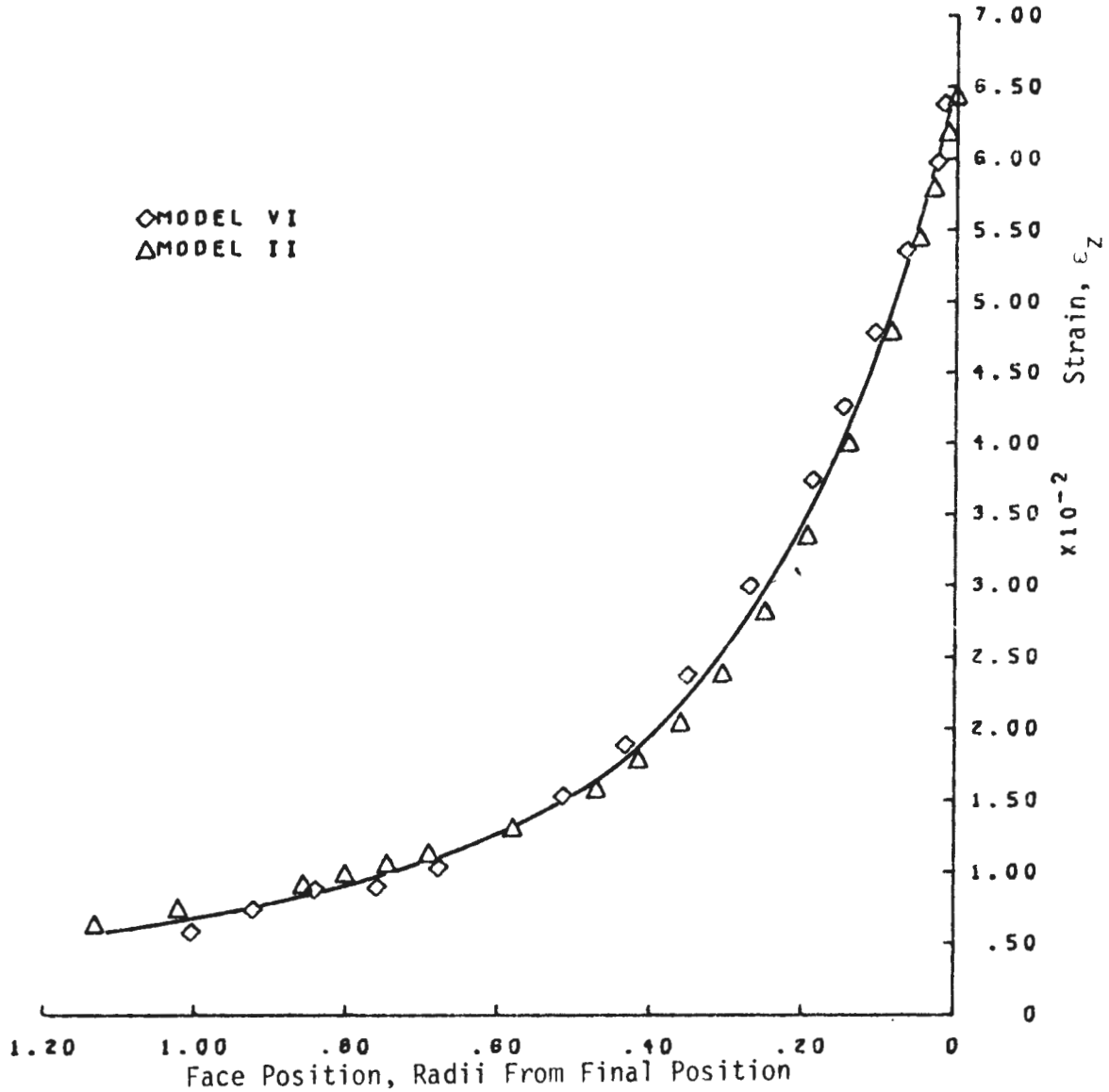

FIGURE VI-20 SIMILARITY OF STRAINS IN MODELS II AND VI.
STRAINS CALCULATED AT POSITION $\frac{x}{A}$ = .4 ON LINE F.

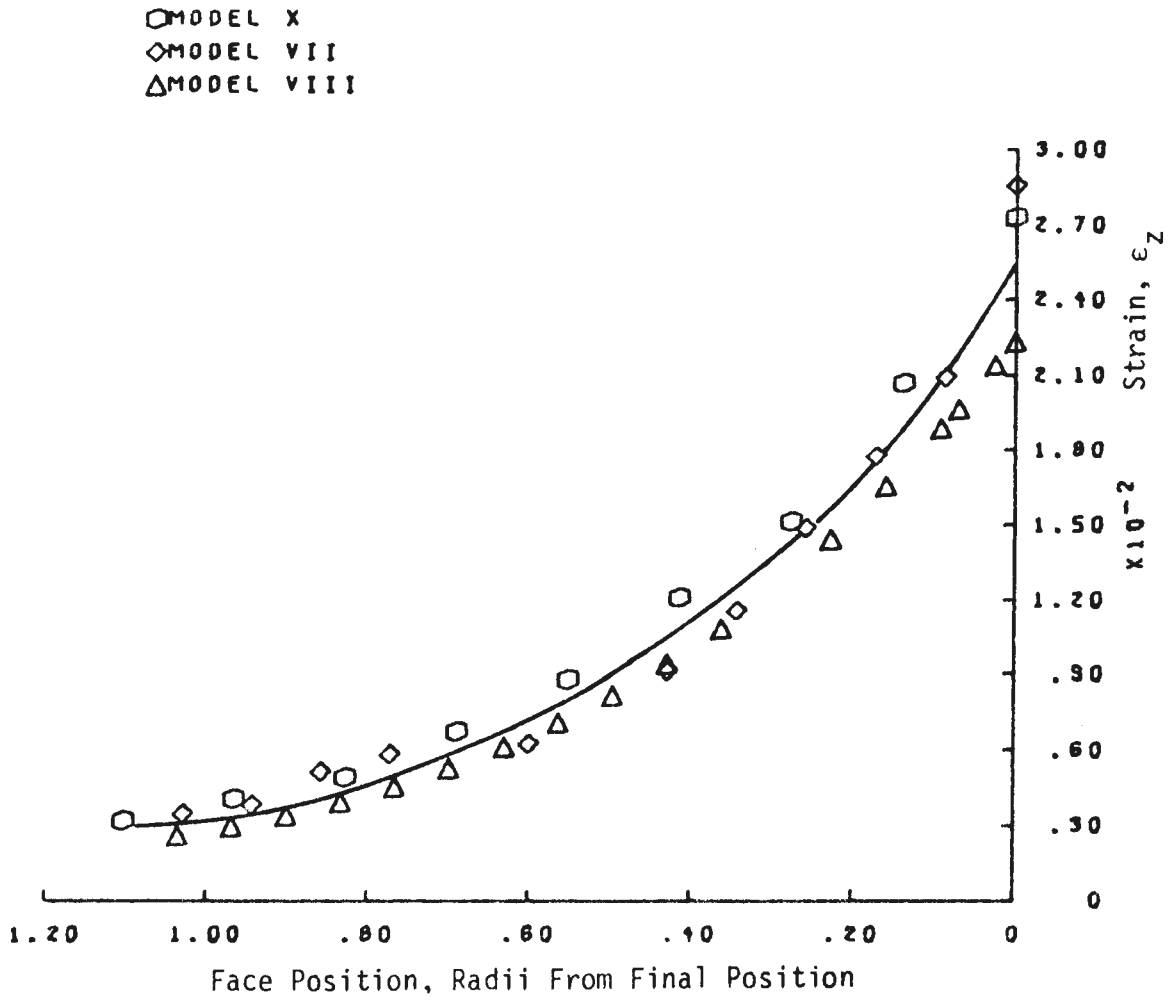

FIGURE VI-21 SIMILARITY OF STRAINS IN MODELS VIII, VII AND X. STRAINS CALCULATED AT POSITION $\frac{x}{A}$ = .4 ON LINE F.

excavation, the deformation behavior was the same for the two openings. This equality of behavior is also shown in Table VI-2 by F_{sr}, T_{st}, and the ratio of strains at the end of excavation all equal to about 1. Tunnel size was the same in Models II and VI but confining pressure and advance rate were different. It was previously seen from a comparison of Models V and VI that an increase in excavation rate at the same confining pressure resulted in a decrease in deformation during excavation. The decrease in deformations resulting from a 5% decrease in confining pressure was noted in comparing Models II and V. Thus, a comparison of Figure VI-20 with Figure VI-6, (Model V results) shows that the increase in excavation rate by a factor of four resulted in behavior during the unsupported period similar to that of a 5% decrease in confining pressure. Results from the face line of Models VII and VIII are plotted on the same graph in Figure VI-21. The agreement between these models is not as good as the agreement between Models II and VI. Values of F_{sr} greater than one in Table VI-2 for a comparison of Models VII and VIII reflect the greater strain at the end of excavation in Model VII. In comparing behavior of Models VII and VIII (Figure VI-21) with Model IX (Figure C-4) a similar conclusion as above can be drawn that the increase in excavation rate resulted in behavior during the unsupported period similar to that of a 10% decrease in confining pressure.

In Figure VI-21 and Table VI-2 it is also seen that most strains in Model X were equal to strains in Model VIII at the same points relative to the face position during excavation. In this case the confining pressure and tunnel size were different while the

advance rate was the same. Models X and IX were previously compared to show the decrease in strains resulting from a decrease in size while holding other parameters constant; and the decrease in deformation due to a decrease in confining pressure was noted in comparing Models VIII and IX. Therefore, in comparing Figure VI-21 to Model IX results, it is seen that a reduction in size by one half to a 6.4 cm (2.5 in) diameter tunnel or a 10% reduction in pressure on the 12.4 cm (4.9 in) tunnel resulted in similar behavior during the unsupported period.

These relations between size, advance rate, and pressure can also be stated conversely. For example, the increase in size from the 6.4 cm (2.5 in) model tunnel to the 12.4 cm (4.9 in) tunnel ought to result in behavior similar to a 10% increase in pressure on the 6.4 cm (2.5 in) tunnel.

Results of Model XII indicate that the magnitude of pressures for equivalent behavior might not increase linearly with size. Model XII was 50% larger in diameter than Model VIII but had the same confining pressure. If the same relationships applied as observed above, strains in Model I and Model XII should have been equal during excavation. It is not clear how much influence the interference of the Model XII boundary had on these results but it seems that the increase in size from the 12.4 cm (4.9 in) tunnel to the 19 cm (7.5 in) tunnel represented a change in behavior at least equal in magnitude to a 10% increase in confining pressure on the Model VIII tunnel. Comparisons of the behavior of Model XII with that of Model II and V indicates the size increase minus boundary interference would not have caused strains greater in magnitude than a 25% increase in pressure on the Model VIII tunnel.

Figure VI-22 summarizes these results and shows the change in size of the 12.4 cm (4.9) diameter tunnel necessary to obtain equal behavior if the ratio of confining pressure to material strength changes. The dotted curves represent the uncertainty caused by the boundary effects of Model XII; the true curve would lie between the two dotted curves. Confining pressure represents depth of cover over a prototype tunnel. It is seen that a 50% decrease in size resulted in at least a 10% decrease in ratio of confining pressure to material strength. If it is assumed that the same behavior would result from an increase in the ratio of confining pressure to strength whether the increase were due to increased pressure or decreased strength, these results could be restated in the following form: a 10% increase in confining pressure or a 10% decrease in strength required at most a 50% decrease in tunnel size to maintain the same degree of stability.

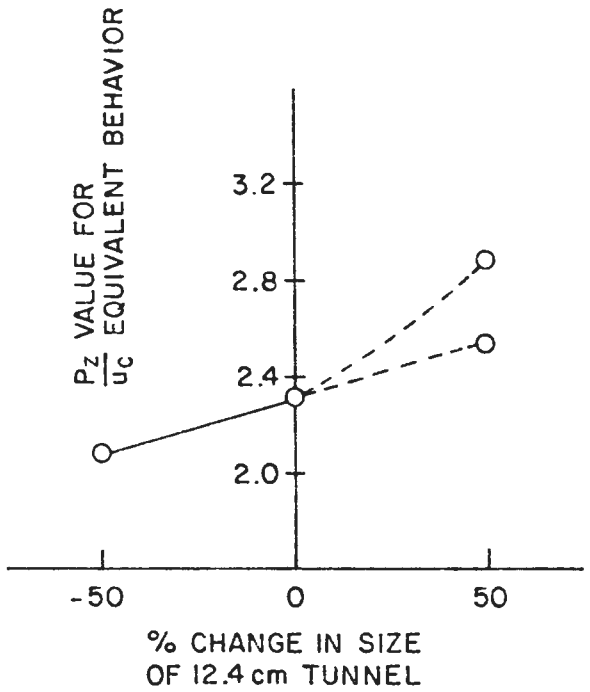

FIGURE V1-22 CHANGE IN SIZE OF 12.4 cm TUNNEL NECESSARY TO OBTAIN EQUAL BEHAVIOR IF RATIO OF CONFINING PRESSURE TO MATERIAL STRENGTH $\left(\frac{P_z}{UC}\right)$ CHANGES. DATA FROM LINE F AT POSITION $\frac{x}{A} = .4$.

TABLE VI-2

Summary Of Model Test Results

Model Y vs Model W	$\frac{P_{zy}}{P_{zw}}$ *	$\frac{r_y}{r_w}$	$\frac{A_{ry}}{A_{rw}}$ ***	$\varepsilon_x/\varepsilon_y$ ++			F_{sr}			T_{st}		
				+line A	+line B	+line F	+line A	+line B	+line F	+line A	+line B	+line F
Model VI vs Model V	1	1	4	0.45	0.5	0.55	0.6	0.6	0.6	0.8	0.7	0.8
Model VII vs ξ Model IX	1	1	4	0.8	0.65	0.65	0.9	0.9	0.7	0.9	0.8	0.8
Model X vs ξ Model IX	1	.5	2	0.55	0.4	0.65	0.5	0.4	0.7	0.7	0.35	0.8
Model VIII vs Model XII	1	.7	1.5	-	-	-	-	-	-	0.5	~0	0.3
Model VI vs Model II	1.04	1	4	.8	1	1	1	1	1	.9	1	1
Model VII vs Model VIII	1.1	1	4	1.4	1.4	1.2	1.8	1.4	1.3	.9	.7	.1
Model X vs Model VIII	1.1	.5	2	1	.8	1.2	1	.7	1.2	1	.75	.09

ξ Model IX ~ Model I

** r is radius

++ Strain values calculated at the end of excavation

* P_z is confining pressure

*** A_r is ratio of advance rate to tunnel radius

+ All values computed using results from sensor line positions .4 radii from final position of tunnel boundary

Chapter 7

Conclusions and Recommendations

The relationship between size, advance rate and stand-up time of tunnels in squeezing ground was studied by observing the effects of changes in size or advance rate on the time dependent deformation in a series of twelve model tests. Because, by definition, stand-up time is the time elapsed before instability, results were first interpreted with the aim of defining the deformation state which represented instability in the models and relating this defined state to prototype behavior. Conclusions could then be drawn with respect to the effects of size and advance rate changes on the time for development of the deformation states indicative of instability.

Rather than being represented by a state of total collapse of the unsupported section of the model tunnels, instability was defined in part by the magnitude of accumulated strains. Though there was some evidence of material failure around the tunnels, collapse in the models occurred only due to interaction of the model boundary with deformations around the tunnel. A definition of instability in terms of deformation magnitudes is not contradictory to realistic prototype behavior in which deformations and deformation rates become large enough to inhibit tunnelling operations though catastropic collapse does not occur. Even if collapse is a factor for consideration, the potential for it would be lessened by limiting the amount of deformations. It was apparent in the model tests, however, that

the collapse sometimes associated with stand-up time problems in squeezing ground is caused by characteristics of the ground other than those modeled by the model material, e.g. discontinuities.

It was also found that instability in the models should be defined not only in terms of the magnitude of the deformations, but also in terms of when during the test the deformations were accumulated. All models in which the excavation phase was completed exhibited increasing post-excavation deformations, but at a decreasing rate, until apparent long term stability was achieved. This post-excavation behavior prevailed even in Model V which was near collapse at the end of excavation. Though collapse in model tunnels was not representative of a true stand-up time problem, the lack of any collapses after excavation stopped and the behavior of Model V indicated that the deformations accumulated after excavation stopped did not have a significant effect on the stability of the models. Stability or instability in the models was therefore defined in terms of the amount of strain accumulated during the excavation phase of the test. These deformations modeled deformations which would be experienced in a continually advanced prototype tunnel.

In order to compare meaningfully stand-up times of model tunnels of different sizes and advance rates during excavation a stand-up time factor, T_{st} was defined which was the time to reach a particular strain expressed as a percent of the unsupported period. The unsupported period is the time in a continually advancing tunnel (model or prototype) that an element of ground remains unsupported.

With an appreciation of the preceeding qualifications and definitions the following conclusions could be drawn regarding the effect on stand-up time of altering tunnel size or advance rates.

1. If the size of a tunnel in squeezing ground is increased, even though the advance rate and ratio of diameter to distance from face to first support remains constant, stand-up time was shown to decrease. The lower stand-up time was shown to be associated with larger deformations accumulated by the end of the unsupported period. For example, in comparing two models which represented an increase in size from a 2.4 m (8 ft) to a 5 m (16 ft) prototype tunnel, the stand-up time factor, T_{st}, for a point near the tunnel face was .8. Thus, relative to the length of the unsupported period, the larger tunnel experienced strains equal to those of the smaller 20% sooner; stand-up time was reduced by 20%. The amount of axial strain accumulated by the end of excavation in the larger tunnel at the same point had increased by over 50%. Deformations were largest ahead of the face in both tunnels, but in comparing the two tunnels at other positions between the face and the first support, T_{st} was lower and the increase in strains was greater in the larger tunnel.
2. A decrease in the rate of advance of a tunnel in squeezing ground was shown to lead to decreased stand-up time and increased deformations by the end of an unsupported period. For example, in comparing models representing a decrease in average prototype advance rates from 1.2 m/hr (4 ft/hr) to 30 cm/hr (1 ft/hr) the stand-up time factor, T_{St}, for a point near the

the face was .8. The axial strain at the same point was 45% lower by the end of excavation than in the more slowly excavated model.

3. Effects of altering size or advance rates on strains accumulated during an unsupported period could be explained as resulting from the effects of these variations on strain rates. However, such an analysis also resulted in the conclusion that size and advance rate effects are at least partially independent phenomena. Though average strain rates decreased in the models as advance rates decreased, the percent decrease in strain rates was less than the percent decrease in advance rates. Because the time an element remained unsupported is the inverse of the advance rate, it is seen that a smaller percent decrease in average strain rate than in advance rate would lead to larger strains by the end of excavation of a model tunnel. To aid in comparing strain rates in models in which tunnel size differed, a ratio (A_r) of advance rate to tunnel radius was defined. Keeping other variables constant, it was found that an increase in tunnel size led to a decrease in average strain rates but the percent decrease was less than the percent decrease in A_r and thus strains were greater by the end of excavation in the larger tunnel. By expressing advance rates in terms of A_r it had been hoped that an equivalence could be established between the changes in strain rates due to altered advance rates and the changes in strain rates due to altered size. However, in using results of two tests in which advance rates were different to predict strain

rate changes due to size differences, the predicted effect of a change in size on strain rates was less than the observed effect.

4. It was found that stand-up time behavior due to changes in tunnel size or advance rate could be equated to behavior due to changes in the ratio of depth of cover to material strength. In the model tests, depth of cover was represented by the model confining pressure. If the confining pressure was increased by 10%, a 50% decrease in size was necessary to yield the same behavior or degree of stability. Material strength was constant in the models, but if it is assumed that the same behavior would result from a 10% increase in the ratio of confining pressure (depth of cover) to strength whether the increase was due to increased pressure (depth) or decreased strength, the results indicate that a strength decrease of 10% in squeezing ground could require a decrease in tunnel size of 50% to maintain the same degree of stability. Making the same assumptions, results similarly indicated that a 5% to 10% increase in depth or a 5% to 10% decrease in strength could require an increase in advance rate of a factor of four to maintain the same degree of stability.

Recommendations For Further Study

Both an increase in size and a decrease in advance rate were found to decrease stand-up time of continually advanced tunnels in squeezing ground, but results indicated the two effects were independent. The relative importance of these effects on stand-up time could be further investigated by performing tests in which tunnel size was varied while the ratio of advance rate to tunnel radius was kept constant. In such tests geometric similarity of the

tunnels would be maintained at all times and any differences in behavior would be indicative only of a size effect.

The models were continuously excavated whereas many tunnels are excavated by rounds in which the face is advanced very quickly and then left stationary for an interval of time. In the models quickly increasing deformation rates invaribly changed to quickly decreasing rates after excavation stopped. It is not clear how closely the deformation history of a continually advanced tunnel resembles the deformation history of a tunnel advanced by discrete increments. Further study is needed to determine the effect on tunnel stability of excavation by discrete rounds.

The effect on model stability of changes in the ratio of confining pressure to material strength were quite significant. In the models the changes in this ratio were effected by changing the model confining pressure, which would be the same as changing the depth of cover in a prototype situation. Further study is needed to determine if behavior resulting from a change in confining pressure is indicative of behavior resulting from a change in strength. Complementary to this would be a study of material parameters most indicative of potential stand-up time behavior.

REFERENCES

Arnold, A.B., R.P. Bisio, D.G. Heyes, and A.O. Wilson (1972). "Case histories of three tunnel-support failures, California Aqueduct," Bull. of the Assoc. of Eng. Geol., Vol. 9, No. 3, pp. 265-299.

Attewell, P.B., and J.B. Boden (1971). "Development of stability ratios for tunnels driven in clay," Tunnels and Tunnelling, May, pp. 195-198.

Attewell, P.B., and I.W. Farmer (1974). "Ground deformations resulting from shield tunnelling in London Clay." Canadian Geotech. J., Vol. II, No. 3 pp. 380-395.

Ayres, M.O. (1969). "Case history - Berkeley Hills twin transit tunnels," Proc. of the 2nd Symp. on Rapid Excavation, Sacramento, H.C. Hartman, ed., pp. 10-26 to 10-37.

Bieniawski, Z.T. (1974). "Geomechanics classification of rock masses and its applications in tunnelling," Tunnelling in Rock, Z.T. Bieniawski, ed., S. African Inst. of Civil Eng., Pretoria, pp. 89-103.

Bishop, A.W. (1966). "The strength of soils as engineering materials," Geotechnique, Vol. 16, pp. 91-128.

Bishop, A.W. and D.J. Henkel (1962). The Measurement of Soil Properties in the Triaxial Test, St. Martin's Press, New York, 227 pp.

Brekke, T.L. and T.R. Howard (1973). Functional Classification of Gouge Materials from Seams and Faults in Relation to Stability Problems in Underground Openings, U.S. Bureau of Mines (ARPA) Contract No. H0220022.

Broms, B.B., and H. Bennermark (1967). "Stability of clay at vertical openings," J. of Soil Mech. and Found. Div., ASCE, Vol. 93, No. SM1, pp. 71-94.

Campanella, R.G. and Y.P. Vaid (1974). "Triaxial and plane strain creep rupture of an undisturbed clay," Canadian Geotech. J., Vol. 11, No. 1, pp. 1-10.

Carnahan, B., H.A. Luther, and J.O. Wilkes (1969). Applied Numerical Methods, Wiley, New York, 604 pp.

Casagrande, A. and S. Wilson (1951). "Effect of rate of loading on strength of clays and shales at constant water content," Geotechnique, Vol. 2, No. 3, pp. 251-263.

Cooling, L.F., and W.H. Ward (1953). "Measurements of loads and strains in earth supporting structures," Proceedings, 3rd Int. Conf. on Soil Mech. and Found. Eng., Zurich, Vol. 2, pp. 162-166.

de Beer, E.E., and E. Buttiens (1966). "Construction de réservoirs pour hydocarbures liquéfiés dans l'argile de Boom à Anvers. Étude des mouvements du sol provoqués par cette réalisation," Traveaux, Sept., pp. 1087-1093, and Oct., pp. 1167-1174.

Den Hartog, J.P. (1952). Advanced Strength of Materials, McGraw-Hill, New York, 379 pp.

Hansmire, W.H., and E.H. Cording (1972). "Performance of a soft ground tunnel on the Washington Metro," Proceedings, North Amer. Rapid Exc. and Tunnelling Conf., Chicago, pp. 287-313.

Hartmark, H. (1964). "Geotechnical observations during construction of a tunnel through soft clay in Trondheim, Norway, " Felsmechanik und Ingenieurgeologie, Vol. 2, No. 1, pp. 9-21.

Hopper, R.C., T.A. Lang, and A.A. Mathews (1972). "Construction of Straight Creek Tunnel, Colorado," Proceedings, North Amer. Rapid Exc. and Tunnelling Conf., Chicago, Vol. 1, pp. 501-538.

Jaeger, J.C. and N.G.W. Cook (1969). Fundamentals of Rock Mechanics, Chapman and Hall LTD, 515 pp.

Jaunzemis, W. (1967). Continuum Mechanics, Macmillan, New York, 604 pp.

Korbin, G.E. (1975). A Model Study of Spiling Reinforcement in Underground Openings, Ph.D. Dissertation, University of California, Berkeley.

Lang, T.A. (1972). "Rock reinforcement," Bull. Assoc. of Eng. Geol., Vol. 9, No. 3, pp. 215-239.

Langhaar, H.L. (1951). Dimensional Analysis and Theory of Models, Wiley, New York, 166 pp.

Lauffer, H. (1958). "Gebirgsklassifizierung für den stollenbau," Geologie und Bauwesen, Vol. 24. No. 1, pp. 46-50.

Mandel, J. (1963). "Tests on reduced scale models in soil and rock mechanics, a study of the conditions of similitude," Inst. J. Rock Mech. Mining Sci., Vol. 1, pp. 31-42.

Merrill, R. (1954). "Design of underground mine opening in oil shale mine,Rifle, Colorado," Report of Investigations 5089, US Bureau of Mines.

Merrill, R. (1957). "Roof-span studies in limestone," Report of Investigations 5406, US Bureau of Mines.

Mitchell, J.K. (1976). Fundamentals of Soil Behavior, Wiley, New York, 422 pp.

Moler, W.A. (1974). Personal communication.

Moretto, O. (1969) in: "Deep excavations and tunnelling in soft ground," Proceedings, 7th Inst. Conf. on Soil Mech. and Found. Eng., Mexico City, Vol. 3, pp. 225-290.

Murayama, S. and T. Shibata (1964). "Flow and stress relaxation of clays (theoretical studies on the rheological properties of clay-part I), " Proceedings, Rheology and Soil Mech. of the Int. Union of Theoretical and Applied Mech., Grenoble, France.

Murphy, G. (1950). Similitude in Engineering, Ronald Press, New York, 302 pp.

Peck, R.B. (1969) in "Deep excavations and tunnelling in soft ground," Proceedings, 7th Inst. Conf. on Soil Mech. and Found. Eng., Mexico City, Vol. 3, pp. 225-290.

Peck, R.B., A.J. Hendron, Jr., and B. Mohray (1972). "State of the art of soft-ground tunnelling," Proceedings, North Amer. Rapid Exc. and Tunnelling Conf., Chicago, Vol. 1, pp. 259-286.

Peters, C.M.F. (1972). "A structural interpretation of the Garlock Fault zone at the Techachapi Crossing," Proceedings, North Amer. Rapid Exc. and Tunnelling Conf., Chicago, Vol. 1, pp. 133-155.

Polshin, D.E., N.Y. Rudnitski, P.G. Chizhikov, and T.G. Yakovleva (1973). "Centrifugal model testing of foundation soils of building structures," Proceedings, 8th Int. Conf. on Soil Mech. and Found. Eng., Moscow, Vol. 1, Pt. 3, pp. 203-208.

Rabcewicz, L.V. (1969). "Stability of tunnels under rock load," Water Power, June, pp. 225-229, July, pp. 266-273, and Aug., pp. 297-302.

Rabcewicz, L.V. (1975). "Tunnel under Alps uses new cost saving lining method," Civil Eng., ASCE, Vol. 45, No. 10, pp. 69-74.

Roscoe, K.H. (1968). "Soils and model tests," J. of Strain Analysis, Vol. 3, No. 1, pp. 57-64.

Scott, R.F. (1963). Principles of Soil Mechanics, Addison - Wesley, Reading, Mass., 550 pp.

Sekiguchi, H. (1973). "Flow characteristics of clays," Soils and Foundations, Japan. Soc. of Soil Mech. and Found. Eng., Vol. 13, No. 1, pp. 45-60.

Semple, R.M. (1973). The Effect of Time-Dependent Properties of Altered Rock on Tunnel Suppot Requirements, Ph.D. Dissertation, University of Illinois, Urbana.

Shibata, T. and D. Karube (1969). "Creep rate and creep strength of clays," Proceedings, 7th Int. Conf. on Soil Mech. and Found. Eng., Mexico City, Vol. 1, pp. 361-367.

Singh, A. and J.K. Mitchell (1968). "General stress-strain-time function for soils," J. of Soil Mech. and Found. Div., ASCE, Vol. 94, No. SM1, pp. 21-46.

Singh, A. and J.K. Mitchell (1969). "Creep potential and creep rupture of soils," Proceedings, 7th Int. Conf. on Soil Mech. and Found. Eng., Mexico City, Vol. 1, pp. 379-384.

Skempton,A.W. (1943). "Discussion to Groves, G.L., 'Tunnel linings, with special reference to a new form of reinforced concrete lining,'" J. ICE, March, pp. 29-64.

Tattersall, F., T.R.M. Wakeling, and W.H. Ward (1955). "Investigations into the design of pressure tunnels in London clay," Proc. ICE, pp. 400-471.

Terzaghi, K. (1946) in: Rock Tunnelling with Steel Supports, Proctor and White, eds., Commercial Shearing and Stamping Co., Youngstown, Ohio, 292 pp.

Underwood, L.B. (1965). "Machine tunnelling on Missouri River dams," J. of the Const. Div., ASCE, May, No. CO1, pp. 1-27.

Underwood, L.B. (1968). "Future needs in site study," Rapid Exc., Problems and Progress, Proc. of Tunnel and Shaft Conf., Minn., pp. 24-31.

Waddell, G., T. Crocker, and E. Skinner (1971). "Technique of measuring initial deformation around an opening," Report of Investigations 7505, US Bureau of Mines.

Ward, W.H. (1969) in: "Deep excavations and tunnelling in soft ground," Proceedings, 7th Int. Conf. on Soil Mech. and Found. Eng., Mexico City, Vol, 3., pp. 320-325.

Ward, W.H., and H.S.H. Thomas (1965). "The development of earth loading and deformation in tunnel linings in London clay," Proceedings, 6th Int. Conf. on Soil Mech. and Found. Eng., Montreal, Vol. 2, pp. 432-436.

Wood, A.M. (1969) in: "Deep excavations and tunnelling in soft ground," Proceedings, 7th Int. Conf. on Soil Mech. and Found. Eng., Mexico City, Vol, 3, pp. 363-367.

Appendix A

TABLE A-1

Relative Compressibilities and Flexibilities of Example Cases

Case	Reference	Lining Type	Radius m (ft)	Thickness cm (in)	Observed Rigidity	Soil Type	Undrained Shear Strength MN/m^2 (psi)	Flexibility F/K_2	Compress-ibility C
London, 1942	Skempton 1943	Bolted Iron Segments	2. (6.4)	3.4 (1.3)	Small Moments	London Clay	.28 (40.)	3.3×10^1	.046
London, 1952	Cooling & Ward, 1953	Bolted Iron Segments	3.9 (12.7)	5.9 (2.3)	Small Moments	London Clay	.33 (49) to to 1.1(153)	2.4×10^1	.07
London, 1961	Ward & Thomas 1965	Concrete Segments	2. (6.6)	23. (9.)	Moments < 12k ft/ft	London Clay	.37 (54) to to .41 (59)	1	.086
London, 1952	Tattersall et al. 1955	Iron Segments	1.3 (4.4)	30. (12.)	Consider-able	London Clay	1.1 (153)	.52	.12
Norway, 1949	Hartmark 1964	Concrete	3.3 (10.8)	66. (26.)	Consider-able	Sensitive Clay	.03 (4.8) to to .06 (8.3)	.012	.005

$$F = \frac{r^2 E_g K_2}{E_\ell t_\ell^3} \qquad C = \frac{r E_g}{E_\ell t_\ell} \qquad E_g = 600\,(S_u) \qquad S_u = \text{Unconfined Shear Strength}$$

Data after Peck (1969)

APPENDIX B

SUPPLEMENTARY RESULTS OF MODEL MATERIAL CHARACTERIZATION

Table B-2 (Cont.)

.7% Paro .5% Shap (Cont.)

4-4/22/75	75	.685	.783	105
1-4/30/75	75	.758	.810	57
3-4/30/75	78	.912	1.215	53.1
4-4/30/75	77	-	-	42
5-4/30/75	76	.643	.766	32
6-4/30/75	76	.991	1.163	53.9
2-2/18/75	50	. 96	1.070	Didn't fail in 10,000
1-2/18/75	50	. 95	1.210	Didn't fail in 10,000
1.3% CD150 Temp. = 7.2°C				
1-5/26/75	73	.290	.329	55
2-5/20/75	77	.291	.358	274-304
3-5/20/75	77	.210	.324	49
3-5/31/75	77	.079	.138	15
2-5/31/75	77	.204	.225	52
2-6/4/75	77	.172	.205	30.8
.6% CD150 .%Shap				
7	90	.370	-	19
8	90	.429	.569	32
9	90	.220	-	9
10	90	.506	.579	25
13	90	.250	.337	9
15	90	.400	.496	5
16	90	.422	.782	8
28	90	.250	.319	13
29	90	.342	.455	10
30	90	.262	.408	9
31	90	.244	.305	19
5	80	.549	.624	85
8	80	.381	.530	1.7

Table B-2 (Cont.)

.6% CD150 .4% Shap (Cont.)

20	80	.470	-	67
21	80	.384	.426	83
22	80	.356	.536	106
23	80	.375	.411	96
25	80	.532	-	63
26	80	.340	.378	79
44	80	.293	.354	113
46	80	.340	.378	79
32	70	.814	.876	780
33	70	.699	.746	1086
34	70	.762	.822	990
35	70	.793	.815	870
19	60	1.016	1.103	2010
20	60	.596	.621	2520
21	60	1.015	1.093	2790
38	60	1.016	1.025	1800
39	60	.771	.782	1470
41	60	.736	-	1680
42	60	.998	1.018	3020
45	60	1.169	-	5500
46	60	.6 -.7	-	10000
1-7/2/75	50	.5- .6	-	Didn't fail in 10,000
2-7/3/75	50	.689	.719	Didn't fail in 10,000
3-7/3/75	50	1.31	1.370	5360
4-7/3/75	50	.686	.691	4512

Appendix B

Table B-3

Unconfined Strength Tests

.6% CD150 .4% Shap

Test	Density g/cm³ (pcf)	Ultimate Stress σ_{ult} KN/m² (psi)	Ultimate Strain ε_{ult} %	
4-7/3/75	1.519 (94.8)	265. (38.5)	.253	
3-7/3/75	1.519 (94.8)	263. (38.2)	.320	
2-7/3/75	1.539 (96.1)	280. (40.6)	.256	
1-7/3/75	1.519 (94.8)	273. (39.6)	.201	
1-9/9/75	1.519 (94.8)	264. (38.3)	.298	Ave σ_{ult} = 2.59
3-9/9/75	1.529 (95.5)	274. (39.8)	.348	
4-9/9/75	1.529 (95.5)	271. (39.3)	.396	St. Dev.= .20
6-9/9/75	1.529 (95.5)	266. (38.6)	.231	Ave ε_{ult} = .247
7-9/9/75	1.539 (96.1)	285. (41.3)	.216	
8-9/9/75	1.539 (96.1)	264. (38.3)	.159	St. Dev. = .07
6-10/17/75	1.529 (95.5)	263. (38.2)	.200	
7-10/17/75	1.529 (95.5)	259. (37.6)	.165	
8-10/17/75	1.539 (96.1)	260. (37.8)	.216	
9-11/21/75	1.519 (94.8)	244. (35.5)	.169	
8-11/21/75	1.529 (95.5)	246. (35.8)	.151	
11-12/1/75	1.529 (95.5)	250. (36.3)	.315	
10-12/1/75	1.529 (95.5)	226. (32.8)	.167	
12-12/2/75	1.539 (95.5)	243. (35.2)	.207	
13-12/4/75	1.529 (95.5)	225. (32.7)	.252	
14-12/4/75	1.529 (95.5)	219. (31.8)	.213	
15-1/6/76	1.529 (95.5)	224. (32.5)	.254	
16-1/13/76	1.529 (95.5)	270. (39.2)	.366	
17-1/13/76	1.529 (95.5)	257. (37.3)	.300	
18-1/30/76	1.529 (95.5)	224. (32.5)	-	
20-2/4 /76	1.529 (95.5)	220. (32.0)	.274	

APPENDIX C

SUPPLEMENTARY RESULTS OF MODEL TESTS

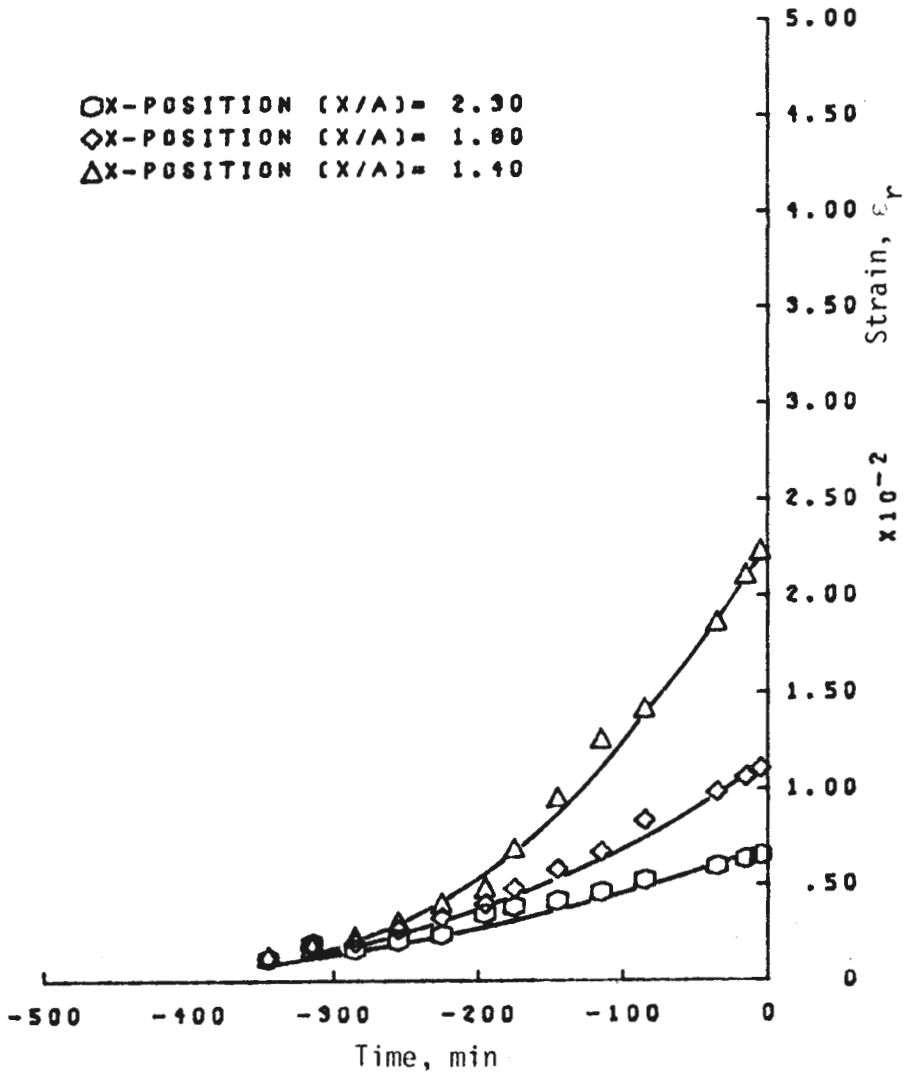

FIGURE C-1 ε_r VS. TIME, LINE A, MODEL IX

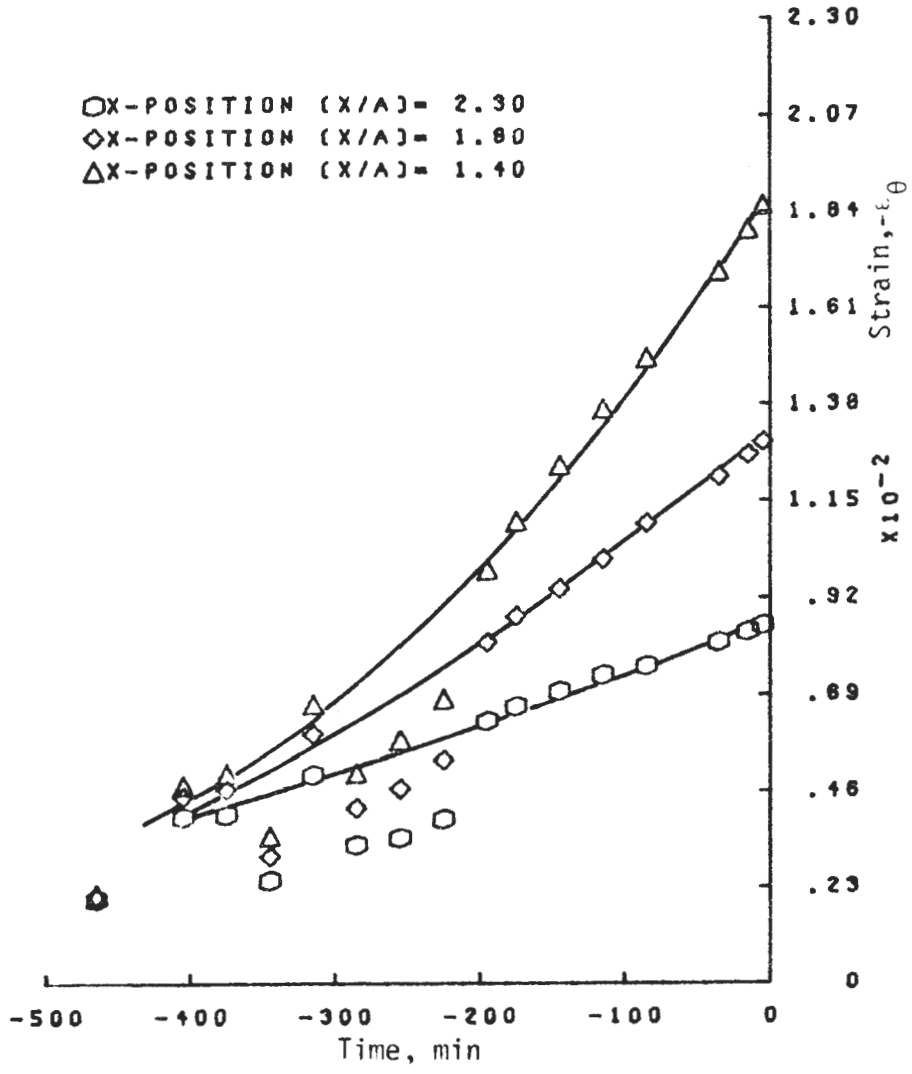

FIGURE C-2 ε_θ VS. TIME, LINE A, MODEL IX.

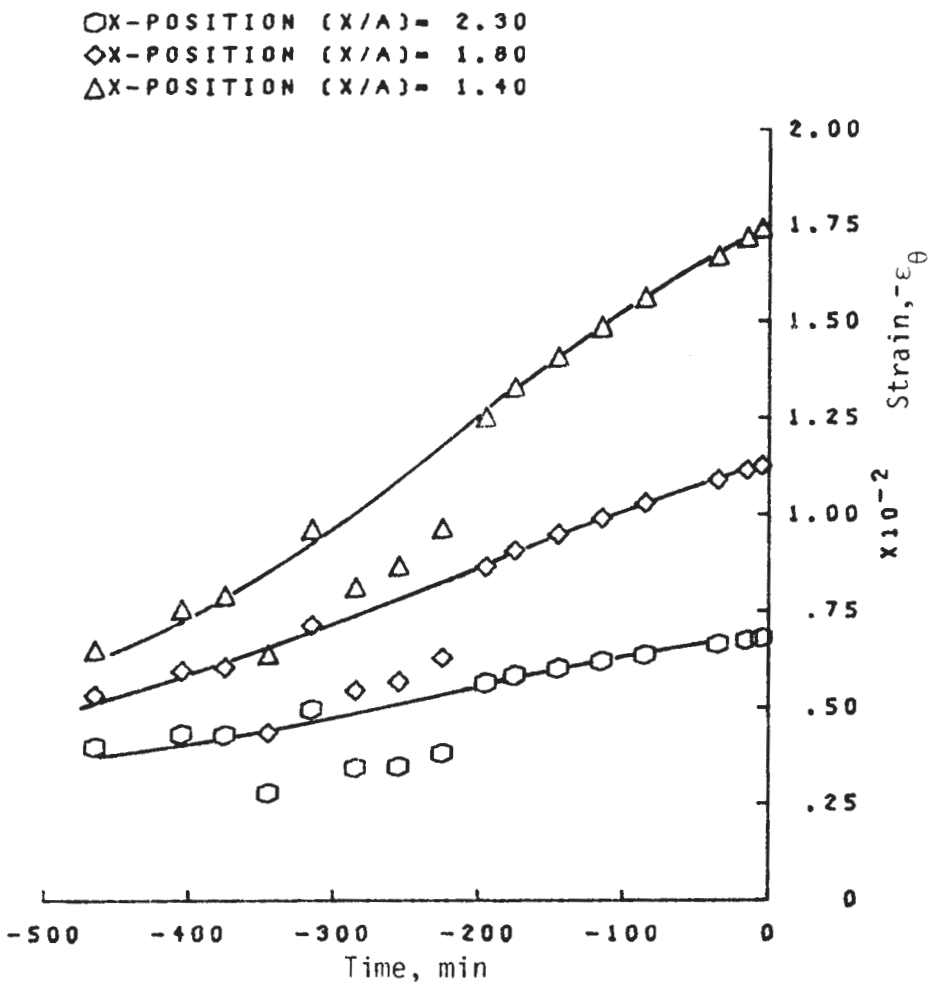

FIGURE C-3 ε_θ VS. TIME, LINE B, MODEL IX

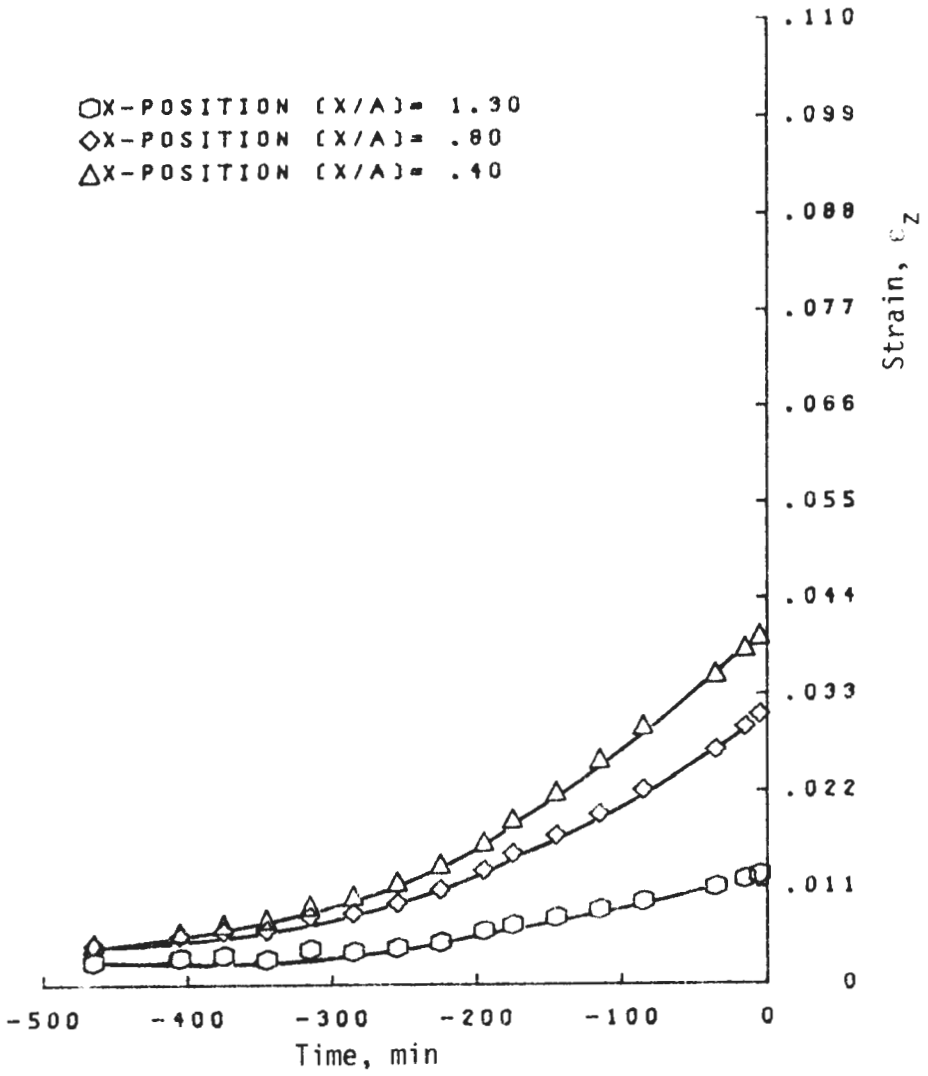

FIGURE C-4 ε_z VS. TIME, LINE F, MODEL IX

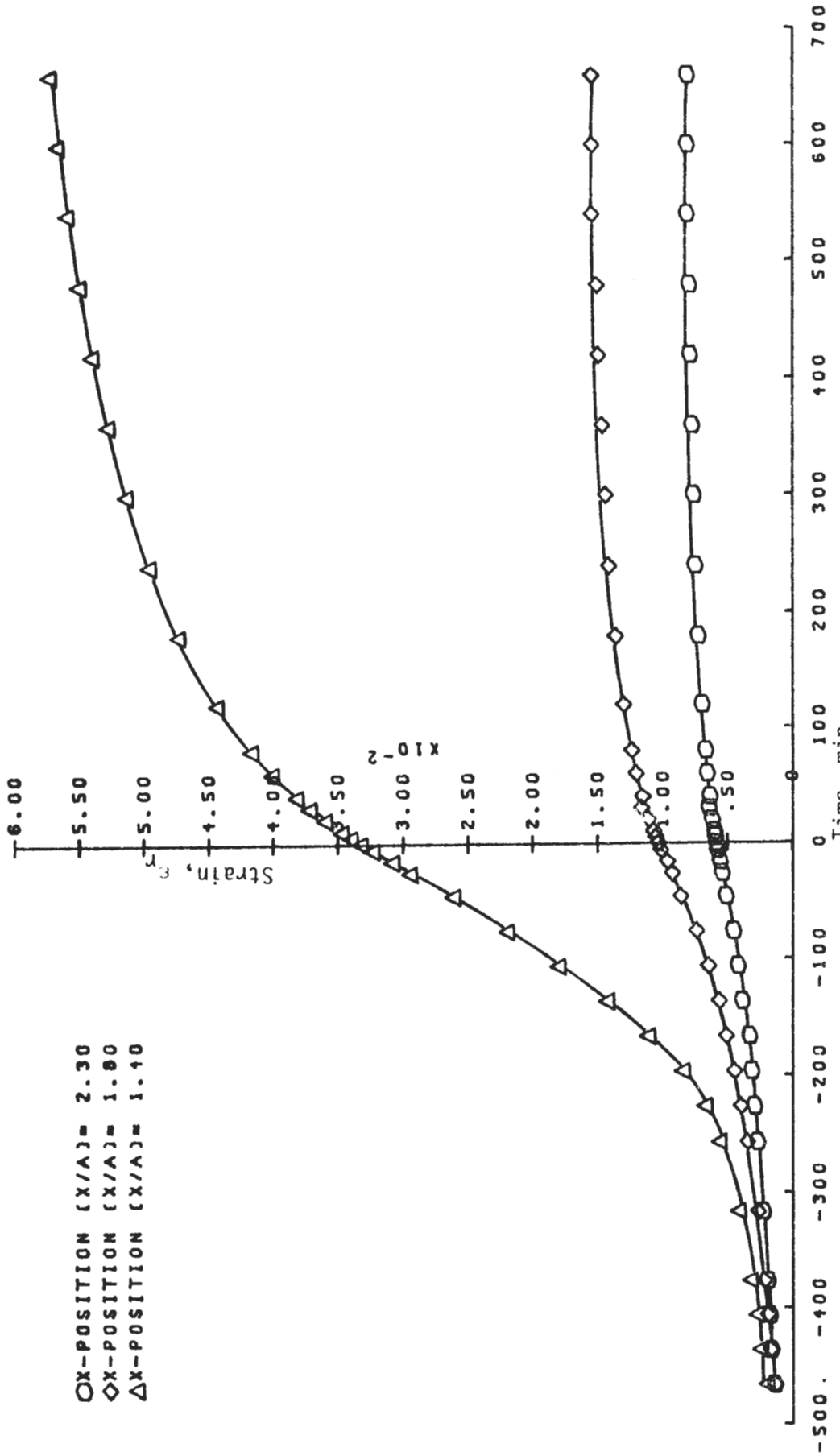

FIGURE C-5 ε_r VS. TIME, LINE A, MODEL II.

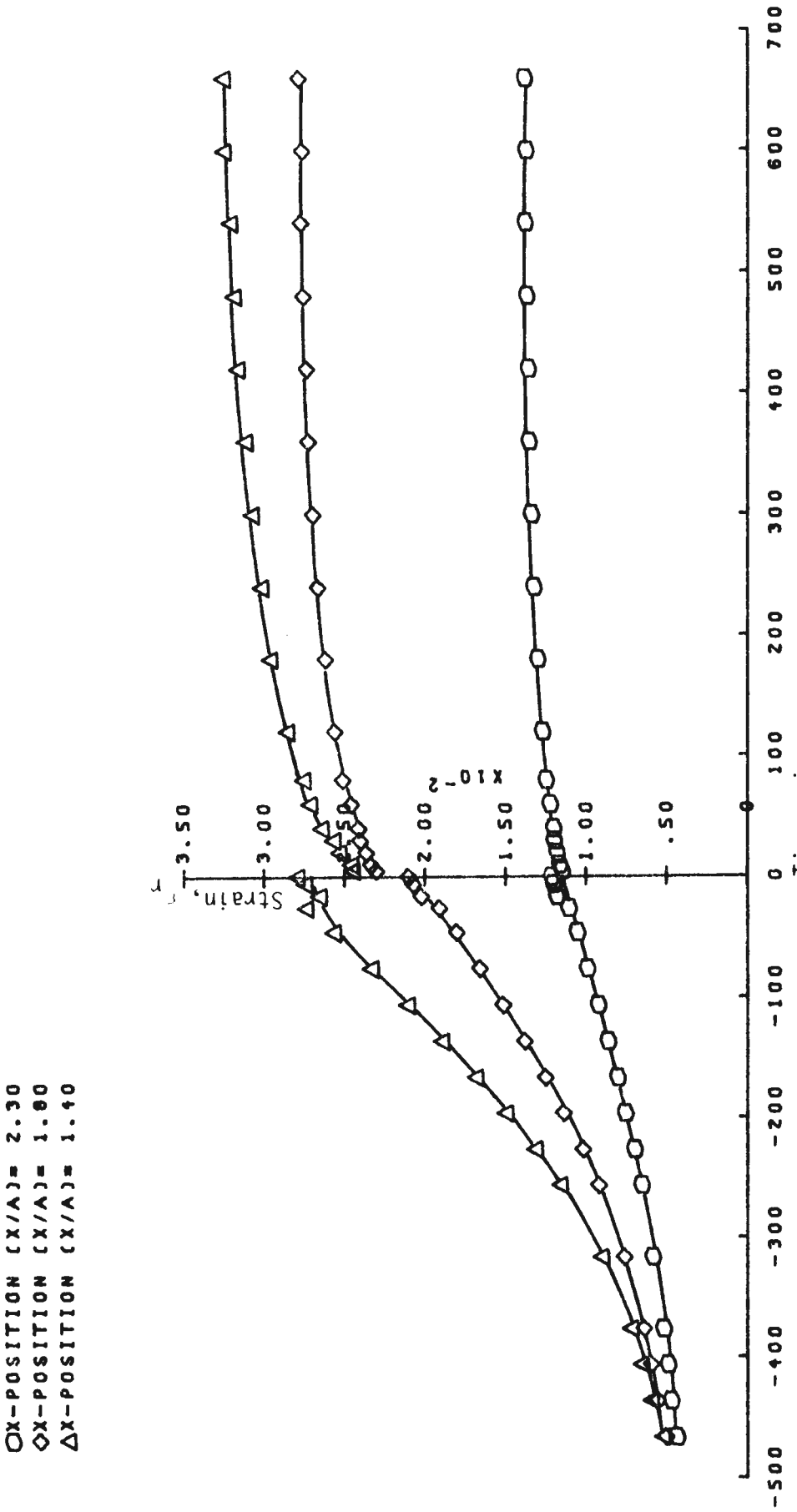

FIGURE C-6 ε_r VS. TIME, LINE B, MODEL II.

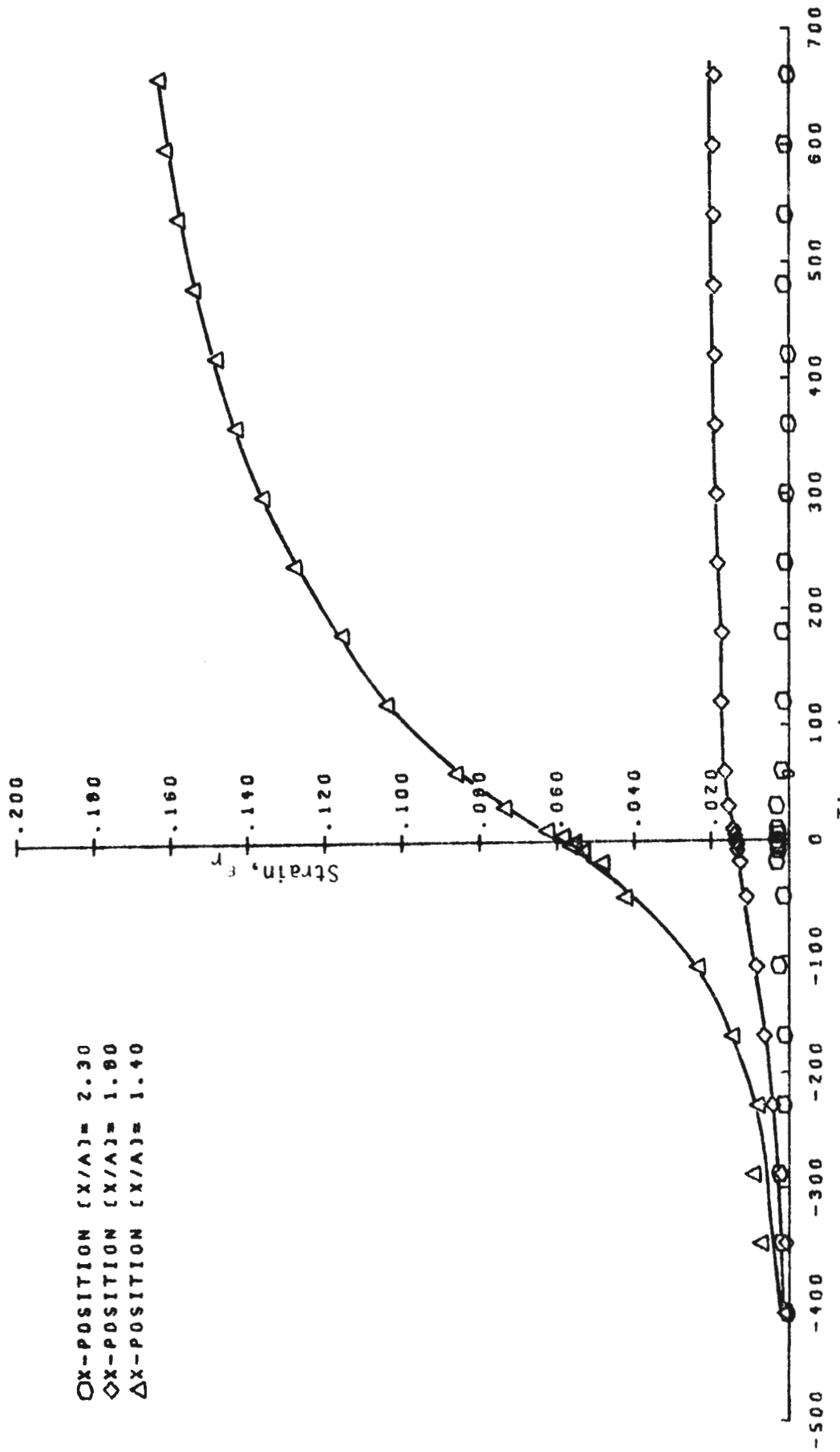

FIGURE C-7 ε_r VS. TIME, LINE A, MODEL V.

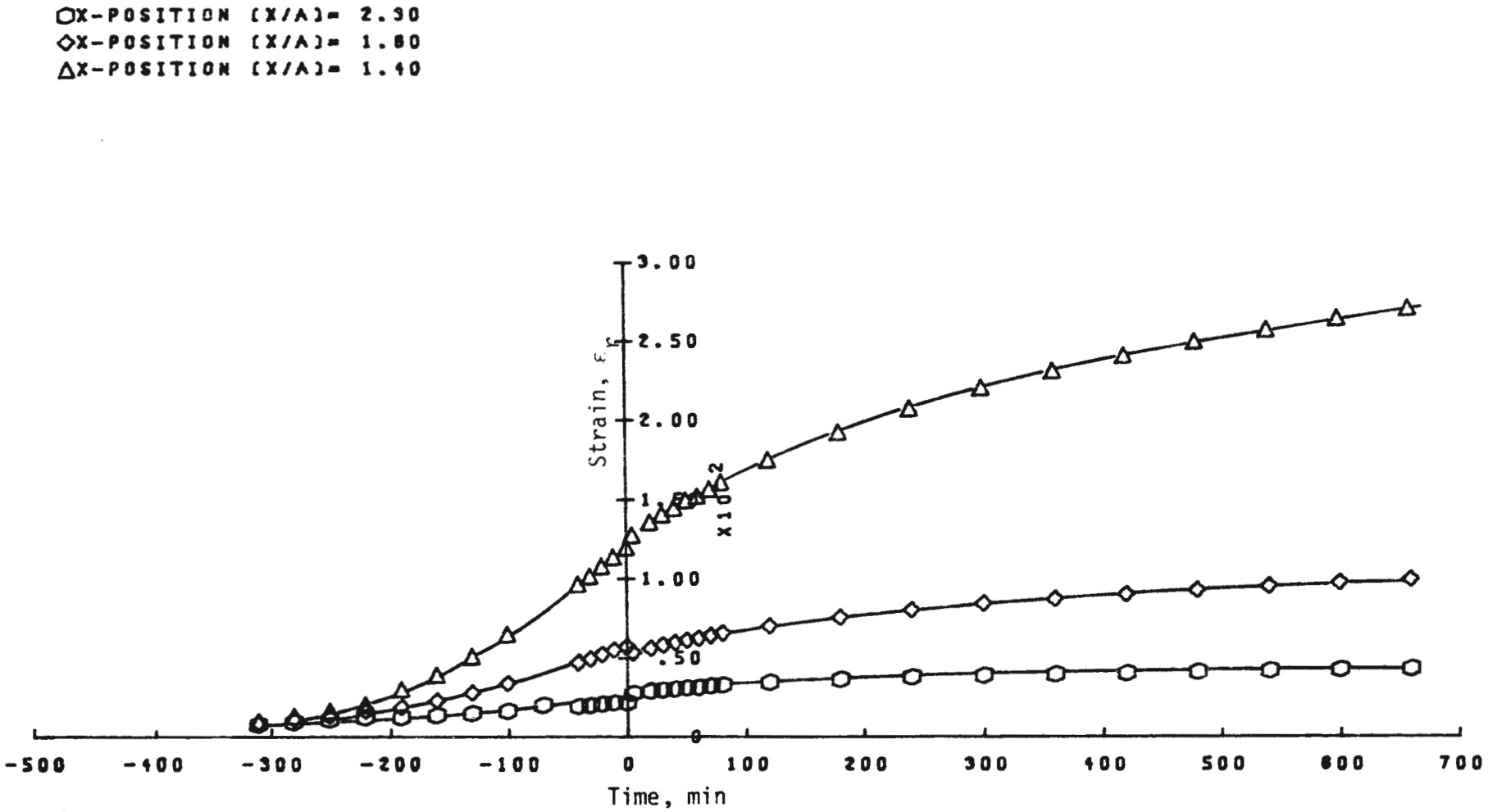

FIGURE C-8 ε_r VS. TIME, LINE A, MODEL VIII.

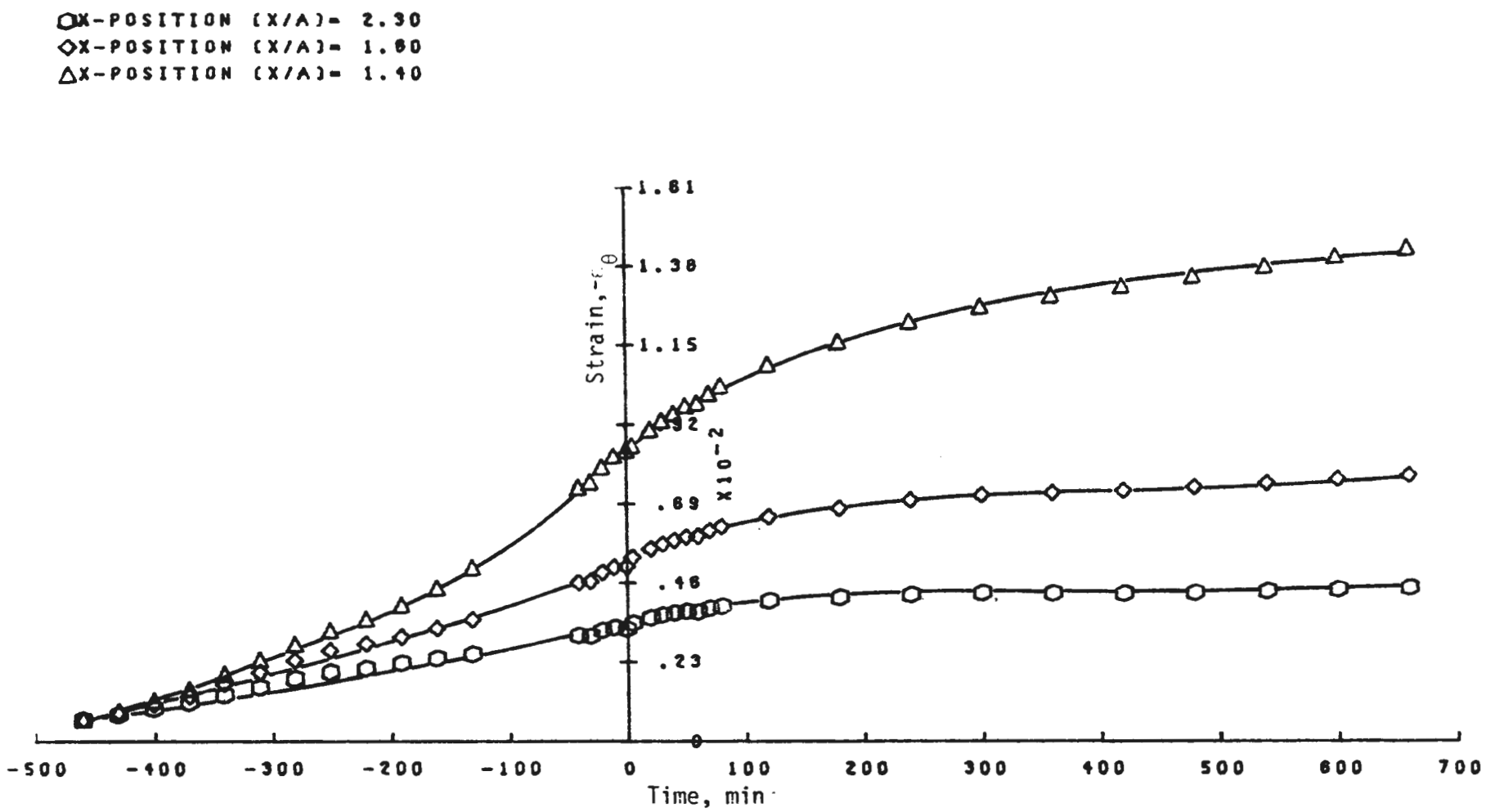

FIGURE C-9 ϵ_θ VS. TIME, LINE A, MODEL VIII

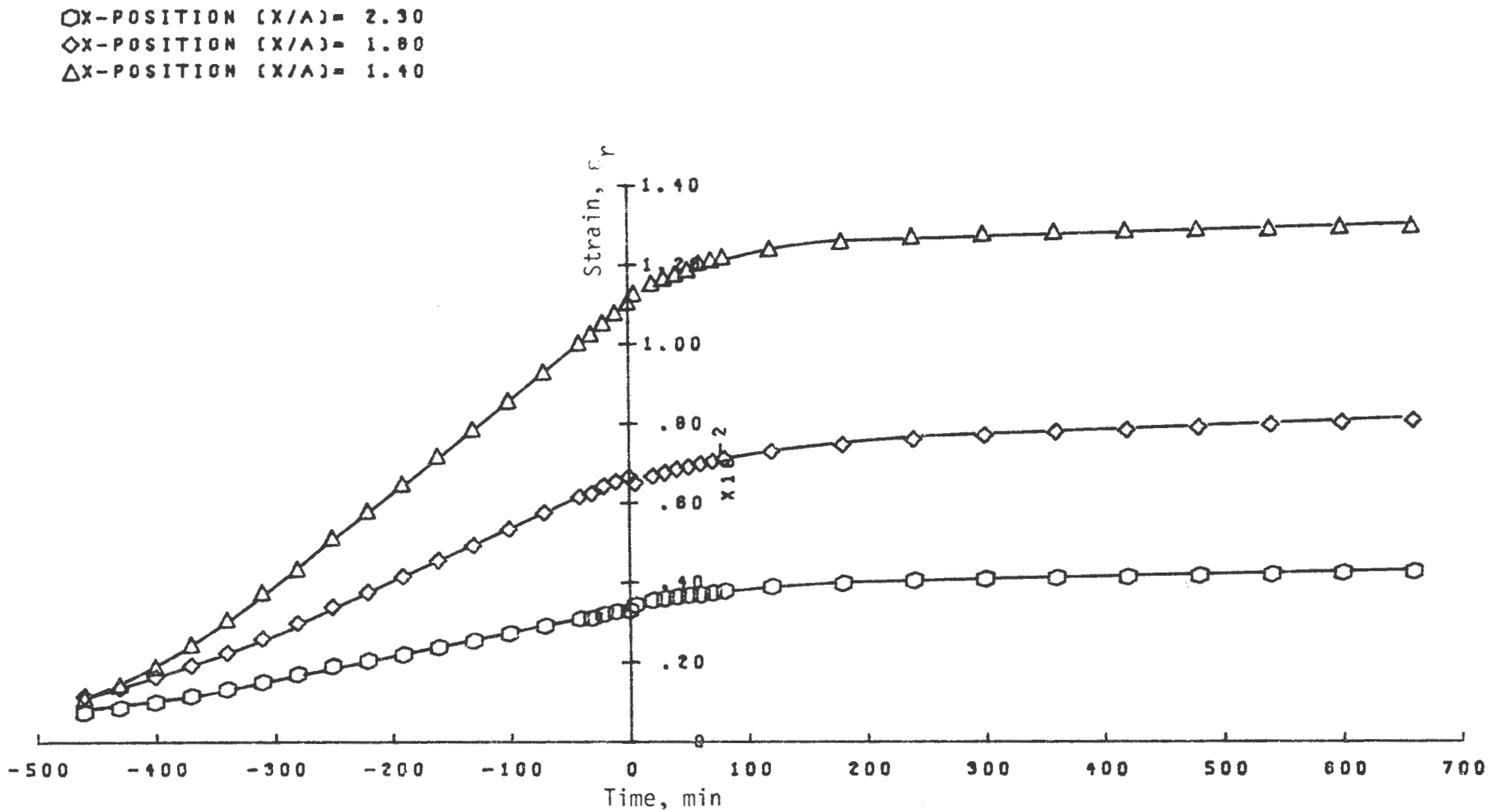

FIGURE C-10 ε_r VS. TIME, LINE B, MODEL VIII.

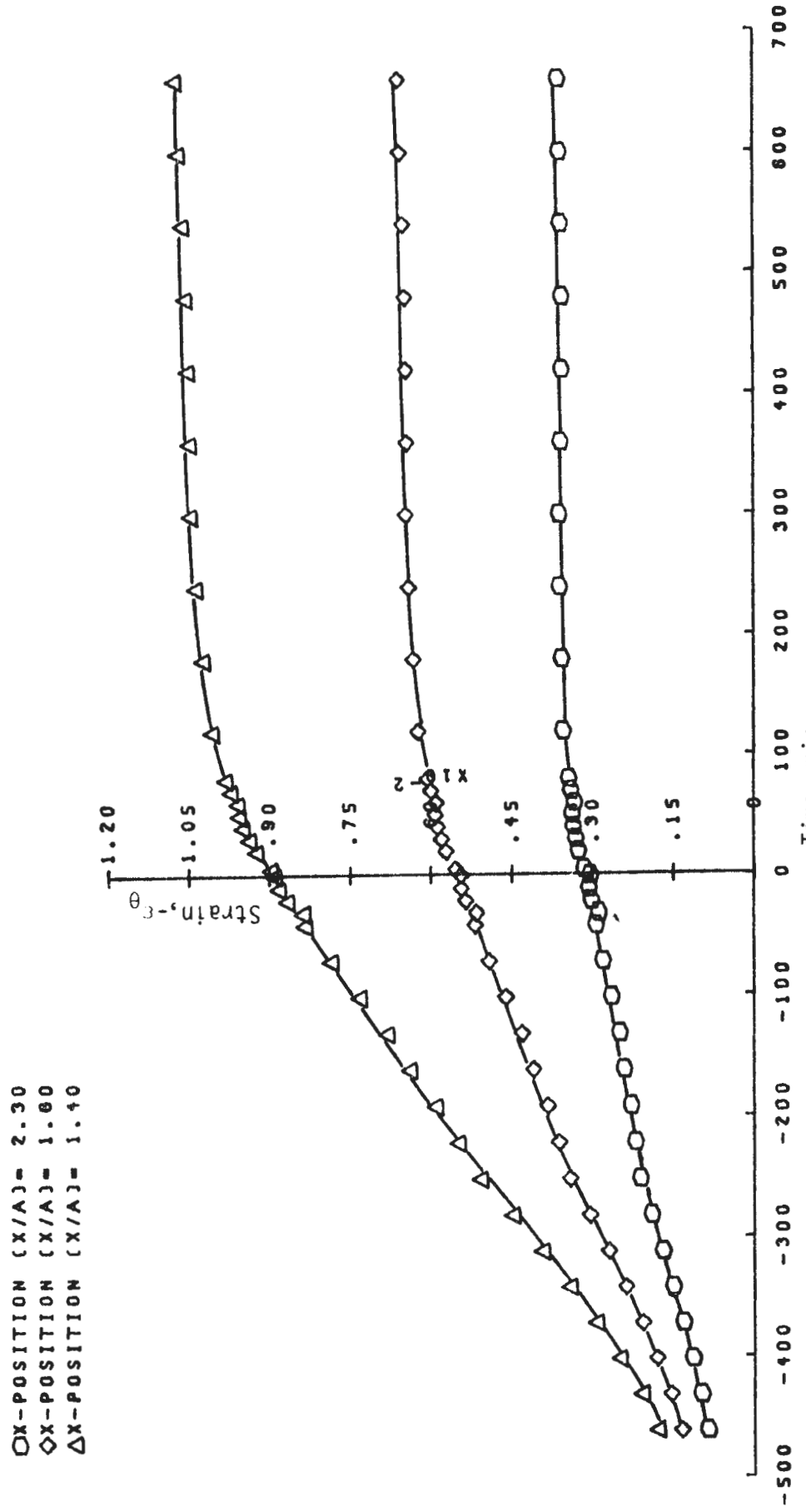

FIGURE C-11 ε_θ VS. TIME, LINE, B, MODEL VIII.

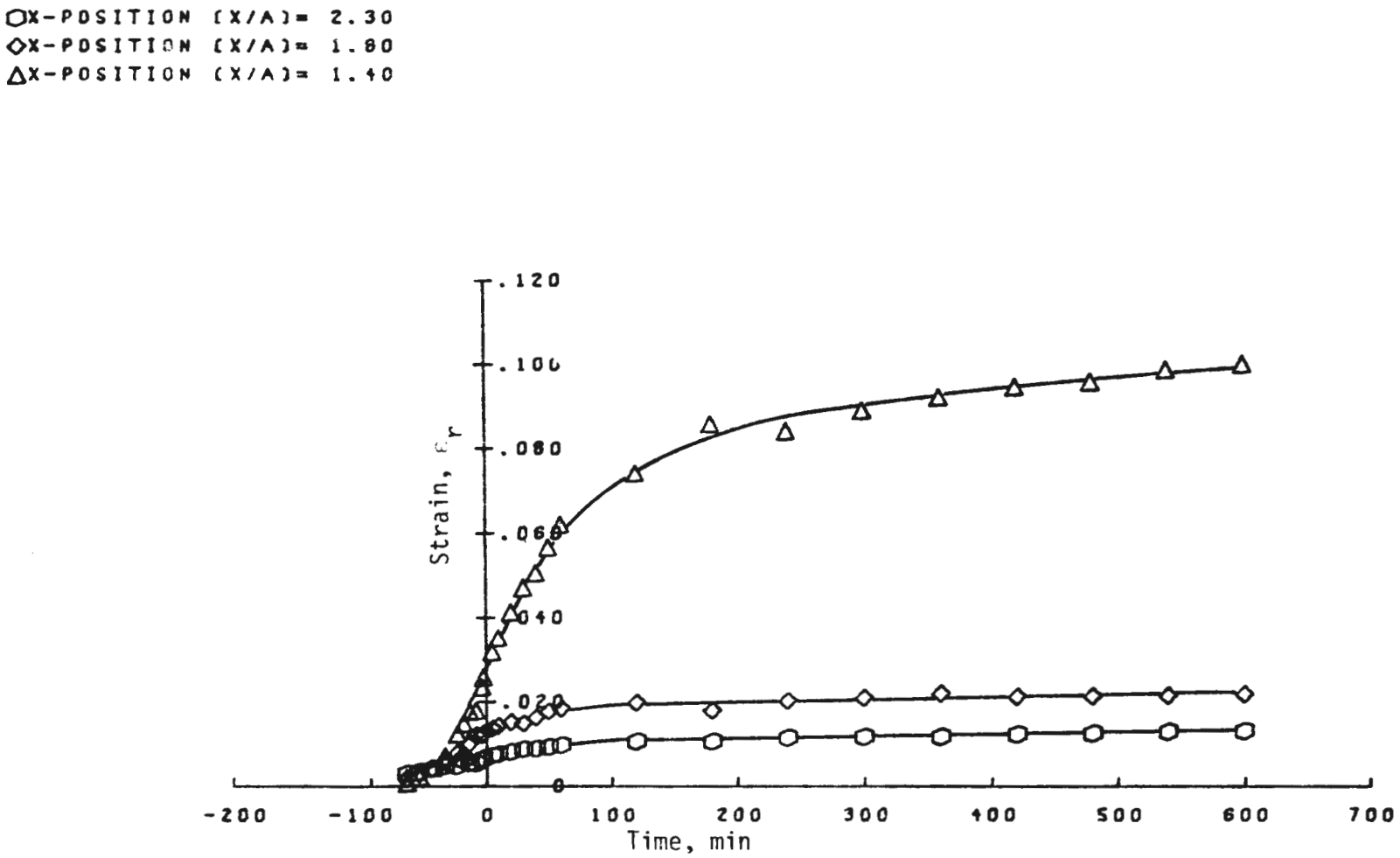

FIGURE C-12 ε_r VS. TIME, LINE A, MODEL V1.

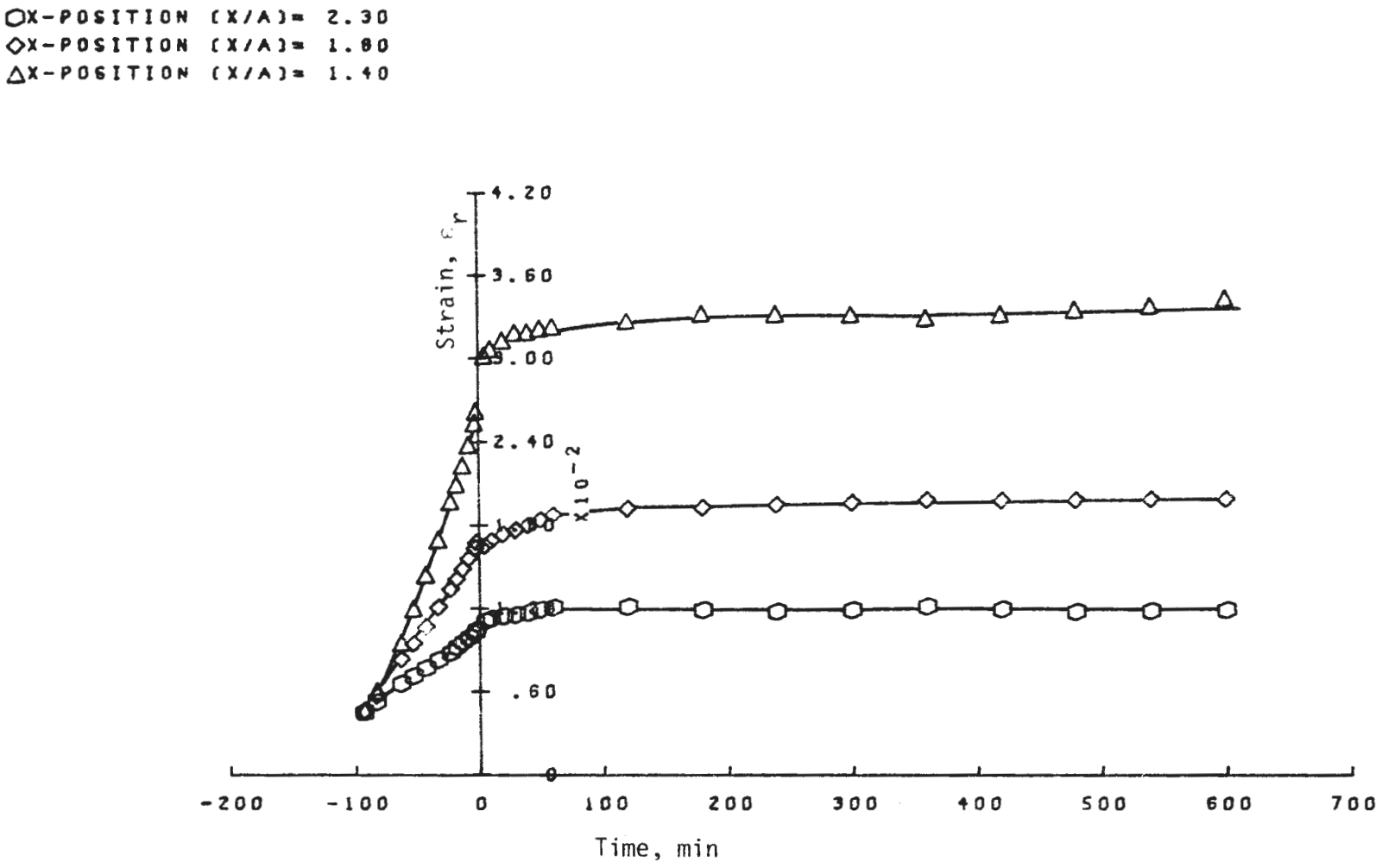

FIGURE C-13 ε_r VS. TIME, LINE B, MODEL V1.

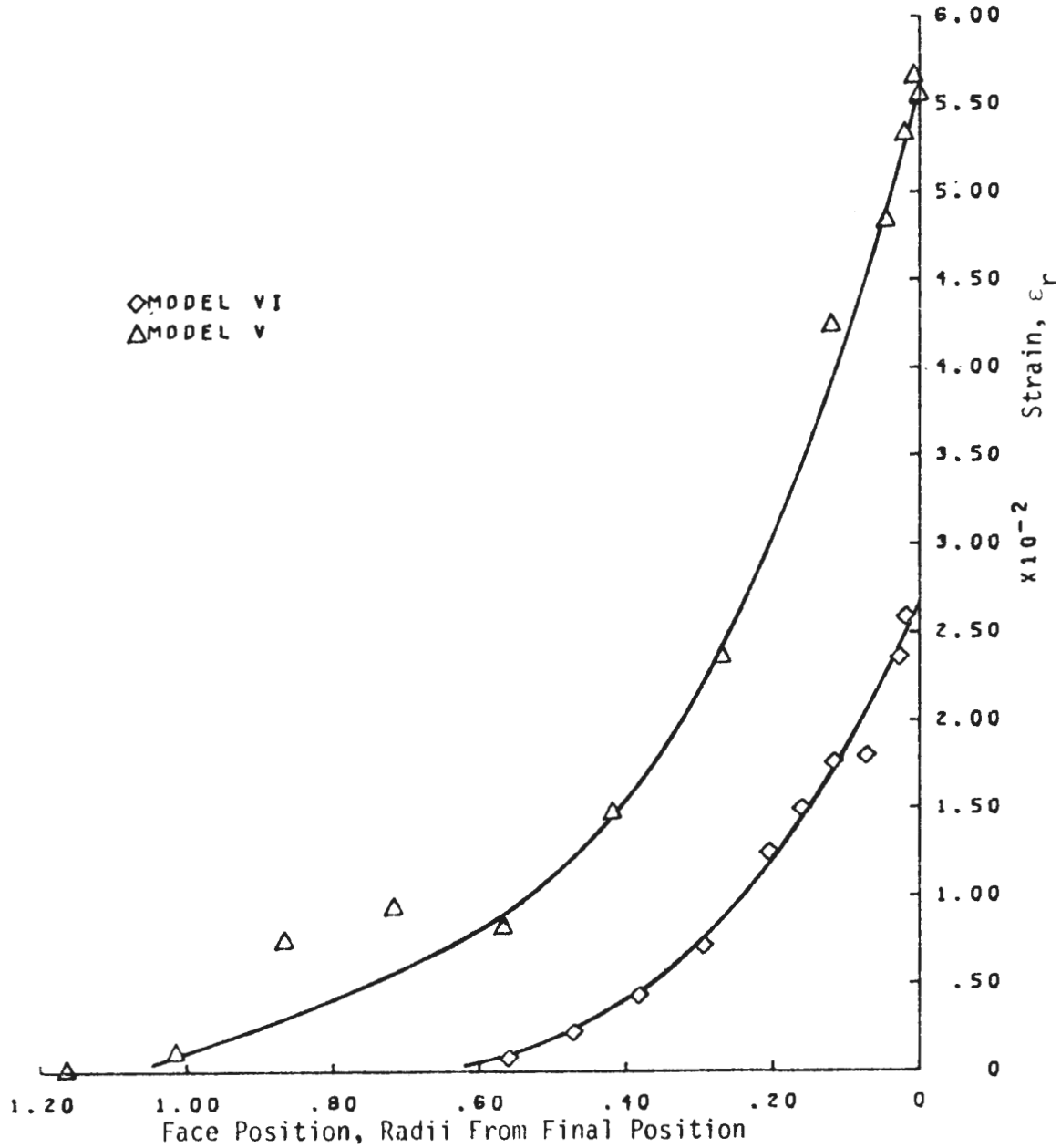

FIGURE C-14 COMPARISON OF ε_r IN MODELS V AND VI ON LINE A AT POSITION $\frac{X}{A} = 1.4$.

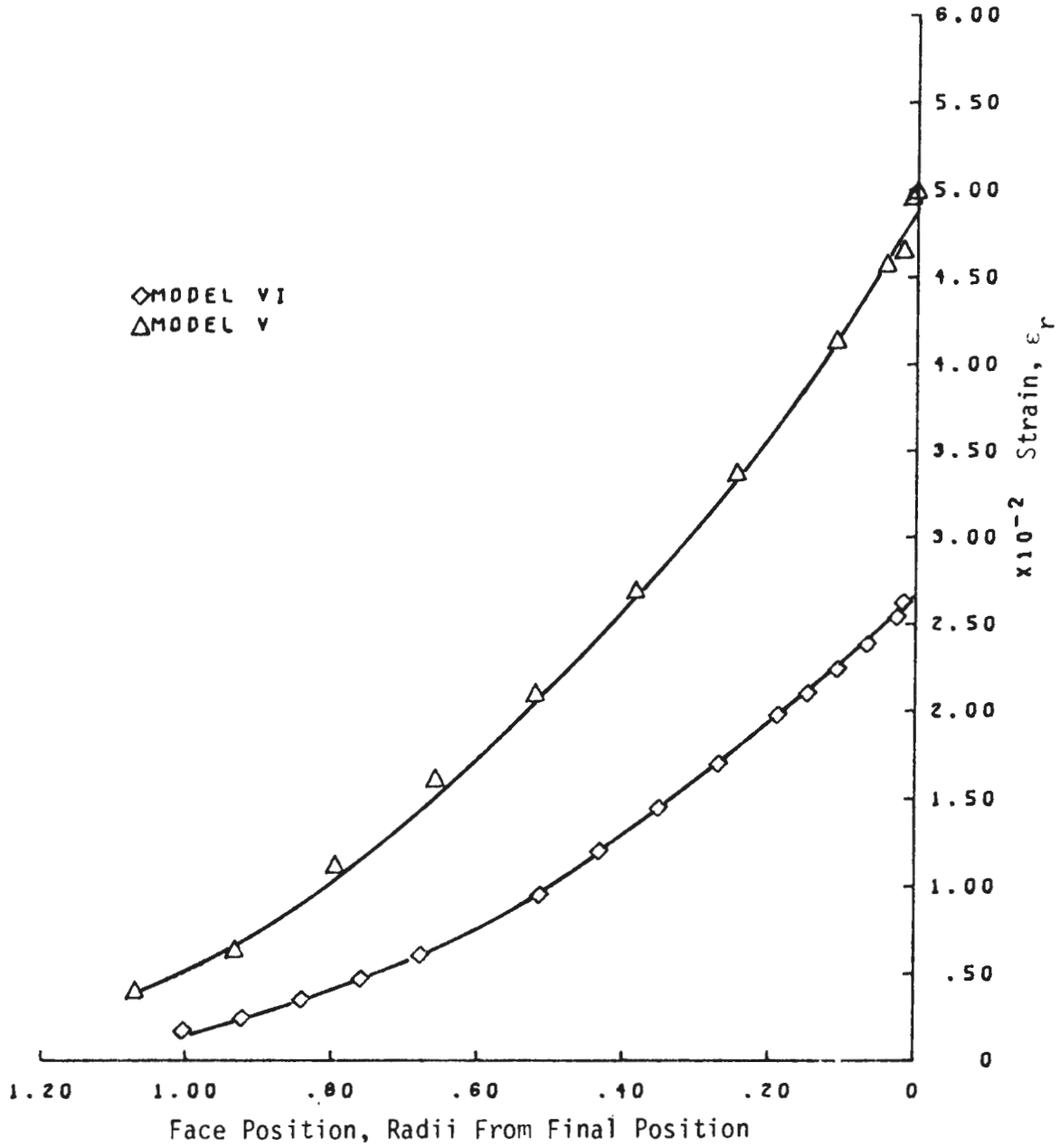

FIGURE C-15 COMPARISON OF ε_r IN MODELS V AND VI ON LINE B AT POSITION $\frac{X}{A} = 1.4$.

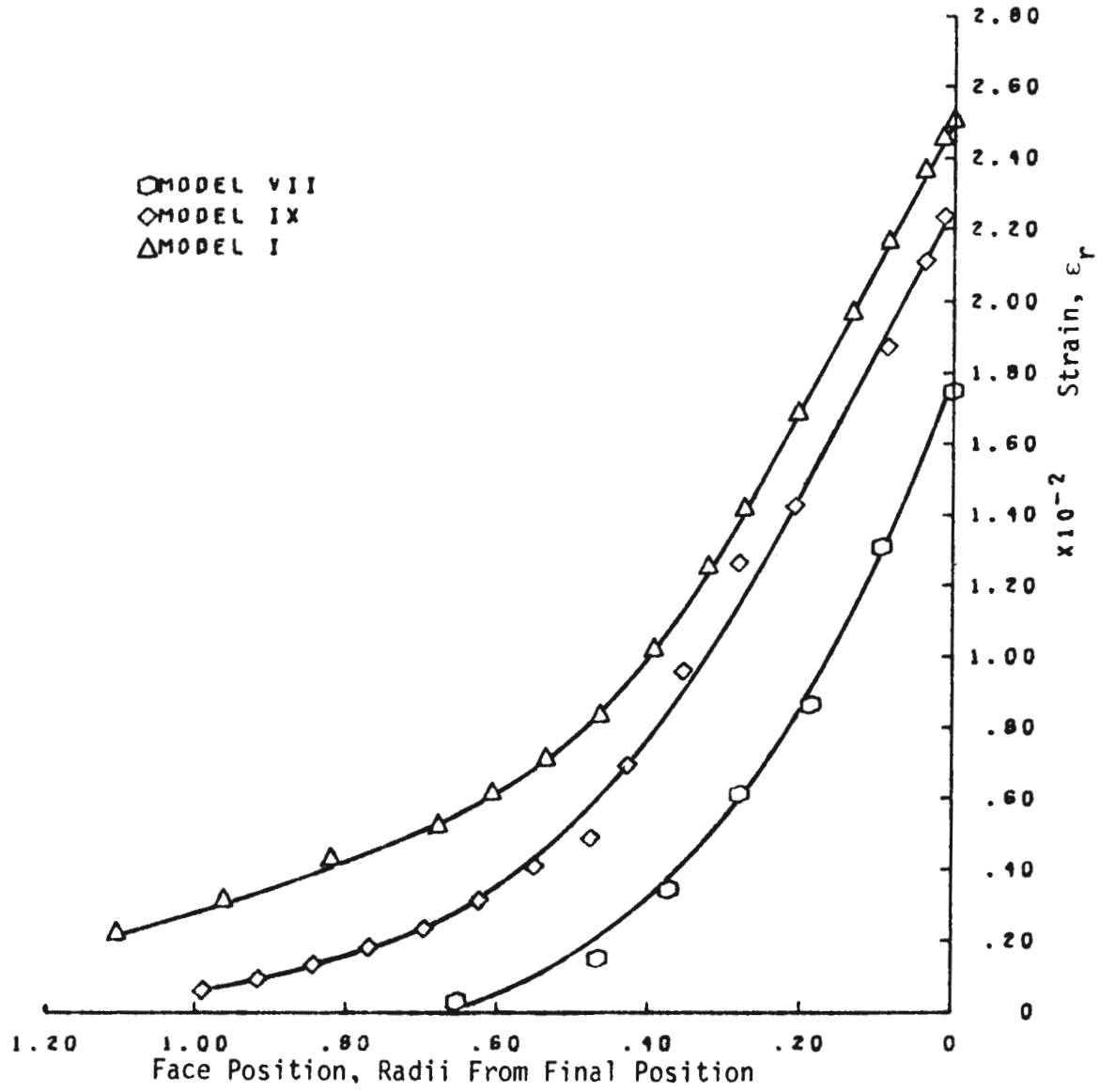

FIGURE C-16 COMPARISON OF ε_r FOR MODELS VII, I AND IX ON LINE A AT POSITION $\frac{x}{A}$ = 1.4.

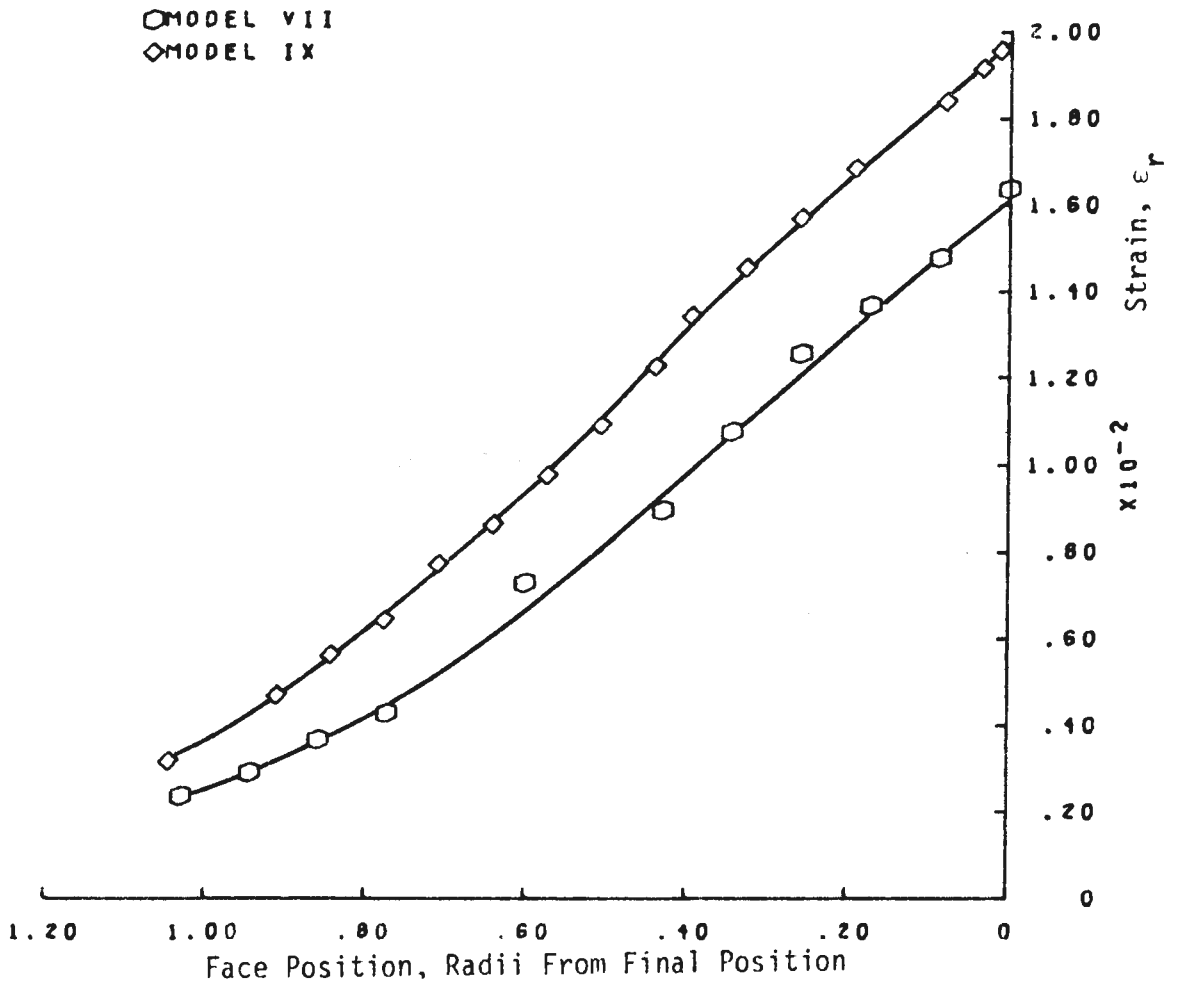

FIGURE C-17 COMPARISON OF ε_r IN MODELS VII, AND IX ON LINE B AT POSITION $\frac{X}{A} = 1.4$.

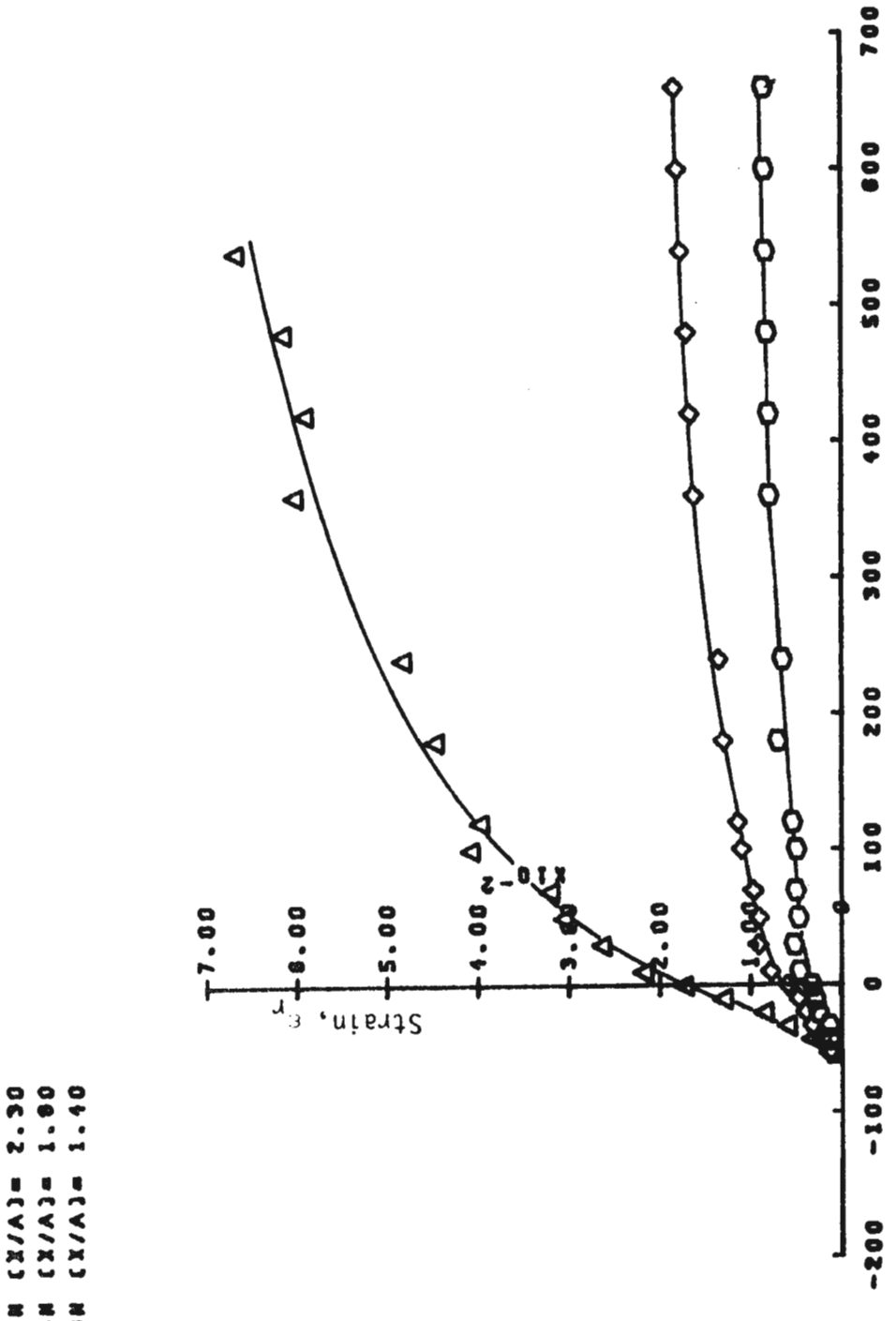

FIGURE C-18 ε_r VS. TIME, LINE A, MODEL V11

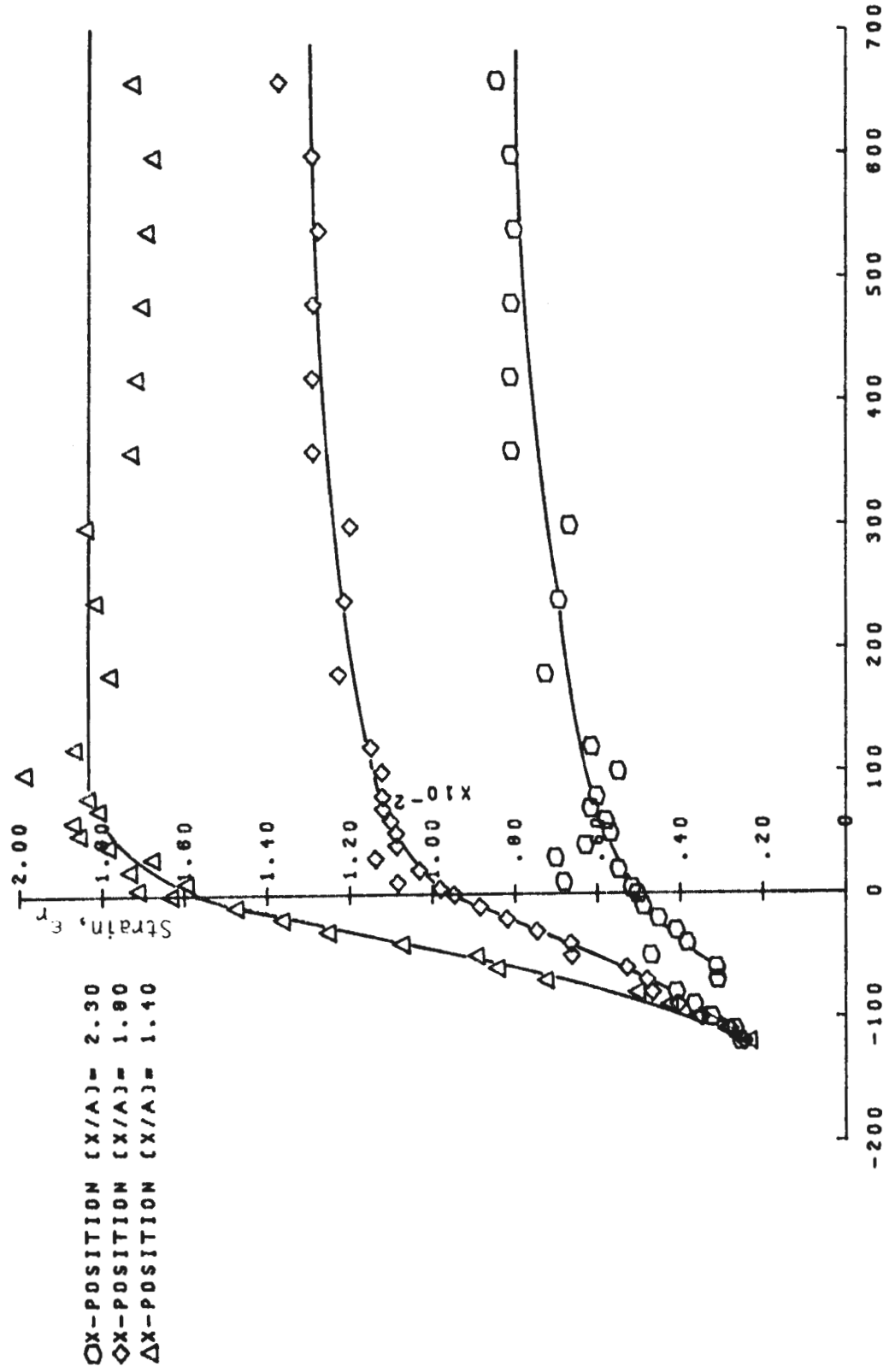

FIGURE C-19 ε_r VS. LINE B, MODEL V11

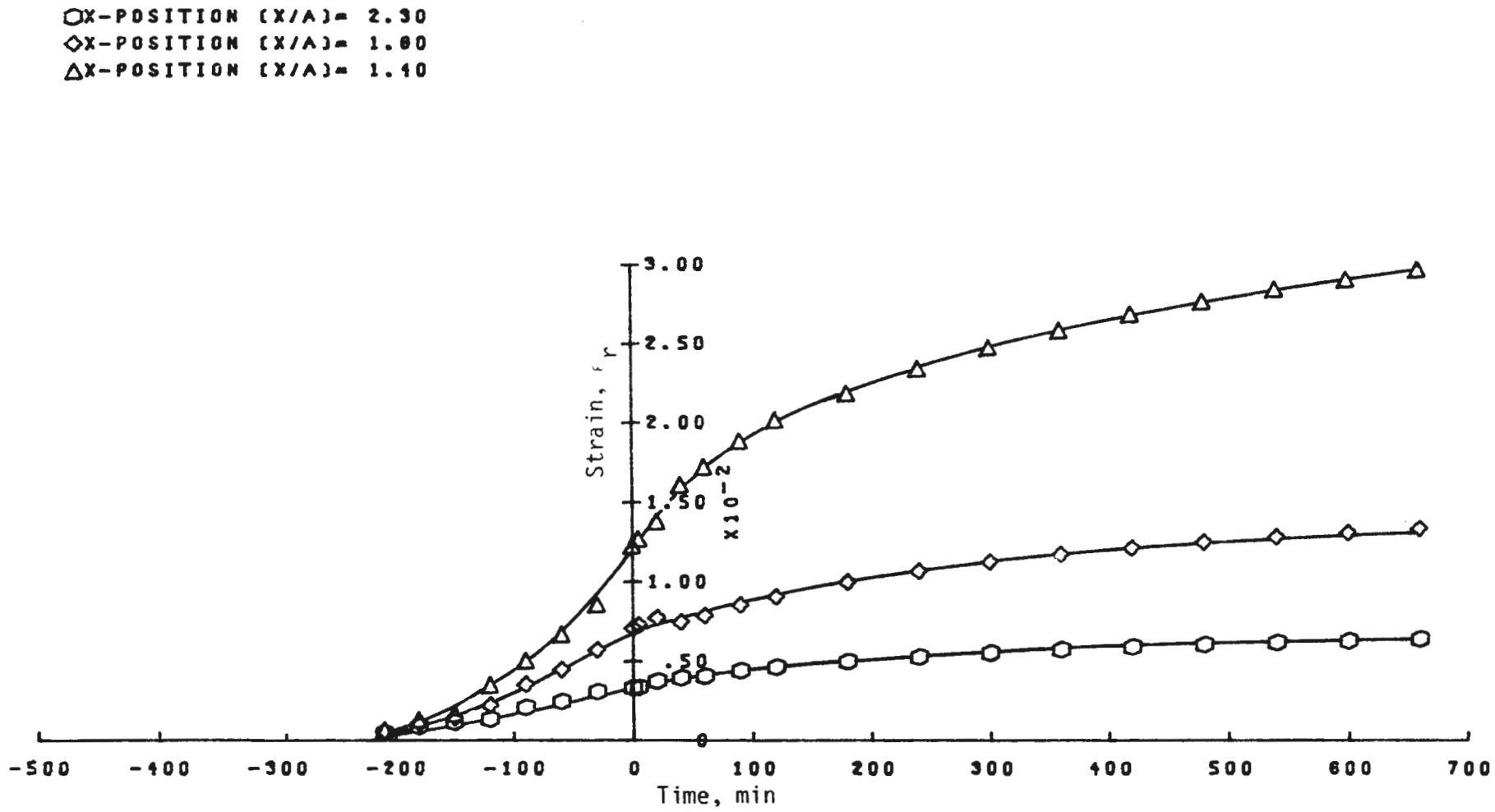

FIGURE C-20 ε_r VS. TIME LINE A, MODEL X

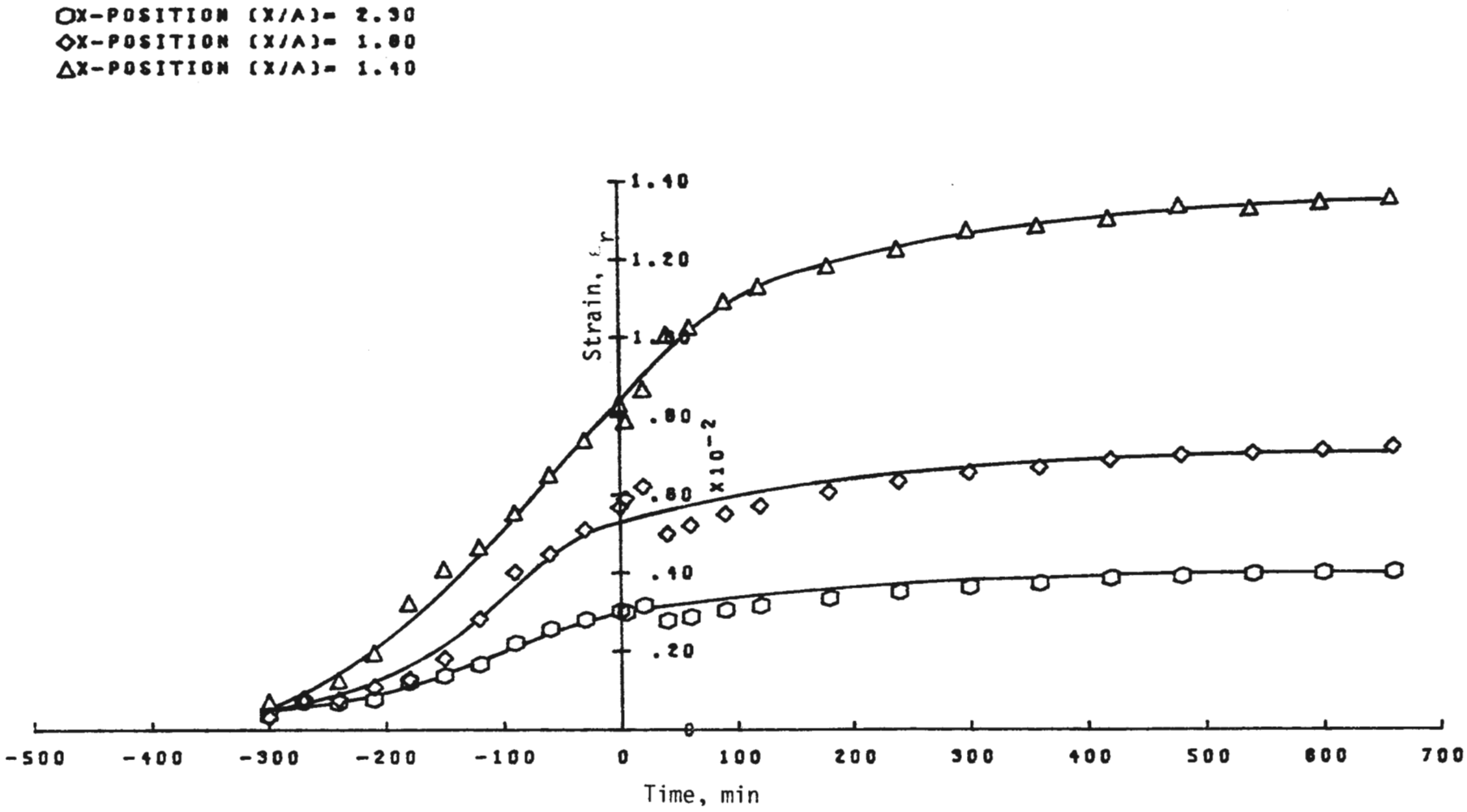

FIGURE C-21 ε_r VS. TIME, LINE B, MODEL X.

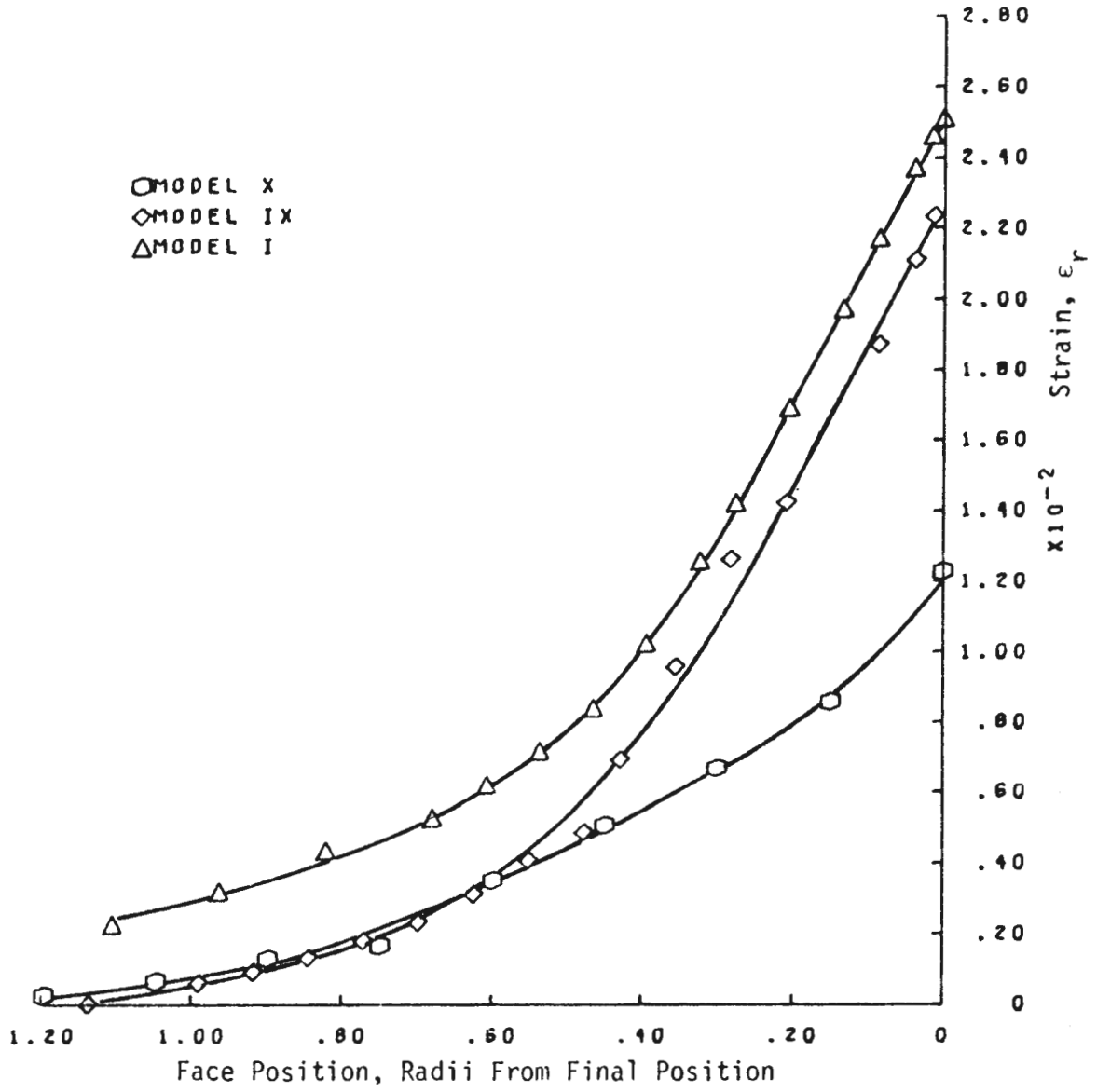

FIGURE C-22 COMPARISON OF ϵ_r IN MODELS X, I AND IX ON LINE A AT POSITION $\frac{X}{A} = 1.4$.

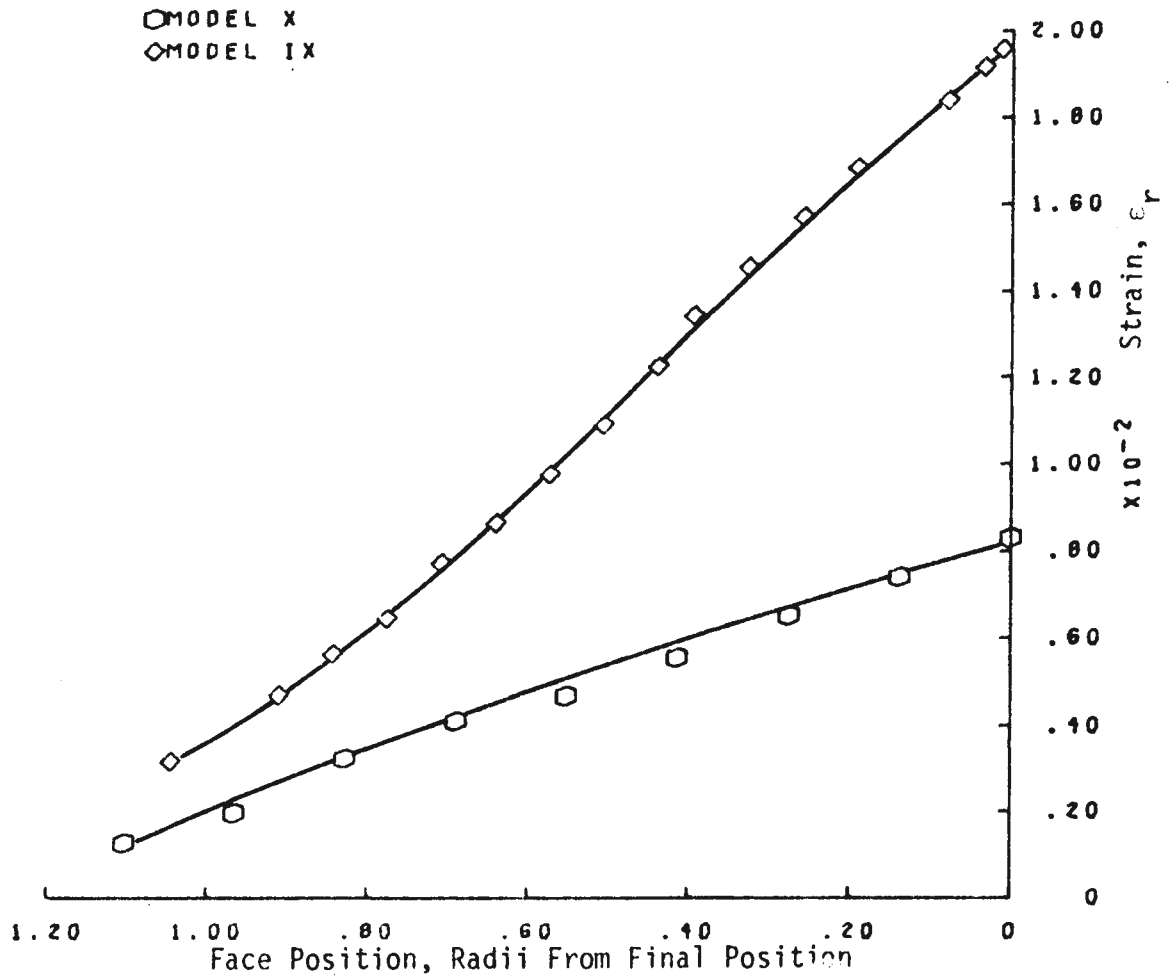

FIGURE C-23 COMPARISON OF ε_r IN MODELS X, AND IX ON LINE B AT POSITION $\frac{X}{A} = 1.4$.

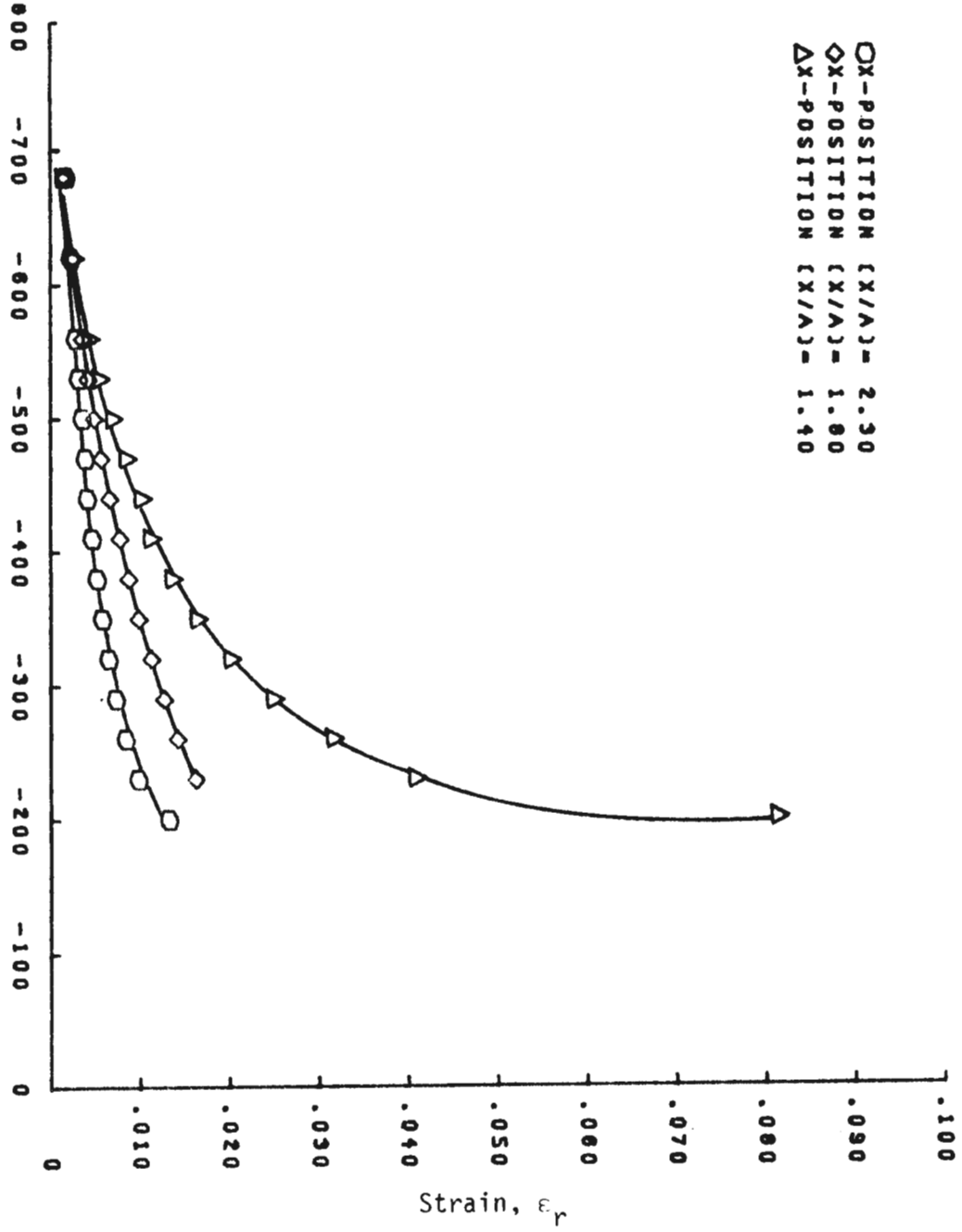

FIGURE C-24 ε_r VS. TIME, LINE A, MODEL X11.

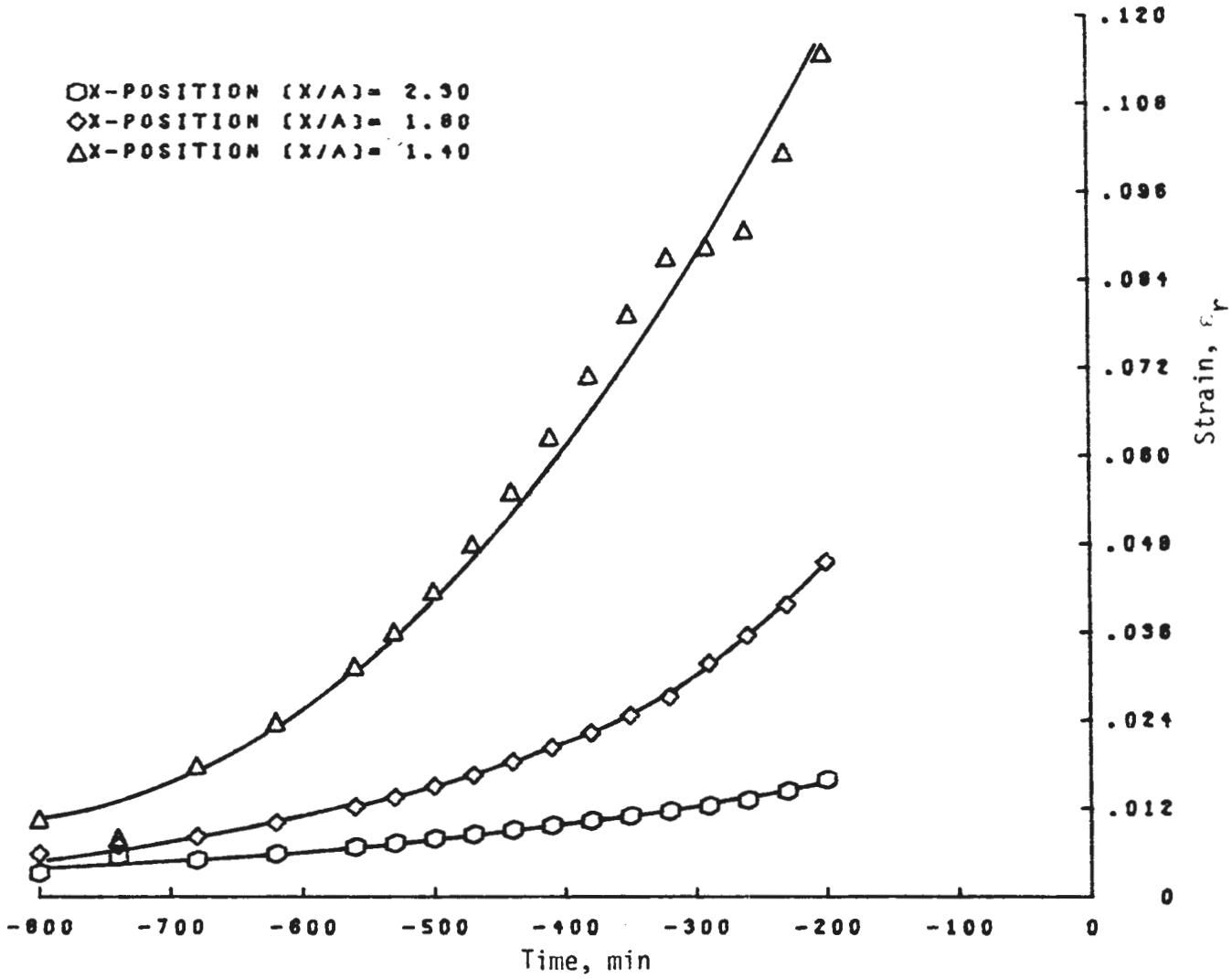

FIGURE C-25 ε_r VS. TIME, LINE B, MODEL X11.

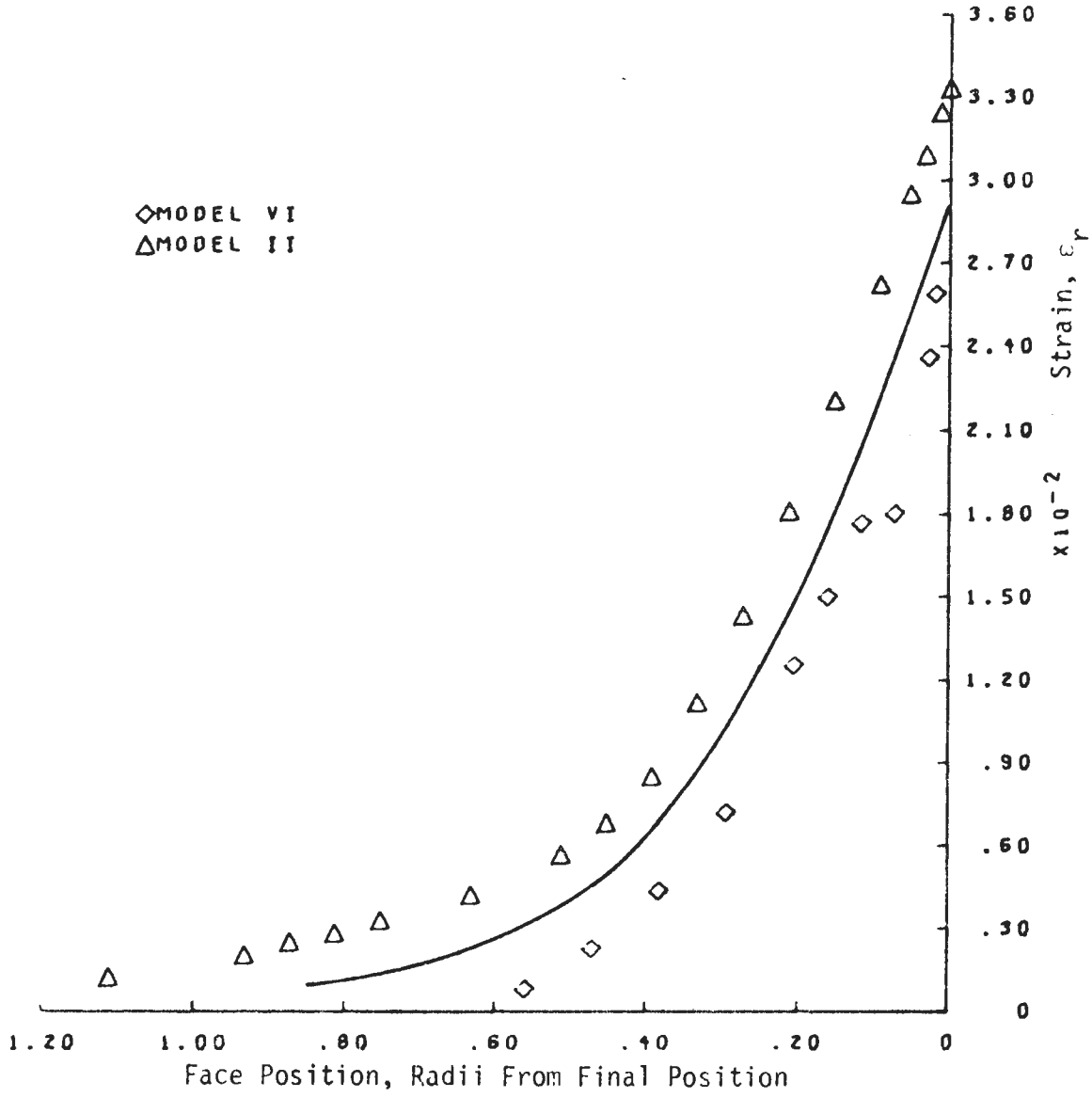

FIGURE C-26 COMPARISON OF ε_r IN MODELS II AND VI ON LINE A AT POSITION $\frac{x}{A} = 1.4$.

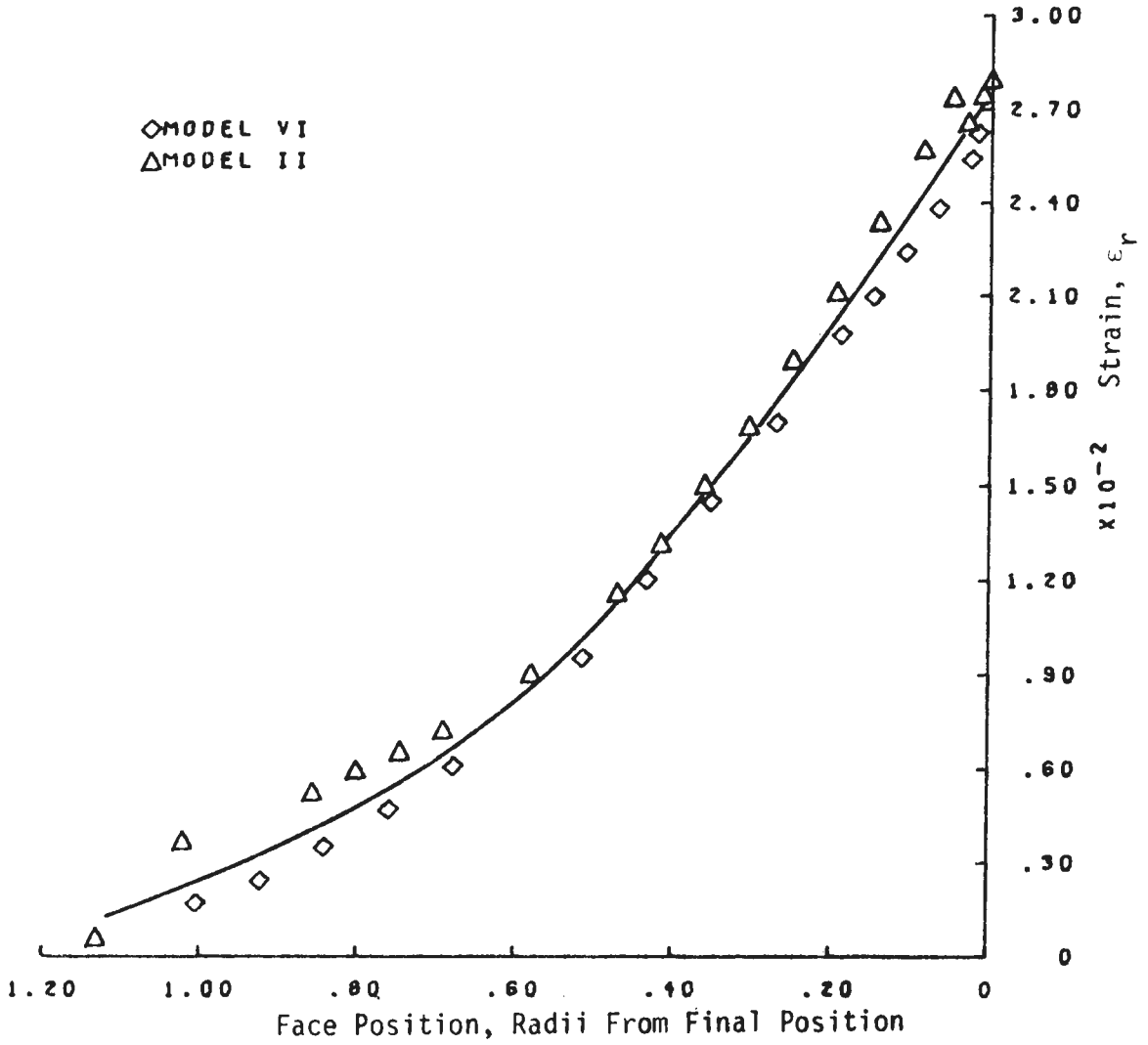

FIGURE C-27 COMPARISON OF ε_r IN MODELS II AND VI ON LINE B AT POSITION $\frac{X}{A} = 1.4$.

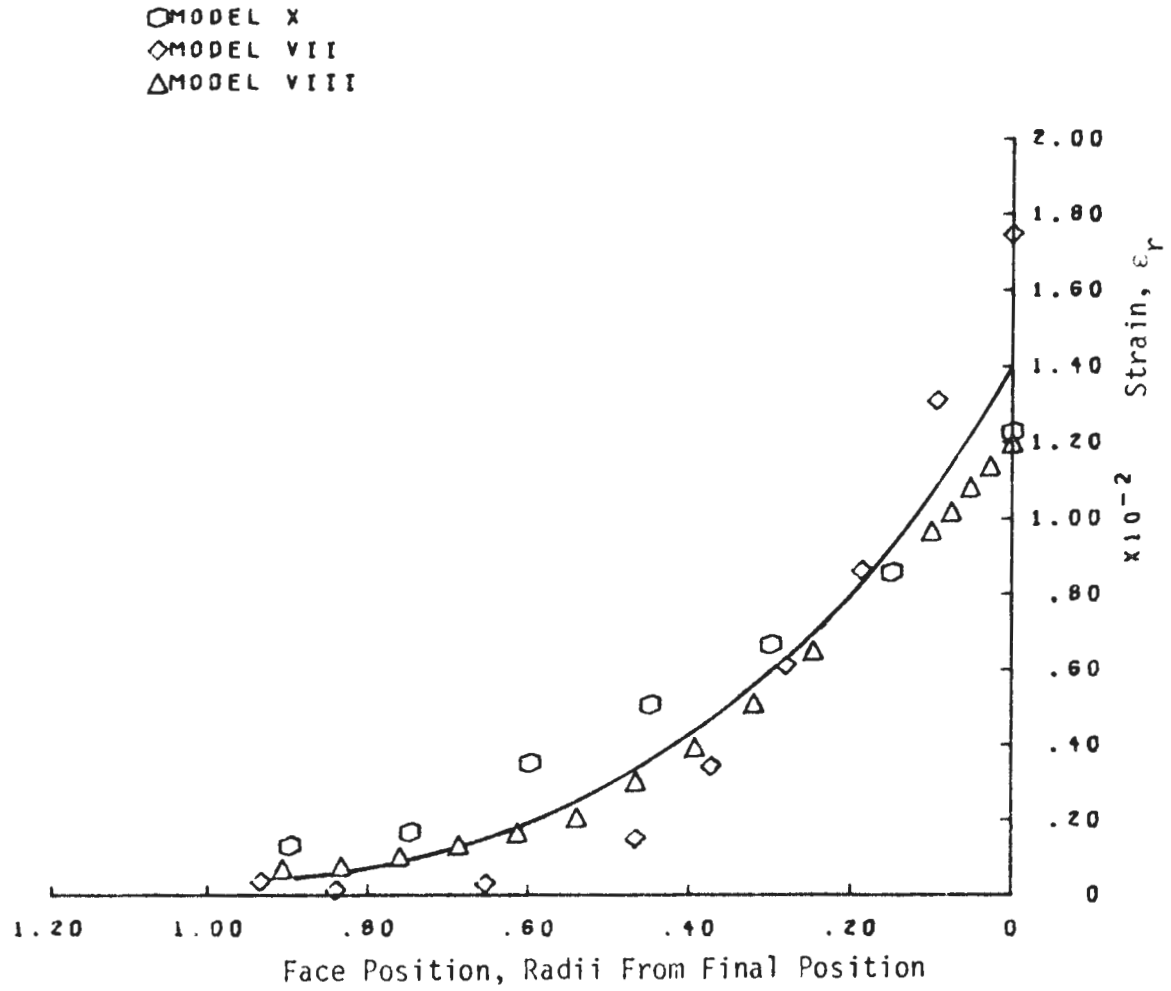

FIGURE C-28 COMPARISON OF ε_r IN MODELS VII, X AND VIII ON LINE A AT POSITION $\frac{x}{A} = 1.4$.

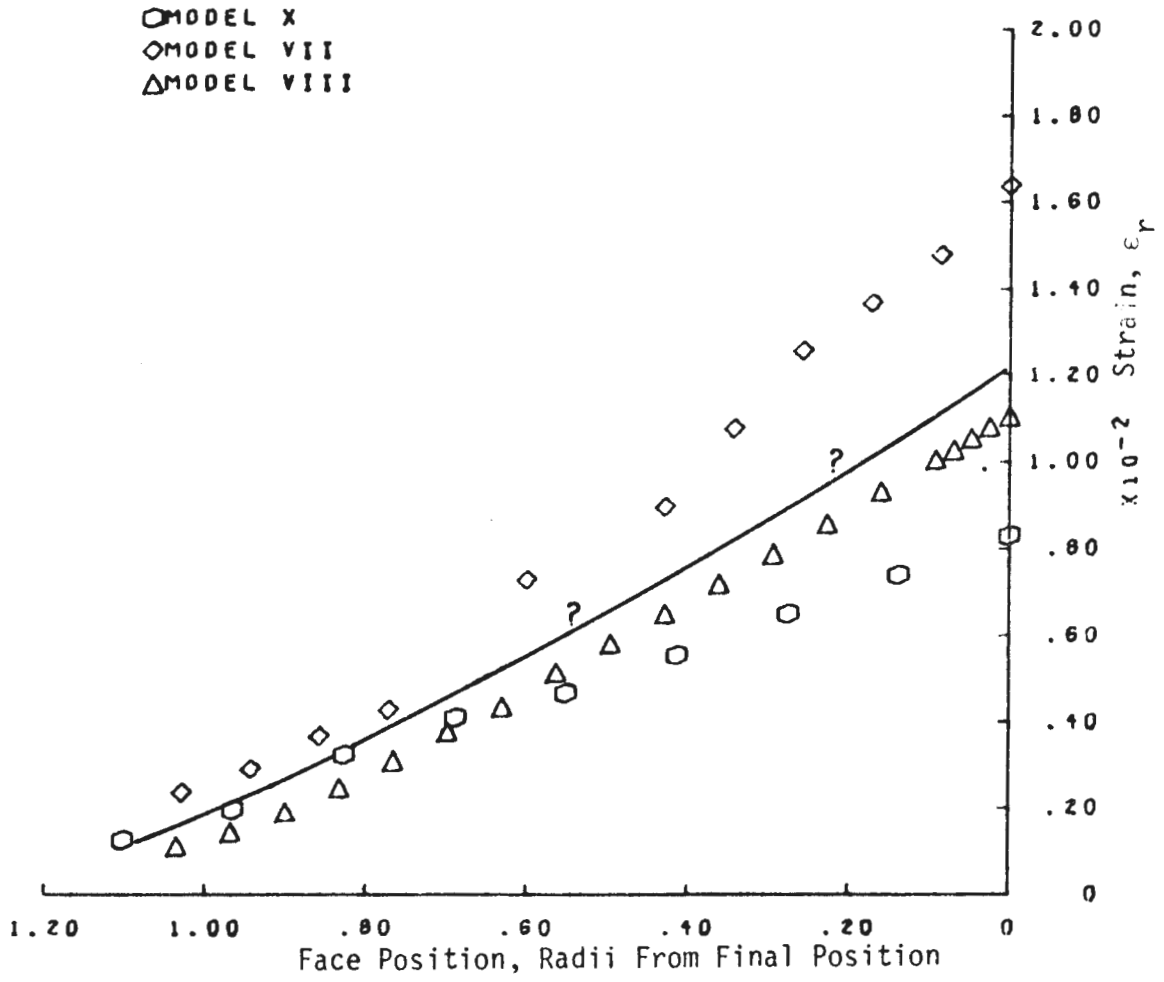

FIGURE C-29 COMPARISON OF ε_r IN MODELS VII, X AND VIII ON LINE B AT POSITION $\frac{x}{A} = 1.4$.

APPENDIX D

LISTINGS OF MAJOR COMPUTER PROGRAMS USED IN STUDY

```
      PROGRAM SENSOR(INPUT,OUTPUT)
C
C     THIS PROGRAM WAS USED TO FIT A CURVE OF THE FORM Y=AXB(EXP(CX)) TO
C     SENSOR CALIBRATION DATA AND OUTPUT THE VALUES OF A, B, AND C.
C
      REAL DATA(30),LDATA(30)
      COMMON/LSTSQ/LDATA,DATA,Z(30)
      PRINT1003
C-M=NO. OF DATA SETS
C- N= NO. OF POINTS
      READ1000,M
      DO 100 I=1,M
      READ1000,N
      READ1001,(Z(J),J=1,N)
      READ1001,(DATA(J),J=1,N)
      DO 101 J=1,N
      Z(J)=ALOG(Z(J))
      LDATA(J)=ALOG(DATA(J))
  101 CONTINUE
      CALL LSTSQ(N,A,B,C)
      PRINT1004,A,B,C
      DO 500 K=1,N
      DUM2=C*DATA(K)
      DUM=B*LDATA(K)
      DUM=EXP(DUM)
      DATA(K)=A*DUM*EXP(DUM2)
  500 CONTINUE
      PRINT1005,(DATA(K),K=1,N)
 1005 FORMAT(1X,8E16.6)
  100 CONTINUE
 1000 FORMAT(1I2)
 1001 FORMAT(8E10.4)
 1003 FORMAT(10X,*A*,15X,*B*,15X,*C*)
 1004 FORMAT(1X,3E16.6)
      STOP
      END



      SUBROUTINE LSTSQ(M,A,B,C)
      COMMON/LSTSQ/X(30),Y(30),Z(30)
      D=FLOAT(M)
      SX=0.
      SXX=0.
      SXY=0.
      SY=0.
      SYY=0.
      SXZ=0.
      SZ=0.
      SYZ=0.
      DO 10 I=1,M
      SX=SX+X(I)
      SY=SY+Y(I)
      SZ=SZ+Z(I)
      SXX=SXX+X(I)*X(I)
```

```
      SXY=SXY+X(I)*Y(I)
      SXZ=SXZ+X(I)*Z(I)
      SYY=SYY+Y(I)*Y(I)
   10 SYZ=SYZ+Y(I)*Z(I)
      DET=D*(SXX*SYY-SXY*SXY)-SX*(SX*SYY-SXY*SY)+SY*(SX*SXY-SXX*SY)
      A=(SZ*(SXX*SYY-SXY*SXY)-SX*(SXZ*SYY-SXY*SYZ)+SY*(SXZ*SXY-SXX*SYZ))
     $/DET
      A=EXP(A)
      B=(D*(SXZ*SYY-SXY*SYZ)-SZ*(SX*SYY-SXY*SY)+SY*(SX*SYZ-SXZ*SY))/DET
      C=(D*(SXX*SYZ-SXZ*SXY)-SX*(SX*SYZ-SXZ*SY)+SZ*(SX*SXY-SXX*SY))/DET
      RETURN
      END
```

```
      PROGRAM DISPLC(INPUT,OUTPUT,TAPE5=INPUT,TAPE1,TAPE2)
C
C     THIS PROGRAM WAS USED TO CONVERT SENSOR READINGS IN TERMS OF
C     VOLTAGES INTO DISPLACEMENTS AND OUTPUT CUMULATIVE DISPLACEMENTS
C     OF EACH SENSOR.
C
      DIMENSION DATA(24,2),IDATA(24,2),CAL(3,21)
      COMMON DATA
      INTEGER TIME
      DATA CAL/16.7245,-.464954,.227689E-04,20.1237,-.437548,-.416505E-0
     $4,8.71441,-.239970,-.580009E-04,8.14430,-.233795,-.650560E-04,8.47
     $100,-.235776,-.576761E-04,8.66734,-.239573,-.534692E-04,8.12091,-.
     $233436,-.642371E-04,17.7974,-.456959,.127089E-04,5.76961,-.255285,
     $-.842062E-04,10.5409,-.273815,-.348747E-04,8.22188,-.234707,-.6625
     $97E-04,8.43655,-.237310,-.599266E-04,8.21644,-.234484,-.635197E-04
     $,8.36574,-.236673,-.614752E-04,15.5359,-.456345, .210192E-04,6.100
     $68,-.273401,-.103662E-03,10.3718,-.269608,-.414403E-04,7.82222,-.2
     $25050,-.715918E-04,9.09359,-.248253,-.553690E-04,8.48799,-.238879,
     $-.623271E-04,8.54078,-.239410,-.559065E-04/
      READ1011,NSETS,INTIM
      CALL INIT(TIME,INTIM,N)
      PRINT1006
  130 READ1010,(IDATA(I,N),I=1,24)
      IF(EOF,5) 120,121
  121 PRINT1007,(IDATA(I,N),I=1,24)
      PRINT1008
      WRITE(2) (IDATA(I,N),I=1,24)
      GO TO 130
  120 ENDFILE2
      REWIND2
      PRINT1005
      PRINT1000
  102 READ(2) (IDATA(I,N),I=1,24)
      IF(EOF,2) 104,114
C-PLACE DECIMAL POINT IN NOS.
  114 DO 105 I=1,24
      IDUM=(IDATA(I,N)/10)*10
      IEXP=IDATA(I,N)-IDUM
      IEXP=IEXP-2
      IF(IEXP) 122,122,123
  123 DATA(I,N)=FLOAT(IDUM)
      DATA(I,N)=DATA(I,N)/(10**IEXP)
  105 CONTINUE
C-CHANGE VOLTAGES TO LOCAL DISPLACEMTNTS
      DO 100 I=2,22
      J=I-1
      D1=CAL(2,J)
      D2=D1*ALOG(DATA(I,N))
      D2=EXP(D2)
      D3=EXP(DATA(I,N)*CAL(3,J))
      DATA(I,N)=CAL(1,J)*D2*D3
  100 CONTINUE
      IF (N.EQ.2) GO TO 112
      GO TO 101
C-ADD TIME TO TOTAL TIME
  112 D1=DATA(24,2)
```

```
      IF(D1.LT.11000.    .AND.D1.GT.9000.     ) GO TO 107
      IF(D1.LT.8999.     .AND.D1.GT.7000.     ) GO TO 108
      IF(D1.LT.6999.     .AND.D1.GT.5000.     ) GO TO 109
      IF(D1.LT.4999.     .AND.D1.GT.3000.     ) GO TO 110
      IF(D1.LT.2999.     .AND.D1.GT.1000.     ) GO TO 111
  107 TIME=(TIME/60)*60+60
      GO TO 113
  108 TIME=(TIME/30)*30+30
      GO TO 113
  109 TIME=(TIME/10)*10+10
      GO TO 113
  110 TIME=(TIME/5)*5+5
      GO TO 113
  111 TIME=TIME+1
C-CALCULATE DISPLACEMENTS RELATIVE TO INITIAL STATION POSITIONS
  113 DO 106 K=1,3
      JJ=K*7+2
      DEL1=0.
      DO 103 I=1,7
      J=JJ-I
      DEL2=DEL1-DATA(J,1)+DATA(J,2)
      DATA(J,2)=DEL2
      DEL1=DEL2
  103 CONTINUE
  106 CONTINUE
  101 PRINT1001,NSETS,TIME,(DATA(I,N),I=2,8)
      PRINT1001,NSETS,TIME,(DATA(I,N),I=9,15)
      PRINT1001,NSETS,TIME,(DATA(I,N),I=16,22)
      WRITE(1) TIME,(DATA(I,N),I=2,22)
      N =2
      NSETS=NSETS+1
      GO TO 102
  104 PRINT1001,NSETS,TIME,(DATA(I,1),I=2,8)
      PRINT1001,NSETS,TIME,(DATA(I,1),I=9,15)
      PRINT1001,NSETS,TIME,(DATA(I,1),I=16,22)
      WRITE(1) TIME,(DATA(I,1),I=2,22)
      ENDFILE1
      GO TO 124
  122 PRINT1004
      GO TO 104
  124 STOP
 1004 FORMAT(10X,*DATA ERROR*)
 1006 FORMAT(20X,*RAW DATA*)
 1007 FORMAT(1X,I9,5I10)
 1008 FORMAT(1X,*--------------------*)
 1011 FORMAT(I5,I1)
 1001 FORMAT(1X,I5,I11,7E16.6)
 1000 FORMAT(1X,*COUNT*,2X,*TIME (MIN)*,3X,*DSPL ST1 (IN)*,3X,*DSPL ST2
     $ (IN)*,3X,
     $*DSPL ST3 (IN)*,3X,*DSPL ST4 (IN)*,3X,*DSPL ST5 (IN)*,3X,*DSPL ST6
     $ (IN)*,3X,*DSPL ST7 (IN)*)
 1005 FORMAT(//39X,*DISPLACEMENTS OF STATIONS OF SENSOR LINES A,B AND F*
     $)
 1010 FORMAT(3X,I7,4X,I7,4X,I7,4X,I7,4X,I7,4X,I7)
      END
```

```
      SUBROUTINE INIT (TIME,INTIM,N)
      COMMON DATA(24,2)
      INTEGER TIME
      GO TO (1,2,3),INTIM
    1 TIME=0
      N=1
      GO TO 10
    2 READ(1) TIME,(DATA(I,1),I=2,22)
      BACKSPACE1
      N=2
      GO TO 10
    3 READ(1) TIME,(DATA(I,1),I=2,22)
      BACKSPACE1
      READ1000,TIME
      N=2
   10 RETURN
 1000 FORMAT(11E)
      END
```

```
      PROGRAM REDUCE(INPUT,OUTPUT,TAPE1,PUNCH)
C
C THIS PROGRAM WAS USED TO FIT NTH ORDER POLYNOMIALS TO POSITION VS.
C     DISPLACEMENT DATA OF THE SENSORS IN EACH SENSOR LINE AND OUTPUT
C     THE DERIVATIVES OF THESE FUNCTIONS.
C
      INTEGER COUNT,TIME,PCPOL,OPT
      REAL INVRX
      COMMON/AREA1/A(11),X(90,3),Y(90,3)
      COMMON/AREA2/NSKIPS(98),N1
      COMMON FCS(6,3)
      READ1000,MIN,MAX,NP,NVP,PCPOL,OPT,NS
      IPCPOL=PCPOL
      N1=0
      KOUNT=1
      GO TO (10,30),OPT
   10 READ1009,((X(I,J),I=1,NP),J=1,3)
      READ1007,(NSKIPS(I),I=1,NS)
   30 COUNT=1
   32 IF(NS-COUNT) 107,33,33
   33 PCPOL=IPCPOL
      CALL OPTION(COUNT,OPT,TIME,NP,PCPOL)
      IF(KOUNT.EQ.4) GO TO 502
      DO 501 IND=1,3
      IF(PCPOL.NE.1) GO TO 501
      IF(IND.EQ.3.AND.OPT.EQ.1) PCPOL=3
  501 CALL FRMC(NP,MAX,IND,PCPOL,KOUNT)
      PCPOL=IPCPOL
  502 DO 500 IND=1,3
      IF(PCPOL.NE.1) GO TO 37
      IF(IND.EQ.3.AND.OPT.EQ.1) PCPOL=3
   37 DO 100 II=MIN,MAX
      N=II
      CALL MLTRGR(NP,N,SING,IND)
      IF (SING) 102,102,103
  102 PRINT1006
      GO TO 500
  103 IF(IND.EQ.1) PRINT1010
      IF(IND.EQ.2) PRINT1011
      IF(IND.EQ.3) PRINT1012
      PRINT1004,N
      PRINT1005,(A(L),L=1,N)
      PUNCH1001,TIME,N,PCPOL
      PUNCH1008,(A(L),L=1,N)
      GO TO (50,51),OPT
   50 PRINT1002
      GO TO 52
   51 PRINT1003
   52 DO 105 J=1,NP
      XX=X(J,IND)
      CALL FRMPOL(N,XX,PCPOL,P,DPDX)
  105 CONTINUE
      IF(OPT.EQ.2) GO TO 100
      K2=NVP-1
      TEMP2=FLOAT(K2)
      IX1=(X(1,IND)/10)*10
```

```
      X1=FLOAT(IX1)
      TEMP1=X1-X(NP,INC)
      TEMP1=ABS(TEMP1)
      DO 104 K=1,NVP
      K1=K-1
      TEMP=FLOAT(K1)
      XX=X1+TEMP1*TEMP/TEMP2
      CALL FRMPOL(N,XX,PCPOL,P,DPDX)
  104 CONTINUE
  100 CONTINUE
  500 CONTINUE
      COUNT=COUNT+1
      GO TO 32
 1001 FORMAT(3IE)
 1009 FORMAT(8E10.4)
 1000 FORMAT(7I2)
 1002 FORMAT(4X,*X-POSITION*,1X,*DISPLACEMENT*,6X,*STRAIN*)
 1003 FORMAT(4X,*X-POSITION*,4X,*STRAIN*,4X,*STRAIN RATE*)
 1004 FORMAT(20X,I2,*TH ORDER POLYNOMIAL REGRESSION COEFFICIENTS*)
 1005 FORMAT(1X,10E13.5)
 1006 FORMAT(20X,*PROBABLE SINGULAR MATRIX*)
 1007 FORMAT(20I4)
 1008 FORMAT(6E13.6)
 1010 FORMAT(30X,*RADIAL LINE A*)
 1011 FORMAT(30X,*RADIAL LINE B*)
 1012 FORMAT(32X,*FACE LINE*)
  107 STOP
      END



      SUBROUTINE FRMPOL(N,XX,PCPOL,P,DPDX)
      COMMON/AREA1/A(11),X(90,3),Y(90,3)
      INTEGER PCPOL
      REAL INVRX
      P=0.
      DPDX=0.
      GO TO (1,2,3,4),PCPOL
    1 INVRX=1./XX
      GO TO 106
    2 INVRX=XX
      GO TO 106
    3 INVRX=1./(1.+XX)
      GO TO 106
    4 INVRX=1./(EXP(XX))
  106 DO 105 J=2,N
      I=N-J+2
      P=P*INVRX+A(I)
      JJ=I-1
      DUM=FLOAT(JJ)
      DPDX=DPDX*INVRX+DUM*A(I)
  105 CONTINUE
      P=P*INVRX+A(1)
      IF (PCPOL .EQ.2) GO TO 108
      DPDX=DPDX*INVRX*(-1.)
```

```
      IF(PCPOL.EQ.4) GO TO 108
      DPDX=DPDX*INVRX
  108 PRINT1003,XX,P,DPDX
      RETURN
 1003 FORMAT(1X,3E13.5)
      END



      SUBROUTINE SYMSOL(NN,SING,EPS)
      COMMON/AREA1/P(11),X(90,3),Y(90,3)
      COMMON A(11,11)
      DO 450 N=1,NN
      N1=N+1
      SING=ABS(A(N,N))
      IF (SING-EPS) 701,701,151
  151 B(N)=B(N)/A(N,N)
      IF (N.EQ.NN) GO TO 500
      DO 250 J=N1,NN
  250 A(N,J)=A(N,J)/A(N,N)
      DO 300 I=N1,NN
      DO 300 J=N1,NN
  300 A(I,J)=A(I,J)-A(I,N)*A(N,J)
      DO 400 I=N1,NN
  400 B(I)=B(I)-A(I,N)*B(N)
  450 CONTINUE
  500 N1=N
      N=N-1
      IF (N.EQ.0) GO TO 700
      DO 600 J=N1,NN
  600 B(N)=B(N)-A(N,J)*B(J)
      GO TO 500
  701 SING=0.
  700 RETURN
      END



      SUBROUTINE MLTRGR(M,N,SING,IND)
      REAL INVRX
      COMMON/AREA1/B(11),X(90,3),Y(90,3)
      COMMON/COEFM/C(60,11,3)
      COMMON SYMC(11,11)
      DATA EPS/1.0E-10/
C-FORM B(N)=TRANSPOSE(X)*Y
      DO 200 I=1,N
      T=0.
      DO 100 J=1,M
      T=T+C(J,I,IND)*Y(J,IND)
  100 CONTINUE
      B(I)=T
  200 CONTINUE
C-FORM TRANSPOSE(X)*X, SYMC(N,N)
      DO 300 I=1,N
```

```
      DO 300 K=1,N
      T=0.
      DO 400 J=1,M
      T=T+C(J,I,IND)*C(J,K,IND)
  400 CONTINUE
      SYMC(I,K)=T
  300 CONTINUE
      CALL SYMSOL(N,SING,EPS)
      RETURN
      END



      SUBROUTINE FRMC(M,N,IND,FCFCL,KCUNT)
      REAL INVRX
      INTEGER FCFCL
      COMMON/AREA1/R(11),X(90,3),Y(90,3)
      COMMON/COEFM/C(60,11,3)
C-FORM X=C(M,N) MATRIX
      GO TO (1,2,3,4),FCFCL
C-MATRIX FOR X=1/X
    1 DO 101 I=1,M
      INVRX=1./X(I,IND)
      C(I,1,IND)=1.
      DO 102 J=2,N
      L=J-1
      C(I,J,IND)=C(I,L,IND)*INVRX
  102 CONTINUE
  101 CONTINUE
      GO TO 170
C MATRIX FOR X=X
    2 DO 150 I=1,M
      C(I,1,IND)=1.
      DO 151 J=2,N
      L=J-1
      C(I,J,IND)=C(I,L,IND)*X(I,IND)
  151 CONTINUE
  150 CONTINUE
      GO TO 170
C-MATRIX FOR X=1/1+X
    3 DO 160 I=1,M
      INVRX=1./(1.+X(I,IND))
      C(I,1,IND)=1.
      DO 161 J=2,N
      L=J-1
      C(I,J,IND)=C(I,L,IND)*INVRX
  161 CONTINUE
  160 CONTINUE
      GO TO 170
    4 DO 162 I=1,M
      INVRX=1./(EXP(X(I,IND)))
      C(I,1,IND)=1.
      DO 171 J=2,N
      L=J-1
      C(I,J,IND)=C(I,L,IND)*INVRX
```

```
171 CONTINUE
162 CONTINUE
170 KOUNT=KOUNT+1
    RETURN
    END


    SUBROUTINE OPTION(COUNT,OPT,TIME,NP,PCPOL)
    COMMON/AREA1/A(11),Y(90,3),X(90,3)
    COMMON/AREA2/NSKIPS(98),N1
    COMMON POS(6,3)
    INTEGER COUNT,TIME,OPT,PCPOL
    DIMENSION DUM(90,6,3)
    GO TO (10,30),OPT
 10 NNI=NSKIPS(COUNT)
    IF(N1-NNI) 11,12,13
 11 N1=NNI
    COUNT=COUNT+1
    N2=NSKIPS(COUNT)
    DO 100 I=N1,N2
100 READ(1)
    GO TO 15
 12 COUNT=COUNT+1
 15 READ(1) TIME, ((X(I,J),I=1,7),J=1,3)
    PRINT1000
    DO 102 I=1,3
    PRINT1002, TIME, (X(J,I),J=1,7)
102 CONTINUE
 13 RETURN
 30 READ1001,NSEN
    READ1009,((POS(K,I),K=1,NSEN),I=1,3)
    DO 104 I=1,NP
    DO 105 K=1,3
    READ1001,TIME,N,PCPOL
    READ1009, (A(KK),KK=1,N)
    Y(I,K)=FLOAT(TIME)
    DO 106 J=1,NSEN
    POSI=POS(J,K)
    CALL FRMPOL(N,POSI,PCPOL,P,DPDX)
    DUM(I,J,K)=ABS(DPDX)
106 CONTINUE
105 CONTINUE
104 CONTINUE
    II=COUNT
    DO 108 K=1,3
    DO 109 J=1,NP
    X(J,K)=DUM(J,II,K)
109 CONTINUE
108 CONTINUE
    PRINT1004
    PRINT1003,(POS(II,I),I=1,3)
    RETURN
1000 FORMAT(13X,*TIME*,37X,*DISPLACEMENTS OF SENSORS*)
1001 FORMAT(3I5)
```

```
1002 FORMAT(1X,I16,7E16.6)
1003 FORMAT(1X,3E16.6)
1004 FORMAT(12X,*X/A POSITIONS OF SENSORS*)
1009 FORMAT(6E13.6)
     END
```

```
      PROGRAM DPLOT(INPUT,OUTPUT,TAPE5=INPUT,TAPE1,TAPE99)
C
C     THIS PROGRAM INTERFACES WITH GOSLIR AND WAS USED TO GENERATE
C     PLOTS OF DISPLACEMENT OR STRAIN VS. TIME OR FACE POSITION.  A
C     SEPARATE GRAPH FOR EACH SENSOR LINE WAS OUTPUT.
C
      INTEGER OPT,TIME,COUNT,OPTA
      DIMENSION SPECS(30)
      DIMENSION GXSPEC(4),XTICK(3,1),YTICK(3,1)
      DIMENSION RAD(3)
      COMMON/SPECSS/SPECSA(30)
      COMMON/CONSTS/COUNT,N2,NC,NS,NSEN,IND,NSEN1(7),NP,RATE
      COMMON/DATA/XDATA(50,7,3),YDATA(50,7,3)
      COMMON/DATA2/XPOS(7,3),TIME(6)
      READ1000,NC,NP,OPT,ITMC,IBX,OPTA,RAD,RATE
      READ1001,(SPECSA(I),I=1,30)
      DO 100 I=1,30
  100 SPECS(I)=SPECSA(I)
      N2=0
      COUNT=1
      GXSPEC(1)=0.
      GXSPEC(3)=1.
      GXSPEC(4)=1.
      XTICK(1,1)=3.
      YTICK(1,1)=3.
      XTICK(2,1)=.1
      YTICK(2,1)=.1
  101 CALL OPTION(OPT,ISIG,ITMC,IBX,OPTA,RAD)
      IF(ISIG.EQ.1) GO TO 501
      DO 500 II=1,OPTA
      READ1001,(SPECSA(I),I=3,10)
      DO 102 I=3,10
  102 SPECS(I)=SPECSA(I)
      GXSPEC(2)=SPECS(6)
      XTICK(3,1)=SPECS(9)
      YTICK(3,1)=SPECS(10)
      CALL GXLILI(GXSPEC,XTICK,YTICK,SPECS)
C-FIND ZERO COORDINATE OF AXIS
      XR=SPECS(3)
      XL=ABS(SPECS(4))
      XS=SPECS(7)
      XS=XS/(XR+XL)
      ZRO=(XS*XL)
      SPECS(7)=ZRO
      CALL NOSLIR(SPECS)
      SPECS(7)=SPECSA(7)
      SPECS(27)=SPECSA(27)
      CALL NOSLIR(SPECS)
      SPECS(24)=SPECSA(24)
      CALL PLOTS(OPT,II)
      CALL NXTFRM(SPECS)
  500 CONTINUE
      GO TO 101
  501 CALL GOSEND(SPECS)
      STOP
 1000 FORMAT(3I2,I5,2I2,4E10.4)
```

```
1001 FORMAT(8E10.4)
     END



     SUBROUTINE FRMPOL(N,XX,PCPOL,P,DPDX,A,RAD,K)
     DIMENSION A(11),RAD(3)
     INTEGER PCPOL
     REAL INVRX
     P=0.
     DPDX=0.
     GO TO (1,2,3,4),PCPOL
   1 INVRX=1./XX
     GO TO 106
   2 INVRX=XX
     GO TO 106
   3 INVRX=1./(1.+XX)
     GO TO 106
   4 INVRX=1./(EXP(XX))
 106 DO 105 J=2,N
     I=N-J+2
     P=P*INVRX+A(I)
     JJ=I-1
     DUM=FLOAT(JJ)
     DPDX=DPDX*INVRX+DUM*A(I)
 105 CONTINUE
     P=P*INVRX+A(1)
     DPDX=DPDX/RAD(K)
     IF (PCPOL .EQ.2) GO TO 108
     DPDX=DPDX*INVRX*(-1.)
     IF(PCPOL.EQ.4) GO TO 108
     DPDX=DPDX*INVRX
 108 RETURN
     END



     SUBROUTINE SYMP(OPT,II,NTIT)
     INTEGER TIME,OPT ,COUNT
     DIMENSION SPECS(30)
     COMMON/SPECSS/SPECSA(30)
     COMMON/DATA2/XPOS(7,3),TIME(6)
     DO 100 I=1,30
 100 SPECS(I)=SPECSA(I)
     DUM=FLOAT(II)
     SPECS(23)=SPECS(23)+(.17*DUM)
     SPECS(16)=DUM
     GO TO (10,20,10,20),OPT
  10 CALL SYMKEY(3.,10HTIME(MIN)=,SPECS)
     SPECS(22)=SPECS(22)+.1
     VALUE=FLOAT(TIME(II))
     CALL DECVAL(1.,VALUE,SPECS)
     RETURN
  20 CALL SYMKEY(3.,17HX-POSITION (X/A)=,SPECS)
```

```
      SPECS(22)=SPECS(22)+.1
      VALUE=XPOS(II,NTIT)
      CALL DECVAL(1.,VALUE,SPECS)
      RETURN
      END



      SUBROUTINE PLOTE(OPT,NTIT)
      INTEGER TIME,OPT,COUNT
      DIMENSION SPECS(30),X(50),Y(50)
      COMMON/DATA/XDATA(50,7,3),YDATA(50,7,3)
      COMMON/CONSTS/COUNT,N2,NC,NS,NSEN,IND,NSEN1(7),NP,RATE
      COMMON/SPECSS/SPECSA(30)
      COMMON/DATA2/XPOS(7,3),TIME(6)
      DO 100 I=1,30
  100 SPECS(I)=SPECSA(I)
      DO 500 II=1,NC
      SPECS(16)=FLOAT(II)
      DO 101 I=1,NP
      X(I)=XDATA(I,II,NTIT)
      Y(I)=YDATA(I,II,NTIT)
  101 CONTINUE
      CALL PSLILI(X,Y,SPECS)
      CALL SYMP(OPT,II,NTIT)
  500 CONTINUE
      RETURN
      END



      SUBROUTINE OPTION(OPT,ISIG,ITMC,IBX,OPTA,RAD)
      INTEGERTIME,OPT,PCPOL,COUNT,OPTA
      DIMENSION NSKIPS(98),DUM(7,1,3),A(11)
      DIMENSION RAD(3)
      COMMON/CONSTS/COUNT,N2,NC,NS,NSEN,IND,NSEN1(7),NP,RATE
      COMMON/DATA/XDATA(50,7,3),YDATA(50,7,3)
      COMMON/DATA2/XPOS(7,3),TIME(6)
      IF(OPT.EQ.4) GO TO 4
    2 IF(COUNT.GT.1) GO TO 119
      IND=0
      READ1000,NS,NSEN,(NSEN1(I),I=1,7),PCPOL
      READ1000,(NSKIPS(I),I=1,NS)
      READ1001,((XPOS(I,J),I=1,NSEN),J=1,OPTA)
      PRINT1006,((XPOS(I,J),I=1,NSEN),J=1,OPTA)
      DO 110 II=1,NP
      N1=NSKIPS(COUNT)
      COUNT=COUNT+1
      IBX=IBX-1
      IF(N2-N1) 111,112,112
  111 N2=NSKIPS(COUNT)
      DO 114 I=N1,N2
  114 READ(1)
  112 READ(1)ITIME,((DUM(J,1,I),J=1,7),I=1,3)
```

```
      RTIME=FLOAT(ITIME)
      IF(IEX)101,102,102
  102 ITIME=ITIME-ITMC
      RTIME=FLOAT(ITIME)
      IF(RATE.LT..000001) GO TO 101
      RTIME=RATE*RTIME
      RTIME=ABS(RTIME)
  101 COUNT=COUNT+1
      DO 115 K=1,OPTA
      DO 115 I=1,NSEN
      NS1=NSEN1(I)
      YDATA(II,I,K)=DUM(NS1,1,K)
      IF (OPTA.EQ.3) GO TO 120
      YDATA(II,I,K)=YDATA(II,I,K)/RAD(K)
      GO TO 121
  120 YDATA(II,I,K)=YDATA(II,I,K)*2.54
  121 XDATA(II,I,K)=RTIME
      IF(RATE.LT. .000001) GO TO 115
      XDATA(II,I,K)=XDATA(II,I,K)/RAD(K)
  115 CONTINUE
      PRINT1004,ITIME,((YDATA(II,I,K),I=1,NSEN),K=1,OPTA)
  110 CONTINUE
      GO TO 118
  119 IND=IND+NC
      ICK=IND+NC
      IF(ICK-NSEN) 117,117,119
  117 DO 113 K=1,OPTA
      JJ=IND
      DO 11 I=1,NC
      JJ=JJ+1
      XPOS(I,K)=XPOS(JJ,K)
      DO 88 J=1,NP
      YDATA(J,I,K)=YDATA(J,JJ,K)
   88 CONTINUE
   11 CONTINUE
  113 CONTINUE
      GO TO 118
  116 ISIG=1
  118 RETURN
    4 IF(COUNT.GT.1) GO TO 135
      IND=0
      READ1000,NSEN
      READ1001,((XPOS(I,J),I=1,NSEN),J=1,OPTA)
      PRINT1006, ((XPOS(I,J),I=1,NSEN),J=1,OPTA)
      DO 130 II=1,NP
      IEX=IEX-1
      DO 90 K=1,3
      READ1002,ITIME,N,PCPOL
      IF(K.GT. OPTA) GO TO 108
      RTIME=FLOAT(ITIME)
      IF(IEX)108,109,109
  109 ITIME=ITIME-ITMC
      RTIME=FLOAT(ITIME)
      IF(RATE.LT..000001) GO TO 108
      RTIME=RATE*RTIME
      RTIME=RTIME/RAD(K)
```

```
      RTIME=ABS(RTIME)
  108 READ1001,(A(L),L=1,N)
      IF(K.GT. OPTA) GO TO 90
      DO 131 I=1,NSEN
      XX=XPOS(I,K)
      CALL FRMPOL(N,XX,PCPOL,P,DPDX,A,RAD,K)
      IF(OPTA.EQ. 3) GO TO 138
      P=P/RAD(K)
      YDATA(II,I,K)=P
      GO TO 140
  138 YDATA(II,I,K)=ABS(DPDX)
  140 XDATA(II,I,K)=RTIME
  131 CONTINUE
   90 CONTINUE
      PRINT1004,RTIME,((YDATA(II,I,K),I=1,NSEN),K=1,OPTA)
      COUNT=COUNT+1
  130 CONTINUE
      GO TO 139
  135 IND=IND+NC
      ICK=IND+NC
      IF(ICK-NSEN) 137,137,136
  137 DO 238 K=1,OPTA
      JJ=IND
      DO 132 I=1,NC
      JJ=JJ+1
      XPOS(I,K)=XPOS(JJ,K)
      DO 91 J=1,NP
      YDATA(J,I,K)=YDATA(J,JJ,K)
   91 CONTINUE
  132 CONTINUE
  238 CONTINUE
      GO TO 139
  136 ISIG=1
  139 RETURN
 1000 FORMAT(20I4)
 1001 FORMAT(6E13.6)
 1002 FORMAT(3I5)
 1003 FORMAT(8E10.4)
 1004 FORMAT (1X,F8.3,16F7.5,F6.4,F5.4)
 1005 FORMAT(1X,I6)
 1006 FORMAT(9X,16F7.5,F6.4,F5.4)
      END
```

* U.S. GOVERNMENT PRINTING OFFICE : 1977 0-729-886/1486

REQUEST FOR FEEDBACK TO
The DOT Program Of University Research

DOT-TST-77-59

YES	NO	
☐	☐	Did you find the report useful for your particular needs? If so, how?
☐	☐	Did you find the research to be of high quality?
☐	☐	Were the results of the research communicated effectively by this report?
☐	☐	Do you think this report will be valuable to workers in the field of transportation represented by the subject area of the research?
☐	☐	Are there one or more areas of the report which need strengthening? Which areas?
☐	☐	Would you be interested in receiving further reports in this area of research? If so, fill out form on other side.

Please furnish in the space below any comments you may have concerning the report. We are particularly interested in further elaboration of the above questions.

Cut Out Along This Line

COMMENTS

Thank you for your cooperation. No postage necessary if mailed in the U.S.A.

RESEARCH FEEDBACK

Your comments, please . . .

This booklet was published by the DOT Program of University Research and is intended to serve as a reference source for transportation analysts, planners, and operators. Your comments on the other side of this form will be reviewed by the persons responsible for writing and publishing this material. Feedback is extremely important in improving the quality of research results, the transfer of research information, and the communication link between the researcher and the user.

FOLD ON TWO LINES, STAPLE AND MAIL.

Fold Fold

DEPARTMENT OF TRANSPORTATION
OFFICE OF THE SECRETARY
Washington, D.C. 20590

Official Business

PENALTY FOR PRIVATE USE, $300

POSTAGE AND FEES PAID
DEPARTMENT OF
TRANSPORTATION
DOT 518

Office of University Research
Office of the Secretary (TST-60)
U.S. Department of Transportation
400 Seventh Street, S.W.
Washington, D.C. 20590

Fold Fold

IF YOU WISH TO BE ADDED TO THE MAIL LIST FOR FUTURE REPORTS, PLEASE FILL OUT THIS FORM.

Name _____ Title _____
Use Block Letters or Type

Department/Office/Room _____

Organization _____

Street Address _____

City _____ State _____ Zip _____